2002

FUNDAMENTAL AND APPLIED MEASUREMENTS IN ICP-MS

CARTER, JULIAN ROBERT

FUNDAMENTAL AND APPLIED MEASUREMENTS IN IOP-MS

JULIAN CARTER

Ph.D. 2002

Signed.....

FUNDAMENTAL AND APPLIED MEASUREMENTS

IN

ICP-MS

By

JULIAN ROBERT CARTER., BSc (Hons), AMRSC

A thesis submitted to the University of Plymouth in partial fulfilment for the degree of

DOCTOR OF PHILOSOPHY

Department of Environmental Sciences

University of Plymouth

Drake Circus

Plymouth

PL4 8AA

In collaboration with Thermoelemental

Ion path Road

Winsford

Cheshire

UK

MAY 2002

ABSTRACT
FUNDAMENTAL AND APPLIED MEASUREMENTS IN ICP-MS
By
JULIAN ROBERT CARTER, BSc., AMRSC

Fundamental and applied aspects of ICP-MS have been investigated to gain an increased understanding of the technique and improve on its analytical capabilities.

Dissociation temperatures of polyatomic ions were calculated using a double-focusing sector instrument, to obtain more reliable mass spectral data with controlled vapour introduction via a Dreschel bottle to allow accurate calculation of the ingredients in the plasma. The equilibrium temperature for the plasma, operated at 1280 W calculated using CO^+ and C_2^+ as the thermometric probes, was c.a. 5800 – 7400 K, while using ArO^+ and ArC^+ as the thermometric probes the temperature calculated was c.a. 2000 - 7000 K. Calculated dissociation temperatures were used to elucidate the site of formation of these ions. Results confirmed that strongly bound ions such as CO^+ and C_2^+ were formed in the plasma whereas weakly bound ions such as ArO^+ and ArC^+ were formed in the interface region due to gross deviation of the calculated temperatures from those expected for a system in thermal equilibrium.

The use of helium gas in a hexapole collision cell attenuated the signals of ArH^+ Ar^+, ArO^+, ArC^+, $ArCl^+$ and Ar_2^+ allowing improved determination of $^{39}K^+$, $^{40}Ca^+$, $^{56}Fe^+$, $^{52}Cr^+$, $^{75}As^+$ and $^{80}Se^+$ in standard solutions. The use of the hexapole collision cell also resulted in an enhancement of analyte signals due to the thermalisation of the ion beam.

The ion kinetic energy of ions sampled from the plasma and those sampled from the skimmer cone were determined using a modified lens stack to assess the significance for memory effects of material deposited on the skimmer cone. The most probable kinetic energy of Be^+ ions sampled from the skimmer cone was found to be 2.4 eV, which was considerably lower than the most probable kinetic energy of Be^+ ions sampled from the plasma, which was found to be 9.5 eV. The low kinetic energy of the ions deposited on the skimmer cone means they will only contribute to the analytical signal under certain instrumental operating conditions.

The feasibility of liquid sample introduction into a LP-ICP-MS system designed for gaseous sample introduction was investigated using a particle beam separator. The low signal was attributed to the low gas kinetic temperature of the plasma which was confirmed by the fact that the signal increased rapidly with increasing temperature of the transfer line between the particle beam separator and the LP-ICP torch. This was also supported by the fact that more volatile compounds gave mass spectra whereas less volatile compounds did not. A limit of detection of 30 mg l^{-1} for chlorobenzene was achieved.

Finally, silicon and phosphorus speciation was performed by HPLC coupled to sector-field ICP-MS. Silicones ranging in molecular weight from 162 g mol^{-1} - 16500 g mol^{-1} were extracted from spiked human plasma and separated by size exclusion chromatography. Limits of detection ranged from 12 ng ml^{-1} Si^+ for the 162 gmol^{-1} silicone to 30 ng ml^{-1} Si^+ for the 16500 g mol^{-1} silicone. Organophosphate pesticides were extracted from spiked plasma and separated by reversed phase chromatography. Recoveries were between 55 - 81 %. Limits of detection were 0.9 ng ml^{-1} P^+, 1.8 ng ml^{-1} P^+, 1.6 ng ml^{-1} P^+ and 3.0 ng ml^{-1} P^+ for dichlorvos, methyl parathion, malathion and quinolphos respectively. Phosphates were extracted from various food products and separated by ion-exchange chromatography. Limits of detection were 1.0 ng ml^{-1} P^+, 2.3 ng ml^{-1} P^+, and 39 ng ml^{-1} P^+ for PO_4^{3-}, $P_2O_7^{4-}$ and $P_3O_{10}^{5-}$ respectively.

CONTENTS

LIST OF TABLES

LIST OF FIGURES

ACKNOWLEDGEMENTS

I would like to thank my supervisors, Dr Hywel Evans and Prof. Les Ebdon for their continuous support and encouragement throughout this Ph.D.

The financial assistance of the EPSRC is gratefully acknowledged. I would like to thank Thermoelemental as the collaborating establishment.

I gratefully acknowledge Dr Peter Sutton and Mr. Andrew Tonkin for synthesising the silanols, which turned out to be a difficult task indeed! Special thanks to Rob Harvey for always being at hand to repair the ICP instruments.

Thanks to everyone I have worked with at the University of Plymouth, past and present including Neil, Jason, Mike, Anita, Andy, Emily, Sarah and Paul. I would like to thank the following friends who have been there through the good and bad times: Frank, Kat, Sharon and Jo. You are all stars!

Finally, I would like to dedicate this thesis to the following people: Mum, Dad, Steve, Nan, Mark, Kevin and Vanessa, for their ceaseless love, support and encouragement.

AUTHOR'S DECLARATION

At no time during the registration for the degree of Doctor of Philosophy has the author been registered for any other university award.

This study was financed with the aid of a studentship from the Engineering and Physical sciences Research Council (EPSRC).

Regular scientific seminars and conferences were attended and external institutions were visited for consultation purposes.

COURSES AND CONFERENCES ATTENDED

- 'European winter conference on Plasma Spectrochemistry', University of Pau, Pau, France, 10-15 January 1999. Poster presented.
- '36th Research and Development Topics in Analytical Chemistry', University of Greenwich, Greenwich, UK, 12-14 April 1999. Poster presented.
- 'Analytical Atomic Spectrometry short course', University of Plymouth, Plymouth, UK, 4-8 October 1999.
- 'Research and Development at the young researchers' meeting and specialist symposium', UMIST, Manchester, UK, 16-17 April 2000. Poster presented.
- 'Tenth Biennial National Atomic Spectroscopy Symposium', Sheffield Hallam University, Sheffield, UK, 17-20 July 2000. Poster Presented.
- Regular lecture presentations at the university of Plymouth research seminars.

PUBLICATIONS RESULTING FROM THIS STUDY

- Carter, J. R. C., Ebdon, E., and Evans E. H., 'The estimation of dissociation temperatures: An insight into the site of formation of polyatomic ions in ICP-MS'. To be submitted

- Carter, J. R. C., Ebdon, E., and Evans E. H., 'Ion stopping experiment to determine the origin of background ions in ICP-MS. Paper submitted.

Signed J. Carter.....

Date 19-10-02.....

CHAPTER 1: INTRODUCTION

1.1 Origins and Development of Inductively Coupled Plasma - Mass Spectrometry

The inductively coupled plasma (ICP) used in the instruments of today was first utilised by Reed in 1961[1]. The potential of the ICP as an atom cell for atomic emission spectroscopy (AES) was realised by Greenfield *et al.* in 1964[2] and Wendt and Fassel in 1965[3], with both groups recognising the potential of ICP-AES to become a useful tool for simultaneous multi-element analysis. However, even before the commercial launch of these instruments work was already under way developing what is generally seen as its successor. Gray[4] first demonstrated that plasma source mass spectrometry was possible using a direct current plasma. This was not an ideal ion source and was replaced by the ICP. The first success in coupling of an argon inductively coupled plasma with a mass spectrometer was reported in 1980 by Houk *et al.*[5] and later by Date and Gray[6]. The first commercial instruments were introduced in 1983 by two manufacturers, VG isotopes (now Thermoelemental, UK) and Sciex (Canada). The success of ICP-MS is reflected in that more than six companies are manufacturing and marketing these instruments world wide today.

1.2 The ICP-MS System Set Up and Operation

Figure 1.1 Shows a schematic diagram of a standard ICP-MS instrument. The instrument consists of three basic units: i) a conventional ICP operated at temperatures of 5000 - 10 000 K, with a nebuliser and spray chamber for liquid sample introduction, ii) an interface unit consisting of two water-cooled nickel cones, each containing a small orifice allowing sampling of the plasma gases and transfer of the ion beam into the mass spectrometer, and iii) a conventional quadrupole mass spectrometer which permits rapid scanning over the mass range 0 - 300 atomic mass units.

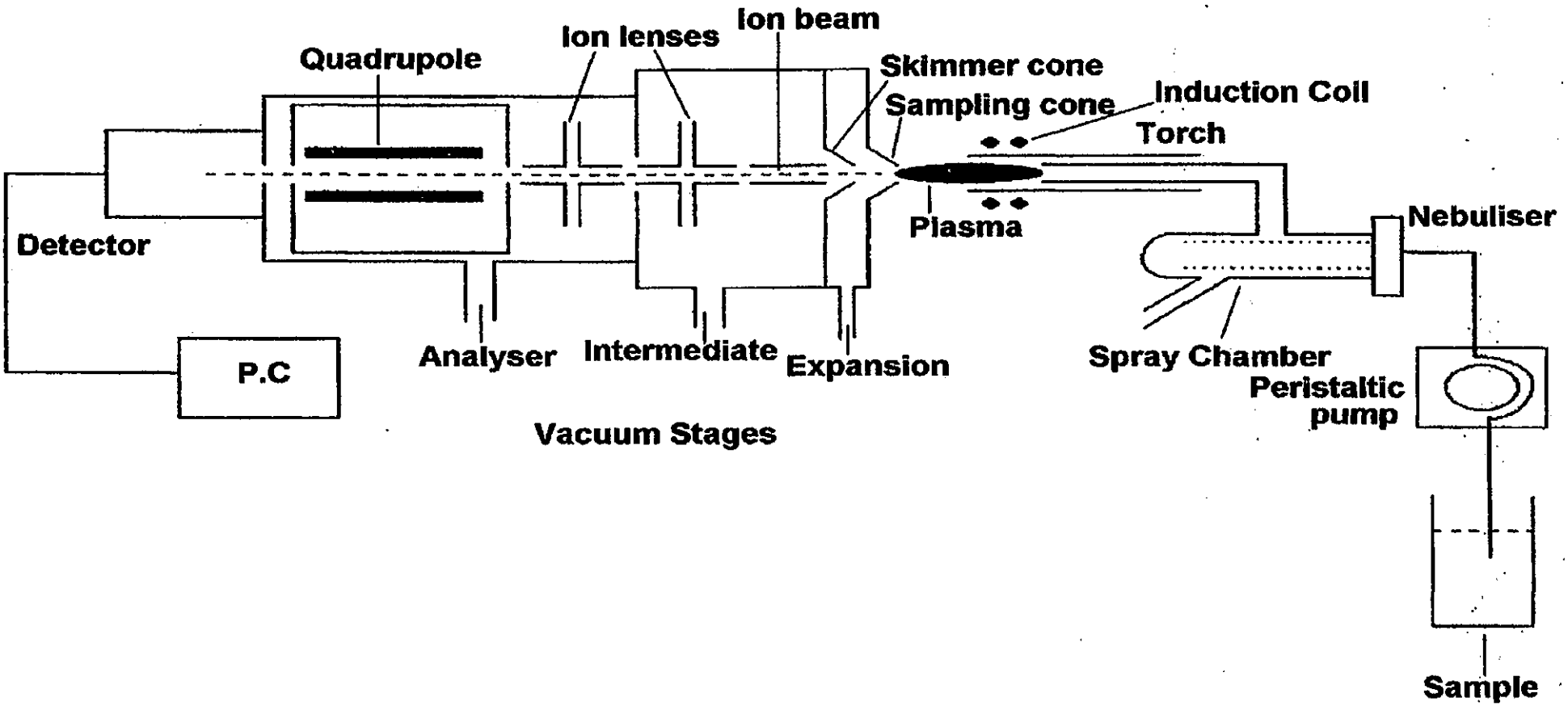

Figure 1.1: Schematic of a conventional ICP-MS.
(Taken from reference 137)

1.2.1: Forming and sustaining the plasma

The ICP ion source is formed within the confines of three concentric tubes (Figure 1.2) made of quartz. Each tube has an entry point for gas, with those of the coolant gas (outer tube) and the auxiliary gas (intermediate tube) being introduced tangentially. Located around the edge of the outer quartz tube is a two or three turn water cooled copper coil. This load coil is connected to a radio- frequency (RF) generator and power input to the ICP is achieved via the load coil typically in the range 1- 2.5 kW at a frequency of 27 or 40 MHz.

Flowing gases, usually argon, are introduced into the two outer tubes of the torch and the RF field is switched on which induces a magnetic field. The ICP is initiated by seeding the gas with electrons from a telsa discharge. These electrons are then accelerated in the magnetic field and cause ionisation of some of the gas atoms. The resulting cations and electrons collide with more argon atoms to produce further ionisation. This collisional ionisation continues in an avalanche reaction resulting in the formation of the ICP discharge. This process is self-sustaining so that argon atoms, argon ions and electrons now co-exist within the confines of the torch and can be seen to protrude from the top in the shape of a bright white luminous bullet. This bullet shape is formed by the escaping velocity of the argon gas causing the entrainment of air back towards the torch itself. The resulting ICP is electrically neutral, however, it is not in local thermal equilibrium and as a consequence excitation, ionisation and gas temperatures have different values. The ICP is sustained within the torch and load coil by the RF energy which is being continually transferred.

In order to introduce the sample aerosol into the hot plasma (5000 - 10000 K) the nebuliser gas is now introduced, this punches a hole in the centre of the plasma, thus creating the characteristic doughnut or toroidal shape of the ICP. This region is cooler than the rest of the ICP, but at 5000 - 6000 K it is sufficiently hot to atomise most

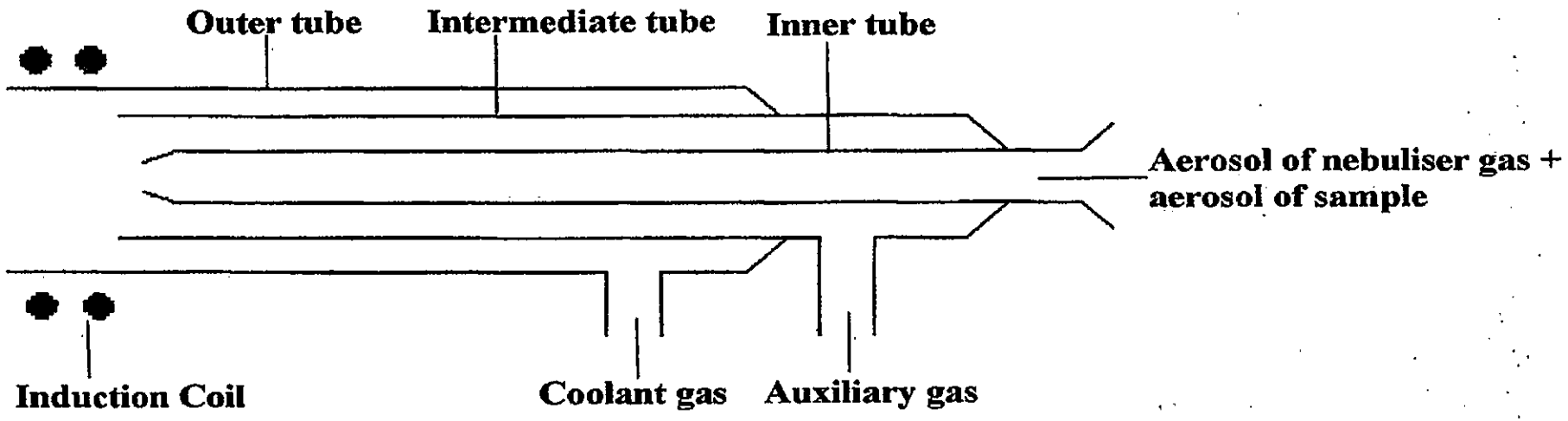

Figure 1.2: Schematic of a standard 'Fassel' quartz torch.
(Taken from reference 137)

samples and to cause varying degrees of ionisation. Figure 1.3, shows the chain of events that occurs from sample to the formation of ions in the plasma. The efficiency of ionisation in the ICP can be calculated by the Saha equation and this shows the formation of singly charged ions is very efficient and that over 54 elements are expected to be ionised with an efficiency of 90 % or more [7].

Once atoms are formed in the ICP there are several processes by which they can be ionised and excited [7]. The main mechanisms for ionisation are:

- **Thermal excitation/ionisation:** caused by collisional energy exchange between atoms, ions and electrons

$$x + e^- \longrightarrow x^+ + 2e^- \quad \textbf{(1.1)}$$

$$M + A \longrightarrow M^+ + A + e^- \quad \textbf{(1.2)}$$

- **Penning ionisation/excitation:** caused by collisions between ground state atoms and argon metastable species.

$$Ar^m + X \longrightarrow Ar + X^+ + e^- \quad \textbf{(1.3)}$$

$$Ar^m + X \longrightarrow Ar + X^{+(*)} + e^- \quad \textbf{(1.4)}$$

- **Charge transfer ionisation/excitation:** caused by the transfer of charge between ions and atoms.

$$Ar^+ + X \longrightarrow Ar + X^+ \quad \textbf{(1.5)}$$

$$Ar_2^+ + X \longrightarrow 2Ar + X^{+(*)} \quad \textbf{(1.6)}$$

1.2.2: Sample introduction into the plasma

Sample introduction into the ICP is most commonly achieved in the liquid phase. The sample solution is delivered to a nebuliser using a peristaltic pump, to minimise physical characteristics, e.g. change in viscosity, at a rate of about 1 ml min^{-1}. The basic

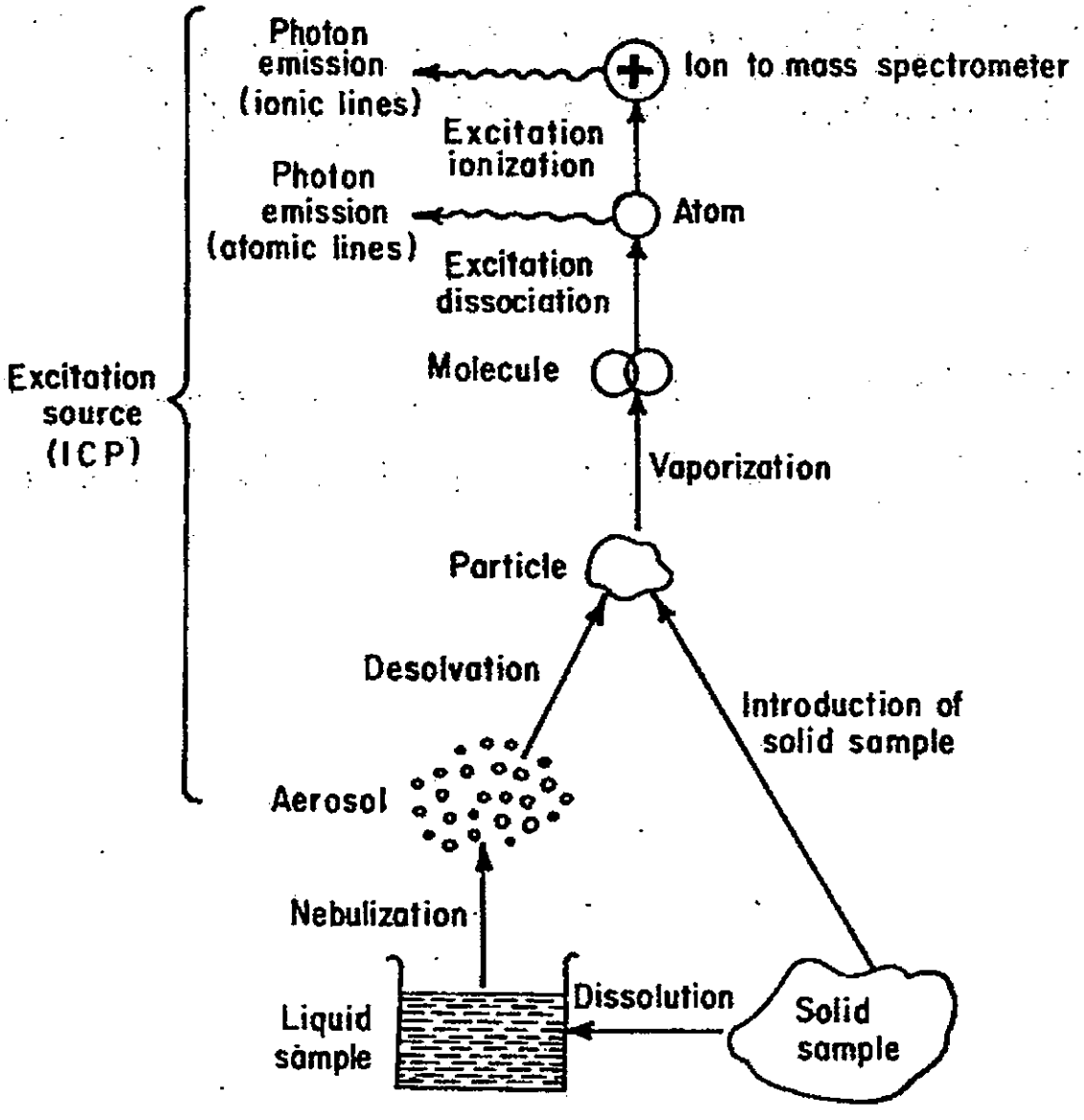

Figure 1.3: The chain of events leading from sample to the formation of ions in the plasma.
(Taken from reference 280)

function of the nebuliser is to convert the sample into an aerosol. The smaller the droplets formed, the more sample reaches the plasma. There are several different types of commercially available nebulisers, one of the most common nebulisers is the concentric glass nebuliser such as the Meinhard (Figure 1.4), other nebulisers include the cross flow nebuliser and Babington nebuliser of which the Ebdon nebuliser is a variety. The aerosol is then carried by the nebuliser gas through a spray chamber where large droplets condense and drain and pass to waste. The spray chamber is required because if large sample droplets were allowed to enter the plasma they would cause signal fluctuations, plasma instabilities and would eventually extinguish the plasma. Droplets in excess of 5-8 μm are effectively removed by the spray chamber and drawn or pumped to waste. The spray chamber also dampens pump noise. The majority of spray chambers are cooled between 2 - 5^0 C. This temperature is maintained throughout an analytical run so that the amount of solvent reaching the plasma is kept constant. This improves the stability of the plasma and the signal intensity.

As well as the conventional aspiration of aqueous samples, as described, there are several other methods of introducing samples into the plasma. These include the direct analysis of solids by laser ablation[8,9], or slurry nebulisation[10,11], the use of electrothermal vaporisation [12, 13, 14, 15] and hydride generation[16], or the use of various chromatographic techniques[17, 18].

Once the sample is injected into the plasma it undergoes several sequential processes as it moves deeper into the plasma: desolvation, vaporisation, atomisation and ionisation (Figure 1.3).

1.2.3: Ion extraction

The main success in the development of this technique was the development of a suitable interface. The interface allows the coupling of the ICP source, at atmospheric pressure, with the mass spectrometer, at high vacuum, while maintaining a high degree

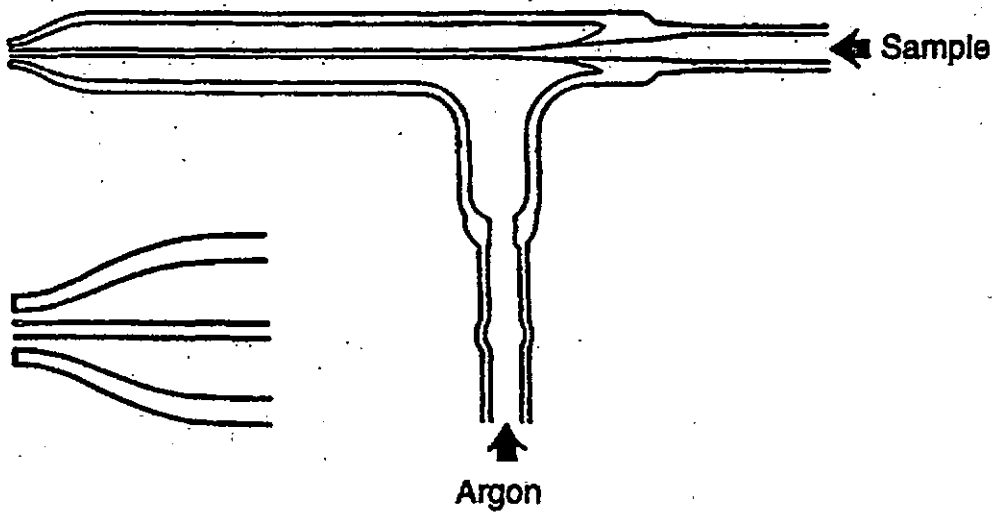

Figure 1.4: The Meinhard pneumatic nebuliser.
(Taken from reference 128)

of sensitivity. The interface (Figure 1.5) consists of a water-cooled nickel sampling cone, which has an orifice of approximately 1mm in diameter, positioned in close proximity to the ICP. The pressure behind the sampling cone is reduced using a rotary vacuum pump. The creation of this pressure differential causes ions from the plasma and the plasma gas itself to be drawn through the sampling orifice and undergo adiabatic expansion to form a shock wave structure, known as the barrel shock. The barrel shock helps prevent the gas jet from mixing with the surrounding gas and therefore helps prevent the formation of molecular species. The region within this expansion cone is called the 'zone of silence' which is representative of the ion species to be found in the ICP. The skimmer cone, which has an orifice diameter of approximately 1 mm and lies about 7mm behind the sampling cone, protrudes into the 'zone of silence'. The ions from the zone of silence pass through the orifice into a second intermediate vacuum chamber as an ion beam. This method of extracting ions directly from the plasma is referred to as continuum sampling, and is a development of the original method of boundary sampling. In this latter method ions were extracted from a cool layer which formed over the sampling cone as a result of the small aperture used in the sampling cones. In continuum sampling the higher gas flow through the sampler breaks through the boundary layer and sheath. The cool layers are still present, but they form along the inside edge of the sampling orifice. This method of sampling leads to a much higher total flow of ions, a more representative sample of ions from the plasma and a greater resistance to being blocked by deposited solids. The extracted ions are then focused by a series of electrostatic lenses into the mass spectrometer. These ion lenses, housed in the intermediate region of the instrument, are basically metal rings with electric potentials applied to them, they focus as many ions as possible from the zone of silence into the entrance of the quadrupole mass analyser. There are several different arrangements in use, but most usually have a photon stop present on the axis to

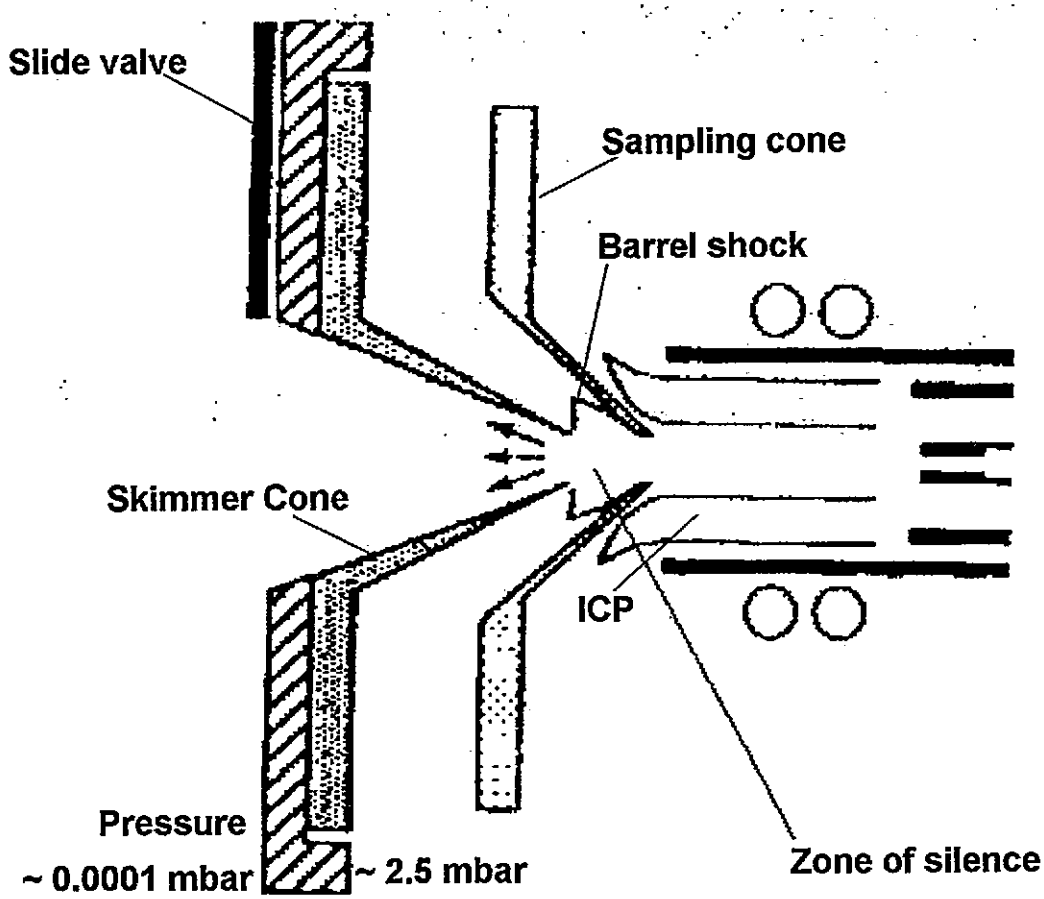

Figure 1.5: Schematic of the ICP-MS interface.
(Taken from reference 281)

prevent photons from the plasma striking the detector and adding to the background signal.

The mass analyser then separates the ions with respect to their mass to charge ratio (m/z). This is traditionally achieved using a quadrupole, but other mass analysers such as magnetic sector-field, time of flight and ion trap analysers are also used. The ions are detected using an electron multiplier, the data from which is transferred to a computer.

1.3: Capabilities of ICP-MS

ICP-MS has become one of the dominant techniques for multielement analysis owing to a number of important capabilities that the technique offers.

One of the main attractions of ICP-MS lies with the low detection limits attainable with mass spectrometric detection compared with optical detection. These detection limits are usually at least three orders of magnitude better than ICP-AES and better or equivalent to those obtained by graphite furnace atomic absorption spectrometry (GF -AAS). It has a much wider elemental coverage than atomic absorption spectrometry (AAS) and furthermore, it has the capability of multielement analysis unlike AAS with which only a limited number of elements at a time can be determined. The linear dynamic range for many elements extends 5 - 6 orders of magnitude allowing major, minor and trace elements in a sample to be determined simultaneously. The spectra are very simple and easier to interpret than optical emission spectra. This is important for samples that contain rare earth elements or heavy elements that yield complex emission spectra. The precision of the technique is typically 0.1 - 1 % and the sample throughput is extremely fast. ICP-MS instruments have the unique capability of providing a very rapid semi-quantitative analysis. This allows the determination of, for example, 70 elements in less than 60 seconds using less than 1ml of solution at a sample uptake rate of 1 ml min^{-1} in an unknown sample. This gives

concentrations within a factor of 2 or 3 of the accepted value. This feature allows the presence of elements to be revealed and dilution steps assessed before the elements are determined more accurately. Other advantages include isotope analysis capability and the flexibility of the instrument. This latter advantage allows other sample techniques such as laser ablation and hydride generation to be coupled to the standard instrument allowing solid and gaseous samples to be analysed. Various chromatographic techniques can also be coupled to the standard instrument allowing information on the chemical form in which an element is present to be obtained. Under standard operating conditions all compounds introduced into the ICP are atomised completely.

Owing to these numerous features, ICP-MS has been applied to the analysis of a wide range of samples. These include, as examples: geological[19], biological[20], clinical,[21] nuclear[22], freshwater[23], seawater[24], environmental[25], metallurgical[26], petroleum products[27] and food[28] and beverages[29].

1.4: Limitations of ICP-MS

Clearly ICP-MS has a number of distinct advantages over rival techniques. However, it is far from being the ideal analytical technique and in its standard configuration, i.e. with a pneumatic nebuliser for sample introduction and with a quadrupole mass analyser ICP-MS shows a number of important limitations. The major limitations are the problem of interferences.

1.4.1:Spectroscopic interferences

This category of interference forms the largest form of interferences. These interferences occur when an ionic species has the same m/z value as an analyte ion. This generally leads to an enhancement in the apparent analyte signal. Such interferences fall into three categories: Isobaric ions, doubly charged ions and polyatomic ions.

Isobaric interferences occur when two or more elements have isotopes which have the same nominal mass. For atomic mass spectrometry with a quadrupole mass analyser, isobaric species are isotopes that differ in mass by less than one unit, whereas with a higher resolution instrument smaller mass differences can be tolerated. Since around 70 % of the elements in the periodic table have more than one isotope isobaric interferences can easily be avoided by selecting an alternative isotope for analysis. For example if determining nickel then $^{60}Ni^{+}$ would be selected rather than the most abundant isotope of nickel, $^{58}Ni^{+}$, which is 67.8 % abundant, because it suffers from an isobaric overlap by $^{58}Fe^{+}$. At atomic mass 60 Nickel is 26.4 % abundant but no interfering isotope occurs. However, there is a problem that by determining the lower abundant isotope there is a loss in sensitivity. Alternatively, the isobaric interference can be corrected for by using appropriate calculations.[30] Most instruments are capable of making such corrections automatically. Some examples of isobaric interferences are shown in Table 1.1.

Elements such as barium, cerium, lanthanum, strontium and thorium, which have relatively low second ionisation potentials, easily form doubly charged species (M^{2+}) in the plasma. For example barium with a second ionisation potential of 10 eV[31] forms approximately 4.1 %[32] $^{138}Ba^{2+}$. The formation of doubly charged species causes two problems, firstly it results in loss of sensitivity of the singly charged species and secondly it gives rise to an ion that causes an isotopic overlap at half the mass of the parent element. Thus $^{138}Ba^{2+}$, causes an interference at mass 69 which interferes with the determination of $^{69}Ga^{+}$. Table 1.2 shows a range of M^{2+} interferences and the affected analytes.

The most troublesome spectroscopic interferences, due to the fact that they are much more difficult to overcome, are those caused by polyatomic ions. Polyatomic ions are molecular species which are formed in the plasma and interface region of the ICP-MS and are of particular problem below m/z 80[32, 33]. Polyatomic ions are formed from

Table 1.1: Examples of isobaric interferences observed in ICP-MS

ISOTOPE	ISOBARIC OVERLAP
$^{36}S^{+}$	$^{36}Ar^{+}$
$^{40}K^{+}$	$^{40}Ar^{+}$ and $^{40}Ca^{+}$
$^{50}V^{+}$	$^{50}Ti^{+}$ and $^{50}Cr^{+}$
$^{58}Ni^{+}$	$^{58}Fe^{+}$
$^{64}Ni^{+}$	$^{64}Zn^{+}$
$^{84}Sr^{+}$	$^{84}Kr^{+}$
$^{92}Zr^{+}$	$^{92}Mo^{+}$
$^{115}In^{+}$	$^{115}Sn^{+}$
$^{124}Te^{+}$	$^{124}Sn^{+}$ and $^{124}Xe^{+}$
$^{148}Nd^{+}$	$^{148}Sm^{+}$
$^{160}Gd^{+}$	$^{160}Dy^{+}$
$^{176}Lu^{+}$	$^{176}Yb^{+}$ and $^{176}Hf^{+}$
$^{196}Pt^{+}$	$^{196}Hg^{+}$
$^{204}Pb^{+}$	$^{204}Hg^{+}$

Table 1.2: Doubly charged ions commonly observed in ICP-MS and the affected analyte

M^{2+}	AFFECTED ISOTOPE
$^{88}Sr^{2+}$	$^{44}Ca^{+}$
$^{138}Ba^{2+}$	$^{69}Ga^{+}$
$^{140}Ce^{2+}$	$^{70}Ge^{+}$
$^{154}Sm^{2+}$	$^{77}Se^{+}$
$^{170}Er^{2+}$	$^{85}Rb^{+}$
$^{176}Yb^{2+}$	$^{88}Sr^{+}$
$^{232}Th^{2+}$	$^{116}Sn^{+}$
$^{238}U^{2+}$	$^{119}Sn^{+}$

interactions between species in the plasma (e.g. Ar) and species in the sample matrix (e.g. Na, Cl, Ca), the solvent used (e.g. O, H, C and also N, Cl, S) or the atmosphere (e.g. O, N, C). These ions interfere with analysis by causing an erroneously large signal at the m/z value of interest. Clearly the extent of the polyatomic interference will depend upon the composition of the sample being analysed. Some examples of polyatomic ions are shown in Table 1.3.

1.4.2: Non - spectroscopic interferences.

Non - spectroscopic interferences are due to the affects of the sample matrix. This interference is quite general in that the presence of nearly any concomitant element will result in a matrix effect which can exert an influence on sample transport, ionisation, ion extraction and ion throughput in the ion beam. Furthermore, the nature and concentration of the sample matrix has a direct bearing on the severity of the effect. Non - spectroscopic interferences are characterised by a reduction or enhancement of the analyte signal. The matrix of the sample will affect the viscosity, density and surface tension of the solvent which leads to a change in the sample delivery rate and thus interfere with and suppress the analyte signal. For example, the 100 mgl^{-1} sodium concentration in the matrix will cause a 20% suppression of cobalt and bismuth signals when the concentration of these elements is 10 mg l^{-1} [34]. This can be overcome by matrix matching of the samples and standards. The analyte signal can be suppressed by deposition of salt on the sampler and skimmer cones[35]. The presence of easily ionisable elements can lead to an enhancement of the analyte signal[36, 37], but most commonly it causes suppression of the analyte signal[36,38,39]. The effects of easily ionisable elements has been attributed to space charge effects[40].

Table 1.3: Polyatomic ions encountered in ICP-MS and the affected analyte

POLYATOMIC ION	AFFECTED ANALYTE
$^{18}H_2O^+$	$^{18}O^+$
$^{28}N_2^+$ and $^{28}CO^+$	$^{28}Si^+$
$^{29}N_2H^+$	$^{29}Si^+$
$^{31}NOH^+$	$^{31}P^+$
$^{32}O_2^+$	$^{32}S^+$
$^{52}ArC^+$	$^{52}Cr^+$
$^{54}ArN^+$	$^{54}Fe^+$
$^{56}ArO^+$	$^{56}Fe^+$
$^{57}ArOH^+$	$^{57}Fe^+$
$^{75}ArCl^+$	$^{75}As^+$
$^{76}Ar_2^+$	$^{76}Se^+$
$^{80}Ar_2^+$	$^{80}Se^+$
$^{103}ArCu^+$	$^{103}Rh^+$
$^{154}BaO^+$	$^{154}Sm^+$ and $^{154}Gd^+$
$^{155}BaOH^+$	$^{155}Gd^+$
$^{181}HoO^+$	$^{181}Ta^+$
$^{192}LuO^+$	$^{192}Os^+$ and $^{192}Pt^+$
$^{254}UO^+$	$^{254}Es^+$ and $^{254}Cf^+$

1.5: Extending the measurement capabilities of ICP-MS

ICP-MS was basically designed for multielement analysis of aqueous samples. In order to extend its measurement capabilities and to achieve accurate, reliable and sensitive results much work has gone into overcoming the problems of interferences. Interferences can be dealt with in two ways either remove the interference or correct for its presence. It has been demonstrated that operating parameters such as the nebuliser gas flow rate, forward power, sampling orifice dimensions, cleanliness of the interface surface and ion lens tuning are all important in determining the levels of polyatomic interferences [38, 41, 42, 43, 44, 45, 46, 47, 48, 49, 50, 51]. The exact settings of these parameters depends upon the identity of the interference and the make of the instrument.

Mathematical correction techniques to account for the presence of polyatomic ions involves either simple calculations[30,52,53] using the isotope abundances of the interference (e.g. correcting for the presence of $^{75}ArCl^+$ by measuring $^{77}ArCl^+$) or using more complex multivariate techniques[54, 55].

One simple, but effective, way to overcome an interference caused by the acid used for digestion is to simply use an alternative acid. For instance if $^{75}As^+$ is to be determined HCl should be avoided and thus $^{75}ArCl^+$ will not be formed in the plasma allowing interference free determination of arsenic. In general nitric acid has been favoured as a dissolution media as it contains only N, H and O which are species present in the plasma gas and entrained gases anyway. This gives rise to simple spectra[33] in comparison with hydrochloric, sulphuric and phosphoric acid which give rise to a larger number of polyatomic ions [54, 28]. The use of alternative dissolution media may not however always be possible, this is particularly true for geological samples.

Alternative sample preparation methods have been investigated for these samples[56, 57, 58]. One method is to grind the sample into a fine suspension or slurry in a suitable dispersant. When the interference is present in the sample matrix itself it is possible to separate the analyte from the interference by precipitation or solvent

extraction. Chloride [21] has been removed in clinical samples by precipitation with silver and thus reducing the interference of $^{75}AsCl^+$ on $^{75}As^+$. Solvent extraction has been used as a means of separating the analyte form the matrix prior to analysis[59]. Precipitation and solvent extraction have generally been used in batch mode and are time consuming. Furthermore, there is the risk of co-precipitation of trace elements along with the interference or increasing the blank levels due to impurities in the extracting solvent.

An elegant alternative to the methods described above is the use of on-line techniques that have the advantage of being rapid. These include using chelating[60,61] or ion exchange resins [19, 62, 63] or chromatographic methods [17, 18]. These are used to either pre-concentrate the analyte or remove the matrix, or to separate the analytes from the interference temporally.

As mentioned earlier ICP-MS is extremely flexible in that the sample introduction system can be modified and this has been exploited in alleviating interferences.

The amount of water vapour entering the plasma and hence the levels of O^+ and OH^+ has been reduced by simply cooling the spray chamber[64,65] and more elaborate desolvation apparatus has also been employed such as Peltier coolers[66], membrane interfaces [67, 68] and heater/condensers[69]. The reduction of water entering the plasma causes a large reduction in the levels of oxide and hydroxide polyatomic ions. The various desolvation techniques employed have also been shown to reduce other polyatomic ions such as $ArCl^+$[70].

Other sample introduction techniques are also used to alleviate interferences, such as laser ablation[8, 9], electrothermal vaporisation[12, 13] and hydride generation[16].

The use of mixed gas plasmas, that is plasmas not solely composed of argon, have been investigated by several workers using N_2[71, 72, 73, 74, 75, 76, 77, 78, 79, 80, 81] He[82], Xe[83], H_2[14, 84], CH_4[75, 85] and C_2H_4 [86] to alleviate polyatomic ions. Mixed gas plasmas are formed when one of these gases is bled into or completely replaces one of the gas flows

in the ICP i.e. the nebuliser, auxiliary, or coolant. Mixed gas plasmas have mainly been used to reduce spectroscopic interferences and to a lesser extent non-spectroscopic interferences. They have also been used to increase analyte sensitivity.

Two groups[87, 88] have investigated using helium inductively coupled plasmas as a source for ICP-MS. The use of helium removes all argon based interferences and also facilitates more effective analysis of difficult to ionise elements owing to its higher ionisation potential. However, helium ICPs are difficult to initiate and sustain due to the resistivity and high thermal conductivity of He compared to Ar. Helium ICPs have thus found limited application and little further research has been undertaken.

The characteristics of the plasma can also be changed by operating the conventional Ar ICP at a lower power, typically 600 - 700 W with a relatively high injector gas flow rate. This may be used with increased sampling depth and desolvation. This 'cold ' plasma condition was first reported in 1988 by Jiang *et al.* [46]. They observed that under these conditions the background mass spectrum become dominated by NO^+ at m/z 30, while nearly all the Ar^+, and ArH^+ signals were markedly reduced. This allowed the determination of $^{39}K^+$ and $^{41}K^+$. Subsequently other workers investigated the use of cold plasmas [89, 90]. In the absence of desolvation the background spectrum is also dominated by water derived polyatomic ions e.g H_2O^+ [90]. There are however, a number of drawbacks using cool plasma conditions for analysis. Sensitivity is related to the ionisation potential of the analyte, decreasing markedly for elements whose ionisation potential is above 8 eV [90]. So, while easily ionised elements such as $Li,^+$ Mg^+, and Fe^+ can be determined by cool plasma conditions elements such as As^+ and Se^+, with high ionisation potentials will not be efficiently ionised. Such elements should be determined in the conventional (hot) plasma. Therefore if multielement analysis of a sample is to be performed a sample will have to be analysed twice, once under standard conditions for most elements with high ionisation potentials and once under cool plasma

conditions for the easily ionised elements. Non-spectroscopic interferences (matrix effects) may become more important in the cool plasma.

The replacement of the quadrupole mass analyser can provide relief from interferences. The principle motives for seeking alternative mass analysers is the limitations of the quadrupole, including its low duty cycle per isotope and a low mass resolution. The ion trap has been successfully coupled to the Ar ICP by Koppenaal and coworkers [91,92,93]. The authors reported that polyatomic ions such as ArO^+, $ArCl^+$, ClO^+ and Ar_2^+ are completely destroyed and that Ar^+ ions are almost completely neutralised. The time of flight mass analyser has also been coupled to the Ar ICP by Heiftje *et al.*[94].

One of the most effective and elegant ways of overcoming spectral interferences is to use a high-resolution mass analyser (Figure 1.6). The high resolution ICP-MS is based on a double focusing sector mass spectrometer. The ability of the mass analyser to separate or resolve two species of the same nominal mass (m) is described by:

$$R = m/\Delta m \quad (1.7)$$

Where R is the resolution and Δm is the mass difference between the two peaks. The peaks are considered to be resolved if the valley between them is less than 10 % of the peak height (for peaks of equal height).

Since the double focusing sector mass spectrometers show a higher mass resolution than quadrupole mass analysers the signals of analyte ions can be resolved from those of interfering ions. This allows unambiguous identification and quantification of analytical results. Most predicted interferences in ICP-MS can be resolved from the isotope of interest with a resolution of up to 10000, although the separation of isobaric interferences requires a resolution of greater than 20000, which is outside the capabilities of the analyser.

Reed *et al.*[95] have investigated several polyatomic ions that arise from common acids used in analysis and those arising from air entrainment into the plasma and the resolution required to resolve these interferences. Table 1.4 shows the resolution

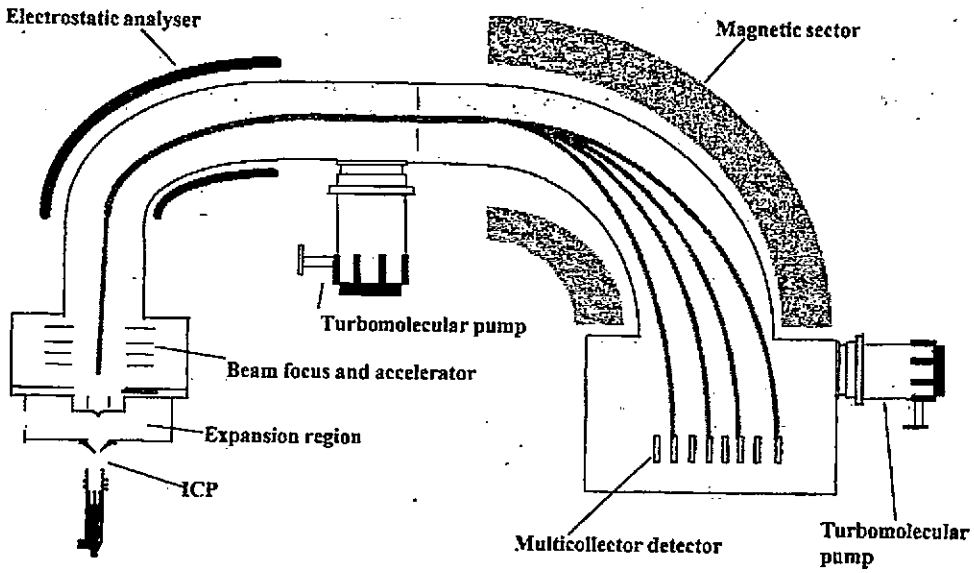

Figure 1.6: Schematic of a double-focusing sector ICP-MS.
(Taken from reference 128)

Table 1.4: Resolution required to separate interfering ions from analyte ions

ANALYTE	POLYATOMIC ION	RESOLUTION
$^{28}Si^{+}$	N_2^{+}	960
$^{28}Si^{+}$	CO^{+}	1600
$^{31}P^{+}$	NOH^{+}	970
$^{32}S^{+}$	O_2^{+}	1800
$^{40}Ca^{+}$	Ar^{+}	193000
$^{52}Cr^{+}$	ArC^{+}	2400
$^{52}Cr^{+}$	$ClOH^{+}$	1700
$^{56}Fe^{+}$	ArO^{+}	2500
$^{75}As^{+}$	$ArCl^{+}$	7800
$^{80}Se^{+}$	Ar_2^{+}	9700

required to separate interfering ions from a number of difficult to analyse elements by quadrupole ICP-MS. High-resolution instruments have been used for multi-element trace analysis of seawater[96], eliminating the need for matrix separation techniques which demonstrates its superiority over quadrupole instruments. After experimentally selecting the appropriate resolution setting for the elements of interest, the sample could be analysed after a 4 - 5 fold dilution. In comparison using a quadrupole instrument, owing to the large number of spectral interferences, separation/pre - concentration steps would have to be included, lengthening analysis time. Other advantages of high-resolution instruments are the superior detection limits obtainable in low-resolution mode and the possibility of controlling the shape of the peaks. The former advantage is due to the double-focusing mass analyser requiring an ion beam with high energy for effective ion transmission and resolution. Such a beam is less affected by space-charge effects, which cause scattering of the ion beam in the quadrupole mass analyser. The latter advantage is useful in isotope ratio analysis. At low resolution it is possible to obtain flat - topped peaks. Using a flat topped peak the measured ion beam intensity is independent of the exact position at which the peak was measured, whereas using a quadrupole, with its rounded peaks, there will be some uncertainty on the position of the measurement. This means isotope ratio analysis is more accurate and reproducible with a double-focusing instrument. Jakubowski *et al.*[97] and Becker and Dietze[98] have reviewed the use of high resolution ICP - MS.

Although the new generation instruments are easier to use and less expensive they are still more complex and more expensive than quadrupole instruments. Furthermore, if high-resolution settings are to be used there will be a loss in sensitivity.

In recent years growing interest has focused on using post plasma reactions to alleviate polyatomic ions. These processes take advantage of differences in reactivities of analytes and interfering ions and for this to be analytically useful polyatomic ions

must be lost efficiently by collision induced dissociation, charge transfer or ion-molecule reactions relative to loss of analyte ions.

While the atmospheric Ar ICP is the most widely used ion source in plasma mass spectrometry other plasma sources have gained attention, the most notable being the microwave induced plasma (MIP). This was initially investigated by Douglas and co-workers[99, 100] and later by Caruso and co - workers using gas chromatography,[101, 102, 103, 104] pneumatic nebulisation[105, 106, 107, 108, 109, 110,] and electrothermal vaporisation[111] as sample introduction methods. An alternative to generation of the plasma at atmospheric pressure is to generate it at low pressure.

1.6: Aims of this study

The aim of this study was to investigate fundamental and applied aspects of ICP-MS to gain an improved understanding of the technique and improve on its analytical capabilities.

ICP-MS is plagued with polyatomic ions which limit the range of analytes that can be successfully analysed. Isobaric overlap can also lead to inaccurate calculations of fundamental properties of the plasma that rely on mass-spectral data. The principle aim of this study was to use a high-resolution instrument to allow unambiguous identification of mass spectral data for use in fundamental and practical studies. Dissociation temperatures can be used to eludicate the site of formation of polyatomic ions, and when these are formed in the plasma the dissociation temperatures can be used to determine the plasma temperature. However, such calculations rely on the measurement of polyatomic ion signals that may suffer from isobaric overlap with analyte signals. Using high resolution ICP-MS to obtain mass spectral data should result in the calculation of more reliable dissociation temperatures.

The attenuation of polyatomic ion signals using helium gas in a hexapole collision cell was investigated.

Materials deposited on the skimmer cone during analysis can re-volatilise and contribute to memory. The significance of this material deposited on the skimmer cone to memory effects was investigated.

Polyatomic ions associated with air entrainment into the plasma can be removed by operating the plasma at low pressure. However, the introduction of liquid samples into such a plasma is difficult to achieve so the feasibility of using a particle beam momentum separator was investigated.

In addition to using high resolution to provide more reliable mass spectral data, the resolution of analyte and polyatomic ion signals will make the speciation analysis of previously difficult to determine elements possible. Silicon and Phosphorus Speciation studies were performed using high resolution ICP-MS.

CHAPTER 2: THE ESTIMATION OF DISSOCIATION TEMPERATURES: An insight into the site of formation of polyatomic ions in ICP-MS

2.1: Introduction

The ICP is a highly efficient ion source that completely atomises samples allowing ultratrace analysis to be achieved. Ideally, only singly charged atomic ions would be observed so that spectral interferences would be few and easy to predict[112]. However, ICP-MS spectra consist of a host of species such as oxides, hydroxides and background species. These species can interfere with analysis by occurring at the same nominal mass as an analyte ion. The most troublesome spectroscopic interferences, due to the fact they are difficult to overcome, are those caused by polyatomic ions.

Polyatomic ions are formed from interactions between species in the plasma gas (e.g. Ar) and species in the sample matrix (e.g. Na, Cl, Ca), the solvent used (e.g. O, H, C and also N, Cl, S) or the atmosphere (O, N, C).

There are several different reaction mechanisms by which these molecular ions may arise:

1. Associative ionisation

$$Ar^{m*} + X \rightarrow ArX^{+} + e^{-} \quad \textbf{(2.1)}$$

Ar^{m*} = metastable excited argon atom

X = metal or non-metal atom

2. Association reaction of an ion and an argon atom

$$X^+ + Ar \rightarrow ArX^+ \quad (2.2)$$

3. Ionisation by electron impact of a neutral argon species

$$ArX + e^- \rightarrow ArX^+ + 2e^- \quad (2.3)$$

4. Association reaction of an argon ion with a metal or non - metal atom

$$Ar^+ + X \rightarrow ArX^+ \quad (2.4)$$

The exact origin of these ions is still unclear. They may possibly be formed in the plasma and not be fully dissociated[43, 113, 114, 115], they could be formed in the boundary layer[43, 113], or they could be formed in the interface region [32, 116]. The initial design of ICP - MS instruments used small apertures in the sample cones and ions were extracted from a cool layer which formed over the sampling cone, known as the boundary layer. In modern instruments larger orifices are used in the sampling cones and ions are extracted directly from the plasma, referred to as continuum sampling. In this method of sampling the higher gas flow through the sampler breaks through the boundary layer and sheath. The cool layers are still present, but they form along the inside edge of the sampling orifice so it is unlikely that formation of polyatomic ions in the boundary layer is the predominant process. It is also possible that polyatomic ions may arise due to reactions occurring in this interface region, between the sampler and skimmer.

Polyatomic ions interfere with analysis by causing an erroneously large signal at the m/z value of a particular analyte ion. This leads to an apparent enhancement of the analyte signal that severely limits the detection limit. While many methods have been employed to overcome polyatomic ion interferences (see section 1.5) an increased understanding of the formation mechanisms and site of formation of polyatomic ions is still of great interest for ICP - MS trace analysis.

Polyatomic ion formation processes, particularly those formed with non-metals such as ArH^+, ArO^+, ArN^+ and ArC^+, have been studied by several groups[117, 118, 119] owing to their interference in the determination of ^{39}K, ^{56}Fe, ^{54}Fe and ^{52}Cr, respectively. Sakata and Kawabata[119] found that the argon molecular ions are formed in the plasma due to a positive plasma potential induced by capacitive coupling with the load coil, and also behind the sampling cone where a secondary discharge may exist. This secondary discharge was thought to affect the formation of M^{2+} and MO^+ ions. This was attributed to an increase in the electron number density at the surface of the sampling cone. However, this secondary discharge has been shown to result from a large RF voltage swing in the plasma compared to the grounded interface, and that a reduction in the plasma potential greatly affected the formation of ArX^+ ions, but has little effect on M^{2+} and MO^+ ions. Becker *et al.*[120] investigated several metal argide ions and found that non-metal argide molecular ions were formed with higher intensities compared with metal argide ions.

Douglas and French[121] have shown that the interface region is not rich in ion-molecule chemistry so oxide formation is unlikely in this region. Lam and Horlick[51] have observed that the analyte/oxide ion ratio decreases with increasing distance of separation between the sampler and skimmer cones. This implies oxides are not formed in the interface region. Furthermore they found that the $ArNa^+$ signal increased as the sampler - skimmer separation was increased, suggesting that ArX^+ species are formed in the interface region.

Togashi *et al.*[122] studied molecular ionisation in the interface region. From their work they suggested that charge exchange between Ar^+ and neutral organic molecules could occur. So the possibility of neutral oxides being ionised in the interface exists.

Vaughan and Horlick[48] showed that the level of oxides depends on the sampler and skimmer orifices. They found that the oxides of La and Ho increased as the sampler orifice diameter decreased from 0.94 mm to 0.51 mm. These orifice diameters are larger than those used in the very first ICP-MS instruments that suffered from boundary sampling of ions from the plasma. However, their data indicates that a cool layer remains along the edges of the sampler and that sampling ions from this zone results in their conversion to oxide ions.

An unexpectedly high intensity of the H_2O^+ peak compared with the intensity of the OH^+ peak was observed by Van Heuzen and Nibbering[123]. They explained this observation by suggesting that a certain amount of water in the ICP is not completely decomposed. They went on to suggest that this water may undergo an ion/molecule reaction with an argon ion to form an argon hydride ion:

$$Ar^+ + H_2O \rightarrow ArH^+ + OH \quad \textbf{(2.5)}$$

Mermet *et al.*[124] showed that oxide levels were very reliant on the efficiency of energy transfer from the plasma to the sample and on sampling position. Tanner[125] determined plasma temperature from ion kinetic energies and concluded that oxides are predominantly formed in the ICP.

A collision induced reaction of neutral argon and an oxygen ion was suggested by Nonose *et al.*[117] to explain the formation of ArO^+, rather than an ionisation reaction of neutral ArO:

$$Ar + O^+ \rightarrow ArO^+ \quad \textbf{(2.6)}$$

Theoretical calculations of metal monoxide (MO) to element (M) ratios, (MO/M), assuming a Boltzmann equilibrium for MO in the ICP, was performed by

Shibata *et al.*[126] to eludicate the mechanism of oxide formation for the rare earth metals. They found experimental MO^+/M^+ ratios were in good agreement with theoretical MO/M ratios which indicated that oxide ion species in the plasma may be derived from undissociated MO.

One possible way to gain an insight into polyatomic ion formation is to study deviations from equilibrium dissociation temperatures. A single temperature in the ICP cannot be determined because the plasma is not in a state of local thermal equilibrium (LTE)[127]. Several statistical distribution functions exist, which are temperature dependent, and can be used to define temperature characteristics of the ICP. These distribution functions include the Maxwell, Boltzmann, and Saha distributions.

The Maxwell distribution can be used to ascertain the gas kinetic temperature (T_g) and the electron temperature (T_e). The population distribution of an excited state of a species, energy levels below the next ionisation potential of the species, is given by the Boltzmann distribution. This describes the excitation temperature (T_{exc}). The degree of ionisation in the ICP is given by the Saha distribution. The Saha distribution determines the ion-to-atom population ratio of a species as a function of the ionisation temperature (T_{ion}). If the plasma was in a state of LTE then $T_g = T_e = T_{exc} = T_{ion}$. However, this has been found not to be the case for an argon atmospheric ICP. Of all these various temperatures used to define the characteristics of the ICP, the dissociation of molecules (i.e. dissociation temperature) is most likely to be governed by T_g[112].

Several different approaches have been adopted to calculate T_g. Tanner[125] estimated gas kinetic plasma temperatures by measuring ion kinetic energies. The plasma temperature derived from the atomic ion kinetic energies was about 6800 K at low nebuliser flow and about 3300 K at high nebuliser flows. The temperatures derived from oxide kinetic energies was about 500 K. The temperature of the plasma can also be determined using emission data rather than mass spectral data. One possible emission temperature that can de determined is the rotational temperature (T_{rot}), which is related

to the vibrational-rotational excitation of molecules or radicals that are present in the ICP such as N_2^+ and OH. The rotational temperature is assumed to be similar to the gas kinetic temperature[128]. Measuring band spectra emitted by N_2^+, T_{rot} values of 5300 - 5500 K have been reported[129, 130], while values of 3200 - 3700 K[130, 131] have been reported using the OH band at 309 nm.

T_g can be determined by measuring the Doppler width. Human and Scott[132] made measurements of the Doppler width of several atomic lines emitted by the ICP. They reported T_g values of 4900 - 5400 K.

There are several different methods that can be used to determine the dissociation temperature within the plasma, all are based on the dissociation of a diatomic molecular ion (AB^+). The majority use the dissociation of metal oxides[112, 121, 126, 133,134, 135, 136]to calculate the temperature, although other diatomic molecules such as ArO^+[112, 137, 138] have been used.

One such method is based on Boltzmann plots. Early attempts at using such plots yielded temperatures of 21 000 K[133], 10 100 K[133] and temperatures in the range of 9000 - 11 500 K[135]. These temperatures are significantly higher than other reported ICP temperatures[129, 139]. Such high temperatures should yield much lower oxide levels than are actually observed. Douglas and French[133] initially took this as evidence that the oxide ion did not originate in the ICP. The high dissociation temperatures were thought to characterise metal oxides formed by ion molecule reactions in the sampling process. However, subsequent calculations showed this region is not rich in ion -molecule reactions and this is unlikely therefore to occur[121]. Longerich[135] showed that the dissociation temperature varied with operating conditions. Such behaviour would be expected with oxide ions formed in the plasma but not oxide ions formed in the interface by ion - molecule reactions. Shibata *et al.* [126] found T_g of 5000 K and Kubota *et al.*[136] found T_g of 6650 K. Kubota *et al's.* data differ from the earlier attempts for the

calculation of dissociation temperatures as they used the partition functions of the ions studied and did not approximate them as constants.

Houk and Praphairaksit[138] have recently pointed out four minor drawbacks of the above studies. Firstly they argue no correction has been made for mass bias. However, Longerich[135] did make such correction when making his calculations, although other workers have not made such corrections. Longerich[135] found that the change in the calculated temperatures on correction for mass bias were not significant compared with the errors contributed by noise in the data and uncertainties in the bond energies.

Secondly, the equations that describe the dissociation constant contain other temperature-dependent terms, such as partition functions. This can introduce, at the very least, scatter about the fitted line when Boltzmann plots are used to calculate the dissociation temperature.

Thirdly, they argue some of the calculations wrongly use the bond dissociation energy (D_0) of the neutral (MO) species and not the ion (MO^+). This is not strictly true, Douglas and French[133], when using Blotzmann plots to determine the dissociation temperature, plotted MO^+/M^+ ratios vs bond strength of the MO^+ ions. Nonose *et al.*[117] derived bond dissociation energies for ArX^+ species to make their calculations and Longerich[135] also used the bond dissociation energies of the monopositive ions of the monoxides and not those of the neutral species when making his calculations.

Fourthly Houk and Praphairaksit argue that some of the studies unfairly compare mass spectral and optical temperature measurements. The latter measurements are made on free-flowing ICPs, not one that is being sampled for MS.

In addition to these drawbacks two further weaknesses, which are addressed in this work, exist. Firstly the use of a quadrupole mass analyser, which only has unit mass resolution, can lead to erroneous signal measurements. The calculations of the dissociation temperature rely on the measurement of the ion signal ratio B^+/AB^+ from the mass spectrum. Inaccuracies in this measurement can arise due to other ions

occurring at the same m/z values of interest. For instance if the dissociation temperature of ArO^+ is to be determined the ion signal for ArO^+ at m/z 56 has to be measured, $^{56}Fe^+$ (present from the reagents used) also occurs at this mass. The quadrupole mass analyser, with unit mass resolution, cannot resolve these species. This may lead to an erroneous signal measurement of the ArO^+ signal and therefore an inaccurate measurement of the O^+/ ArO^+ ratio and ultimately an inaccurate dissociation temperature being calculated. In this study a high resolution instrument was used to allow separation of ionic species of interest from interfering species allowing unambiguous identification and quantification and hence the calculation of more accurate dissociation temperature measurements.

Secondly, the sample introduction system employed can lead to inaccurate determination of the density of the species in the plasma which are needed for the calculation of the dissociation temperatures. This will be discussed later.

2.2: Theory

This method for the determination of the dissociation temperature was suggested by Houk and Niu[112] and is based on the theory that the dissociation of a diatomic molecule at a gas kinetic temperature is governed by an equation similar to the Saha equation[112].

The main reaction for the dissociation of a polyatomic ion AB^+ is

$$AB^+ \leftrightarrow A + B^+ \quad (2.7)$$

and the equilibrium constant is

$$K_d = n_A\, n_{B+} / n_{AB+} \quad (2.8)$$

(n = number of atoms)

The equilibrium constant may be written in terms of the partition functions[140]

$$\frac{n_A\, n_{B^+}}{n_{AB^+}} = \frac{q^e_A\, q^t_A\, q^e_{B^+}\, q^t_{B^+}}{q^e_{AB^+}\, q^t_{AB^+}\, q^v_{AB^+}\, q^r_{AB^+}} e^{-D_0/KT} \quad (2.9)$$

Where

q^t = translational partition function

q^e = electronic partition function

q^r = rotational partition function

q^v = vibrational partition function

D_0 = dissociation energy of the molecule

k= Boltzmann constant

T = gas kinetic temperature of plasma

Substitution of the appropriate equations for the partition functions, which can be obtained from a textbook on physical chemistry[141] and simplification leads to the following equation:

$$\frac{N_A N_{B^+}}{N_{AB^+}} = \left[\frac{q_A^e q_{B^+}^e}{g_{AB^+}}\right]\left[\frac{2\pi KT}{h^2}\right]^{3/2}\left[\frac{m_A m_{B^+}}{m_{AB^+}}\right]^{3/2}\left[\frac{hcB}{KT}\right]\left[1 - e^{-hc\omega/KT}\right]e^{-D_0/KT} \quad (2.10)$$

Where

N = number density, atoms per m^3

T = gas kinetic temperature, K

D_0 = bond dissociation energy of AB^+, J

ω = vibrational constant, m^{-1}

B = rotational constant, m^{-1}

h = Planck constant, 6.626 08 x 10^{-34} Js

k = Boltzmann constant, 1.380 66x10^{-23} JK^{-1}

c = speed of light, 2.997 024 58 x 10^8 ms^{-1}

m = mass, Kg

g = statistical weight of the ground electronic state of AB^+

Other workers have used a logarithmic form of this equation [112, 117, 126, 138].

Temperature measurements using this equation may be inaccurate due to the use of partition function values, which are, by definition, temperature dependent. However, in the case of the ions and neutral atoms the electronic partition function can be calculated using equation 2.11, with the appropriate constants[142].

$$B(T) = a + b\,(T/10^3) + c(T/10^3)^2 + d(T/10^3)^3 + e(T/10^3)^4 + f(T/10^3)^5 \quad (2.11)$$

The calculation of the partition functions did not rely on a single temperature value as a spreadsheet was set up, so the value of the partition function for a particular species changed as the temperature was altered.

The statistical weight of the ground electronic state, g, of the molecule is given by $g = 2J + 1$ [143] and can be calculated from the term symbol which is composed of several different quantum numbers that describe the electronic state of an atom or molecule. The term symbol for the ground electronic state of CO^+ is $^2\Sigma^+$ [144]. The letter Σ, is the total orbital angular momentum quantum number L which has the values 0, 1, 2, ... for Σ, π, Δ.... The left superscript (i.e. 2) is the multiplicity, which has the value $2S + 1$, where S is the total spin angular momentum quantum number. The total angular momentum quantum number, J, has the value $S + L$. Therefore for CO^+:

$2S + 1 = 2 \quad S = 1/2$

$L = O$

$J = 0 + 1/2$

$J = 1/2$

$g = (2 \times 1/2) + 1$

$\underline{g = 2}$

The statistical weight of the ground electronic state of ArC^+, ArO^+ and C_2^+ were calculated in the same way. Table 2.1 shows the values of g calculated and spectroscopic data taken from the literature in order to calculate T_g for the species ArO^+, ArC^+, CO^+ and C_2^+. The specific dissociation equilibrium this data applies to is also shown in Table 2.1. Two argide polyatomic ions and two non-argide polyatomic ions were selected for study. These species were also selected as they cover a range of bond dissociation energies from weakly bound to strongly bound ions.

From the experimental count rates obtained, an experimental value for $K_d(AB^+)$ was determined by measuring the signals due to the ions B^+ and AB^+ to give the B^+/AB^+ ratio. This was then multiplied by the amount of neutral product A in the ICP, which can be calculated from the solvent introduced into the plasma.

Table 2.1: Spectroscopic constants (Data applied to a temperature of 5000.K)

Species	Dissociation Equilibrium	B (cm^{-1})	ω (cm^{-1})	D_0 (eV)	g	Reference
ArC^+	$ArC^+ \leftrightarrow Ar + C^+$	0.41	304	0.992	4	145
ArO^+	$ArO^+ \leftrightarrow Ar + O^+$	0.2804	289.197	0.416	4	117, 146
CO^+	$CO^+ \leftrightarrow C^+ + O$	1.9772	2214.24	8.338	2	144
C_2^+	$C_2^+ \leftrightarrow C + C^+$	1.659	1350	5.32	4	144

Table 2.2: ICP-MS operating parameters for the introduction of propionic acid/water vapour

Forward Power (W)	1280 or 700 (with and without M- Plasmascreen)
Coolant (L min^{-1})	14
Auxiliary (L min^{-1})	0.7
Nebuliser (L min^{-1})	$0 \rightarrow 0.9$
Resolution	6000
Detection mode	Multiplier and Faraday
Dwell time (ms)	50
Peak width	10
Points per peak	20
Number of scans	3
Number of sweeps	1

2.3: Experimental

2.3.1: Instrumentation

Experiments were conducted using a VG Elemental Axiom high resolution ICP-MS instrument (Thermoelemental, Winsford, Cheshire, UK). Instrumental conditions are shown in Table 2.2.

2.3.2: Controlled introduction of solvent

A 17.7 %, by weight, propionic acid - water solution was prepared by adding 35.4 g of propionic acid (Fluka, Gillingham, Dorset, UK) to 164.6 g of deionised water (18 MΩ) from a milli-Q analytical grade water purification system (Millipore, Bedford, MA, USA). This gives an azeotropic mixture[31], so the composition of the vapour introduced into the ICP is the same as the composition of the liquid i.e. 17.7 % propionic acid and 82.3 % water.

Vapour was introduced directly into the back of the ICP torch using a Dreschel bottle (Figure 2.1). Argon gas in the range of 0.1 - 0.9 $lmin^{-1}$, controlled by a mass flow controller, was introduced through the Dreschel bottle. The argon gas exiting the Dreschel bottle was made up with another flow of argon gas, controlled by the mass flow controller of the nebuliser flow of the ICP-MS instrument, to give a total flow rate of 0.9 l min^{-1} entering the ICP. The water/propionic mixture in the Dreschel bottle was kept in a water bath at 16^0C in order to ensure a constant vapour pressure. This temperature was lower than room temperature to avoid condensation of the vapour in the gas lines but sufficiently high to give good signals in the mass spectrum. A vial containing a small droplet of Hg and covered in PTFE tape was attached to the side arm of the frit to facilitate tuning the instrument and to perform cross - calibration of the instrument. Adjusting the gas flow through the Dreschel bottle, which had been previously calibrated (Table 2.3) altered the amount of vapour entering the plasma. The detector was set up to monitor the ions shown in Table 2.4.

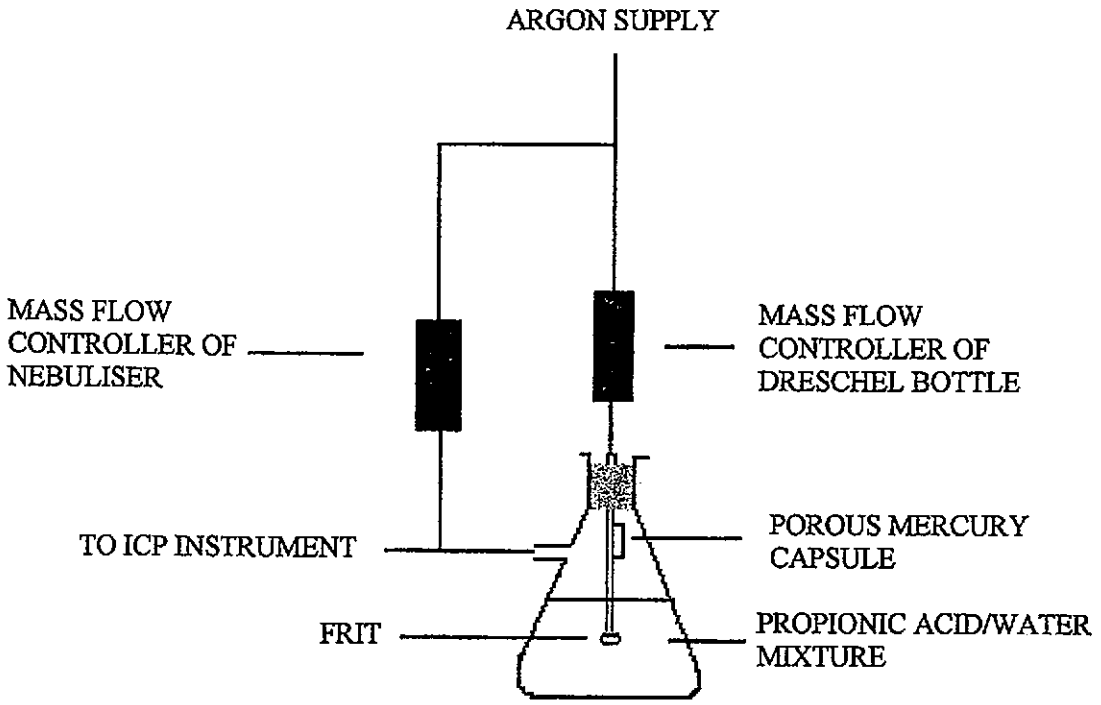

Figure 2.1: Schematic of Dreschel bottle used to introduce propionic acid/water vapour into ICP-MS

Table 2.3: Calibration of Dreschel bottle at 16^0C.

Argon flow rate ($Lmin^{-1}$)	Vapour ($g\ h^{-1}$)			Mean vapour ($g\ h^{-1}$)
0.1	0.14	0.20	0.18	0.17
0.2	0.34	0.36	0.38	0.36
0.3	0.41	0.47	0.52	0.47
0.4	0.59	0.54	0.56	0.56
0.5	0.62	0.67	0.64	0.64
0.6	0.69	0.71	0.74	0.71
0.7	0.82	0.76	0.79	0.79
0.8	0.91	0.85	0.92	0.89
0.9	1.02	1.08	1.09	1.06

Table 2.4: Isotopes studied during the introduction of propionic acid/water vapour

Species	Mass	Abundance (%)
C^+	12	98.9
O^+	16	99.8
C_2^+	24	97.8
CO^+	28	98.7
ArC^+	52	98.5
ArO^+	56	99.4

Four different plasma conditions were studied: 1280 W and 700 W with the M-plasma screen device(TJA Solutions, Winsford, Cheshire, UK) and 1280 W and 700 W without the M-Plasma device. The M-Plasma device is a Pt cylinder positioned over the torch shielding it from the load coil.

2.3.2 Procedure

Taking ArC^+ as an example, the dissociation of the polyatomic ion is:

$$ArC^+ \leftrightarrow C^+ + Ar \quad K_d(ArC^+) = n_{C+}n_{Ar}/n_{ArC+}$$

the experimental K_d value was obtained by measuring the signals due to C^+ and ArC^+, to give the C^+/ArC^+ ratio. This ratio was corrected for isotopic abundance and then multiplied by the concentration of argon assumed to be in the plasma calculated by the ideal gas law as outlined below.

$PV = nRT$

P = pressure (atmospheric pressure, 1×10^5 Pa)

n = moles

R = universal gas constant (8.314 Pa m^3 K^{-1} mol^{-1})

T = temperature

Assuming T = 5000 K

$n/V = 1 \times 10^5$ Pa /(8.314 Pa m^3 K^{-1} mol^{-1} x 5000 K)

$= 2.4$ M^3 mol^{-1}

number of atoms per $m^3 = 2.4$ m^3 mol^{-1} x 6.022×10^{23} mol^{-1}

$= \underline{1.45 \times 10^{24}\ m^{-3}}$

The density of argon calculated is itself temperature dependent. Therefore, as with the partition functions calculated, the density of argon assumed to be in the plasma was not reliant on a single temperature and altered as the temperature was changed in the spreadsheet.

Species such as ArO^+ and ArC^+ are thought to form in the interface as well as the ICP. Therefore another K_d value was calculated using the argon assumed to be in the interface using equation 2.12.

$$n_{x(interface)} = 0.161 n_{x(plasma)} (D_0/X^2) \quad (2.12)$$

$n_{x(interface)}$ = the density of species x in the interface

$n_{x(plasma)}$ = the density of species x in the plasma

D_0 = the sampling diameter

X = the position downstream from the sampling orifice

For the CO^+ ion the fundamental data apply to the dissociation equilibrium:

$$CO^+ \leftrightarrow C^+ + O$$

Therefore the ionic ratio C^+/CO^+ was determined experimentally and this was then multiplied by the concentration of oxygen added to the plasma, from the Dreschel bottle, which was calculated as follows:

At a Dreschel flow rate of 0.1 L min^{-1} the amount of vapour produced, determined experimentally, was 0.17 g h^{-1}.

The mixture is azeotropic ∴ composition of liquid = composition of vapour

17.7 % of the vapour is propionic acid.

Propionic acid vapour = 0.177 x 0.17 g h^{-1}

= 0.03009 g h^{-1} or 8.358 x 10^{-6} g s^{-1}

Total flow of argon entering plasma is 0.9 l min^{-1} or 15 cm^3 s^{-1}

Mass of propionic acid per ml of Ar entering plasma = 8.358 x 10^{-6} g s^{-1}/15 cm^3 s^{-1}

= 5.572 x 10^{-7} g cm^{-3}

Number of mol of propionic acid = 5.572 x 10^{-7} g cm^{-3}/74 g mol^{-1}

= 7.53 x 10^{-9} mol ml^{-1}

Number of molecules of propionic acid = 7.53 x 10^{-9} mol cm^{-3} x 6.022 x10^{23} mol^{-1}

= 4.535 x 10^{15} molecules cm^{-3}

The density of oxygen atoms is therefore 4.535 x 10^{15} cm^{-3}x2x1000000 = 9.07 x10^{21} atoms m^{-3}

Oxygen will also originate from the water.

82.3 % of the vapour is water.

Water vapour = 0.823 x 0.17 g h^{-1}

= 0.1399g h^{-1} or 3.886 x 10^{-5} g s^{-1}

Total flow of argon entering plasma is 0.9 l min^{-1} or 15 cm^3 s^{-1}

Mass of water per ml of Ar entering plasma = 3.886 x 10^{-6} g s^{-1}/15 cm^3 s^{-1}

= 2.5909 x 10^{-6} g cm^{-3}

Number of mols of water = 2.5909 x 10^{-6} g cm^{-3}/18 g mol^{-1}

= 1.439 x 10^{-7} mol cm^{-3}

Number of molecules of water = 1.439 x 10^{-7} mol cm^{-3} x 6.022 x10^{23} mol^{-1}

= 8.668 x 10^{16} cm^{-3}

The density of oxygen atoms is therefore 8.668 x 10^{16} cm^{-3} x 1000000 = 8.67 x10^{22} atoms m^{-3}

The total concentration of oxygen entering the plasma from the Dreschel bottle is therefore:

8.67 x10^{22} m^{-3} + 9.07 x10^{21} m^{-3} = 9.58 x 10^{22} atoms m^{-3}

To calculate the dissociation temperature using the C_2^+ polyatomic ion, the C^+/C_2^+ ratio was multiplied by the density of C added to the plasma, this can be calculated in a similar way to the density of oxygen originating from the propionic acid.

As the gas enters the plasma the increase in temperature from 289 K (water bath temperature) to the temperature of the plasma causes the vapour to expand, and therefore the density of vapour is less. The ratio 289 K/ T_g takes account of the temperature change. As with the density of argon and the partition functions, the density of carbon and oxygen were not reliant on a single temperature and are calculated explicitly as T_g is altered in the spreadsheet.

2.3.3: Mass bias correction

As stated in the introduction the ionic ratios measured must be corrected for mass bias.

The signals for Li, Mg, K, Ti, Cr and Fe were determined 10 times at a resolution of 6000 for a 50 $\mu g\ l^{-1}$ solution at 1280 W and a 100 $\mu g\ l^{-1}$ solution at 700 W using the instrumental conditions in Table 2.5.

Mass response curves were constructed (Figure 2.2) at each of the four plasma conditions studied. The ion signals measured were corrected for isotope abundance.

Figure 2.2 shows the mass response of the instrument can be modelled with polynomial equations. The measured ratios were corrected for mass bias using these curves.

Once an experimental value of K_d had been determined, as described above, it was compared to the theoretical K_d value, calculated from equation 2.10. Using a spreadsheet, the value for the gas kinetic temperature was systematically varied until the theoretical K_d value matched the experimental K_d value. As stated varying this temperature also varied the values of the partition functions and the density of carbon, argon and oxygen in the plasma. The temperature determined by this procedure was assumed to be the equilibrium dissociation temperature of the species.

2.4: Results and Discussion

2.4.1: The accurate measurement of the ionic ratio and the density of the neutral species

One draw back to this method is that for ions such as ArO^+ and ArC^+, which are weakly bound, a small change in the measured ratio results in a large change in the dissociation temperature calculated[147]. Slight changes in the measured ratio for strongly bound ions such as CO^+ do not result in large changes in the calculated dissociation temperature. The presence of a significant concentration of another ion at the same

Table 2.5: Instrumental conditions used for mass bias determination

Forward power (W)	1280 and 700 (with and without M-Plasmascreen)
Coolant (L min^{-1})	14
Auxiliary (L min^{-1})	0.7
Nebuliser (L min^{-1})	0.85
Torch	Fassel type
Spray chambers	Cyclone connected to impact bead at 5 ^{0}C
Resolution	6000
Detection	Multiplier
Dwell time (ms)	50
Peak width	10
Points per peak	20

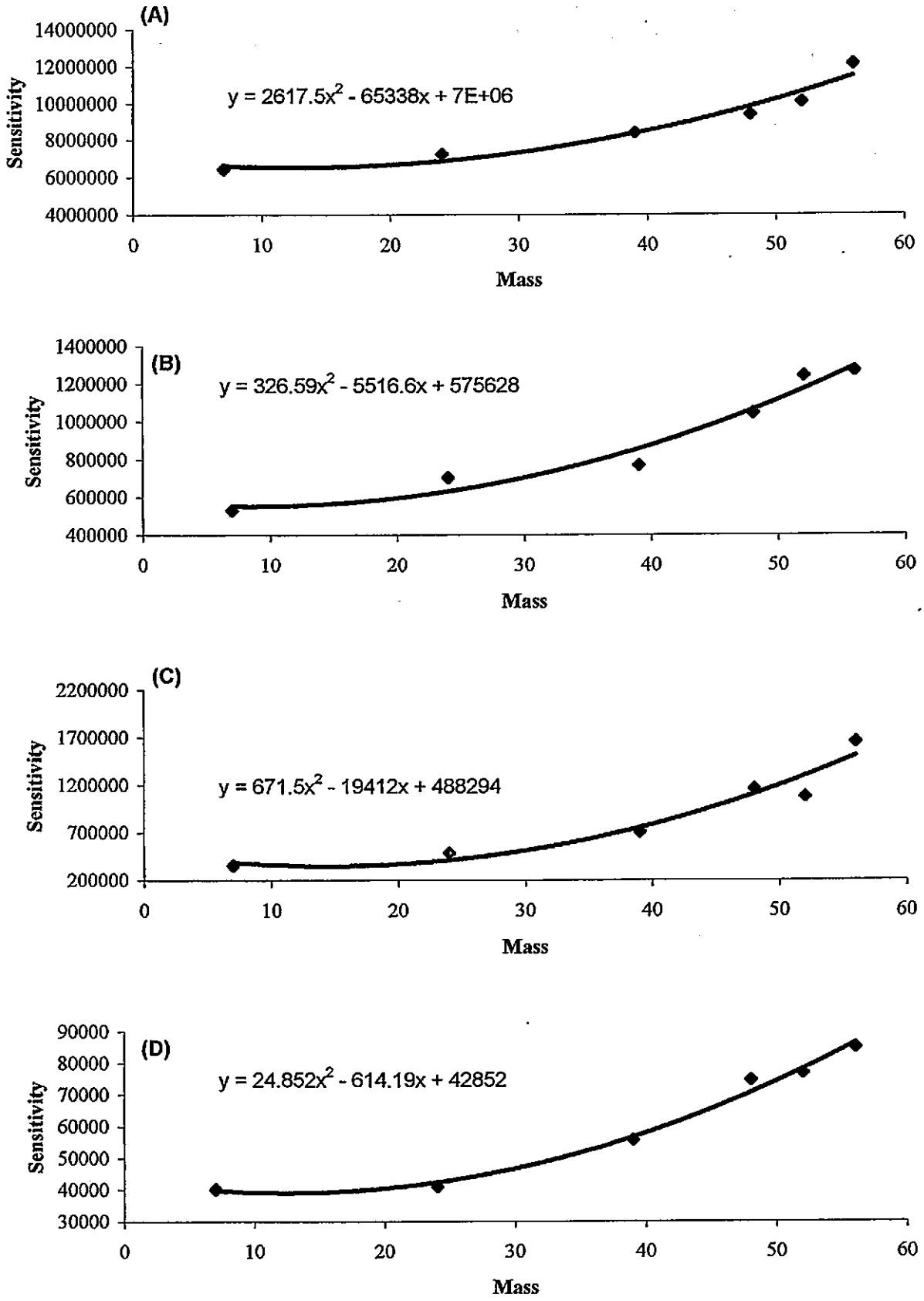

Figure 2.2: Mass response curves: (A) 1280 W with the M-plasmascreen; (B) 1280 W without the M-plasmascreen; (C) 700 W with the M-Plasmascreen and (D) 700 W without the plasmascreen

nominal mass as one of the ionic signals will result in an inaccurate ionic ratio (B^+/AB^+) being determined for a strongly bound ion and hence lead to an inaccurate temperature being calculated. It is therefore essential to make the correct measurement of the ion ratios and hence make accurate measurements of the ion signals, this is particularly important for ions such as ArO^+.

The significance of making accurate measurement of the ion signals is exhibited in Figures 2.3 - 2.6. These spectra clearly show that the various polyatomic ion signals that were measured in order to calculate the temperature suffered from isobaric interferences from the elements present in the reagents used. These contributions are shown in Figure 2.3 - 2.6, where the contribution of $^{56}Fe^+$, $^{52}Cr^+$, $^{24}Mg^+$ and $^{28}Si^+$ to the ion signals of ArO^+, ArC^+, C_2^+ and CO^+ can clearly be seen. The CO^+ ion also suffers from an interference from $^{28}N_2^+$ which cannot be seen in Figure 2.6 as the signal is slightly lower than that needed to be recorded by the Faraday detector. If a quadrupole based instrument had been used for this study then the recorded ArO^+, ArC^+, C_2^+ and CO^+ signals in this case would be wrong and hence the dissociation temperatures calculated would be inaccurate.

Samples are commonly introduced into the ICP by the aspiration of aqueous samples using a nebuliser to produce an aerosol consisting of a mixture of gases, wet droplets, particles and solvent vapour. Cool vapour clouds surrounding large wet droplets have been reported[125, 148, 149]. Tanner [125] reported that MO^+ ions have slightly lower kinetic energy than atomic ions of similar m/z values. This was attributed to cooling of species in clouds surrounding large water droplets. The introduction of vapour directly into the ICP via the Dreschel bottle avoided encountering such problems, which would yield inaccurate temperatures. Similarly for this reason Houk and Praphairakist [138]desolvated the aerosol when making their measurements.

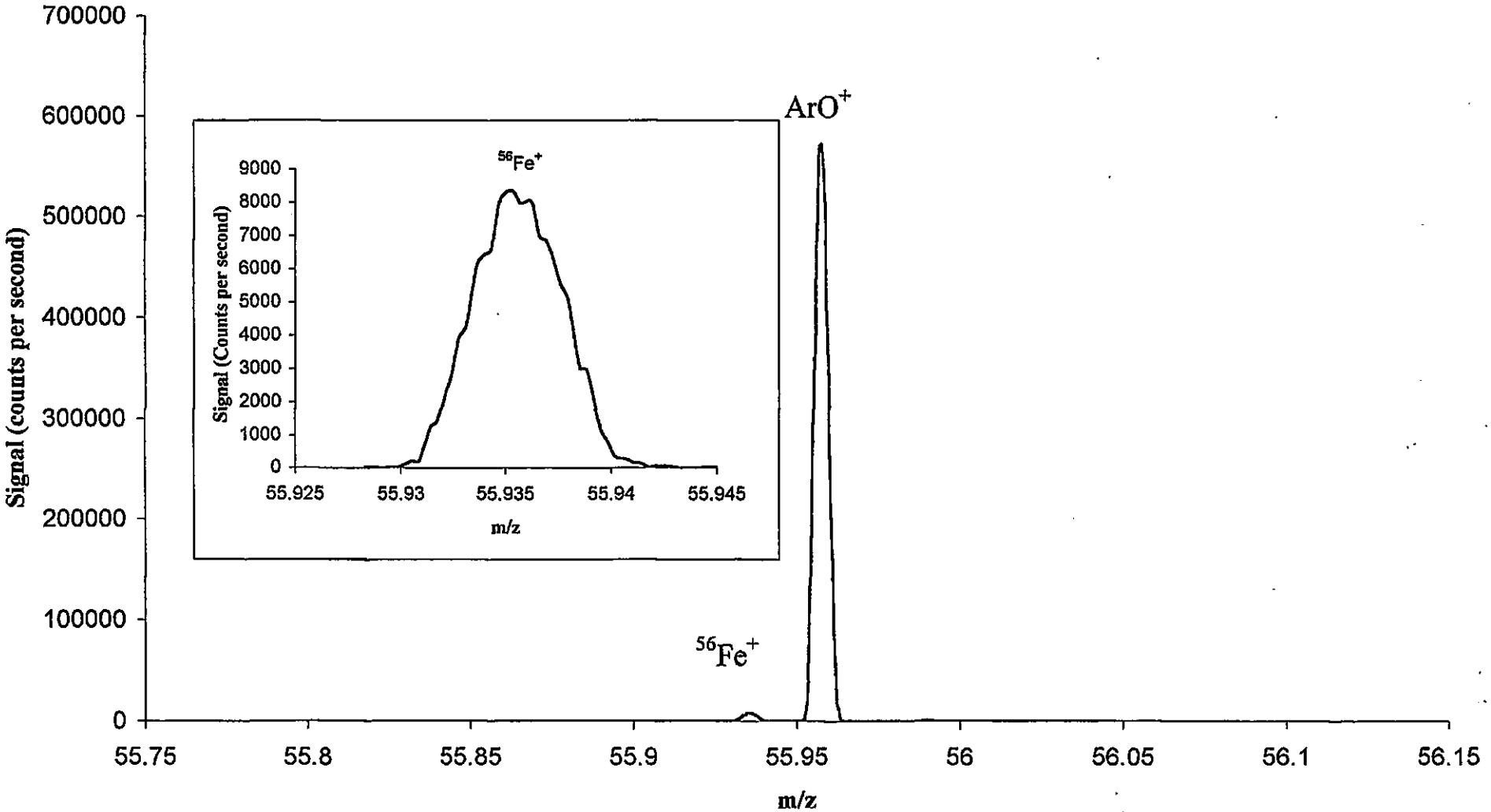

Figure 2.3: Mass spectrum at m/z 56 acquired at 1280 W with the plasmascreen and a vapour loading of 1.06g/h

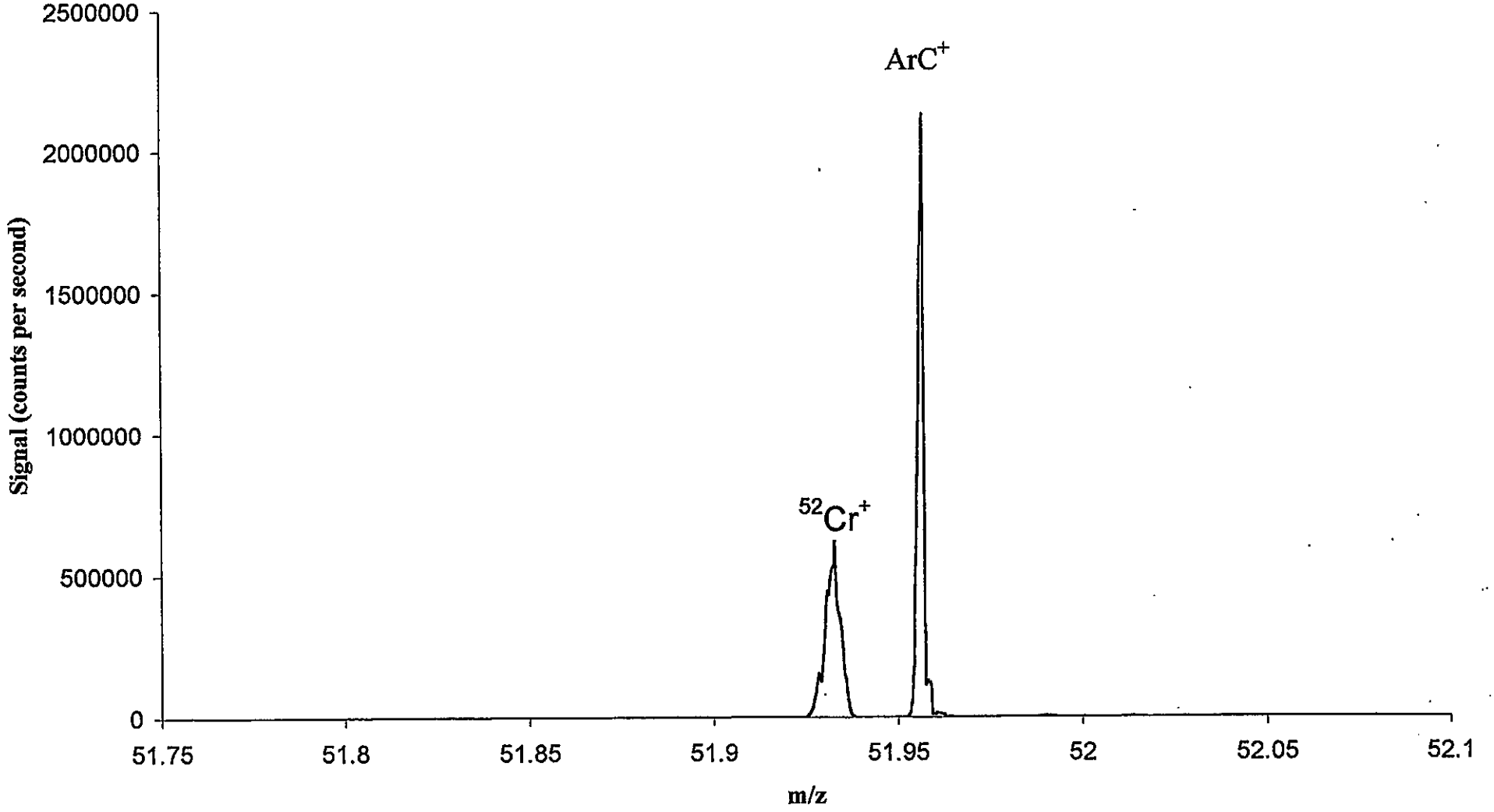

Figure 2.4: Mass spectrum at m/z 52 aqcuired at 1280 W with the plasmascreen and a vapour loading of 1.06 g/h

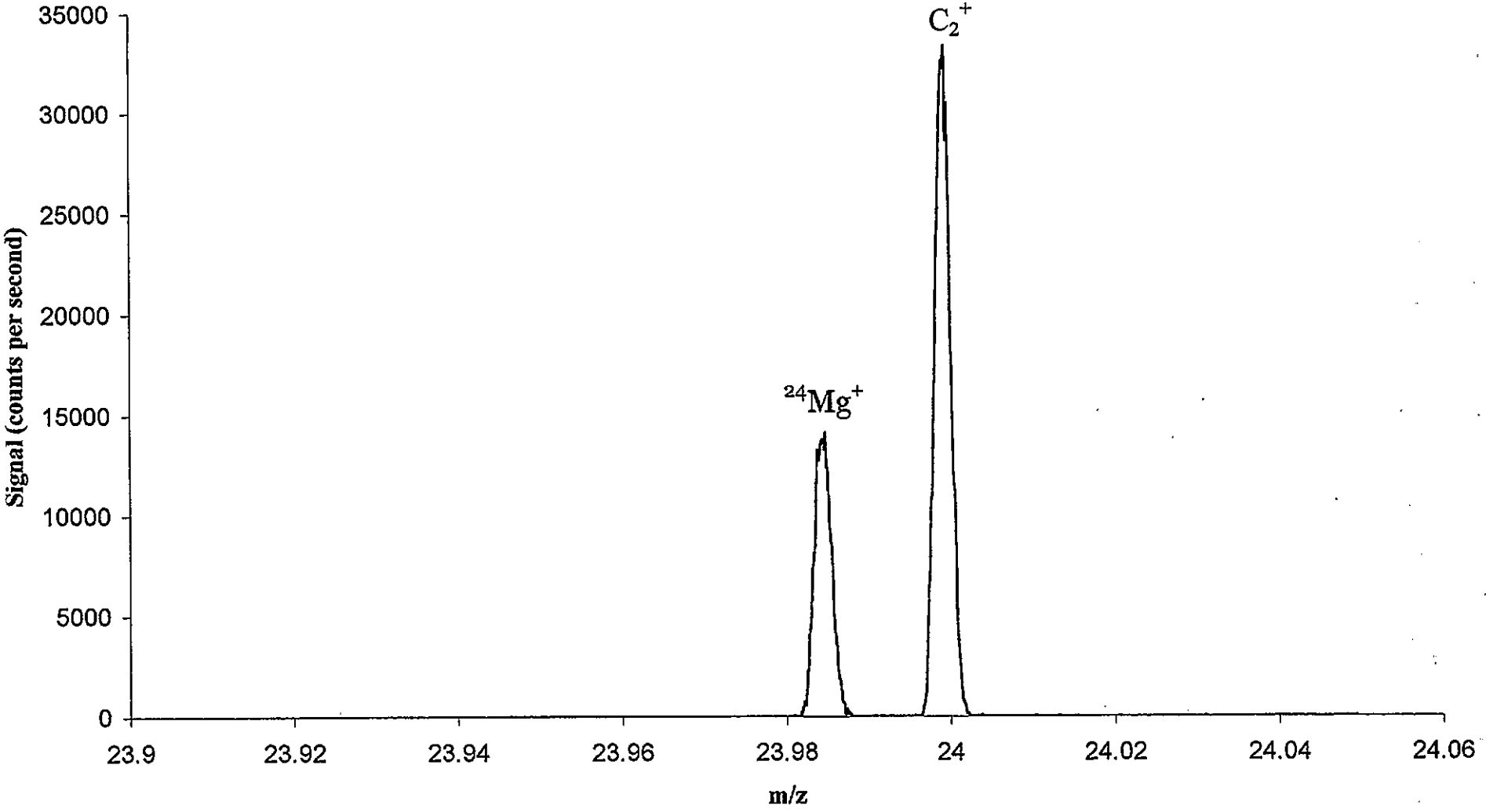

Figure 2.5: Mass spectrum at m/z 24 acquired at 1280 W with the plasmascreen and at a vapour loading of 1.06 g/h

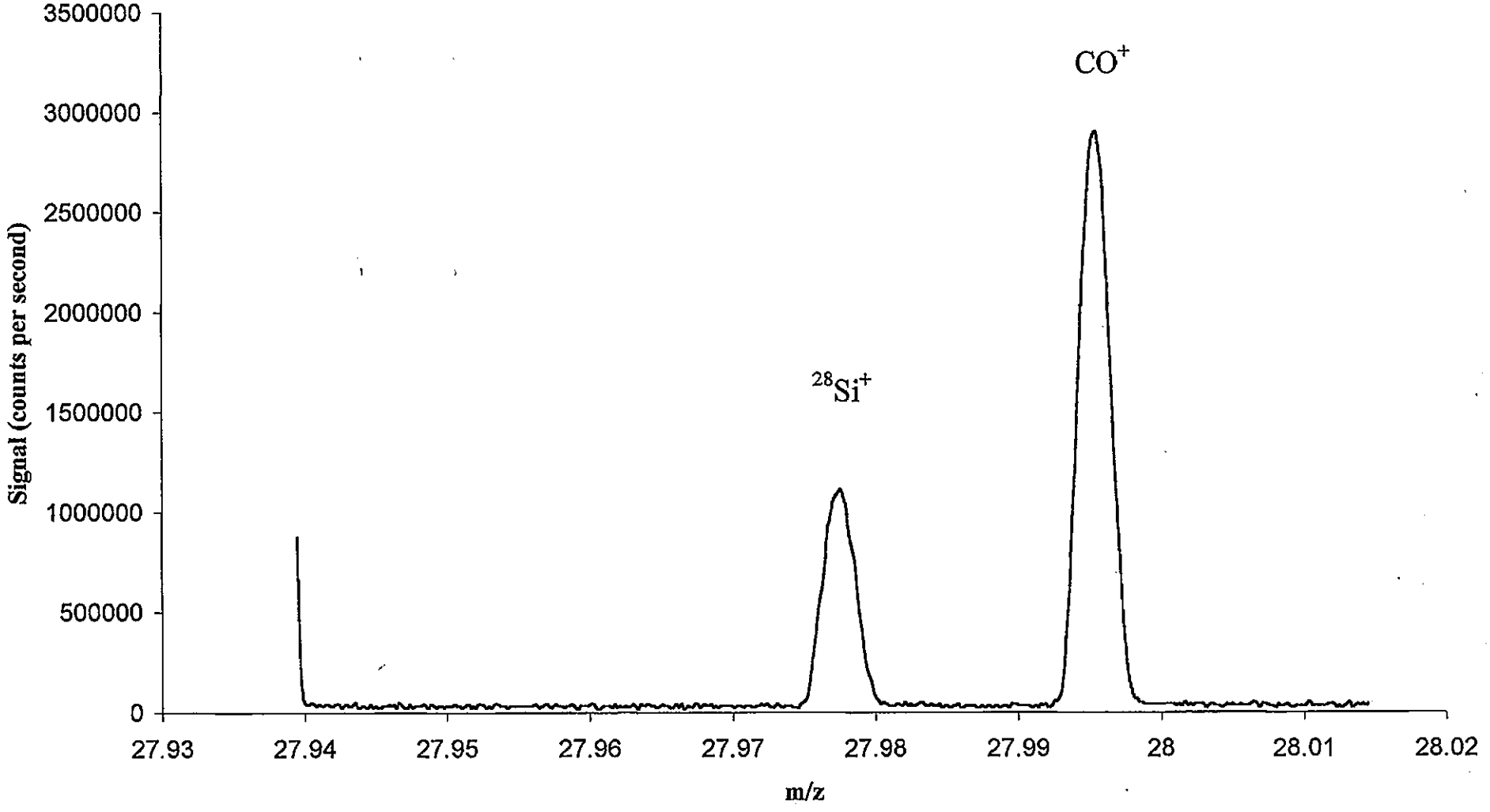

Figure 2.6: Mass spectrum at m/z 28 acquired at 1280 W with the plasmascreen at a vapour loading of 1.06 g/h and recorded using the Faraday detector

The determination of the dissociation temperature, for example for CO^+ and C_2^+, requires that the number density of the neutral species (i.e. O and C) present in the plasma be known. If a sample is introduced by nebulisation (as in the case of previous work) then an estimation of the nebuliser efficiency must be made if the densities of these species are to be calculated. Introducing vapour directly into the ICP using the Dreschel bottle avoided this problem because the vapour loading was determined experimentally. Hence more reliable calculations of the density of the species can be made and ultimately more reliable dissociation temperatures are made.

2.4.2: Dissociation temperatures calculated assuming equilibrium in the plasma

Table 2.6 summaries the dissociation temperatures calculated on the assumption of equilibrium in the plasma. It can be seen that the dissociation temperatures calculated for ArO^+ at 1280 W with no plasmascreen, i.e. hot plasma conditions, are significantly lower than those calculated for the other three species. In order for the ICP to be in local thermodynamic equilibrium all the dissociation temperatures of all the species must be equal. The fact that they are not could be an indication that the plasma is not in local thermodynamic equilibrium. Using the strongly bound ions C_2^+ and CO^+ as the thermometric probes, at 1280 W, the temperature of the plasma would be between 5000 - 7500 K. These temperatures are similar to the temperature expected in the plasma (5000 - 10 000 K)[139]. Using these strongly bound ions thus gives a good indication of the plasma temperature making them ideal thermometric probes. Using the weakly bound ion ArO^+ as the thermometric probe the temperature of the plasma at 1280 W would lie between 1800 - 3300 K. These temperatures are lower than would be expected for the hot plasma. The calculation of the dissociation temperatures is based on the assumption of local thermal equilibrium prevailing in the plasma so the low temperatures calculated for ArO^+ may indicate a deviation from local thermal

Table 2.6: Dissociation temperatures calculated for the four polyatomic ions assuming equilibrium in the plasma

Species	The Dissociation Temperatures calculated (K) for vapour loading between 0.17 - 1.06 (g h^{-1})			
	1280 W (no plasmascreen)	1280 W (plasmascreen)	700 W (no plasmascreen)	700 W (plasmascreen)
ArO^+	2000 - 3270	1807 - 2312	2470 - 4530	7480 -10800
ArC^+	3920 - 6970	2585 - 5275	4530 - 6940	3460 - 4625
C_2^+	6143 - 6658	5288 - 6625	4732 - 5050	4882 - 5281
CO^+	5871 - 7370	5754 - 7102	5118 - 5578	5028 - 5520

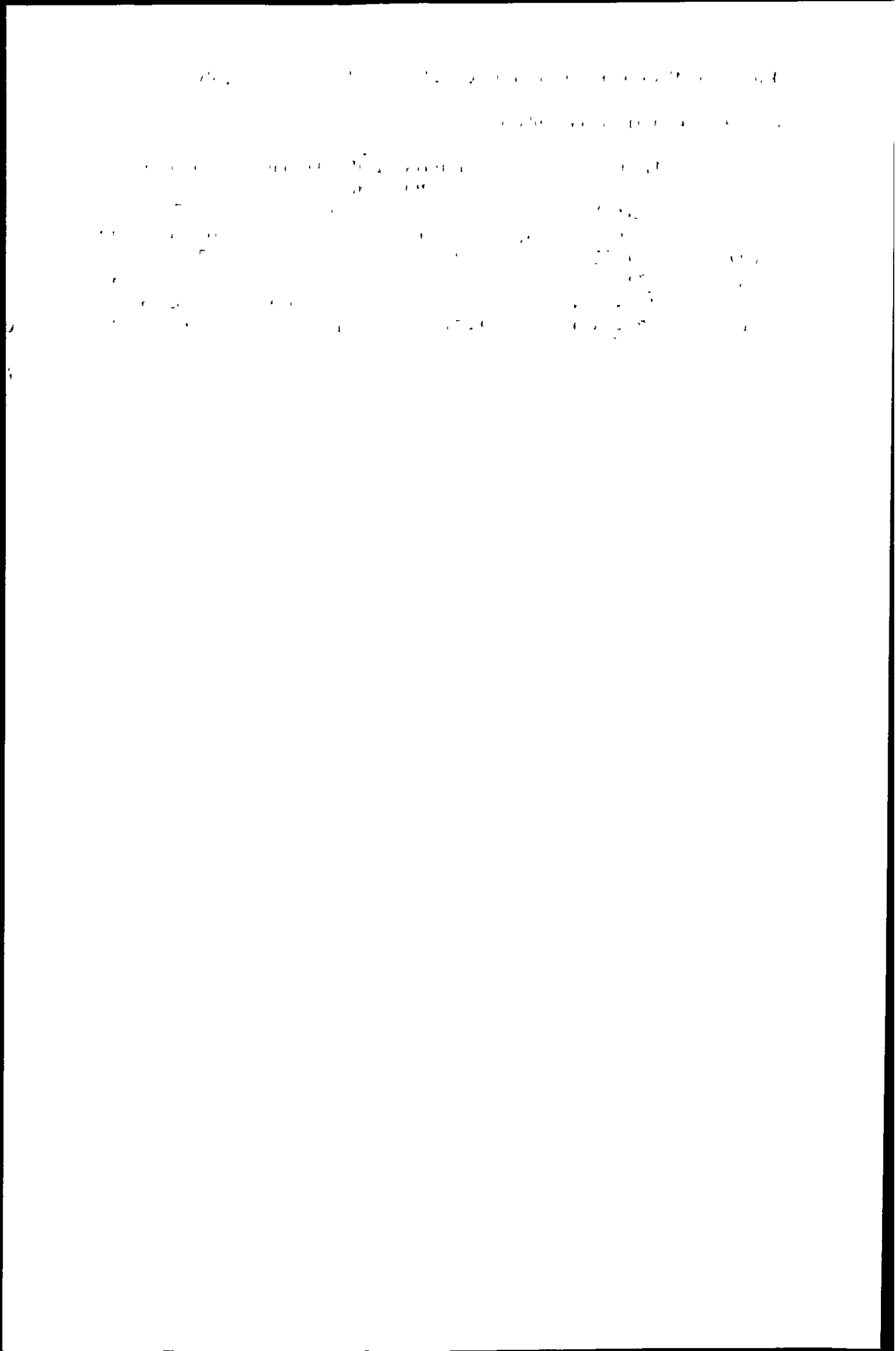

equilibrium. However, it is more likely that this deviation from an expected temperature of the plasma indicates that the site of the dissociation equilibrium of ArO^+ does not occur in the hot part of the plasma. Thus ArO^+ is formed elsewhere in the ICP-MS, i.e. in the interface region, where local thermal equilibrium does not prevail. The dissociation temperatures calculated for ArC^+ at 1280 W with no plasmascreen were between 3920 K, which is slightly lower than would be expected for the plasma, and 6970 K which is typical for the hot plasma. This indicates that the ArC^+ dissociation equilibrium lies between the hot and cooler regions of the plasma. This indicates ArC^+ is probably formed in the plasma and also in the interface regions of the ICP-MS in the same way as ArO^+.

2.4.2.1: The effect of the plasmascreen on the dissociation temperatures

Under normal operation of the Axiom it is equipped with a grounded Pt ring placed in between the load coil and the ICP torch (the M-plasmascreen device). The capacitive decoupling of both components leads to a considerable reduction of the plasma potential. A reduction in the plasma potential causes a reduction in the energy distribution of the extracted ions. Thus the extracted ions become easier to focus and the ion transmission efficiency and, hence, the signal intensity increases.

Table 2.6 shows that the dissociation temperatures calculated at 1280 W with the plasmascreen are slightly lower than those calculated when the plasmascreen is absent. The use of the plasmascreen reduces the plasma potential removing some of the energy within the plasma. Thus with less energy in the plasma the temperature would be expected to be lower. However, these differences are probably insignificant due to the uncertainties in the individual temperature measurements, this is particularly true for the weakly bound ions.

2.4.2.2: The effect of power on the dissociation temperatures

Table 2.6 shows that for the species C_2^+, and CO^+ the dissociation temperatures calculated at 700 W with no plasmascreen are slightly lower than those calculated at 1280 W with no plasmascreen. It would be expected that at a higher power more energy would enter the plasma and so the temperature within the plasma would increase. This increase in temperature at the higher power was also observed for CO^+ and C_2^+ when the plasmascreen was used. A decrease in the temperature reflects a decrease in the B^+/AB^+ ratio and therefore an increase in AB^+ relative to B^+. This is consistent with less power being available to dissociate CO^+ and C_2^+ and reflects that their site of formation is in the plasma. ArC^+ showed no significant difference in the range of dissociation temperatures calculated at 1280 W without the plasmascreen and those calculated at 700 W without the plasmascreen. This was also true for the range of dissociation temperatures calculated for ArC^+ at 1280 W and 700 W when the plasmascreen was used. However, the uncertainties in the individual temperature measurements probably mean these findings are not significant.

The dissociation temperatures calculated for ArO^+ at 700 W and those calculated at 1280 W without the plasmascreen are not significantly different. However, the dissociation temperatures calculated at 700 W with the plasmascreen i.e. cool plasma conditions do show a significant increase over those calculated at 1280 W with the plasmascreen.

The main function of the plasmascreen is to remove the capacitive coupling between the electronic fields of the load coil and the plasma and this reduces the secondary discharge. Therefore argide polyatomic ions should be reduced since the secondary discharge is believed to promote their formation[150]. Under these conditions of lower power and plasmascreen, the ArO^+ signal will be significantly reduced compared to the oxygen signal and hence the O^+/ArO^+ ratio will increase and hence the temperature calculated will increase. Thus under these conditions the deviation of the

dissociation temperature of ArO^+ from that obtained at 1280 W is an indication of the reduction of the polyatomic ion and not a reflection of an increase in the plasma temperature. This reflects that the site of formation of ArO^+ occurs in the interface.

These findings differ from those of Houk and Praphairaksit[138]. They found that the T_g value for ArO^+ dropped from 6350 K to 1810 K for the hot plasma when the load coil was shielded. They suggested that in the absence of the shield ArO^+ would be dissociated in the interface region due to the ion being accelerated towards the skimmer as a result of the presence of the secondary discharge. Whereas when the load coil is shielded the attenuation of the secondary discharge resulted in ArO^+ being created in the interface. Thus a low T_g value was evidence of additional formation of polyatomic ions by collisions in the interface. The results for this study showed no significant difference in the T_g values calculated for ArO^+ at 1280 W with and without the plasmascreen (i.e. shielded and non-shielded). Houk and Praphairaksit[138] also found that under cool plasma conditions, i.e. low power and shielded load coil, the T_g value for ArO^+ was also reduced (1040 K) suggesting that ArO^+ is formed by collision induced reactions in the interface under such circumstances. However, the results to this study clearly show that ArO^+ is reduced under cool plasma conditions and therefore a higher T_g value was calculated. These results are consistent with the function of the plasmascreen with low power on instruments that have an unbalanced load coil design[150]. Furthermore they are consistent with the findings of Sakata and Kawabata[119] and Nonose *et al.* [117] who showed that the presence of a grounded electric shield between the load coil and the torch with low power resulted in the reduction of argon-derived polyatomic ions. Sakata and Kawabata[119] and Nonose *et al.*[117] showed that ArX^+ ions are formed in the interface region of the ICP-MS.

2.4.2.3: The effect of vapour loading on the dissociation temperatures

Figures 2.7a - 2.7d show the effect of vapour loading on the dissociation temperatures for the four species, at the four experimental conditions studied, calculated on the assumption of equilibrium in the plasma.

Figure 2.7 shows that the greatest variation in the calculated temperature at each vapour loading occurs for the weakly bound ions and in particular for ArO^+. This is due to the fact that a very small change in the measured ratio will result in a significant change in the temperature calculated. Therefore due to the uncertainty in the temperature calculated at each vapour loading it is not possible to use the weakly bound ions as thermometric probes to assess the effect of increasing vapour loading on the temperature of the plasma. Furthermore, as discussed previously, the dissociation equilibrium of these ions does not occur in the plasma so cannot be used to assess the plasma temperature. By contrast, the two strongly bound ions CO^+ and C_2^+ show little variation in the temperatures calculated at each vapour loading, so they can be used as thermometric probes to assess the effect of vapour loading on the plasma temperature. The dissociation temperatures calculated for these two ions remained relatively constant with increasing vapour loading for the four plasma conditions studied. Thus, the plasma temperatures remained constant with increasing vapour loading.

Vapour introduced into the plasma influences the coupling of the plasma with the RF field, which in turn affects the power absorbed by the plasma[151]. In addition energy is required to dissociate water[152]. Boumans and De Boer estimated that the water vapour entering the central channel would consume about 20 % of the total power input to the plasma, implying a decrease in temperature with water present[153]. This would also imply that as the vapour loading increased more energy would be required to dissociate the vapour and so the temperature of the plasma would decrease. When organic solvents are introduced, a drop in plasma temperature compared to aqueous introduction has been reported[154, 155, 156]. Temperature decreases have been attributed to

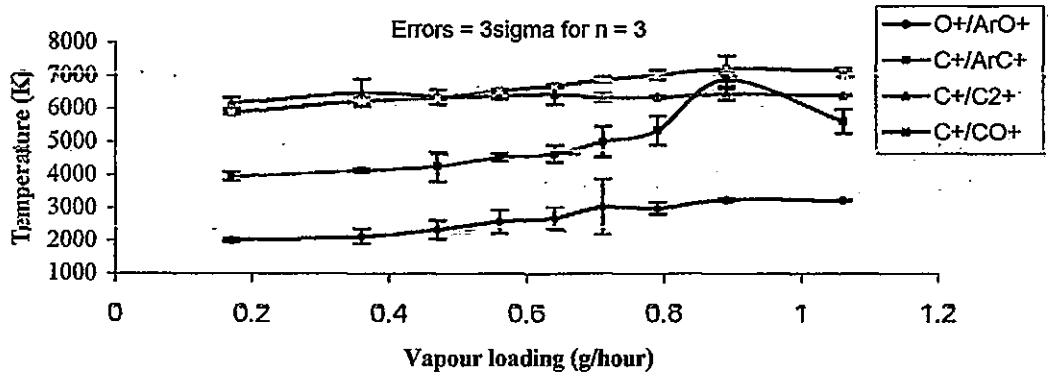

Figure 2.7a: The effect of vapour loading on the dissociation temperatures at 1280 W with no plasma screen (assuming equilibrium in the plasma)

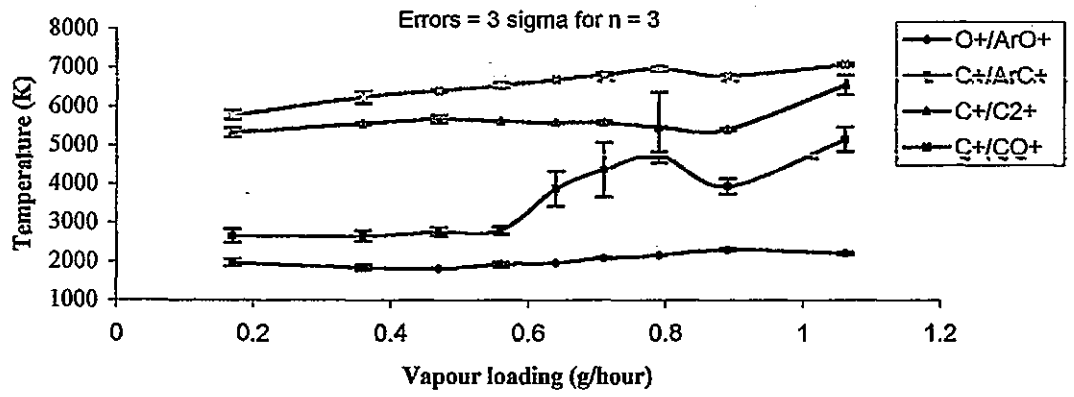

Figure 2.7b: The effect of vapour loading on the dissociation temperatures at 1280 W with the plasma screen (assuming equilibrium in the plasma)

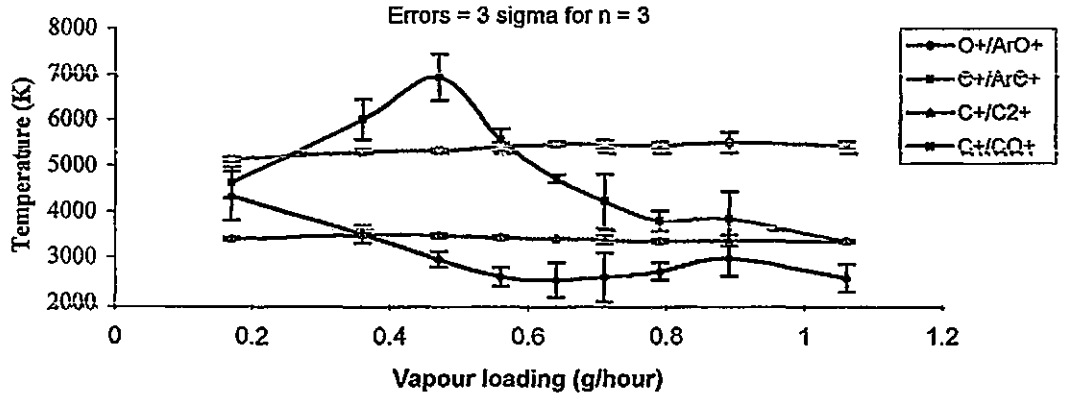

Figure 2.7c: The effect of vapour loading on the dissociation temperatures at 700 W with no plasma screen (assuming equilibrium in the plasma)

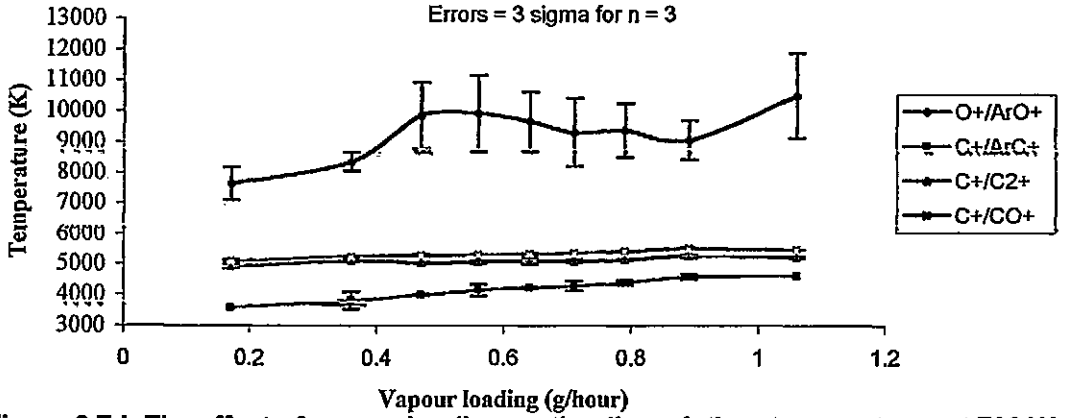

Figure 2.7d: The effect of vapour loading on the dissociation temperatures at 700 W with the plasma screen (assuming equilibrium in the plasma)

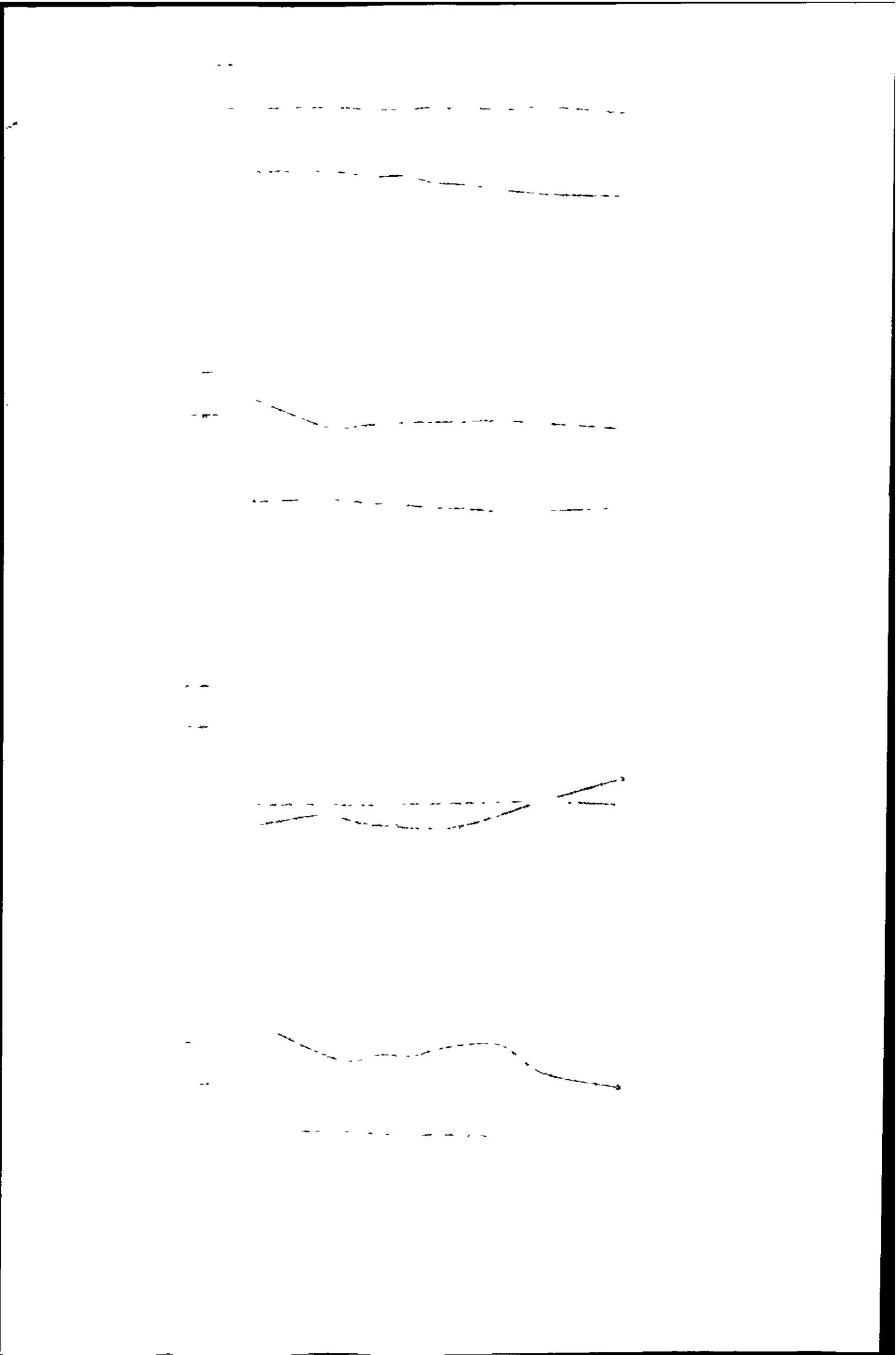

absorption of RF power in the central channel by the large vapour loading of these highly volatile solvents. For organic solvents the C_2^+dissociation plays a critical role on the thermal properties of the central channel[157]. Blades and Caughlin [157] suggested that the drop in excitation temperature of the ICP with xylene introduction when compared to the aqueous ICP was due to the consumption of energy by the dissociation of C_2. Again this would imply a decrease in temperature with increasing vapour loading. However, these results do not reflect this and show that there was no significant change in the temperature of the plasma with increasing vapour loading. Previous studies have indicated that the transfer of energy between the plasma and the central channel is very critical in an ICP[158]. The vapour introduced into the ICP dissociates, although not fully, into C, H, and O. It has been shown [152] that the presence of H results in an improvement of energy transfer from the plasma towards injected species along the central channel. This is as a result of the higher thermal conductivity of H compared to Ar. It has also been shown that[159, 160] the presence of H results in an increase in the temperature along the central channel. Therefore with increasing vapour loading there is an increase in the amount of H present in the ICP and so this would result in an increase in the temperature of the ICP. So, although the dissociation of the vapour and in particular the dissociation of C_2 requires a large amount of energy, the amount of atomic H present improves the heat transfer considerably. The overall effect of this is to cause the temperature of the plasma to remain relatively constant with increasing vapour loading. Furthermore the vapour introduced is only 17.7 % propionic acid so the quantity of organic vapour is not sufficient to cause a drop in temperature.

2.4.3: Dissociation temperatures calculated assuming equilibrium in the interface

Species such as ArO^+ are thought to form in the interface of the ICP-MS rather than in the plasma, so dissociation temperatures were calculated on the assumption of

equilibrium in the interface. Table 2.7 summaries the dissociation temperatures calculated on this assumption.

The dissociation temperatures calculated on the assumption of equilibrium in the interface are lower than those calculated on the assumption of equilibrium in the plasma.

Table 2.7 shows that the dissociation temperatures calculated for the weakly bound ions ArO^+ and ArC^+ are significantly lower than those calculated for the strongly bound ions C_2^+ and CO^+. The dissociation temperatures for ArO^+ are particularly low at less than 1012 K for all four of the plasma conditions studied. The temperatures thought to prevail in the interface are less than 3500 K[117]. Furthermore, the dissociation temperatures calculated for ArO^+ (assuming equilibrium in the interface) are of the same magnitude as the T_g of 155 K at the skimmer cone estimated by Douglas and French[121]. Hence, the low temperatures calculated for ArO^+ and ArC^+ correspond to those thought to prevail in the interface which suggests that they are formed in the interface rather than the plasma. Therefore these species cannot be used as thermometric probes to make accurate temperature measurements of the plasma. Furthermore, these temperatures calculated for the interface cannot be considered to be accurate measurements of the temperature in the interface as this method relies on the assumption of LTE and thermal equilibrium certainly does not prevail in this low pressure environment.

The dissociation temperatures calculated for C_2^+ and CO^+ are in most instances higher than the temperature thought to prevail in the interface region, as determined by Nonose *et al.*[117] (3500 K), and are significantly greater than the T_g value at the skimmer cone (155 K) estimated by Douglas and French[121]. This suggests that these species are formed in the plasma and not the interface region. Therefore these species are ideal thermometric probes to determine the temperature of the plasma.

Table 2.7: Dissociation temperatures calculated for the four polyatomic ions assuming equilibrium in the interface

Species	The Dissociation Temperatures calculated (K) for vapour loading between 0.17 - 1.06 (g h^{-1})			
	1280 W (no plasmascreen)	1280 W (plasmascreen)	700 W (no plasmascreen)	700 W (plasmascreen)
ArO^+	654 - 769	630 - 689	693 - 840	940 - 1012
ArC^+	1372 - 1668	1147 - 1528	1280 - 1679	1305 - 1406
C_2^+	4001 - 4218	3613 - 4206	3334 - 3507	3415 - 3607
CO^+	4406 - 5213	4340 - 5063	3965 - 4240	3933 - 4204

The dissociation temperatures calculated based on the assumption of LTE in the interface cannot be used to assess accurately changes in temperatures with operating conditions such as the power, vapour loading or the use of the plasmascreen. This is due to the fact that LTE does not prevail in the interface. Rather they should be used to assess if the dissociation equilibrium temperature of the ion is similar to the temperatures expected in the interface or similar to those expected in the plasma and hence indicate the site of formation of the ion in ICP-MS.

2.4.4: Comparison of results to previous work

The dissociation temperatures calculated using ArO^+ for the hot plasma, i.e. 1280 W with no plasmascreen, are approximately 3000 K lower than those reported by Houk and Praphairaksit[138], while those calculated for the cool plasma conditions are approximately 4000 - 5000 K higher. The magnitude of the O^+/ArO^+ is influenced by many factors such as the gas flow rates, the extent of desolvation, air entrainment into the plasma and the design of the load coil and interface. Therefore it is hardly surprising that different workers calculate different dissociation temperatures using ArO^+ as the thermometric probe.

The results of this study show the polyatomic ions can be divided into two groups according to their site of formation. The weakly bound argide polyatomic ions probably form in the interface while the strongly bound ions probably form in the plasma. Previous studies have also found this to be the case. Shibata *et al.*[126] proposed that metal oxide polyatomic ions, MO^+, (strongly bound ions) were derived from undissociated MO in the ICP because the theoretical MO/M ratios in the ICP agreed with the experimentally determined MO^+/M^+ ratios. Nonose *et al.*[117] proposed that ArO^+ was formed by a collision-induced reaction of neutral Ar and O^+ due to the differences in signal behaviour of ArO^+ and MO^+ in the ICP. They also estimated the dissociation equilibrium temperature for ArO^+ and ArH^+ by comparing the theoretical ratio of

[ArH^+] to [ArO^+] with the experimental ratio of the ion signals of ArH^+ to that for ArO^+. The temperature at which the two agreed was found to be 3500 K, which was also the OH rotational temperature measured in the interface, suggesting that the dissociation equilibrium for ArX^+ species is established in the interface region and not the ICP. Sakata and Kawabata[119] found that argide polyatomic ions were formed in the plasma, due to a positive plasma potential and also behind the sampler due to a secondary discharge. In contrast Houk and Praphairaksit[138] found that ArO^+ and ArN^+ were dissociated at high plasma potentials. They found that the strongly bound ions O_2^+ and MO^+ for the rare earth elements were observed at levels consistent with T_g in the plasma. All the previous work refers to temperatures calculated using quadrupole instruments and not a magnetic sector field instrument as in the case of this work.

2.5: Conclusions

The mass spectra obtained during this study demonstrated the importance of making the correct measurement of the ion signals used in order to calculate an experimental K_d value. Polyatomic ions by their very nature interfere with the analysis of analyte ions and therefore it follows that the polyatomic ions whose dissociation temperature we wish to determine will be interfered with by the analyte ions. Using a magnetic sector-field instrument unambiguous identification and quantification of the ion signals can be made which ultimately results in more reliable temperatures being calculated using this method.

The temperature calculated for the plasma depends upon the polyatomic ion used. The weakly bound ions ArO^+ and ArC^+ showed dissociation temperatures lower than the strongly bound ions CO^+ and C_2^+. Therefore if the ICP temperature is to be calculated using this method then the polyatomic ion used as the thermometric probe cannot be picked arbitrarily. Strongly bound ions, such as CO^+ and C_2^+ studied in this work, give dissociation temperatures corresponding to those expected in the plasma,

while weakly bound ions such as ArC^+ and ArO^+ reflect temperatures elsewhere. The polyatomic ions CO^+ and C_2^+ can therefore be used to give reliable temperature conditions in the plasma under different operating parameters. The low temperatures calculated using ArO^+ based on equilibrium in the plasma might be an indication that the plasma is not in local thermal equilibrium.

The deviation of the temperatures calculated using ArC^+ and ArO^+ from expected values provided useful information on their possible site of formation, i.e. the interface region. At high power the low temperatures calculated indicate they could not be formed in the plasma, while for ArO^+ at low power with the plasmascreen (cool plasma conditions) the increase in temperature from an expected decrease is again an indication ArO^+ is not formed in the hot plasma. The apparent increase in temperature is as a result of the ArO^+ signal decreasing due to the removal of the secondary discharge that promotes its formation.

The results showed that using the two strongly bound ions as the thermometric probes, there was no significant increase in the temperature of the plasma with increasing vapour loading. This was attributed to a balance between an increasing amount of organic loading into the plasma, which would cause a drop in the plasma temperature, and an increasing amount of H in the plasma which helps improve the energy transfer to the central channel.

Advances in ICP-MS result in lower and lower signals being measurable and this has revealed the presence of new polyatomic ions. Recently experimental evidence has been reported for the formation of the doubly charged polyatomic ions ThO^{2+} and $ThOH^{2+}$ that interfere with tin analysis[161]. The use of sectorfield instruments has allowed the analysis of new analytes, for example sulphur, which could not be determined using quadrupole instruments. However, analysing samples containing sulphur leads to the formation of the polyatomic ions S_2^+ and SO^+[95]. These interferences often occur in regions of other elemental ions making their identification difficult.

Using sectorfield instruments their identification becomes possible, and where the necessary fundamental data exists, their site of formation may be revealed using the method outlined in this work. This method may be used to determine the site of formation of any molecular species as long as the necessary fundamental data are known.

The determination of the dissociation temperature provides a useful, simple and non-invasive method for the determination of the site of formation of a molecular ion. Such information is invaluable as it can aid in the continual process of development of ICP-MS instruments.

CHAPTER 3: PRELIMINARY INVESTIGATION INTO THE APPLICATION OF A HEXAPOLE COLLISION CELL

3.1: Introduction

The main goal in instrumental development and the development of new analytical procedures is to obtain the lowest possible detection limits while maintaining good precision and accuracy, the rapid analysis of samples and a wide linear range. In the case of ICP-MS this has meant considerable attention has focused on minimising interferences, particularly those produced by analyte oxide ions, MO^+, and argide ions, ArX^+. Tactics employed to overcome interferences include mixed gas plasmas, cool plasma conditions, alternative sample preparation and introduction, the use of alternative mass analysers and, most recently, the use of collision cells.

Collision cells have been employed in organic tandem MS/MS for the production of fragment ions to aid structural eludication, and collision cells used in ICP-MS are based on this instrumentation. However, in ICP-MS a collision cell is employed to completely remove an unwanted molecular ion thereby allowing the determination of an analyte ion occurring at the same nominal mass. Generally ions sampled from the plasma pass through a series of RF rods (a multipole) in an enclosed housing filled with one or more collision gases e.g. He, H_2, N_2, Xe or NH_3. The density of this collision gas is high enough to remove the undesired ions while collisional cooling [162] and the focusing properties of the multipole help retain many of the analyte ions.

The first approach considered for implementing a collision cell in ICP-MS was to combine the ICP source with a triple quadrupole mass spectrometer [163]. The purpose was to dissociate polyatomic ions in the middle quadrupole by collisions with argon gas while transmitting the analyte ions. Douglas [163] found that the density of argon required to drive such dissociation reactions lead to a loss of analyte ions by scattering. However, more success was achieved by utilising ion-molecule reactions, instead of

dissociation to remove unwanted ions. Air was admitted as the collision gas and preliminary results showed that CeO^+ was reduced. Rowan and Houk[164] used a double quadrupole arrangement and also found that collision induced dissociations were insufficient to remove most polyatomic ions. However, they found that if a chemically reactive gas (i.e. CH_4 or Xe) was used then the polyatomic ions ArO^+, Ar_2^+, and ArN^+ were attenuated to sufficient levels for analytical purposes. While these ions were lost to some extent by scattering, which would also lead to loss of analyte ions, the two main mechanisms for loss of polyatomic ions were attributed to collision induced dissociation and reactions of the collision gas with the polyatomic ions. The latter process resulted in new peaks in the mass spectrum from products of ion - molecule reactions between both interfering ions and background ions with the collision gas.

The current interest in collision cells for ICP-MS stems mainly from the work undertaken by Koppenaal *et al.*[91, 92, 93] who demonstrated highly efficient removal of argide ions in the ion - trap. They attributed this to ion - molecule reactions between water vapour present in the ion trap. Similar experiments with the deliberate addition of H_2 yielded similar results [93]. Koppenaal's group[165] later added a RF octopole collision cell between the ion source and the ion trap mass spectrometer and found that it could be used to eliminate Ar^+, using H_2 in the cell, prior to trapping the ion beam in the mass spectrometer. This resulted in lower levels of chemical ionisation of the background gases in the trap thus enhancing sensitivity. Oxygen was also added to the collision cell to eliminate isobaric interferences[165].

Initially two different approaches for implementing collision cells in ICP-MS were adopted by manufacturers. One approach was to use an inert collision gas, such as He, to dissociate the polyatomic ions into their component atoms or ions, which should selectively reduce all argon - based polyatomic ions. Atomic ions also lose kinetic energy as a result of collisions with the gas but due to the high ionisation potential of the collision gas, charge exchange and neutralisation of the analyte ions should not

occur. The second approach was to use a reaction gas to selectively remove polyatomic ions using controlled ion - molecule chemistry.

Turner *et al.*[166] reported on the use of a hexapole collision cell for argide polyatomic ion removal to the ppb - equivalent level. It was reported that this was achieved using He as the collision gas. A more thorough report on the operation and application [167, 168] of the same instrument noted the addition of H_2 as reaction gas to promote the desirable chemical reactions of the polyatomic interference ions. The role of water in the collision cell has recently been demonstrated by Dexter *et al.*[169] It has therefore become apparent since the work of Turner *et al.*[166], and the work undertaken in this chapter, that He does not attenuate polyatomic ions by dissociation but the effect can be attributed to significant contamination of the He gas with either water or H_2. It therefore follows that in all collision cells polyatomic ions are reduced by chemical reactions occurring in the cell and that all 'collision cells' are essentially 'reaction cells'. The presence of He serves as a buffer gas to thermalise the ions, improving ion transmission through the MS interface.

Douglas and French[162] first demonstrated that the cell could be used to reduce the kinetic energy spread of various ions, thus reducing the peak tailing observed in the spectra. Turner *et al.*[166] demonstrated the cooling effect for atomic ions in ICP- MS. A multipole-collector, magnetic single focusing instrument equipped with a collision cell is available commercially[170]. Such an instrument allows high-precision isotope ratio measurements by the very low energy spread of ions leaving the hexapole collision cell stage of the MS interface. A light, chemically unreactive collision gas such as He is generally used for such a purpose. Bandura and Tanner[171] have used neon as a collision gas to dampen plasma noise to allow improved determination of lead and silver isotopes.

The theory, design, operation and analytical performance of a collision cell has been discussed in detail by Tanner and associates[172, 173, 174]. Marchante - Gayon *et al.*[175,

[176] added He/ H_2 to a collision cell to reduce interferences caused by the Argon dimers $^{40}Ar\ ^{40}Ar^+$ and $^{38}Ar\ ^{40}Ar^+$ on the main isotopes of selenium. This enabled speciation of Se in nutritional supplements[175] and human urine[176]. Various other gases have also been used in collision cells. Chang and Jiang[177] used ammonia as the collision gas to reduce the intensity of ArC^+, $ClOH^+$, $ArCH^+$ and ClO^+ that interfere on $^{52}Cr^+$ and $^{53}Cr^+$. This allowed ICP-MS to be used as a liquid chromatographic detector for the speciation of chromium in water samples. Vollkopf *et al.*[178] used ammonia to attenuate ArH^+, Ar^+, ArC^+, ArO^+ and $ArOH^+$ to allow the determination of K^+, Ca^+, Cr^+, Fe^+ and Mn^+ in high purity hydrogen peroxide. Bollonger and Schleisman [179] used ammonia as the collision gas to determine a range of metal contaminants in semiconductor grade acids. Carbon and chloride based interferences were attenuated by Neubauer and Vollkopf[180] allowing ng L^{-1} levels of Cr^+, Mn^+ and As^+ to be determined in carbon and chloride based matrices, again using ammonia as the collision gas. Hattendorf and Gunther[181] have investigated the use of a collision cell for laser ablation. Ammonia and H_2 have been used as reactive gases in a collision cell with the addition of He, Ne and Xe as buffer gases to enhance thermalisation in the cell. This resulted in the reduction of Ar - ions and argide ions (e.g. $ArCr^+$) on the main isotopes of Ca and Nb, a reduction of the limit of detection for Ca in quartz, and an improvement of accuracy for the determination of Nb in a chromium matrix. Bandura *et al.*[182] used ammonia to reduce ArN^+ and ArO^+ interferences to allow precise isotope ratio measurements of normally interfered isotopes of Fe^+. They also demonstrated collisional dampening of the ICP noise in the collision cell using ammonia which resulted in a reduction of the RSD of isotope ratio measurements.

All the above work has concentrated on the removal of argon - ions and argon containing ions, ArX^+, which are weakly bound. Strongly bound analyte oxide ions, MO^+, are also problematic in ICP-MS. Du and Houk[183] have used a collision cell for the attenuation of strongly bound metal ions using a mixture of He and H_2 gas in the

hexapole collision cell. They found that by adjusting the collision conditions, in particular the composition and flow rate of the collision gas and the hexapole dc bias voltage, the MO^+/M^+ signal ratio was suppressed by a factor of up to 60 for CeO^+ and LaO^+ while maintaining 20 % of the original analyte signal, M^+. They also found that the same collision cell conditions used to reduce the MO^+ signals served to remove ArO^+, ArN^+ and Ar_2^+ from the background spectrum. The authors concluded that the reduction of MO^+ using the collision cell was not as extensive as that possible by reducing O atom density in the plasma by solvent removal, but may be an appropriate technique to use when there is no solvent to remove, e.g. laser ablation.

Moens *et al.*[184] used ion - molecule chemistry within a collision cell to eliminate the isotopic overlap of ^{87}Rb and ^{87}Sr. This was achieved by selective reaction of Sr with CH_3F in the collision cell enabling the accurate determination of the Sr isotopes by measuring the intensity of the corresponding SrF^+ ion beams. In contrast Rb does not react with CH_3F. This technique was used for the Rb/Sr age determination of magmatic rocks, without the need for sample treatment except for the dissolution of the sample.

There are a number of drawbacks in implementing a collision cell to remove unwanted interferences. Firstly, it is often necessary to use different reaction gases to remove different interferences. Furthermore, some analytes are better determined under conventional operating conditions i.e. with no reaction gas in the collision cell. Therefore a sample may have to be analysed two or more times, initially under conventional operating conditions and finally under collision cell conditions using various reaction gases. Secondly, the ion - molecule reactions used to remove polyatomic ions will lead to product ions that could appear in the mass spectrum potentially hampering its interpretation and interfering with the determination of other analyte ions. The product ions also have the potential to react further in the collision cell, complicating matters more. This can be overcome by ensuring that the product ions fall outside the stability region of the multipole reaction cell so that the ion will collide

with the rods of the multipole collision cell and be neutralised [173]. Alternatively, a negative dc pole bias can be operated in relation to that of the quadrupole mass analyser so that most ions produced in the collision cell do not have sufficient kinetic energy to enter the quadrupole[183]. Finally, collision cells are extremely sensitive to contamination. The presence of water vapour, which reacts with most elemental and molecular argide ions, may create new interferences[172] and even ultratraces of organic compounds (e.g. a trace of oil vapour in the mass spectrometer) may lead to the generation of background species across the entire mass range[185].

Nevertheless, the use of post plasma reactions is an attractive approach to remove polyatomic ions because it can be used with the ICP operating under normal power taking full advantage of the ICP as a highly efficient ion source, so none of the matrix induced effects encountered with a cool plasma or the inefficient ionisation of ions such as Se or As are observed.

The aim of this work was to investigate the application of a hexapole collision cell for the attenuation of polyatomic ions in ICP-MS.

3.2: Experimental

3.2.1: Instrumentation

The work in this chapter was performed at Thermoelemental using a PQ ExCell inductively coupled plasma mass spectrometer (Thermoelemental, Winsford, Cheshire, UK) shown schematically in Figure 3.1. The ions were extracted through a conventional sampler and skimmer from an ICP operated at 1280 W, and then accelerated and injected into a hexapole collision cell. Helium gas in the range of 0 - 7 ml min^{-1} was added to the collision cell via a mass flow controller operated from a dial on the control panel. Operating conditions are shown in Table 3.1.

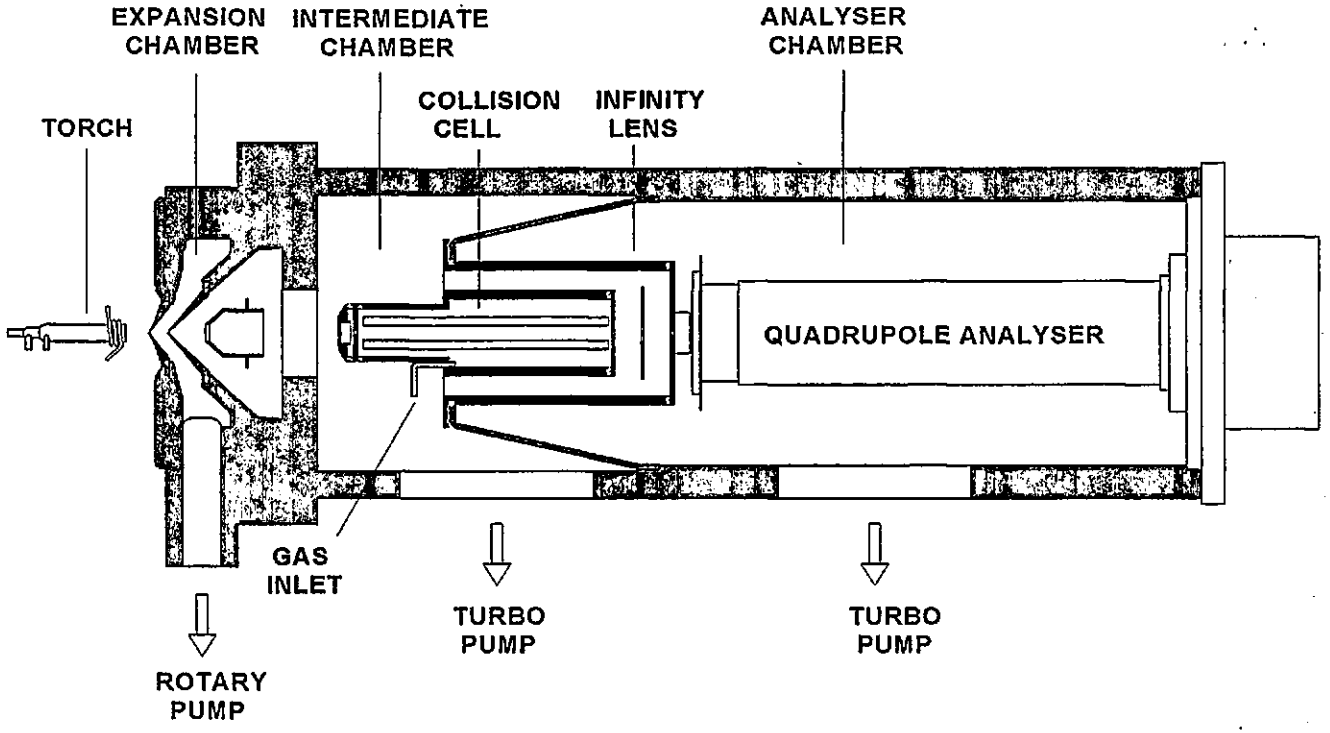

Figure 3.1: Schematic diagram of ICP-hexapole collision cell-quadrupole MS.
(Courtesy of TJA solutions)

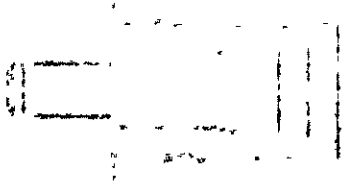

Table 3.1: Operating conditions for the PQExCell in two modes, with and without a collision gas.

	Without collision gas	With He collision gas
Forward Power (W)	1280	1280
Coolant ($l\ min^{-1}$)	15	15
Auxiliary ($l\ min^{-1}$)	1	1
Nebuliser ($l\ min^{-1}$)	0.95	0.95
Detection mode	Dual	Dual
Channels per amu	3	3
Dwell time (μs)	10000	10000
Spray chamber	Impact bead	Impact bead
Spray chamber temperature (^0C)	5	5
Collision gas flow rate ($ml\ min^{-1}$)	0	0- 7
Hexapole bias (V)	-5	0
Quadrupole bias (V)	0	-5
Solution uptake ($mlmin^{-1}$)	1	1

Values stated are typical settings under these conditions and parameters were optimised throughout the experiments.

3.2.2: Procedure

Experiments were performed to investigate the use of helium as a collision gas. Experiments were performed while aspirating a 1 ng ml^{-1} standard tune solution containing $^{59}Co^{+}$ and $^{115}In^{+}$ which was prepared from 1000 ug ml^{-1} standard solutions (BDH, Poole, Dorset, UK). Standards were made up with 2 % (v/v) HNO_3 or 2 % (v/v) HCl, using Aristar grade HNO_3 or HCl respectively (BDH, Poole, Dorset, UK). In order to assess He as a collision gas for the determination of Cr, which suffers from Carbon related interferences a 1 ng ml^{-1} tune solution was prepared in de-ionised water spiked with 1 % (v/v) methanol.

Limits of detection were determined for selected analytes by analysing a blank solution 10 times and two standards of increasing concentration. For the determination of K^{+} and Fe^{+} in an unpressurised cell 0.5 and 1 μg ml^{-1} standards were used, while in a pressurised cell 5 and 10 ng ml^{-1} standards were used. For the determination of As^{+} and Se^{+} 5 and 20 ng ml^{-1} standards were used. For the determination of Ca^{+} in a pressurised cell 1 and 2 μg ml^{-1} standards were used.

In order to evaluate the effectiveness of He as a collision gas experiments on standard solutions were also performed using the same instrument without pressurisation of the collision cell with He. The operating conditions used are shown in Table 3.1.

3.3: Results and Discussion

3.3.1: The effect of He in the collision cell on the In^{+} and Co^{+} signals

In order for the collision cell to be effective it must attenuate the interference while maintaining the analyte signal. When helium was introduced into the hexapole collision cell it resulted in the loss of both analyte and polyatomic ion signals due to scattering of the ions sampled from the plasma. For this reason the ICP-MS instrument must be tuned at each He flow rate in the collision cell to give the maximum signal.

Optimal conditions were obtained by nebulising a solution of 1 ng ml^{-1} of $^{59}Co^{+}$ and $^{115}In^{+}$. Figure 3.2 shows the effect of He flow rate in the collision cell on the $^{59}Co^{+}$ and $^{115}In^{+}$ response, in counts per second. The response at 0 ml min^{-1} corresponds to the signal obtained with an unpressurised cell. Figure 3.2 shows that the signals initially decreased on pressurisation of the cell with helium followed by an increase in the signals as the atomic ions were thermalised by the helium gas in the cell. After this point a further increase in the helium flow rate caused a decrease in the signals as the ions were probably lost by scattering.

3.3.2: The effect of He in the collision cell on various argon based polyatomic ions

Figure 3.3 shows the effect of He flow rate in the cell on various argon based interferences while aspirating a 1 ng ml^{-1} tune solution made up in 2% HNO_3. The instrument was retuned at each He flow rate to maximise the In^{+} and Co^{+} response.

Figure 3.3 shows that the most significant attenuation occurred for the argon dimer, $^{80}Ar_2^{+}$, which interferes with the main isotope of selenium. The signal was attenuated six orders of magnitude from 1 x 10^7 cps to 40 cps. The ArO^{+} signal obtained under standard operating conditions, i.e. unpressurised collision cell, was 5 x 10^6 cps contributed by $^{56}Fe^{+}$ in the nitric acid as well as ArO^{+} formed in the ICP-MS. On pressurising the cell this signal was attenuated from 5 x 10^6 cps to 2 x 10^3, a fall of over three orders of magnitude. The $^{39}ArH^{+}$ and $^{40}Ar^{+}$ signals were attenuated by 3 and 4 orders of magnitude respectively. The initial decay in the signals is likely to be dominated by the reactions of ArO^{+}, Ar^{+} and ArH^{+} with contaminants in the collision gas i.e. H_2 or H_2O. The signals then plateau after this initial fall, probably corresponding to the reduced reaction rates of $^{56}Fe^{+}$, $^{40}Ca^{+}$ and $^{39}K^{+}$ which are contaminants in the nitric acid.

Figures 3.4 and 3.5 show the Co^{+}/ interference ratio and In^{+}/interference ratio, respectively. From these graphs it can be seen that the maximum response to minimal

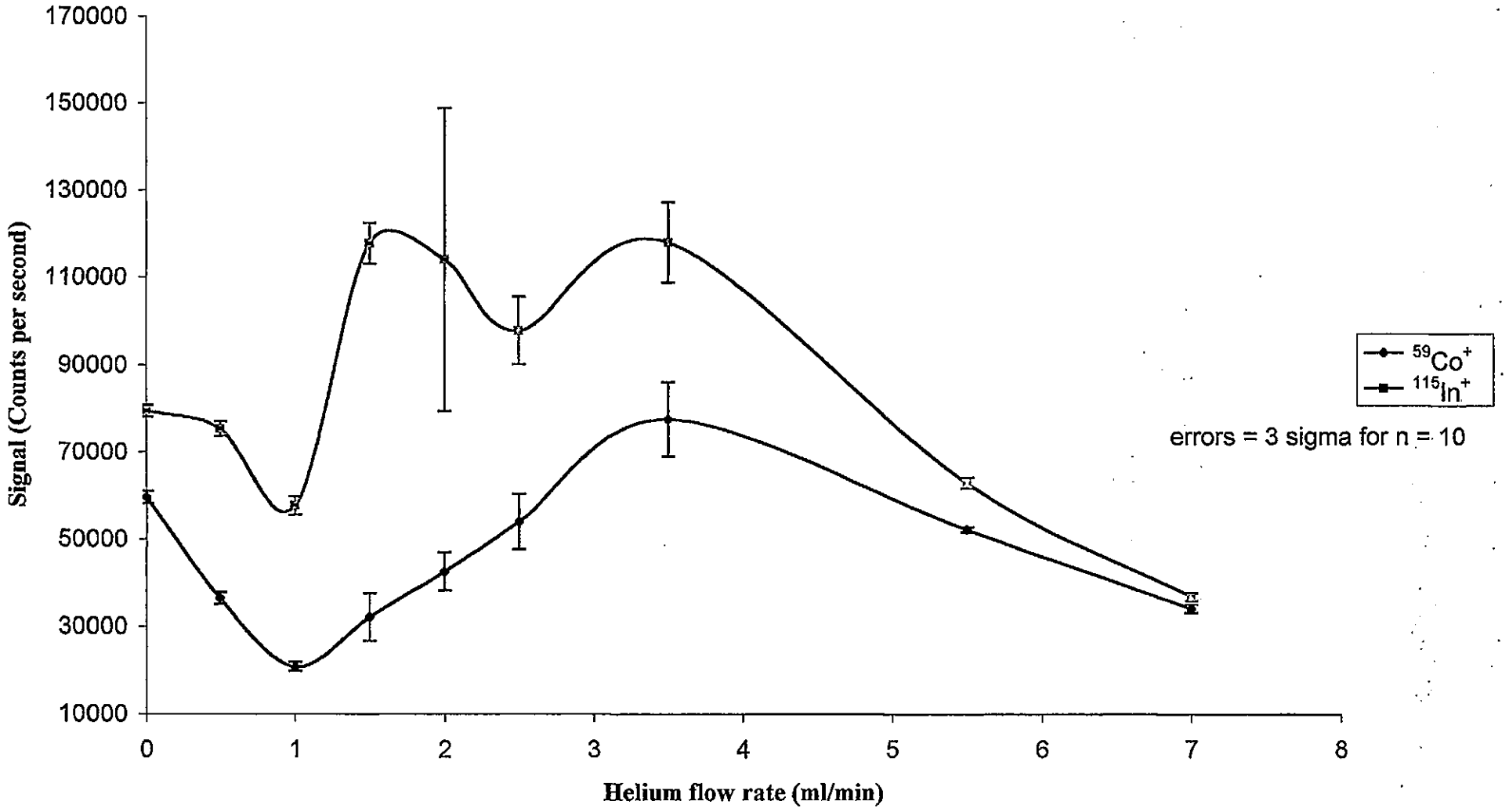

Figure 3.2: The effect of Helium flow rate in the collision cell on the $^{115}In^{+}$ and $^{59}Co^{+}$ signals

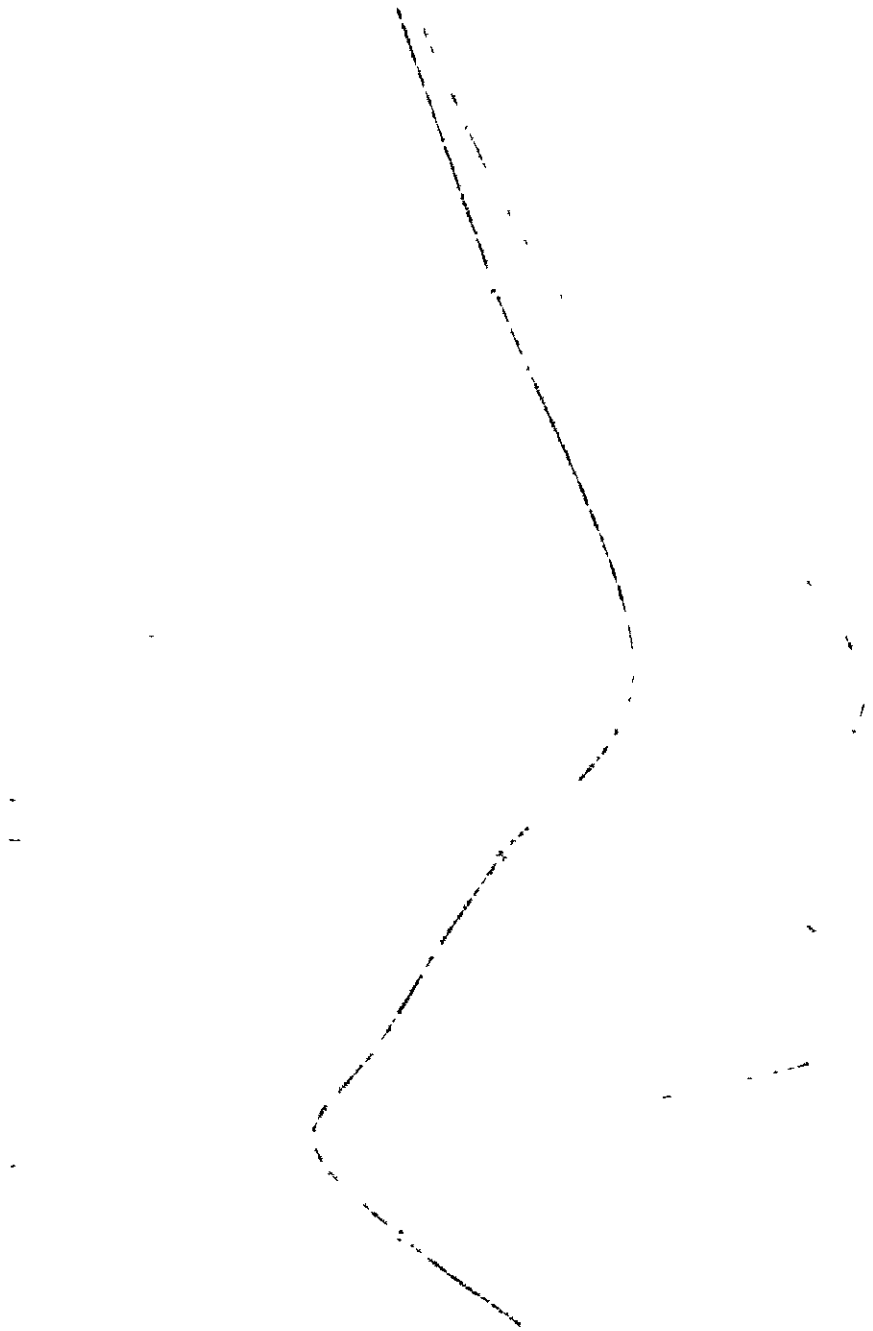

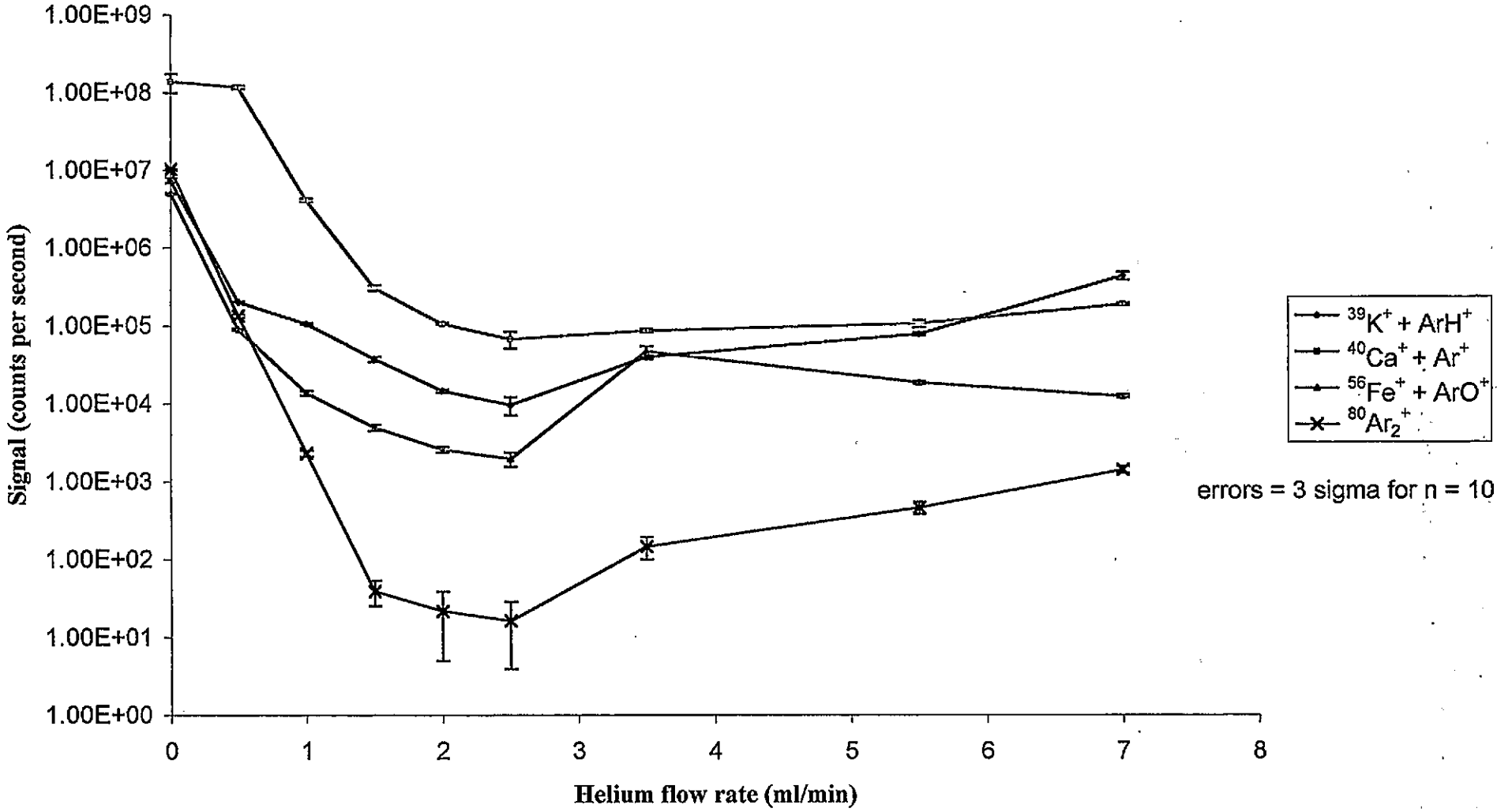

Figure 3.3: The effect of Helium flow rate on various interferences

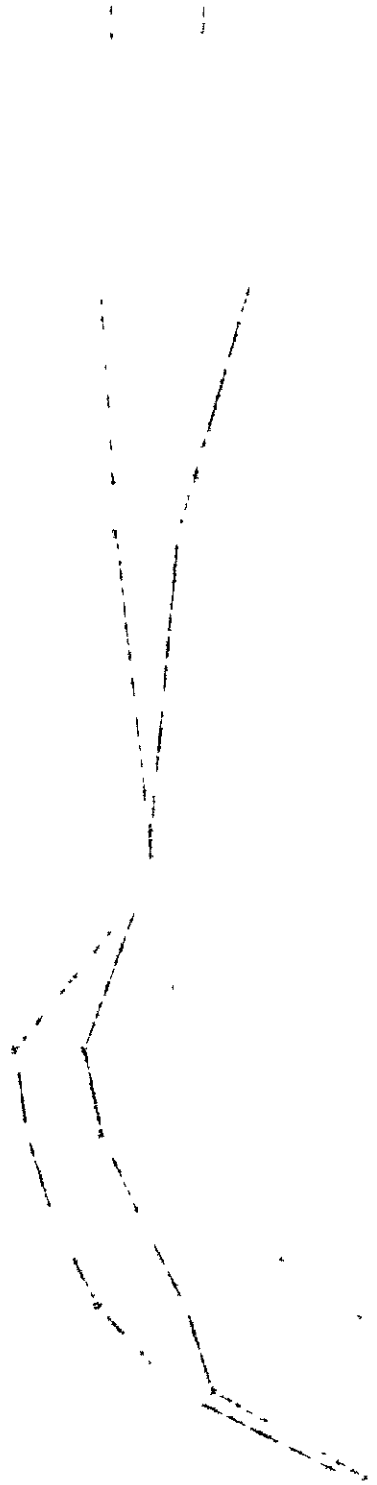

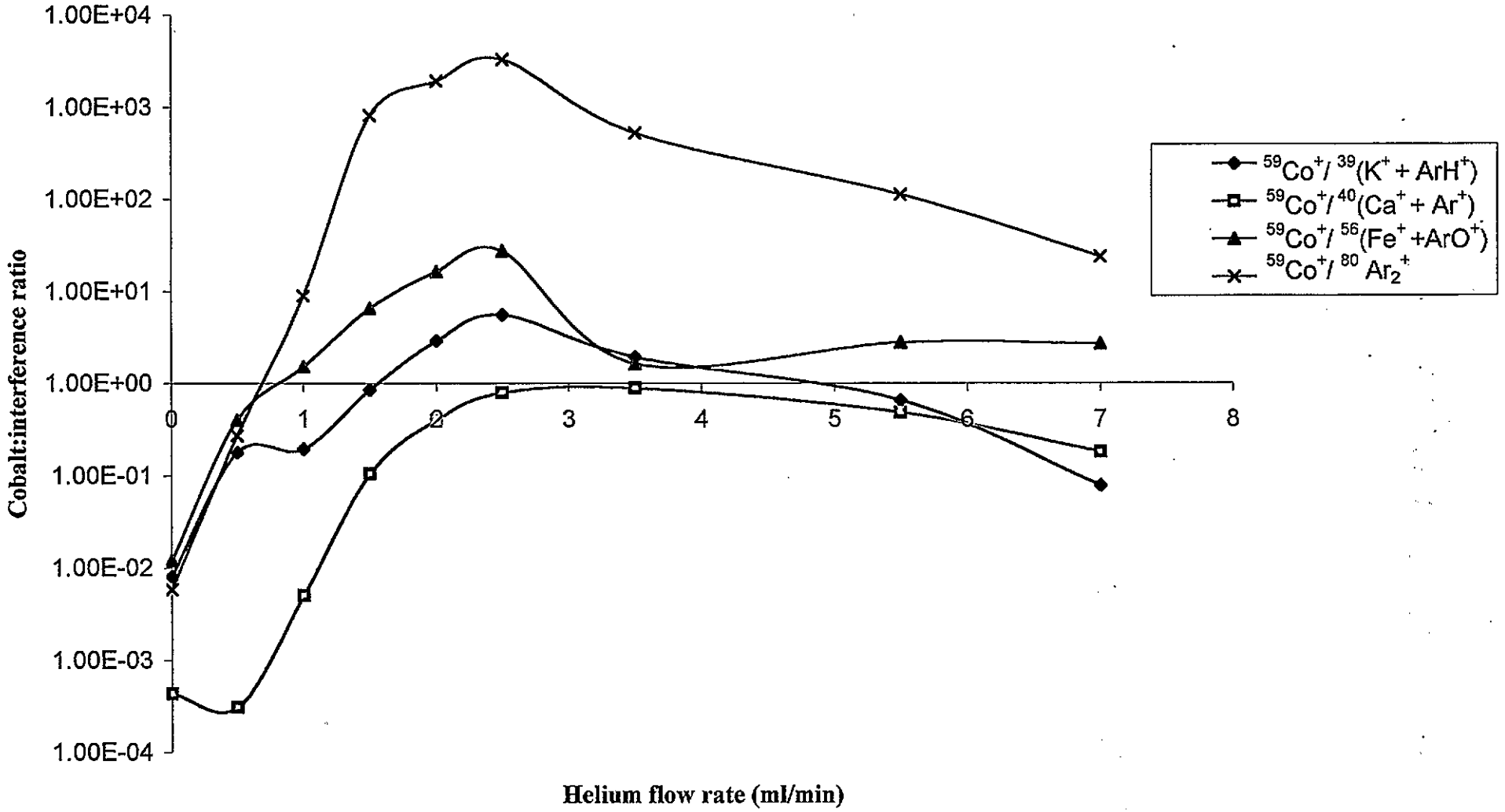

Figure 3.4: The effect of Helium flow rate on the $^{59}Co^{+}$:interference ratio

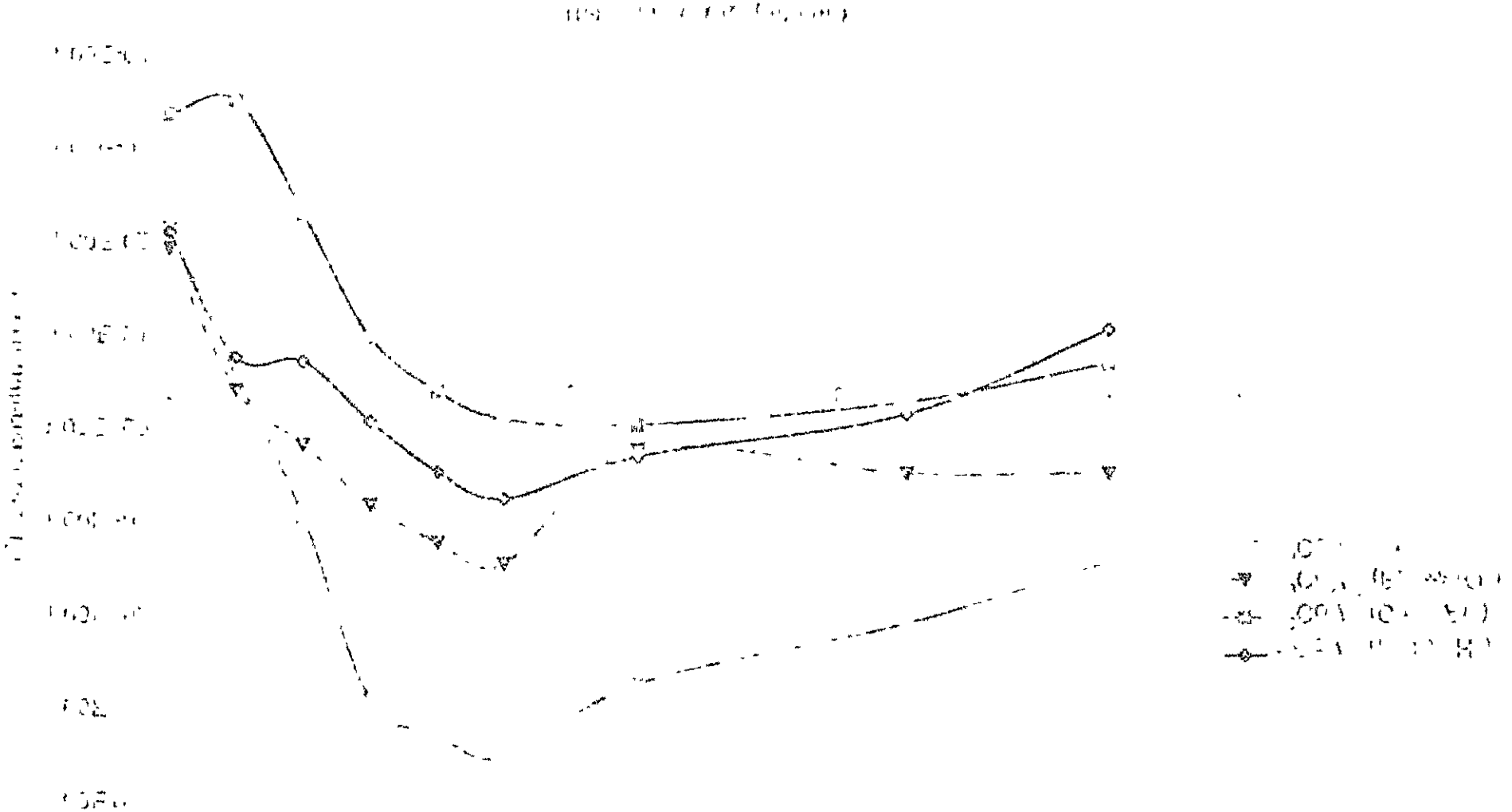

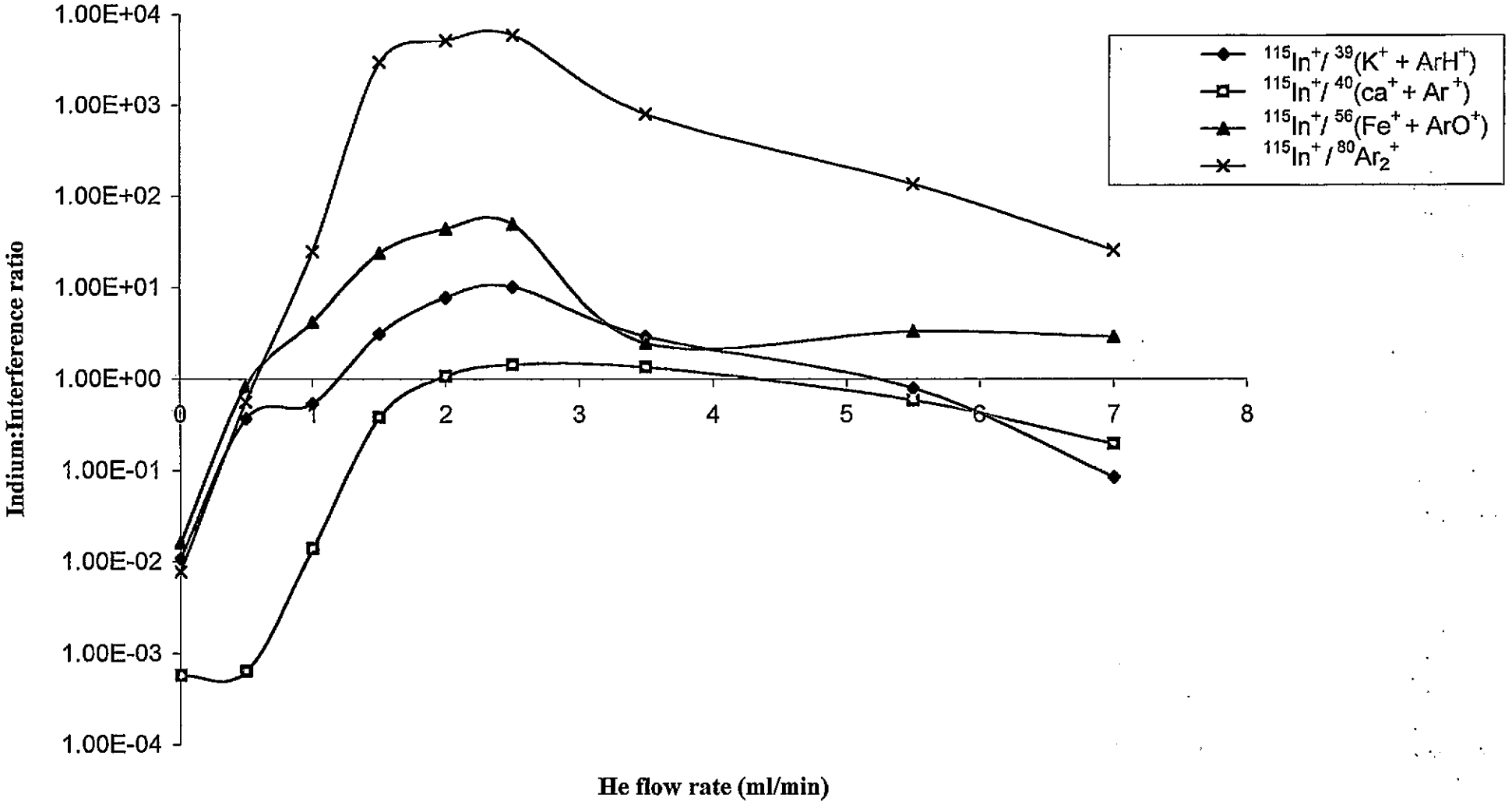

Figure 3.5: The effect of Helium flow rate on the $^{115}In^+$:interference ratio

interference occurs at approximately 2.5 ml min^{-1} helium. This flow rate was chosen to determine the limit of detection of $^{39}K^+$, $^{40}Ca^+$, $^{56}Fe^+$ and $^{80}Se^+$ in standard solutions. Table 3.2 shows the 3σ limits of detection determined at these conditions. Table 3.2 also shows the limits of detection determined in a standard solution of 2% hydrochloric acid as well as in 2% nitric acid. A similar pattern of attenuation of these interferences was observed in 2% HCl. The limits of detection of $^{39}K^+$, $^{40}Ca^+$, $^{56}Fe^+$ and $^{80}Se^+$ determined using conventional operating conditions are shown for comparison. The most important points of note are the limit of detection for $^{56}Fe^+$ is reduced by 3 orders of magnitude and the main isotopes of Ca and Se can be determined, under conventional conditions the background is too high to allow their determination at these isotopes.

3.3.3: The effect of He in the collision cell on the $ArCl^+$ signal

In the presence of chloride the determination of vanadium and arsenic are problematic due to the formation of ClO^+ and $ArCl^+$, respectively. Figure 3.6 shows that pressurisation of the collision cell had little effect on the ClO^+ signal. Therefore the use of helium as a collision gas offers no advantage for the determination of $^{51}V^+$ over conventional operating conditions. However, Figure 3.7 shows that the $ArCl^+$ signal was attenuated 2 orders of magnitude, the most rapid decay in the signal occurring between 0 - 3 ml min^{-1} helium. The background counts were reduced from 24080 counts per second, in an unpressurised collision cell, to 829 counts per second at a flow rate of 7 ml min^{-1} He. Figure 3.8 shows the $^{59}Co^+/ArCl^+$ ratio. The maximum ratio occurred at a helium flow rate of 7ml min^{-1}. This is in contrast to the maximum $^{59}Co^+$/interference ratio for Ar^+, ArH^+ and ArO^+ which was found to be approximately 2.5 $mlmin^{-1}$. Therefore, for different analytes, different collision cell conditions are required for their optimum determination. This severely limits the rapid multielement analysis of a sample in one acquisition. The 3 σ limits of detection for $^{75}As^+$ in 2 % HCl determined at a helium flow rate of 7 ml min^{-1} and in an unpressurised collision cell are shown in

Table 3.2: Detection limits obtained with and without pressurising the hexapole collision cell with helium

Detection limits ($ngml^{-1}$)				
	Without a collision cell (unpressurised cell)		With a collision cell (pressurised cell)	
Element	**2 % HNO_3**	**2 % HCl**	**2 % HNO_3**	**2 % HCl**
^{39}K	2.3	3.9	0.29	0.30
^{40}Ca	ND*	ND*	25	ND*
^{56}Fe	9.8	4.6	0.0045	0.009
^{75}As	0.034	0.86	0.036	0.030
^{80}Se	ND*	ND*	0.045	0.032

* Not determined

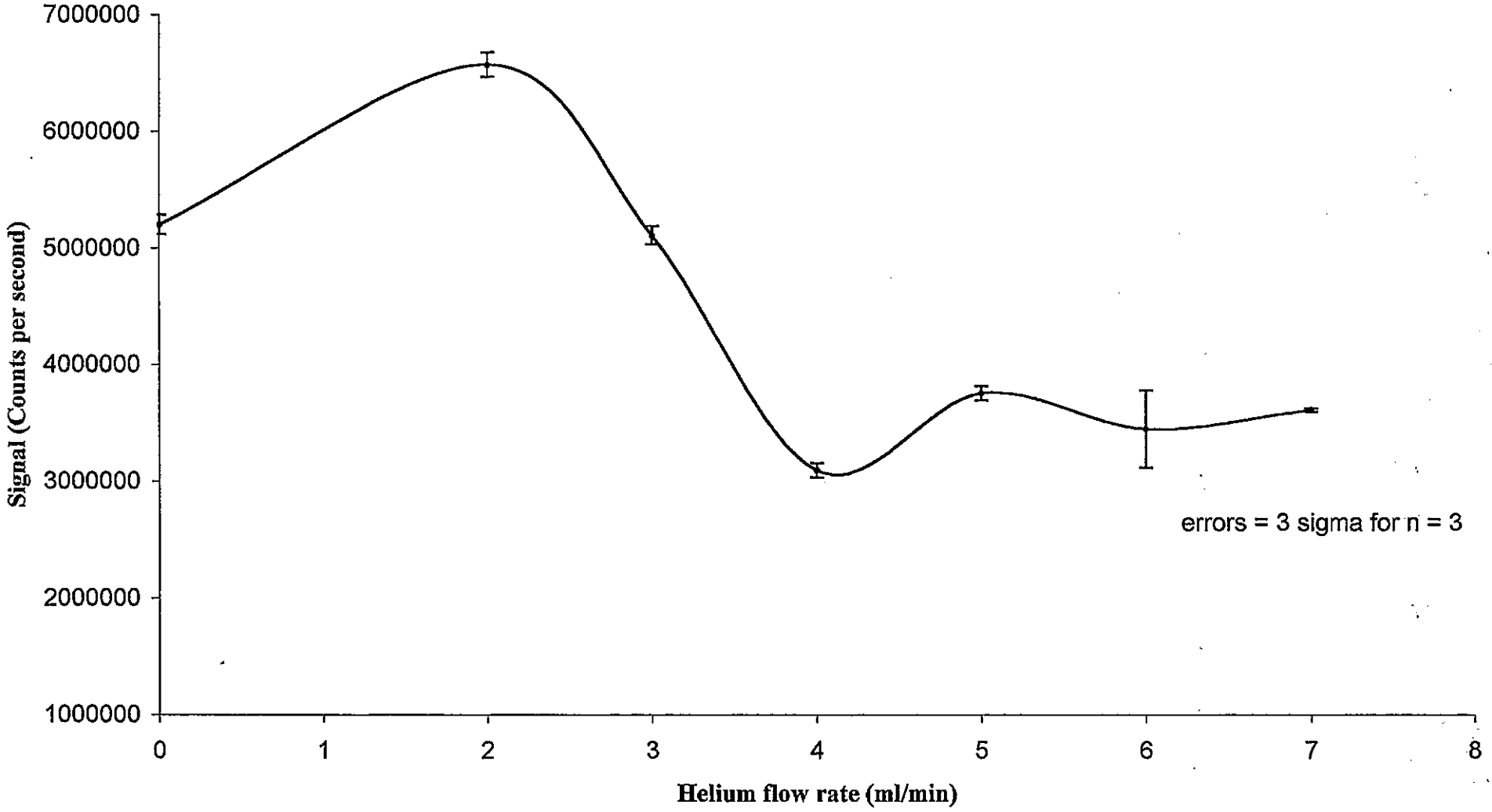

Figure 3.6: The effect of Helium flow rate on the ClO^+ signal

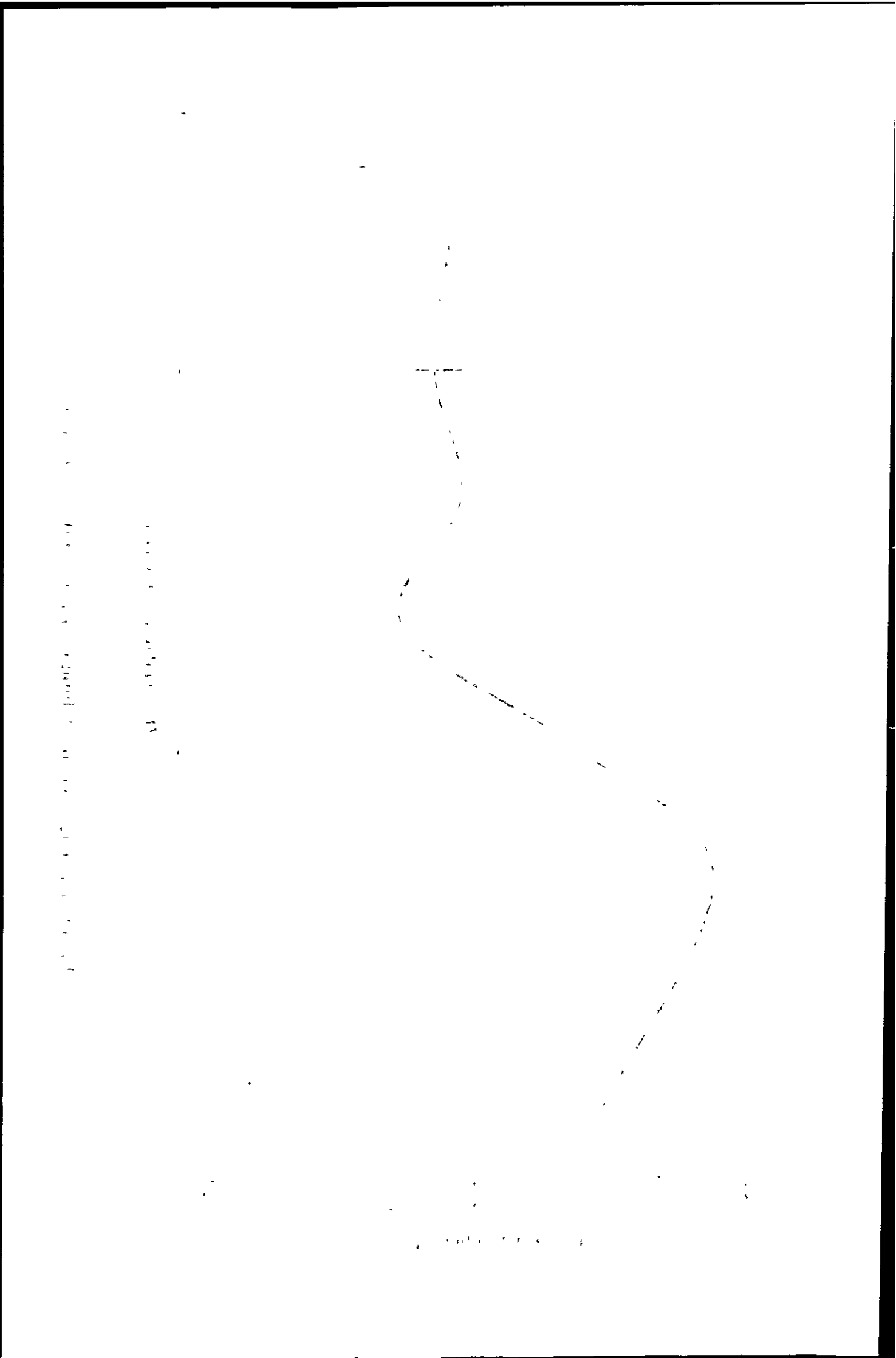

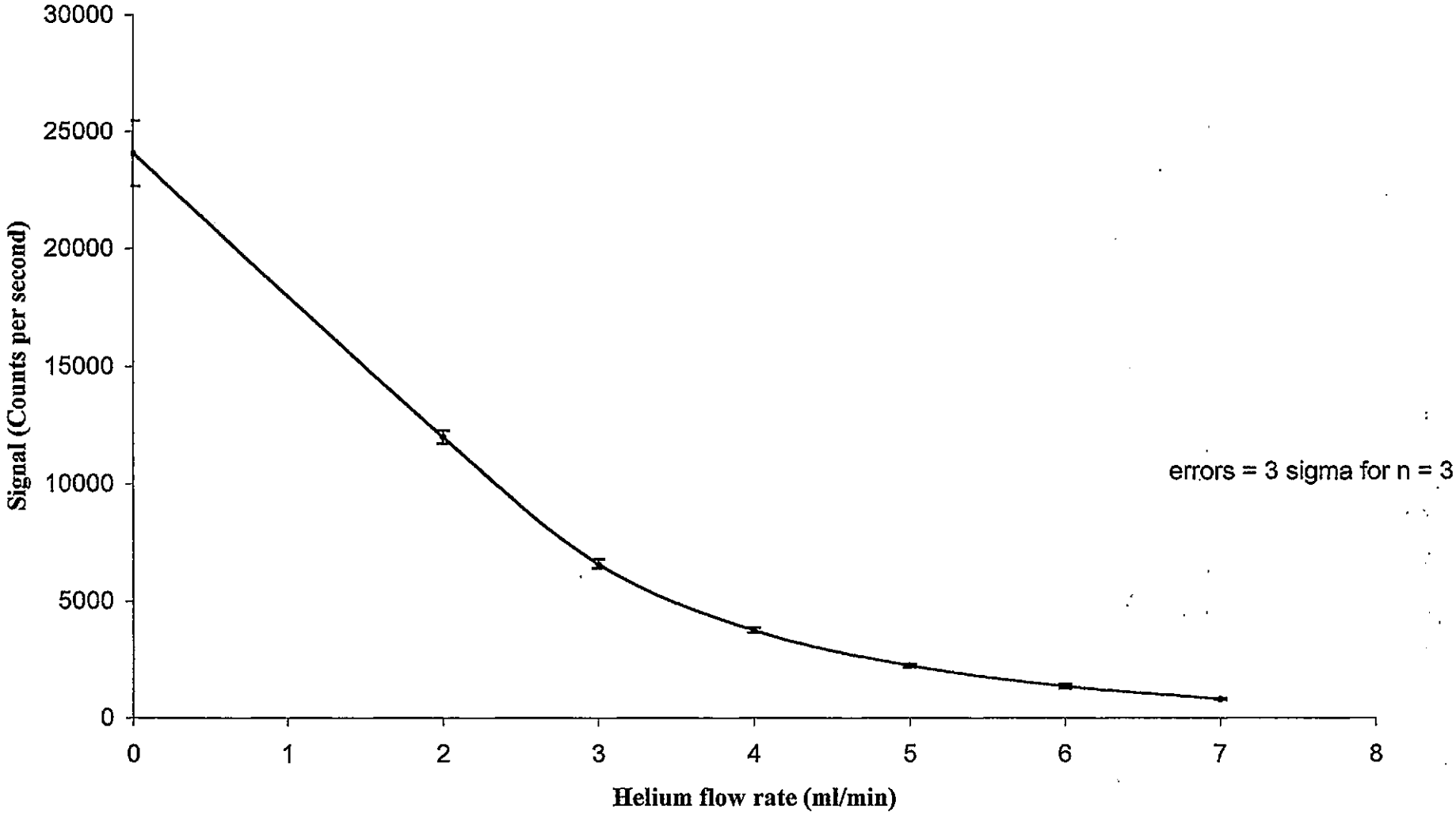

Figure 3.7: The effect of Helium flow rate on the $ArCl^+$ signal

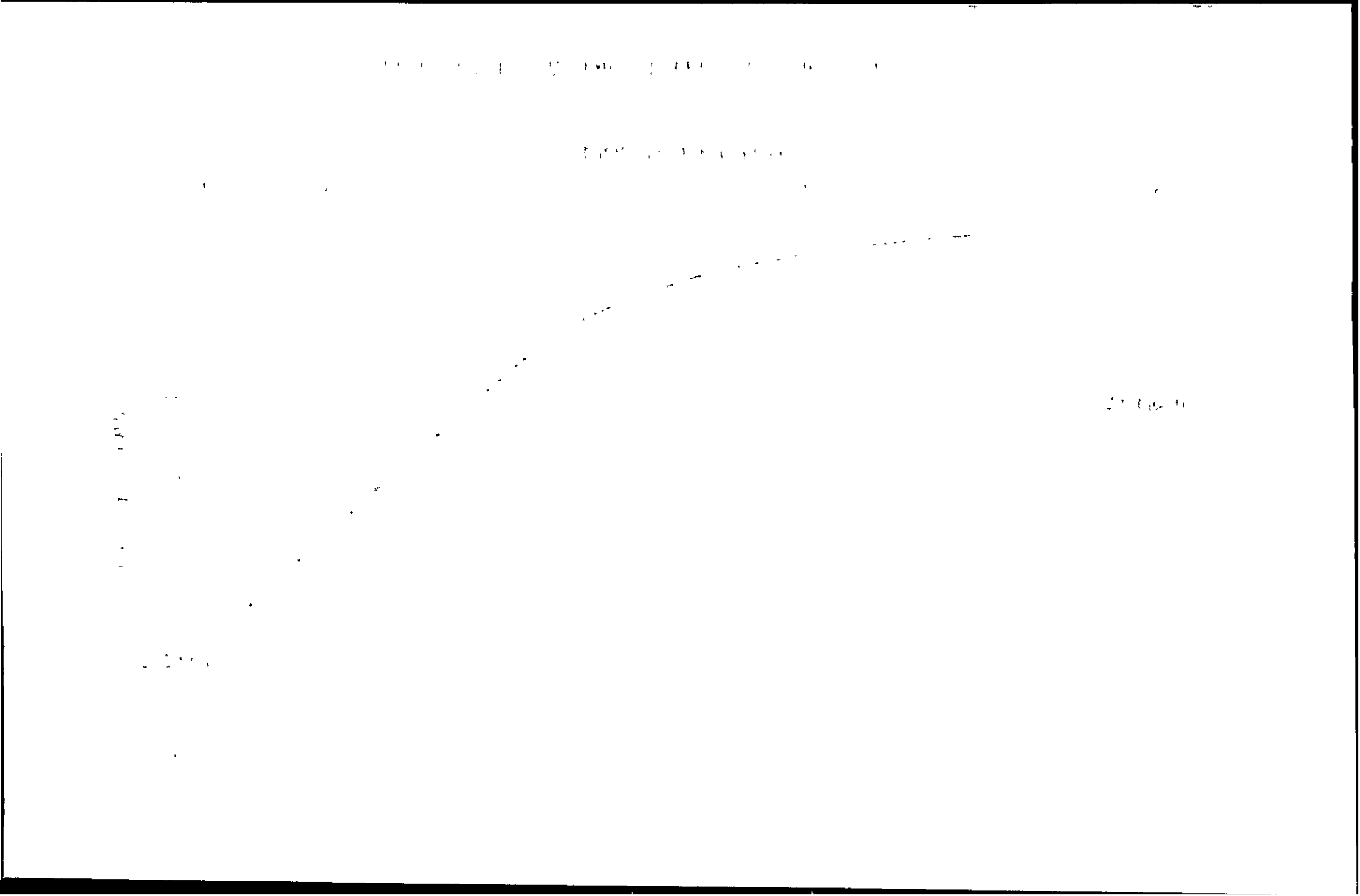

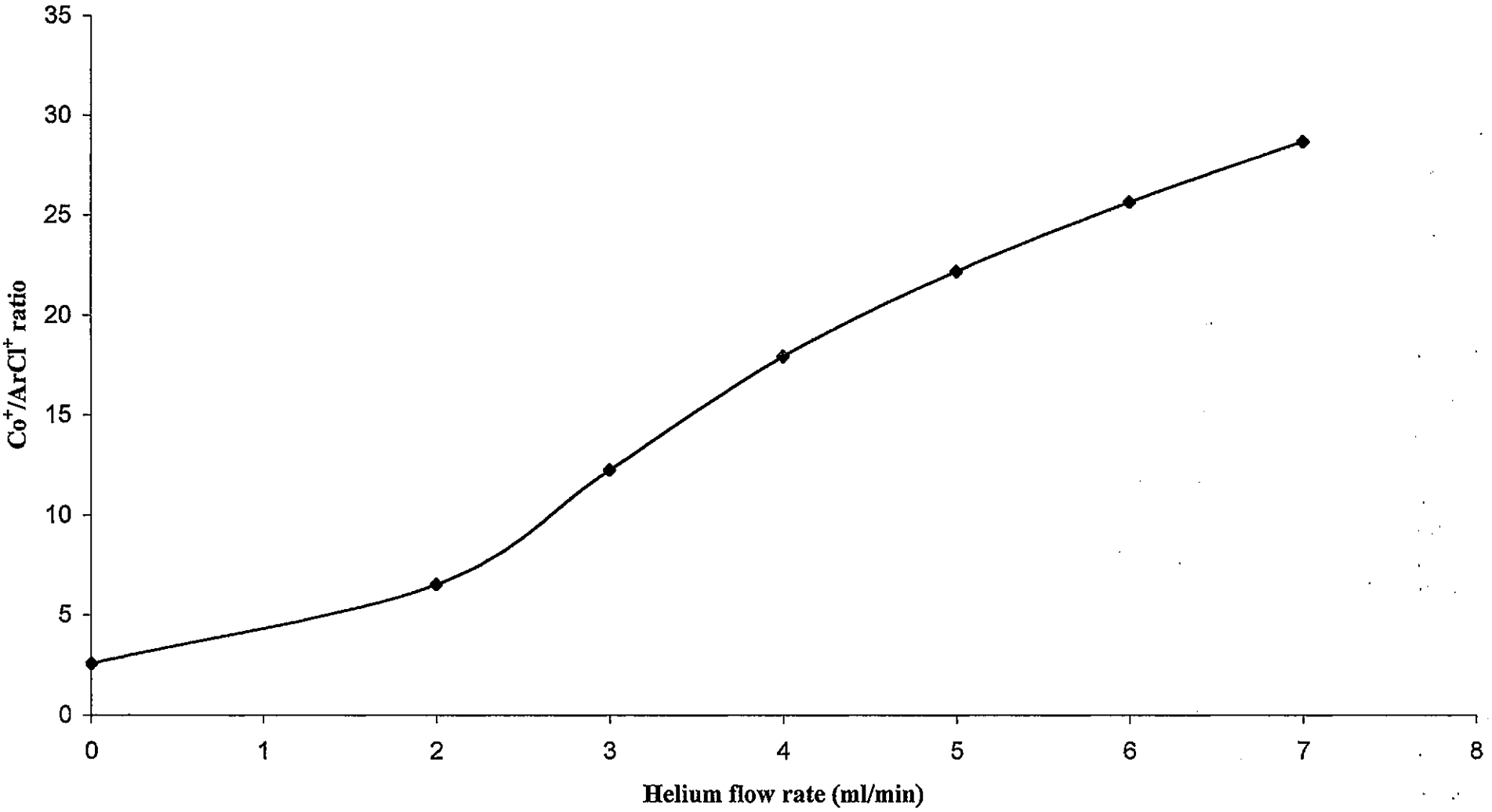

Figure 3.8: The effect of Helium on the $^{59}Co^{+}$: $ArCl^{+}$ ratio

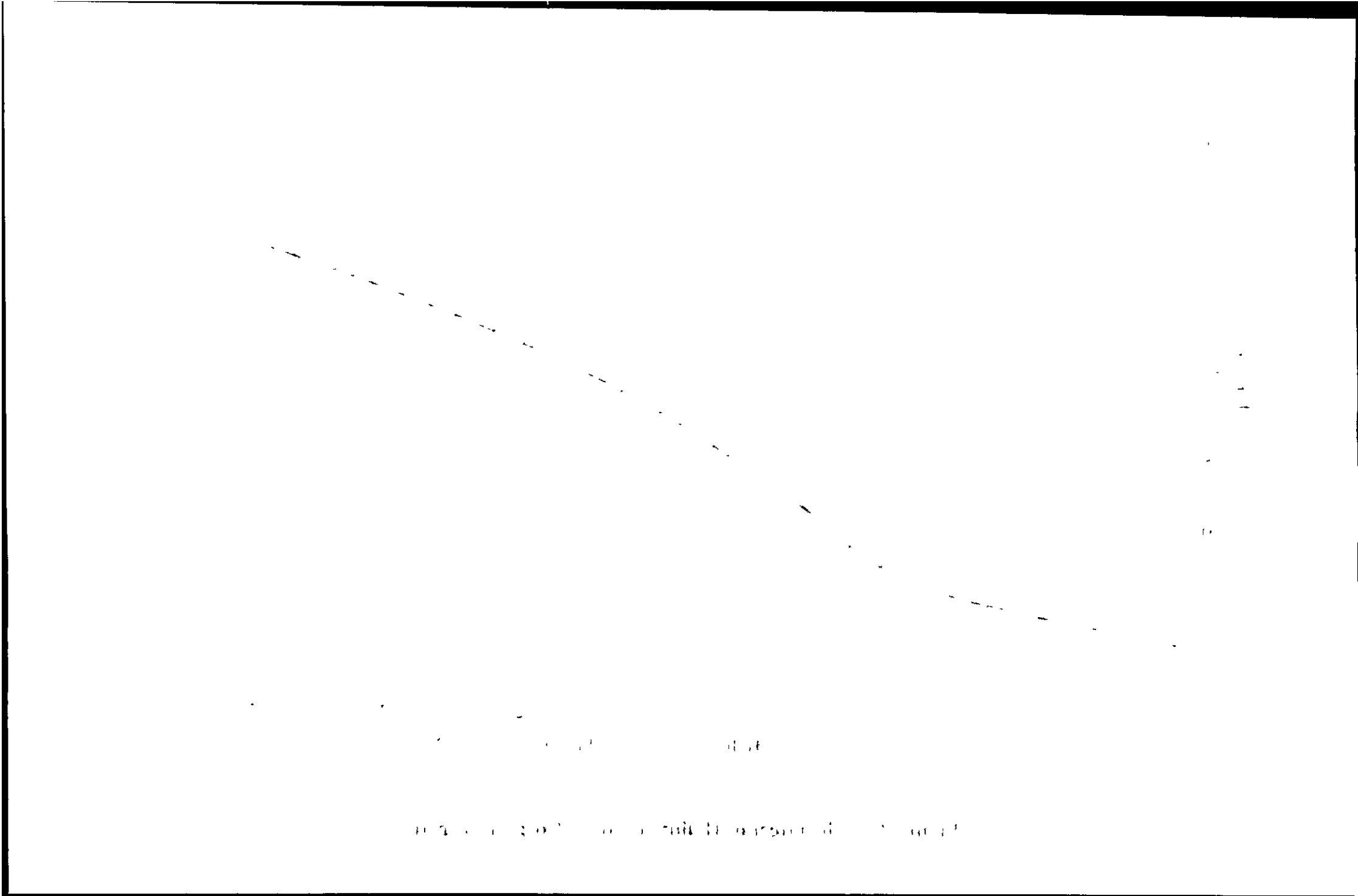

Table 3.2. Also shown in Table 3.2 are the limits of detection determined for arsenic in 2 % HNO_3. The use of the collision cell offers no advantage for the determination ofarsenic in nitric acid over conventional operating conditions because the limit of detection is virtually the same. Note that the limit of detection for arsenic in 2 % HCl using helium in the collision cell was the same as the normally attainable limit of detection for arsenic in the absence of chloride i.e. in 2% HNO_3. Thus, the use of a collision cell will allow the determination of arsenic in matrices that are high in chloride.

3.3.4: The effect of He in the collision cell on the ArC^+ signal

In an organic matrix, carbon based polyatomic ions interfere with the determination of some analytes. The formation of ArC^+ results in the direct spectral overlap interference with $^{52}Cr^+$. The effect of helium in the collision cell on the ArC^+ signal obtained while aspirating a 1 ng ml^{-1} tune solution spiked with 1 % methanol is shown in Figure 3.9. As the helium flow rate was increased, the ArC^+ signal decreased with the most dramatic reduction occurring between 0-3 ml min^{-1}. This decay is probably caused by the rapid reaction of contaminants in the collision gas with the ArC^+ and after this the decay is less rapid as the reaction of any chromium in the acid is slower or does not occur. Figure 3.10 shows the effect of helium on the Co^+:ArC^+ ratio.

Under conventional operating parameters a limit of detection for $^{52}Cr^+$ in a standard solution spiked with 1 % methanol of 0.2 ng ml^{-1} was obtained. This detection limit was improved to 0.02 ng ml^{-1} using a pressurised collision cell due to the reduction of the ArC^+ signal.

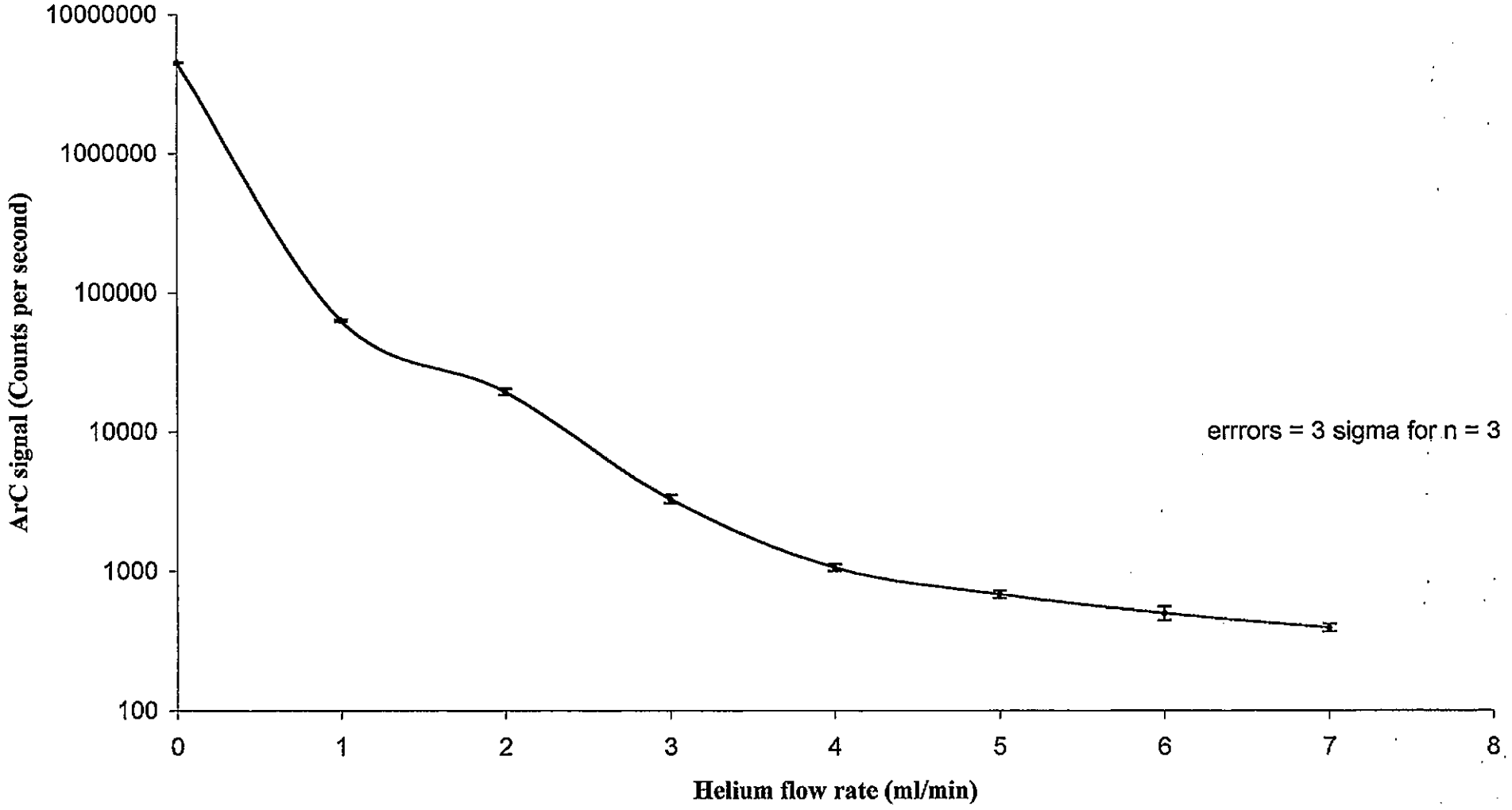

Figure 3.9: The effect of Helium on the ArC^{+} signal

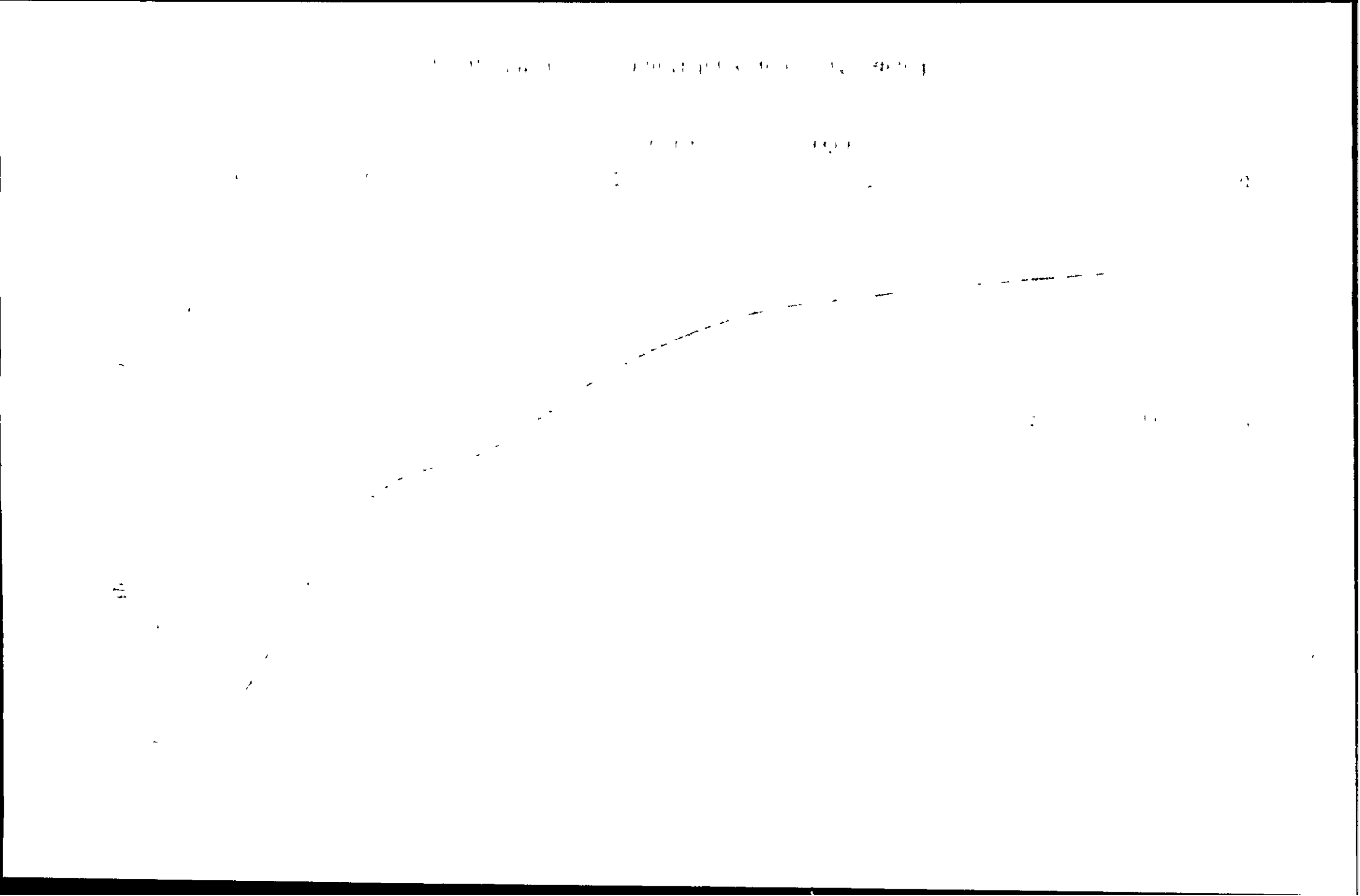

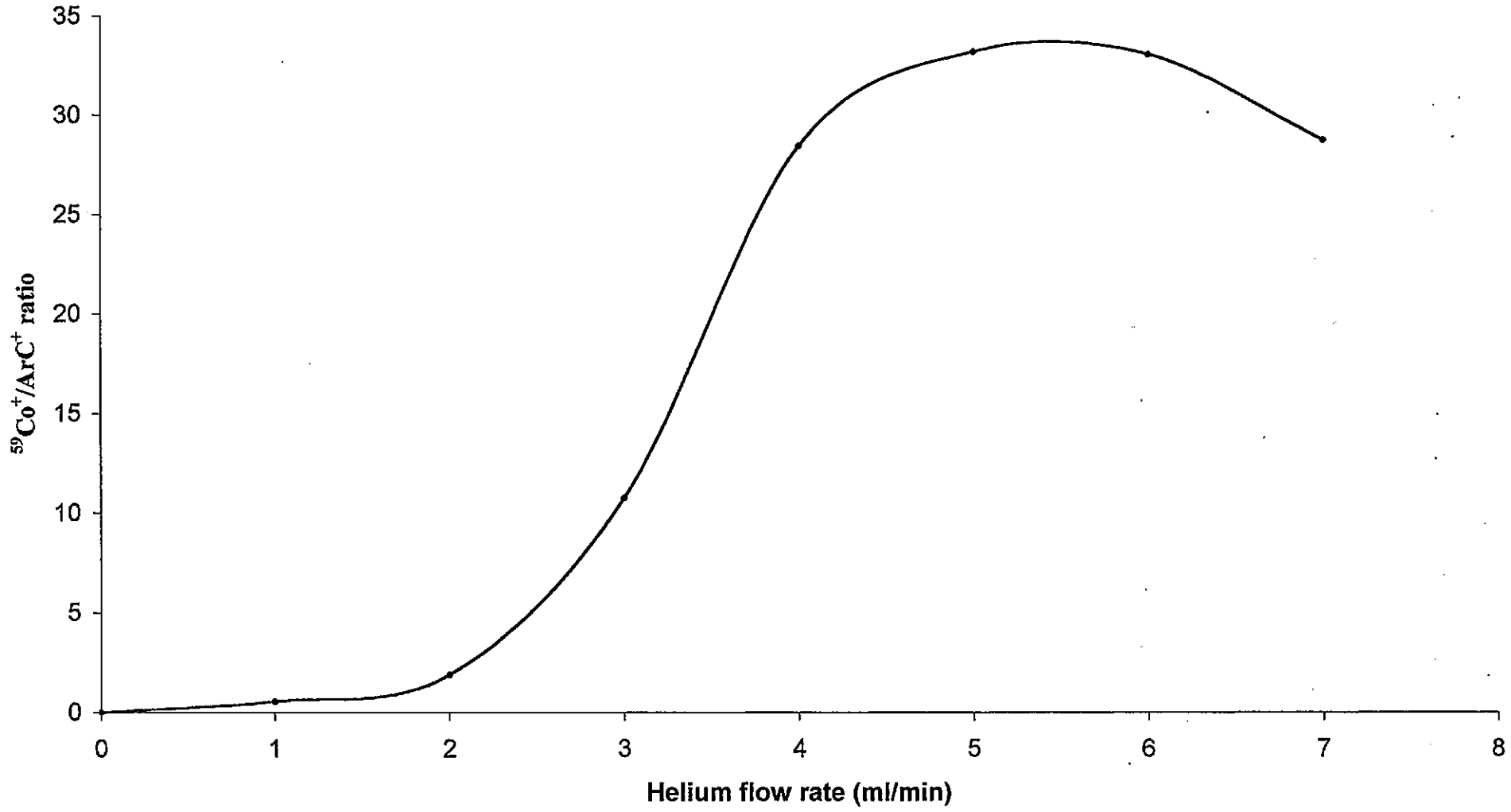

Figure 3.10: The effect of Helium on the $^{59}Co^{+}$:ArC^{+} ratio

3.3.5: The effect of He in the collision cell on various analyte signals

Figure 3.11 shows the effect helium in the collision cell had on the response, in counts per second, on Li^+, Co^+, Pb^+, Bi^+ and U^+ while aspirating a 2% (v/v) HNO_3 acid solution in which the analyte ions were present at a concentration of 1 ng ml^{-1}. The instrument was tuned at each helium flow rate to give the maximum $^{59}Co^+$ response. Figure 3.11 shows that the response of all the ions on pressurising the collision cell with helium was improved, to various degrees, compared with their response for the unpressurised collision cell. Helium in the collision cell had the least improvement on the $^7Li^+$ and $^{238}U^+$ signals. While the greatest improvement occurred for the $^{208}Pb^+$response, which was improved by a factor of almost 5, and the $^{209}Bi^+$ response, which was improved by a factor of 7. Uranium having a larger kinetic energy (due to its higher mass) is not significantly affected by the collisions with He and therefore no improvement in its signal was observed. It would be expected that U^+ at higher He flow rates to be thermalised and hence its signal to increase. Thus, the reason for the decrease in the signal at 4 ml min^{-1} is unclear. The reason for Li^+ being unaffected by the collision gas is also unclear. Collisional focusing should be effective for all ions of mass greater than the collision gas[162]. Furthermore, with the quadrupole operated at a negative pole bias with respect to the hexapole, all ions from the ICP which have lost kinetic energy in the collision cell should be able to pass into the quadrupole for mass separation and detection. The slight improvement of the atomic analyte ion signals occurs due to collisional focussing of the ions in the collision cell. As the ion beam from behind the skimmer cone is directed into the RF hexapole collision cell the ions undergo collisions with the helium gas. The presence of the RF field ensures that the scattered ions are focused back towards the axis of the hexapole where further collisions will take place. Each collision results in the ions losing kinetic energy and after sufficient collisions have occurred the comparatively wide and energetic ion beam

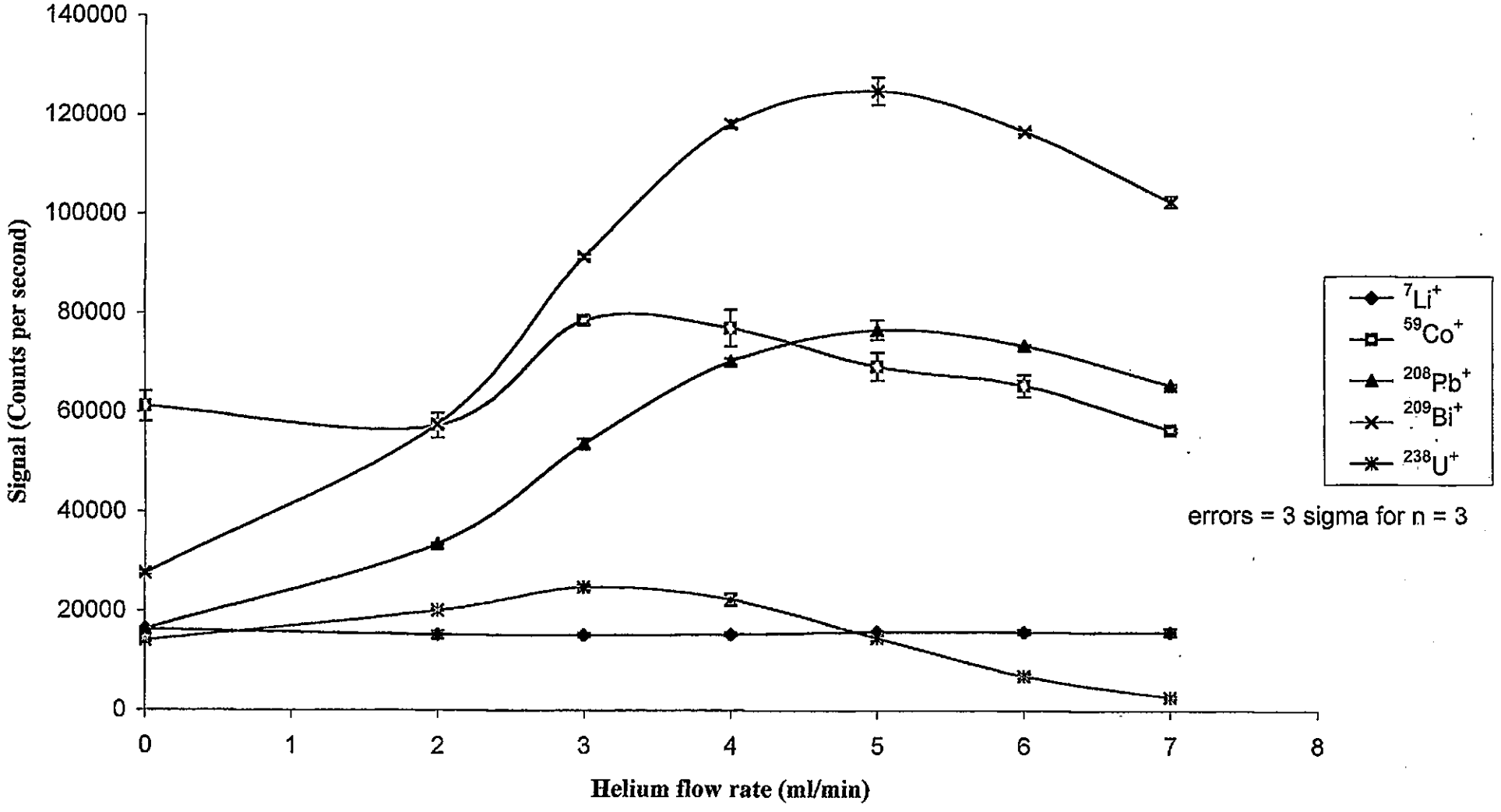

Figure 3.11: The effect of Helium flow rate on various atomic analyte ions present at a concentration of 1ng ml^{-1}

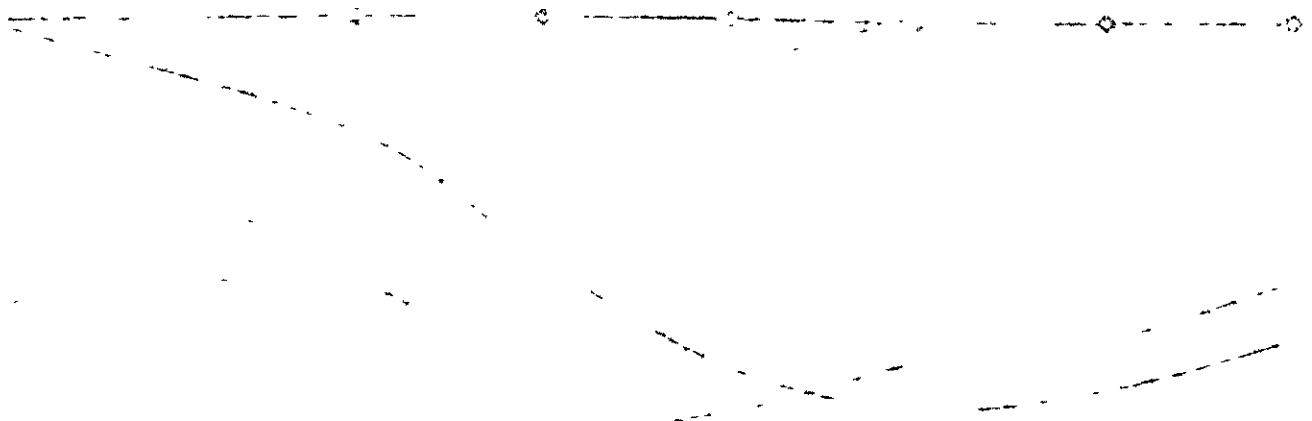

becomes an ion beam with a much narrower spread of kinetic energies. This beam is easier to focus and thus the transmission and hence signal of the ions is increased.

3.4: Conclusions

The pressurisation of a hexapole collision cell with helium is effective in the removal of a range of polyatomic ion interferences and thus offers improved limits of detection for standard solutions. The use of the hexapole collision cell also resulted in a slight improvement of the analyte signals. The use of a collision cell has facilitated the analysis of calcium and selenium at m/z 40 and 80, respectively, which could not be achieved under conventional operating conditions, as the background signals are too large. Furthermore it has been demonstrated that a collision cell will facilitate the analysis of a range of samples for elements that were previously difficult, e.g. arsenic in a chloride matrix and chromium in a carbon matrix.

CHAPTER 4: THE SIGNIFICANCE FOR MEMORY IN ICP-MS OF MATERIAL DEPOSITED ON THE SKIMMER CONE

4.1: Introduction

The main success in the development of ICP-MS was the development of a suitable interface. The interface allows the coupling of the ICP source at atmospheric pressure, with the mass spectrometer at high vacuum, while maintaining a high degree of sensitivity. The interface consists of a water cooled nickel sampling cone, which has an orifice of approximately 1 mm in diameter, positioned in close proximity to the ICP. The pressure behind the sampling cone is reduced using a rotary vacuum pump. The creation of this pressure differential causes ions from the plasma and the plasma gas itself to be drawn through the sampling orifice and expand to form a shock wave structure. The region within this expansion cone is called the zone of silence which is representative of the ion species to be found in the ICP. The skimmer cone, which lies about 7 mm behind the sampling cone, protrudes into the zone of silence. The ions from the zone of silence pass through the orifice into a second intermediate vacuum chamber as an ion beam. The extracted ions are then focused by a series of electrostatic lenses into the mass spectrometer. This ion extraction process is one of the most critical aspects of ICP-MS while being the least understood process that occurs in an ICP-MS instrument.

Unfortunately, not all the ions passing through the skimmer cone are attracted by the voltage applied to the ion lenses and transmitted to the mass analyser. The overall transmission and detection efficiency from the skimmer to the mass analyser is around 1 analyte ion detected for every 500 - 5000 ions passing through the skimmer[112]. This low transmission is attributed to space charge effects in the ion beam leaving the skimmer. The beam passing through the skimmer has approximately equal numbers of ions and

electrons. However, as the gas pressure and density in the beam decreases behind the skimmer the mobility of electrons increases. As a result of the electrons having higher mobility than ions they are lost to the walls of the skimmer. This leaves a beam behind the skimmer with an excess of positive charge. There is an electrostatic repulsive force between the ions, which causes ions to be deflected and lost from the ion beam. Olivares and Houk[113] first suggested that space charge effects maybe important in ICP-MS. They found that the ion current measured at the entrance of the mass spectrometer ion optics was less than was estimated from gas dynamic theory. Tan and Horlick[36] observed that the transmission efficiency was dependent upon the mass of the ion and that the addition of a concomitant element affected the transmission of the target element and this effect was dependent upon the mass of the concomitant element. Gillson *et al.*[40] provided a theoretical and experimental study to attribute the matrix effect to changes in the flux and composition of the ion beam. These changes arise due to space charge effects within the skimmer.

Material deposited on the skimmer from a heavy matrix may revolatilise and contribute to memory effects [186] (Figure 4.1). Lithium[187] and uranium[115] have been reported to be deposited on the skimmer cone and contribute to memory. The effect has been attributed to residual ions being trapped in the boundary layer that forms along the edges of the sampling orifice[115]. Those ions sampled from the plasma and those entering the quadrupole following revolatilisation from the skimmer cone will have different ion kinetic energies. If the kinetic energy of ions deposited on the skimmer cone are too low they may not posses sufficient energy to enter the quadrupole and be detected and thus make no significant contribution to a memory effect.

The kinetic energy is the energy an ion possesses as a virtue of its motion. Ions gain kinetic energy from the positive plasma potential and when the ions leave the plasma they gain kinetic energy during the expansion of the plasma into the vacuum.

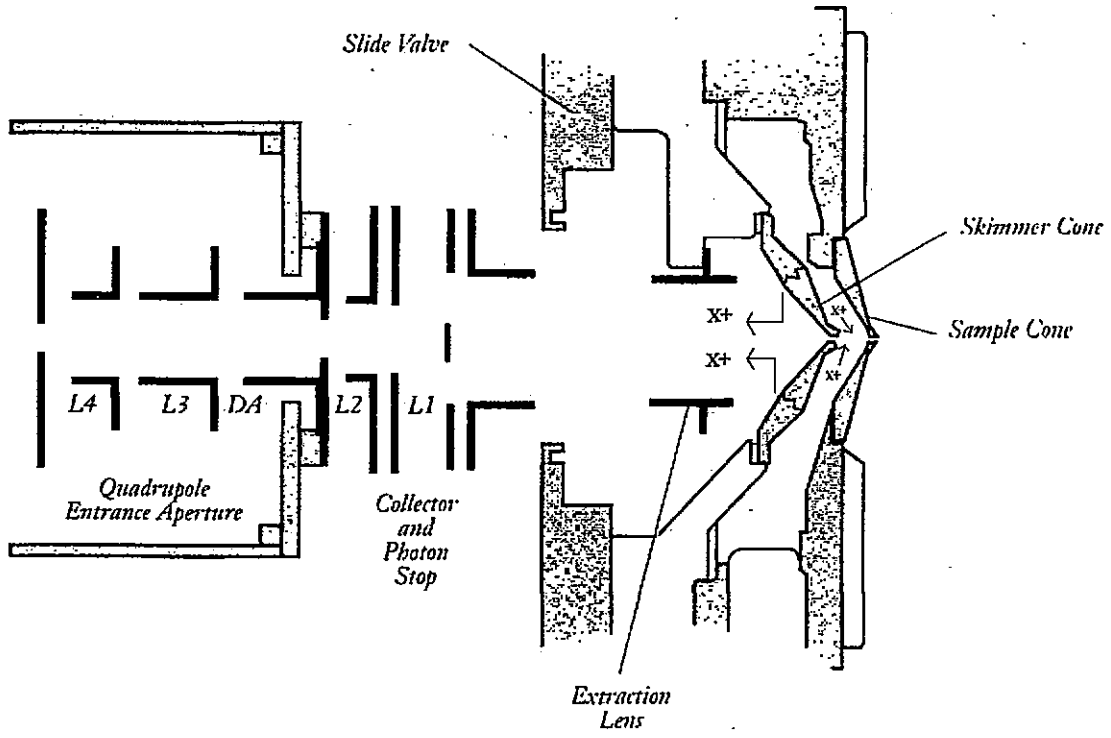

Figure 4.1: A schematic of the skimmer memory effect. Ions deposited on the skimmer cone (x^+) may re-volatilise and enter the detector for mass separation and detection along with ions sampled from the plasma and thus give an erroneously large signal for a particular analyte (x^+).

(Adapted from reference 187)

The ions are then attracted by the voltage on the extraction lens and their kinetic energy, KE, is the product of their charge, z, and the accelerating voltage, V:

$$KE = zeV = 0.5mv^2$$

Where v is the velocity of the ion after acceleration, m is its mass and e is the electronic charge ($e = 1.60 \times 10^{-19}$ C).

Hence, there are three contributions to the kinetic energy of the ions:

1. as a result of the plasma potential;
2. during ion extraction through the interface;
3. as result of acceleration, primarily by the extraction lens.

It is important to know the ion kinetic energy of ions extracted from the plasma, because this influences the ease of operation. A spread in kinetic energies will affect the sensitivity and resolution of the quadrupole mass analyser. Ion kinetic energies have been reported for a number of different ICP-MS instruments [42, 188, 189, 190, 191]. Various approaches have been taken but in all instances ion kinetic energy measurements are made by placing a retarding potential on a lens element, increasing the potential gradually, and observing the ion transmission as a function of this potential which gives rise to an ion stopping curve. Ion kinetic energies have been obtained by applying a retarding DC quadrupole rod bias to the analysing quadrupole[42, 188, 189]and by placing a small orifice retarding plate in front of the mass analyser [191]. There are several drawbacks in using the pole bias as a retarding device. Firstly, even at a very high positive pole bias the transmission of ions is not totally suppressed and there is some residual current even at 20 V. This is particularly true for heavier ions. Secondly, this method gives different quantitative results due to focusing effects within the quadrupole. To overcome these problems Douglas[192] described the use of a three lens ion stopping grid for kinetic energy measurements, which was later used by Tanner[193]. In this system, in contrast to the other systems used for kinetic energy measurements, the data are not subject to bias resulting from focusing effects. Kinetic energy

measurements were originally used to assess the extent of the secondary discharge at different plasma operating powers[188]. Douglas and Fulford[189] investigated the relationship between ion mass and kinetic energy and found that the ion kinetic energy increased linearly with ion mass. Tanner[193] used ion kinetic energies to calculate a gas kinetic temperature of the ICP.

The aim of this work was to determine the ion kinetic energies of ions sampled from the plasma and those sampled from the skimmer cone. The kinetic energy of the ions sampled from the skimmer cone will determine whether they will contribute significantly to a memory effect in ICP-MS.

4.2: Experimental

4.2.1: Instrumentation

Experiments were performed using a PlasmaQuad (PQ2) Inductively coupled plasma mass spectrometer (Thermoelemental, Winsford, Cheshire, UK) with a modified lens stack.

An ion stopping curve was generated by placing three parallel grids behind the skimmer cone (Figure 4.2). The potential on the central grid is increased in small steps. Ions with a kinetic energy higher than the grid potential will pass through the grid and the count rate will be recorded. As the potential is increased eventually all the ions will be stopped from passing through the grid. A plot of the transmission versus the potential is referred to as a stopping curve. The grids either side of the central grid were grounded and provided electrostatic shielding from any electric fields from the plasma or mass analyser.

The triple grid was constructed from nickel mesh (Goodfellows, Huntingdon, UK) which had a nominal aperture of 0.34 mm, a wire diameter of 0.041 mm and an open area of 80 %.

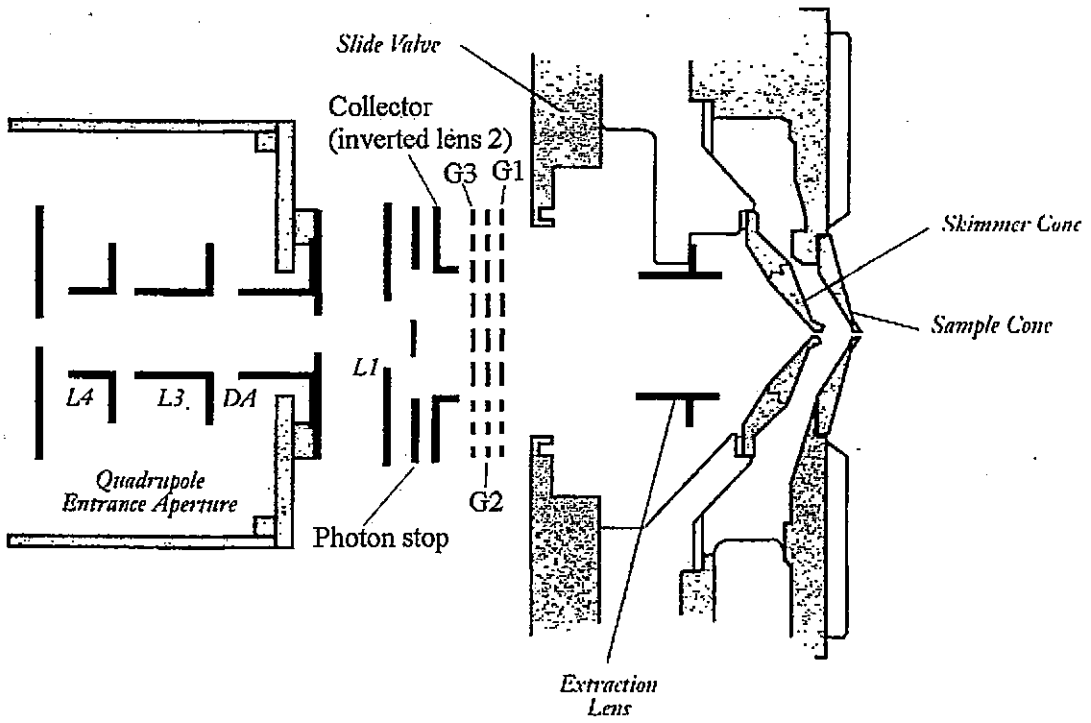

Figure 4.2: Schematic of apparatus used to measure the kinetic energy of ions. G1, G2 and G3 are nickel mesh grids with an open area of 80 %. A potential is applied to G2, the stopping grid, while G1 and G3 are grounded.

(Adapted from reference 187)

Figure 4.3 shows a photograph of the ion lens stack from the PQ2. Due to the instrumental design there is insufficient room behind the slide valve to simply extend this lens stack and add the triple grid to the end. For this reason the configuration of the lens stack shown in Figure 4.4 was adopted. The important features to note are as follows:

1. Lens 2 had the least effect on the transmission of ions under normal operating conditions, so it was removed and its voltage supply used for the stopping grid. Lens 1 was found to be crucial to the transmission of ions so was retained.
2. An inverted lens 2 replaced the collector to allow room for the three nickel mesh grids.
3. Grids 1 and 3 were grounded.
4. The distance between lens 1 and the photon stop was reduced from 1.5 cm to 1 cm. This was found to have no measurable effect on the transmission of ions.
5. The three lens stopping grid was placed behind the extraction lens. Therefore ions sampled from the plasma will have energy derived from the plasma, the initial expansion and the extraction lens, while ions sampled from the skimmer will have energy derived from the extraction lens only.
6. Apart from the extraction lens there were no other ion optics between the interface and the triple grid structure, which would act as energy filters. The potential is imposed on the extraction lens so that ions deposited on the skimmer cone will be attracted and focused into the mass analyser.
7. The remaining ion optics behind the triple grid served to focus the ions into the quadrupole for mass separation and detection.
8. The modified lens stack without the three nickel grids resulted in 80% transmission of ions compared to the normal set up.

The overall transmission of ions through the modified lens stack can be calculated assuming that the transmission through each of the grids was proportional to their open

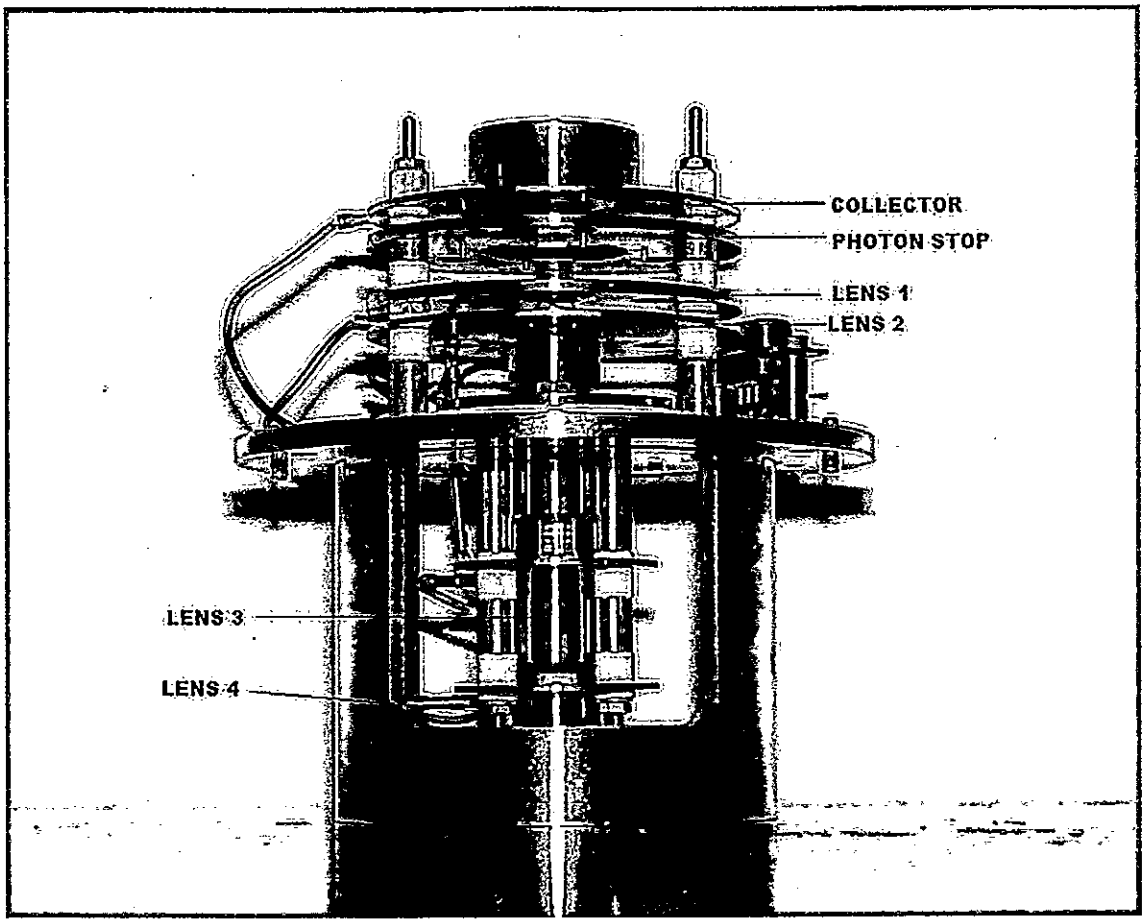

Figure 4.3: Photograph of the lens stack from the PQ2.

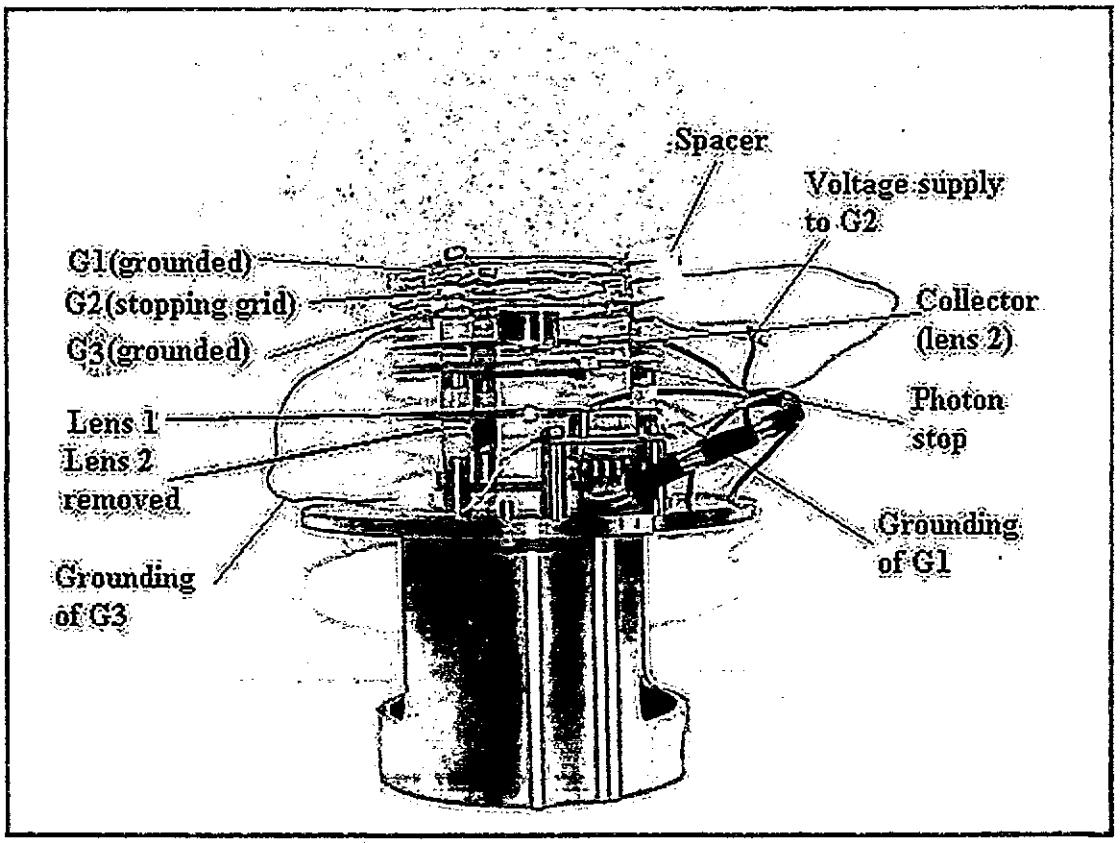

Figure 4.4: Photograph of the lens stack as set up to determine the kinetic energy of ions. G1 and G3 were grounded. G2 was attached to the voltage supply of lens 2, which has been removed. To ensure the maximum transmission of ions lens 1 was in the same position as it is usually found on the lens stack under normal operating conditions. To allow the triple grid to fit on the end of the lens stack the collector has been replaced by an inverted lens 2. Paper spacers ensure there was no contact between the three nickel grids.

area (i.e. 80 %). Hence, the overall ion transmission efficiency was 0.8^4, i.e. 41 % compared to the unmodified lens stack.

The operating conditions are shown in Table 4.1. Note that the potentials on the collector and extraction lenses were more negative than used under normal operating conditions. Under normal operating conditions a slight positive potential, 2 V, was imposed on the quadrupole (i.e. pole bias). For the determination of the ion kinetic energies using the modified lens stack the pole bias was left at 0 V so that ions were mass analysed at kinetic energies gained from the initial expansion into the vacuum chamber and from the extraction lens voltage. A 100 ng ml^{-1} In solution gave a signal of 2.4×10^5 counts per second for the modified lens stack with the triple grid compared to 6.2×10^5 cps under normal operating conditions. This was a 39 % relative transmission efficiency and was very close to the 41 % estimated.

4.2.2: Procedure

Stopping curves were generated for a 100 ng ml^{-1} solution of Be^+, Co^+, In^+, Ce^+, Pb^+ and U^+ at an extraction voltage of -300 V. This gave the ion kinetic energies of ions sampled from the plasma.

The stopping curves were generated by setting the stopping grid (G2) to a particular potential and averaging 5 measurements of each of the ions monitored. The stopping potential was incremented in equal steps (1.3 V) between 0 - 20 V and then decremented in equal steps (1.3 V) at the mid-range of the incremented steps. This was done to minimise any hysteresis. This yielded one stopping curve for each of the ions monitored. The first derivative of this curve yielded the ion kinetic energy distribution of a particular ion and the most probable energy.

In order to measure the ion kinetic energy of ions deposited on the skimmer cone controlled contamination of the skimmer cone was performed. This involved aspirating a 100 μg ml^{-1} multi-element solution for 3 hours while the extraction lens

Table 4.1: Operating conditions for the PQ2 with and without the modified lens stack

	Lens stack as normal	**Modified lens stack with triple grid**
Forward Power (W)	1350	1350
Coolant (L min^{-1})	12	12
Auxillary (L min^{-1})	0.9	1
Nebuliser (L min^{-1})	0.85	0.9
Torch	Fassel	Fassel
Spray chamber	Scott double pass at 5^0C	Scott double pass at 5^0C
Sampler	Ni 1mm orifice	Ni 1mm orifice
Skimmer	Ni 1mm orifice	Ni 1mm orifice
Extraction lens (V)	-220	-300
Collector (V)	4.78	-1.2
Lens 1 (V)	2.44	0.1
Lens 2 (V)	-9.78	-2.5 (stopping grid)
Lens 3 (V)	-7.32	0.3
Lens 4 (V)	-68.4	-54.5
Pole bias (V)	2	0
In Signal (100 ng ml^{-1} (cps))	6.2×10^5	2.4×10^5

voltage was left at -100 V and the slide valve was shut. After this time a clean spray chamber and torch were used that had been left in 10 % HNO_3 for at least 24 hours and clean pump tubing and a clean sampling cone was used. A 2 % HNO_3 solution was then aspirated and stopping curves were generated as described previously.

4.3: Results and Discussion

4.3.1: Ion kinetic energies of ions sampled from the plasma

The ions sampled from the plasma have kinetic energy derived from the plasma, the initial expansion into the vacuum chamber and the voltage on the extraction lens. Figure 4.5 a and b shows the stopping curves generated for various ions. The curves show that there was a little hysteresis in the data. This was particularly true for the Co^+ stopping curve where a clear difference in the signal obtained on the incremented steps and the decremented steps can be seen.

The stopping curves generated by this method show a sharp cut off in ion signal, except in the case of the Be^+ ion stopping curve. This is in contrast to stopping curves generated using the pole bias as a retarding device, which tend to be more exponential in shape, resulting in a more gradual decrease in the transmitted ion signal as a function of the voltage. Therefore, in this case it was far easier to determine the potential which was an indication of the most probable energy of the ions of a particular element.

The derivative plot of the stopping curves (Figures 4.6 a and b) gives the distribution of ion kinetic energies and therefore the most probable energy of the ions. The lowest kinetic energy was for Be^+ (9.5 eV) and the highest was for U^+ (12.8 eV). This is as expected as the kinetic energy of an ion is directly proportional to its mass. Figure 4.6 shows that the spread in kinetic energies for each ion was less than 3 eV. The ion kinetic energies determined in this study did not exceed 20 eV so were well within the acceptance limit for a quadrupole.

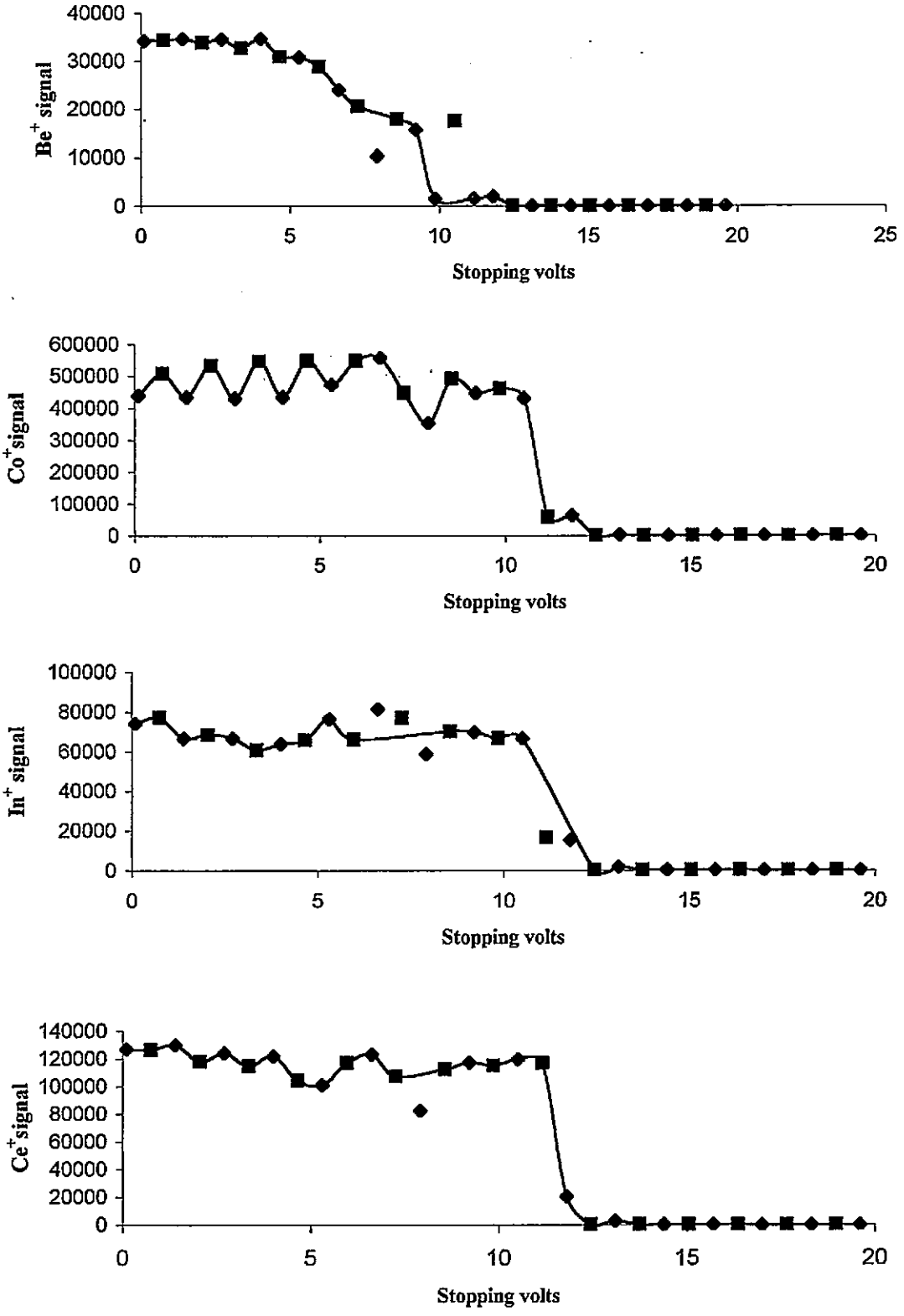

Figure 4.5a:Ion-stopping curves obtained for several ions. Data shown are the transmitted ion signals as a function of the potential applied to the stopping grid (G2).

◆ Incremental steps

■ Decremental steps

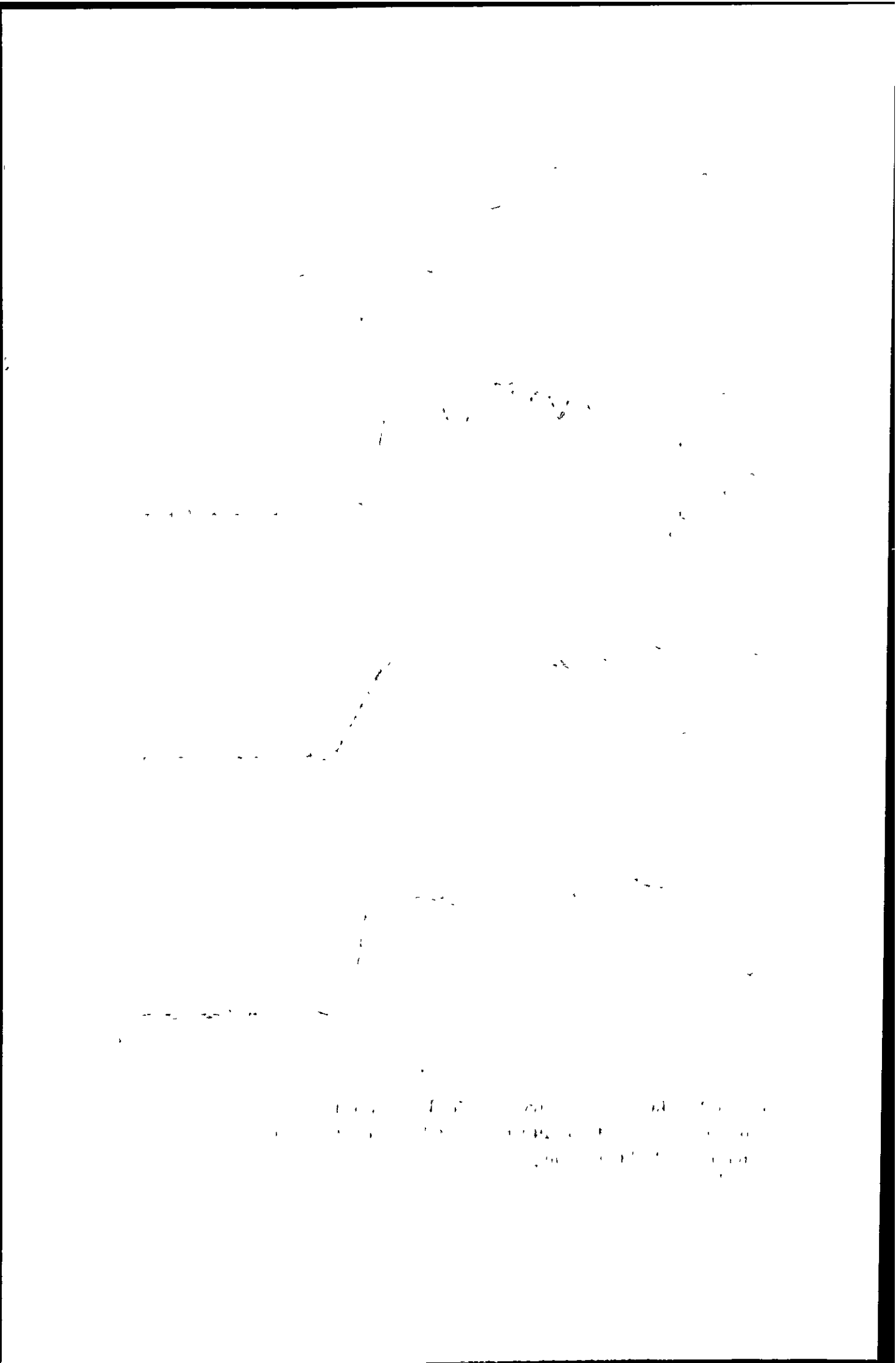

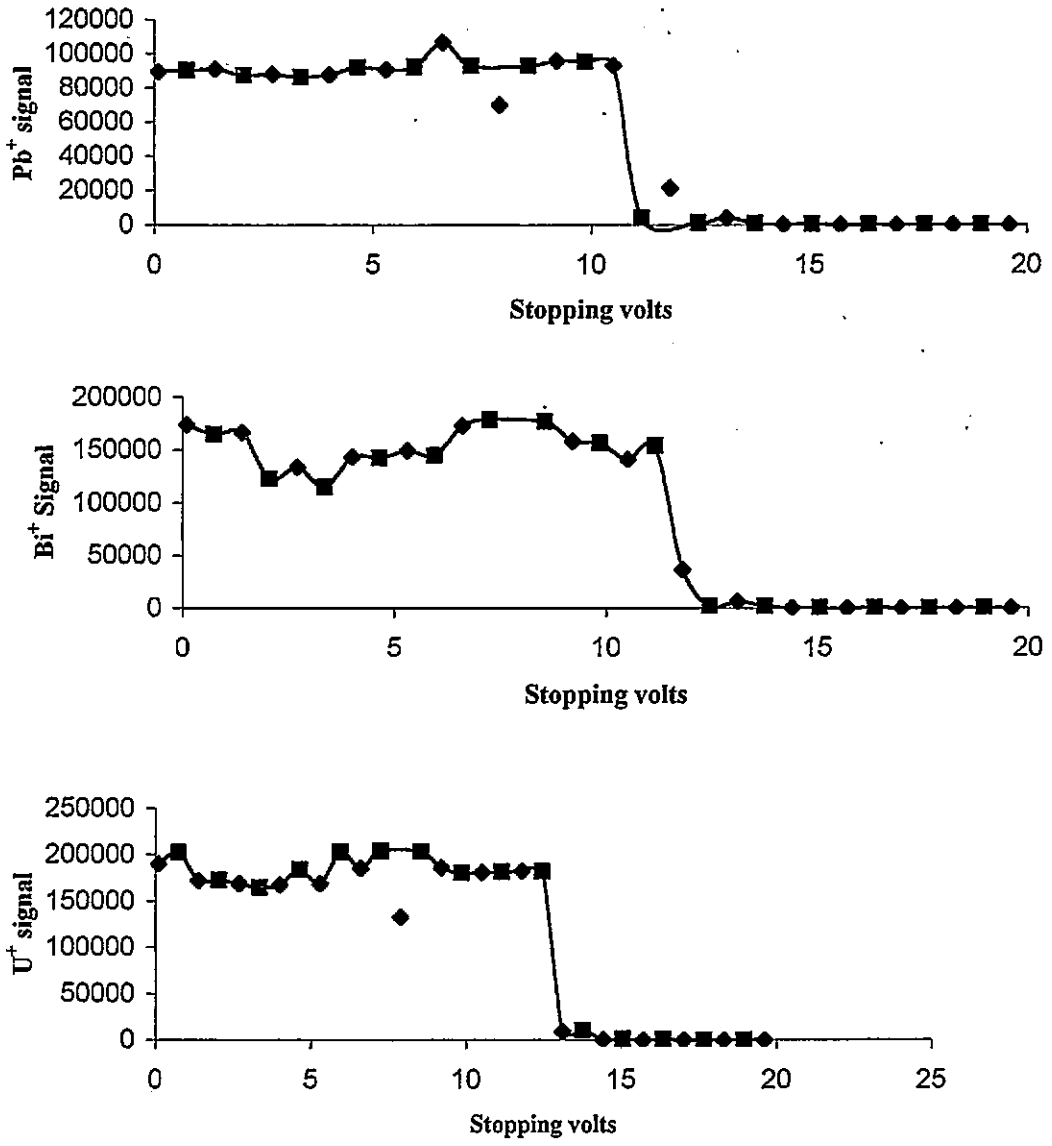

Figure 4.5b:Ion-stopping curves obtained for several ions. Data shown are the transmitted ion signals as a function of the potential applied to the stopping grid (G2).

◆ Incremental steps
■ Decremental steps

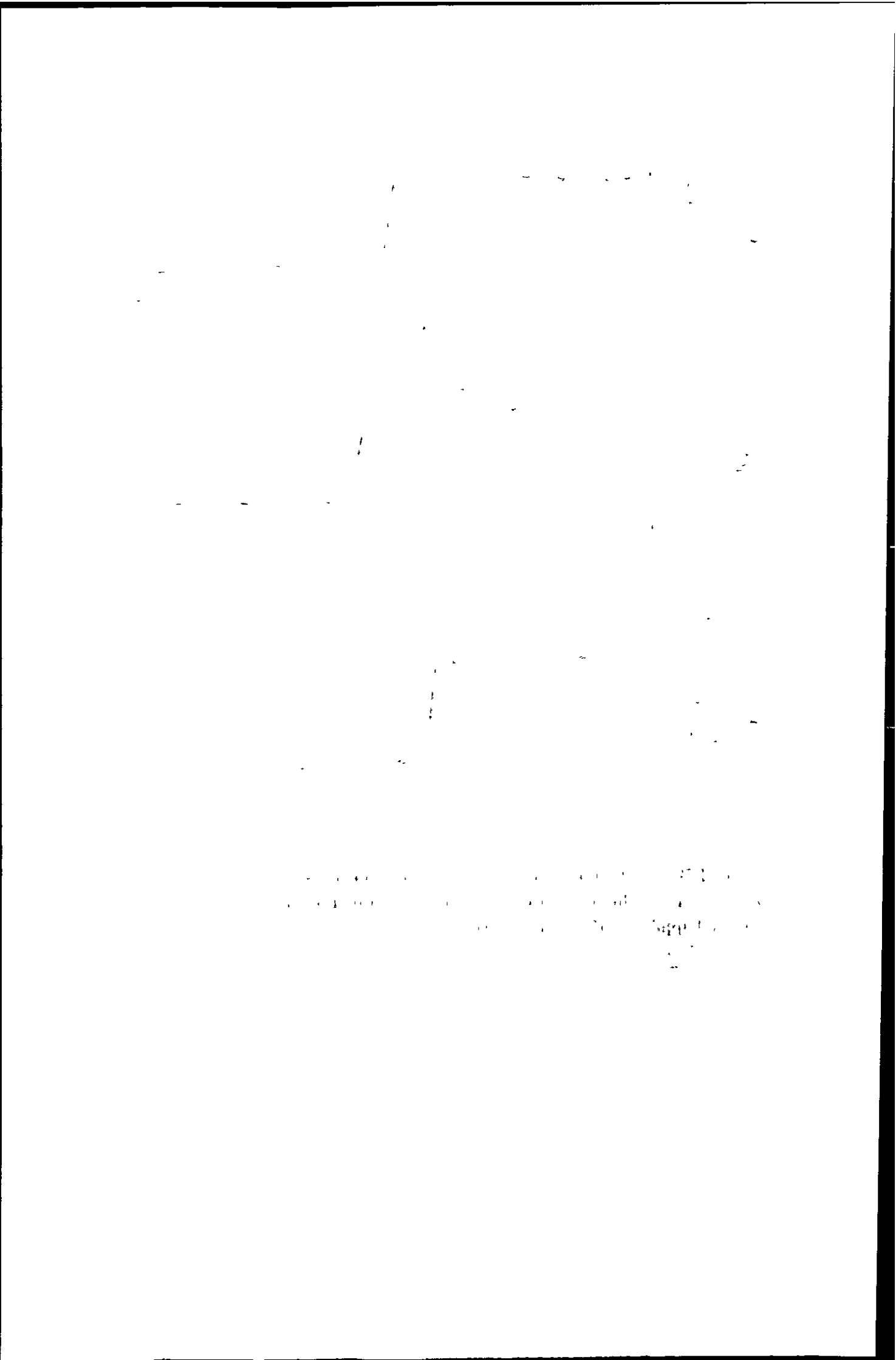

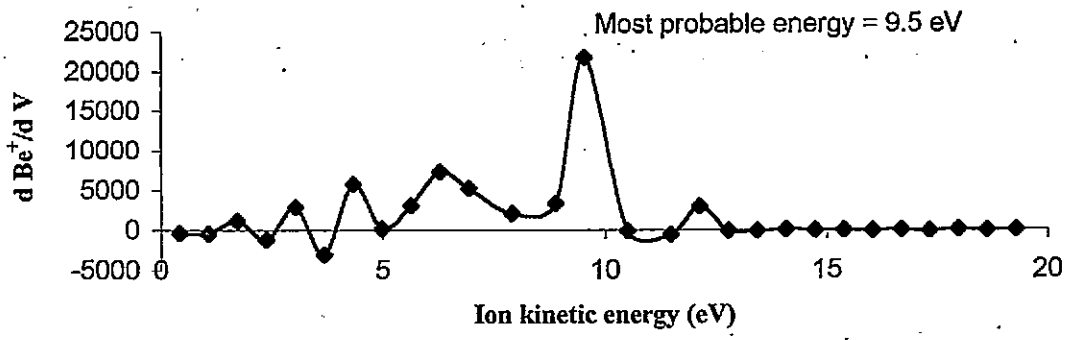

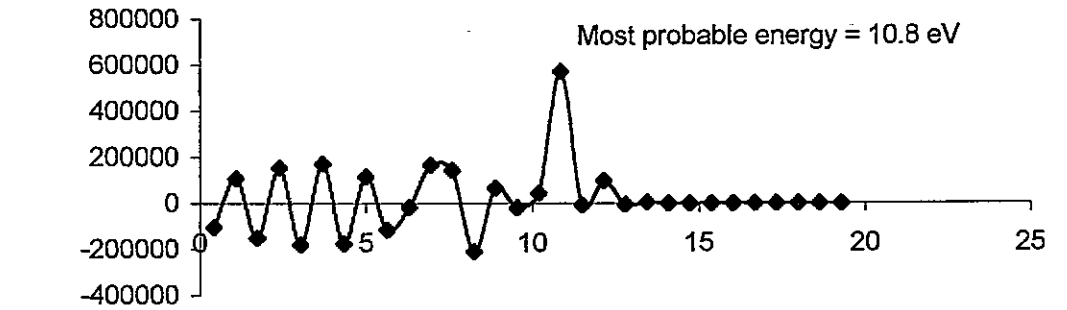

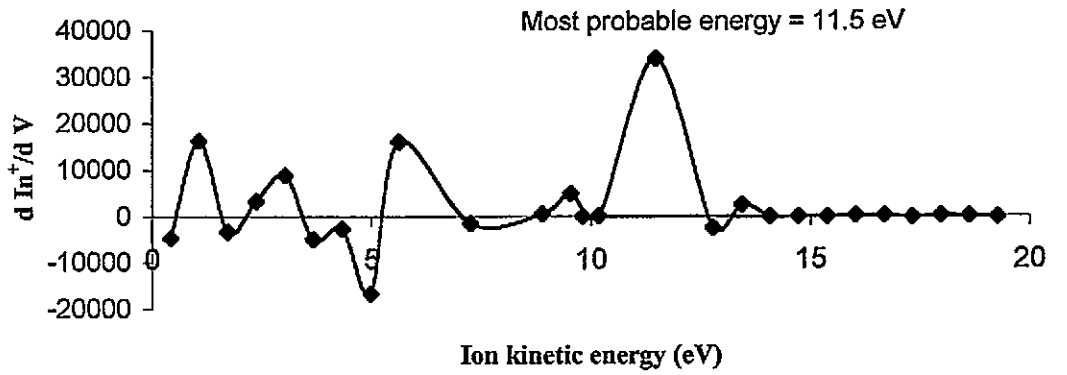

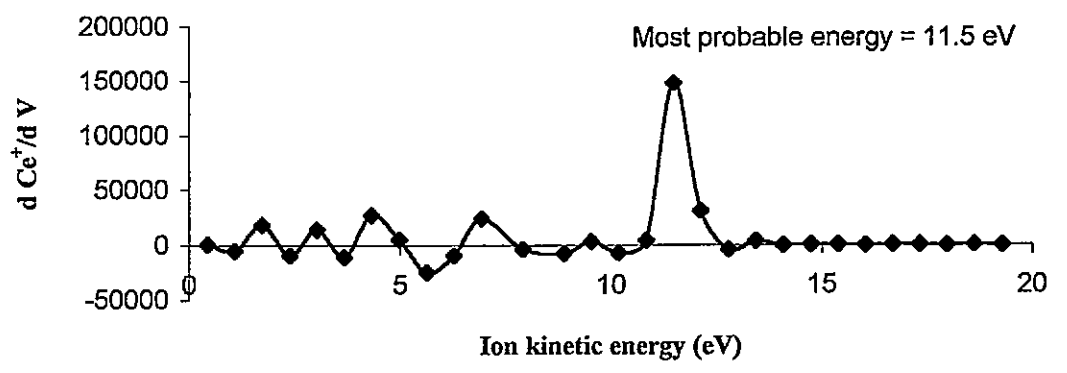

Figure 4.6a: Derivative plots of the ion stopping curves from figure 4.5a.

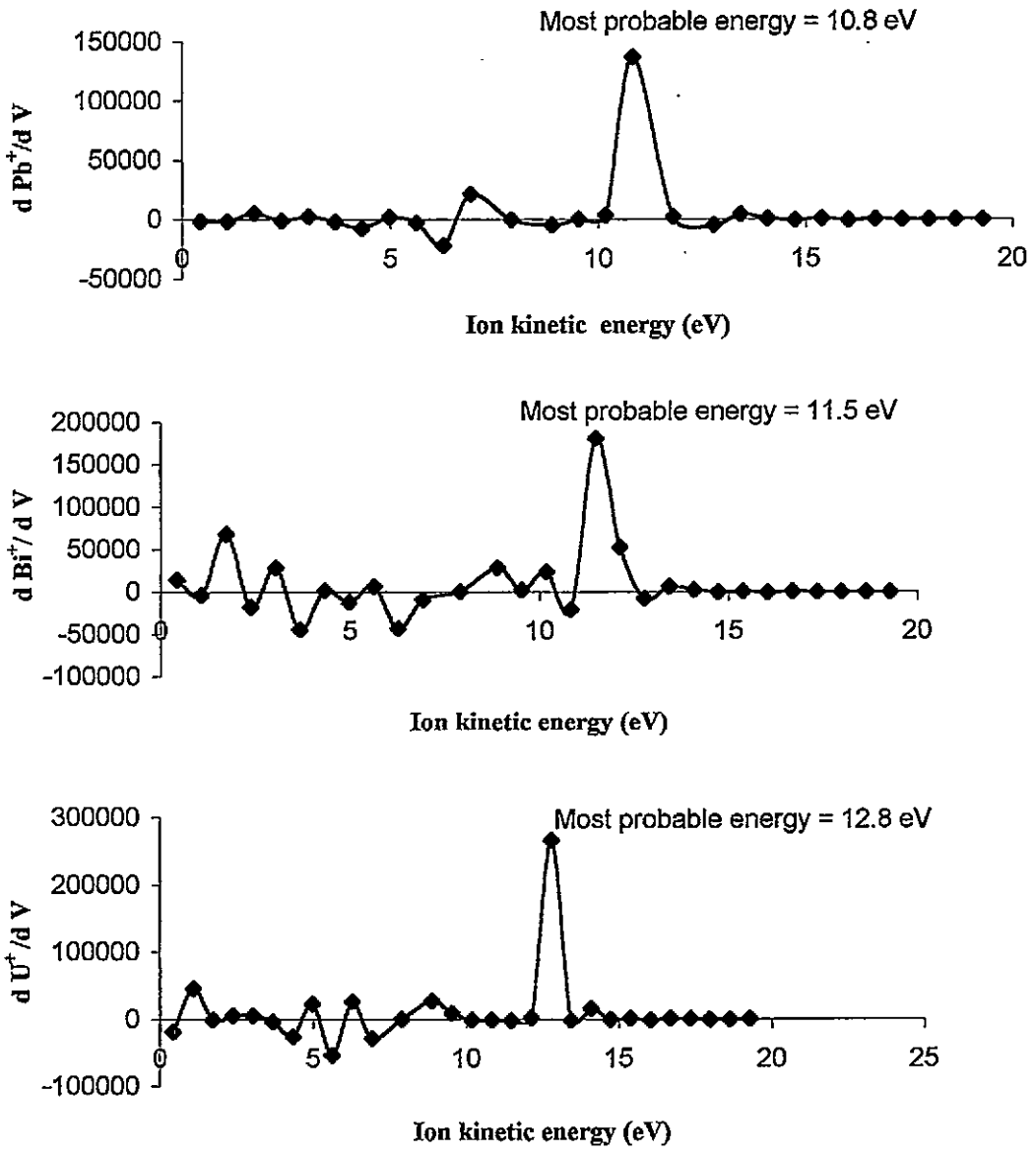

Figure 4.6b: Derivative plots of the ion stopping curves from figure 4.5b.

4.3.2: Ion kinetic energies of ions sampled from the skimmer cone

After controlled contamination of the skimmer cone, as described in section 4.2, only Be^+ gave a measurable signal. Contamination with higher concentrations lead to the sampling cone and the injector of the torch becoming blocked. The Be^+ signal rapidly disappeared upon increasing the voltage on the stopping grid, indicating the ions had a very low kinetic energy. The signal did reappear during the decremental stage in the generation of the stopping curve. After 60 minutes the signal fell back to the normal signal obtained for Be^+ in 2 % HNO_3.

Figure 4.7 shows the stopping curve generated for Be^+ during the aspiration of 2 % HNO_3 following controlled contamination of the skimmer cone. As with the stopping curves generated during the aspiration of a 100 ng ml^{-1} multi-element solution there was a sharp cut off in the ion signal at a given stopping voltage. Figure 4.8 shows the derivative of this curve. The most probable kinetic energy of the Be^+ sampled from the skimmer cone was 2.4 eV, which was significantly lower than the kinetic energy determined for Be^+ sampled from the plasma (9.5 eV). This confirms that the Be^+ memory effect was a result of contamination of the skimmer cone rather than from contamination of the 2 % HNO_3.

The kinetic energy of the ions from the skimmer cone was less than 5 eV, whereas the typical and recommended setting for the pole bias is 5 V[187]. The pole bias offsets the quadrupole above or below zero volts as a whole. It therefore alters the mean ion kinetic energy of the ions seen by the quadrupole. A positive pole bias setting will act as a retarding device to slow ions down as they enter the quadrupole so that they can experience more RF cycles for improved resolution. This is detrimental to the signal because ions with kinetic energy below the positive voltage setting will be rejected by the quadrupole because they are unstable. However, a setting of 5 V is the recommended setting on the instrument used in this study, since such a setting ensures good sensitivity and retards the ions sufficiently to give good resolution. Hence, if a

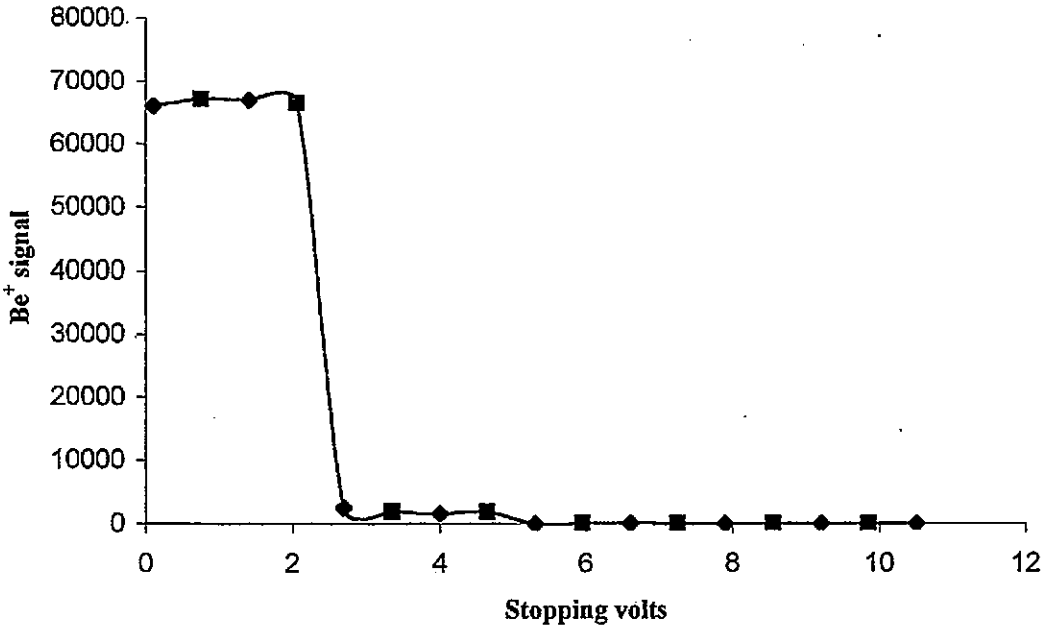

Figure 4.7: Ion-stopping curve obtained for Be^+ following controlled contamination of the skimmer cone.
Data shown is the transmitted ion signal as a function of the potential applied to the stopping grid (G2).

◆ Incremental steps
■ Decremental steps

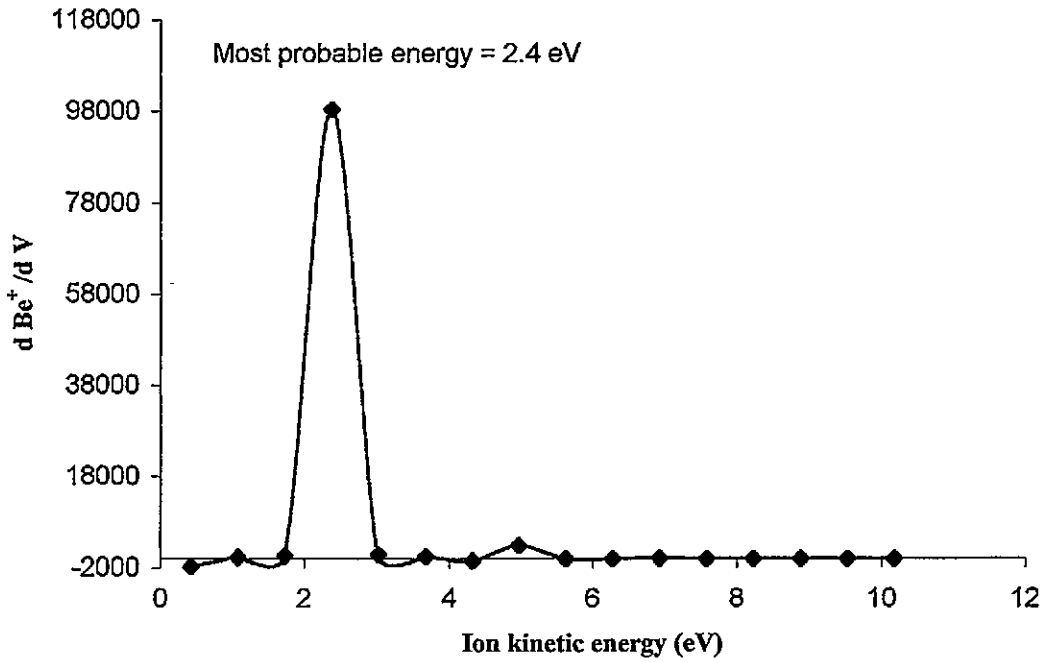

Figure 4.8: Derivative plot of the ion stopping curve obtained for Be^+ following controlled contaimination of the skimmer cone.

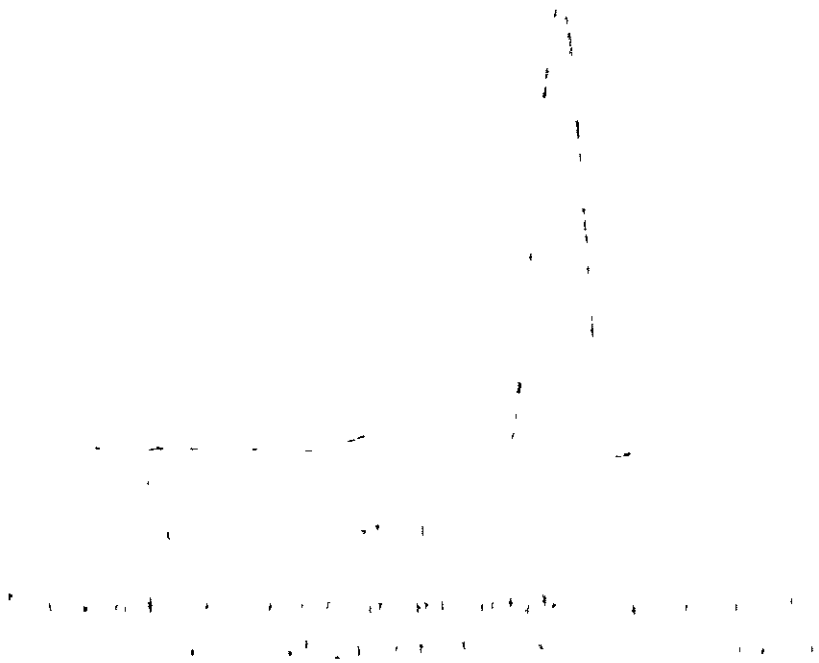

pole bias setting of 5 V was used then the Be^+ ions from the skimmer cone would have insufficient kinetic energy to enter the quadrupole for mass separation and detection. Thus they would make no contribution to the measured Be^+ signal in such circumstances and the skimmer memory effect would be insignificant.

A pole bias of zero volts means the ions are mass analysed at kinetic energies corresponding to the kinetic energy gained from the plasma, the initial expansion into the vacuum chamber and the voltages on the ion lenses. A negative pole bias only serves to increase the kinetic energy of the ions. In both these circumstances the Be^+ ions sampled from the skimmer cone would make a contribution to the measured Be^+ signal giving rise to an erroneous result and thus the skimmer memory effect could be significant.

The ion lenses will also alter the mean ion kinetic energy of the ions detected. A lens element at a more positive voltage than the ion energy (typically 8 eV to 12 eV), tends to inhibit ion transmission[187]. The operating conditions for the instrument with the normal lens stack, shown in Table 4.1, gave an optimum In^+ signal with a collector voltage of 4.78 V and a lens 1 voltage of 2.44 V. Therefore under these conditions the Be^+ ions from the skimmer cone should not be transmitted.

4.4: Conclusions

Following controlled contamination of the skimmer cone only Be^+ gave a measurable signal. The kinetic energy of these ions deposited on the skimmer cone were significantly less than those ions sampled from the plasma. The low kinetic energy of the Be^+ ions deposited on the skimmer cone means they will not contribute significantly to the signal in most instances, as they will be rejected by the quadrupole. Heavier ions than Be^+ deposited on the skimmer cone may cause a memory effect as they will have larger kinetic energies. However, the skimmer cone had no significant effect on system

memory for the other ions investigated in this study since they gave no measurable signal following controlled contamination of the skimmer cone.

If the instrument is operated using a more negative pole bias than the recommended setting, i.e. less than 5 V, in order to improve sensitivity, then the Be^+ ions will make a contribution to the back ground signal. The Be^+ ions from the skimmer cone will also be detected when the voltage on the lens elements is more negative than the kinetic energy of the ions.

In this case controlled contamination of the skimmer cone was performed in order to achieve a measurable signal, however, manufacturers are continually striving to produce ICP-MS instruments capable of achieving lower and lower limits of detection and hence the skimmer memory effect will become increasingly important.

CHAPTER 5: THE FEASIBILITY OF SOLUTION SAMPLE INTRODUCTION INTO A LOW PRESSURE ICP

5.1: Introduction

There is a requirement in the fields of pharmacological and environmental sciences for analytical techniques that are selective, highly sensitive and can provide both atomic and molecular information. Such information is vital as the toxicity of all elements is dependent upon their chemical form. However, there is no single instrument to accomplish this task. Inductively coupled plasma mass spectrometry has become the method of choice for trace element and isotope analysis. The conventional atmospheric ICP operated at around 1000 W is a 'hard' ionisation source that is used to totally atomise analytes allowing ultra-trace analysis. Quantification is sensitive and selective for a particular elemental species, however, such a harsh ionisation source provides no molecular information about the analytes and identification relies solely on chromatographic separation and co-injection of standards, or a separate analysis with another technique. Many ionisation sources such as electron ionisation (EI), chemical ionisation (CI) and electrospray (ES) have been coupled with mass spectrometry and have proven to be powerful techniques for qualitative analysis, however they lack the sensitivity of ICP-MS.

Low pressure inductively coupled plasmas (LP-ICPs) have been used as alternative plasma ion sources for mass spectrometry. Evans and Caruso developed a low pressure inductively coupled plasma mass spectrometer (LP-ICP-MS) using helium and argon[194]. A helium LP-ICP-MS has been used successfully for the analysis of halogenated compounds, using gaseous sample introduction[195]. The LP-ICP was operated at 100 W with 430 - 460 $mlmin^{-1}$ He and lead to total atomisation of the sample yielding elemental spectra. The concept behind the use of this source was to

exclude air and therefore reduce molecular interferences in the plasma associated with air entrainment. Table 5.1 shows the polyatomic ions associated with air entrainment into the atmospheric plasma and the affected analytes.

A reduction of the pressure not only excludes air and therefore many polyatomic ions it also results in less collisions between electrons and plasma gas and analyte atoms and molecular species. This results in a plasma not in thermodynamic equilibrium. In such a plasma the electron temperature is much higher than that of heavier particles and the gas kinetic temperature is relatively low. Therefore the LP-ICP can be used as a soft ionisation source providing molecular information of the analytes. Evans *et al.* obtained atomic and molecular spectra using a LP-ICP-MS by simply altering the plasma gas, torch pressure and forward power[196]. Molecular spectra of benzene containing halogens[197, 198], organotin species and organolead species[197] and organomercury species[199] have been achieved using LP-ICP-MS.

Sample introduction into the above LP-ICPs has been achieved by gas chromatography. The coupling of liquid chromatography (LC) to a LP-ICP-MS mass would extend the well established gas chromatography-LP-ICP-MS method to a wider range of sample types amenable only to LC i.e. non-volatile or thermally fragile analytes. Castillano *et al.*[200] achieved solution sample introduction into a 2 L min^{-1}, 200 W helium LP-ICP using ultrasonic and glass frit nebulisers. Only elemental spectra were obtained. The direct introduction of liquid samples via a nebulisation process is not practical into a low pressure plasma operated to give molecular information, as it cannot accommodate the presence of a wet aerosol. The introduction of an aerosol would make it difficult to sustain the plasma as heat transfer from the LP-ICP would not be sufficient to reduce the droplets to vapour, here the solvent must be removed before it reaches the plasma. There are several devices that can be utilised for desolvation. One method commonly employed for aerosol desolvation when LC is coupled to ICP-MS is

Table 5.1: Polyatomic ions associated with air entrainment and the affected analytes

Polyatomic ion	Affected analyte
N_2^+	$^{28}Si^+$
NO^+	$^{30}Si^+$
NO^+	$^{31}P^+$
O_2^+	$^{32}S^+$
ArO^+	$^{56}Fe^+$

a membrane separator [67, 68]. Gustavsson and co-workers [67, 68] obtained 94 - 99 % water removal using such a device. Recently such a device was used by Sung and Lim[201] for liquid sample introduction into a low pressure plasma operated at 200 - 300 W with a plasma gas flow of 0.2 - 1 $lmin^{-1}$. Although successfully achieved, this system only provides atomic information.

The analytical utility of the LP-ICP-MS system, used in this study, developed for gaseous sample introduction was regarded to be the production of molecular fragment mass spectra, in contrast to the atomic spectra produced by atmospheric ICPs[202]. This was also the prime objective for the introduction of liquid samples. The production of molecular spectra requires the use of much lower powers and plasma gas flows than those utilised by previous workers[201]. While the membrane desolvator may be very efficient in solvent removal, it operates with carrier gas flow rates of up to 1 L min^{-1} which could not be introduced into a LP-ICP operated at low power. The coupling of LC to such a LP-ICP system requires an efficient method of solvent removal, resulting in the formation of a desolvated aerosol composed of dry particles. The most promising approach to separating particles from gases appears to be the particle beam interface. In this aerosol beam technique, high-mass particles can be separated from relatively low mass solvent molecules when the aerosol is expanded into a vacuum because of momentum differences. In this work a previously built LP-ICP-MS system[202] was used to investigate the feasibility of a particle beam (PB) interface for liquid sample introduction into a LP-ICP. The initial studies using this instrument [197, 198, 202] indicated that, by altering the composition of the plasma gas alone, it was possible to utilise the LP-ICP as a soft ionisation source yielding molecular spectra or as a harsh ionisation source providing elemental information only. The particle beam (PB) interface has been successfully employed for the introduction of liquid samples into glow discharges (GD) with AES [203, 204, 205, 206, 207] and MS[208] detection.

5.2: Experimental

5.2.1: Instrumentation

A schematic of the instrumentation is shown in Figure 5.1. The low pressure ICP-MS system used in this work has been described in detail previously[197, 202]. Sample introduction in these reports was achieved via a GC.

5.2.1.1: The low pressure ICP-MS Instrument

The mass spectrometer used was a Hewlett-Packard (Stockport, Cheshire, UK) mass selective detector (MSD) that was modified to analyse samples from the LP-ICP. A low pressure plasma was sustained using a modified RF generator and matching network in a 140 mm long quartz tube of 0.5 inch od with a 0.25 inch od side arm to which a calibration vial containing perfluorotributylamine (PFTBA) was attached. The torch was connected to the ion sampling interface via a low pressure sampling cone that had a 2 mm orifice and an ultra-torr fitting for a 0.5 inch tube. This enabled a vacuum seal to be formed between the LP torch and the ion sampling interface. The plasma gas, controlled by a rotameter, entered the torch via the side arm tube of the torch.

5.2.1.2: The particle beam interface

The particle beam interface used was a Hewlett Packard particle beam HP LC/MS interface (Stockport, Cheshire, UK). The particle beam interface incorporates a pneumatic nebuliser, a heated desolvation chamber and a two-stage momentum separator. The liquid sample was passed into the nebuliser through a fused silica capillary (0.15 mm i.d., 85 mm in length) within a stainless steel capillary (0.5 mm i.d.). In the nebuliser the liquid eluent and compressed helium were combined coaxially. This dispersed the liquid into an aerosol of tiny droplets that consisted of a mixture of sample, solvent and helium. The solvent was partially evaporated from the sample in the desolvation chamber to leave partially desolvated sample droplets. The momentum

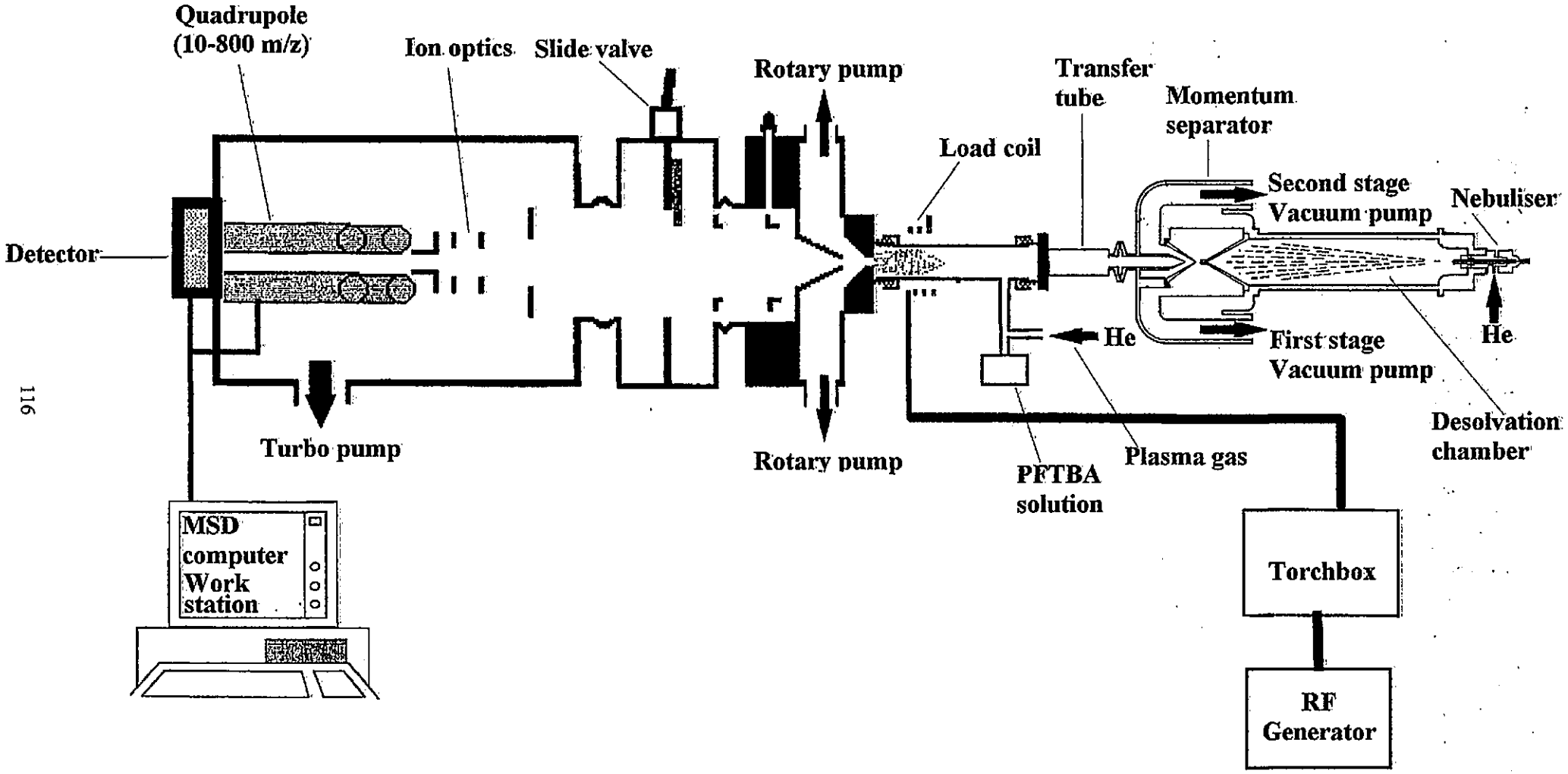

Figure 5.1: Schematic of PB-LP-ICP-MS
(Adapted from references 202 and 209)

separator was partitioned into two stages, the first between the nozzle and the first skimmer and the second between the first and second skimmer. Each stage was connected to its own mechanical vacuum pump, see Figure 5.1. The pressure in the first stage was maintained at < 10 torr and that in the second chamber to <0.8 torr.

During the expansion into the first chamber the particles are accelerated to a velocity approaching that of the helium gas. The high momentum particles tend to remain on axis while the light molecules are deflected and drawn away by the vacuum pumps. This process is repeated using a second skimmer and chamber for further sample enrichment and pressure reduction and the resulting dry, high-velocity PB passes through a short transfer line to the LP-ICP for fragmentation and ionisation. Typical operating conditions are shown in Table 5.2

5.2.1.3: Liquid chromatography pump and injection system

A Pharmacia LC system was used to introduce methanol at a flow rate of 0.5 ml min^{-1}. A flow injection manifold comprising a 500 µl injection loop on a six-port valve (model 5020, Rheodyne, Cotati, CA, USA) and HPLC grade methanol (BDH, Poole, Dorset, UK) was used throughout this study. All samples were degassed with helium prior to use.

5.2.2: Interfacing the particle beam and LP-ICP-MS

The particle beam interface was connected to the back of the low pressure plasma torch using a stainless steel transfer line (100 mm in length). This transfer tube was fitted to the end of the particle beam using a flange fitting and to the back of the plasma torch using a swagelock ultra-torr fitting. This ensured a good vacuum was maintained.

Table 5.2: PB-LP-ICP-MS operating conditions

Forward power (W)	6
Reflected power (W)	0
Plasma gas flow	3 ml min^{-1}
Desolvation chamber pressure (Torr)	200
PB first stage pressure (Torr)	9
PB second stage pressure (Torr)	0.7
Interface pressure (Torr)	0.04
Analyser pressure (Torr)	2×10^{-6}

5.2.3: Test of the PB-LP-ICP-MS

The mass spectrometer was tuned using PFTBA (Perfluorotributylamine, Fluka, Gillingham, Dorset, UK). Initially the LP-ICP-MS efficiency was tested, as the instrument had not been used for more than 12 months.

To assess the feasibility of the coupling of the PB interface to the LP-ICP-MS, methanol was used at a flow rate of 0.5 $mlmin^{-1}$. Visual studies of the PB interface were made after the continuous flow of caffeine which gave an indication of the efficiency of the PB interface. Four compounds were used to asses the quality of the mass spectrum produced. These were caffeine, progesterone (Fluka, Gillingham, Dorset, UK), chlorobenzene and 1,2-dibromobenzene (Aldrich, Gillingham, Dorset, UK). Caffeine and progesterone were used as they are frequently used in PB applications and they are the test compounds for the particular PB interface used in this study[209]. Caffeine has been used in PB-GD-MS[208]. Chlorobenzene and dibrombenzene were used as these compounds gave good results when the LP-ICP-MS was used for gaseous sample introduction[202].

5.3: Results and Discussion

5.3.1: The effects of plasma parameters on the mass spectra of PFTBA

The custom built LP-ICP-MS had previously been used for gaseous sample introduction. Since this instrument had not been used for over 12 months it was important to assess its efficiency. Furthermore, the LP-ICP was sustained by helium carrier gas from the GC. The LP-ICP could not be sustained from helium gas from the nebuliser of the PB interface. This suggests that all the helium from the nebuliser is pumped away by the two stage momentum separator and demonstrates the excellent gas-separating characteristic of the particle beam interface. Figure 5.2 shows the three peaks for the fragments of PFTBA used to tune the instrument and its mass spectrum.

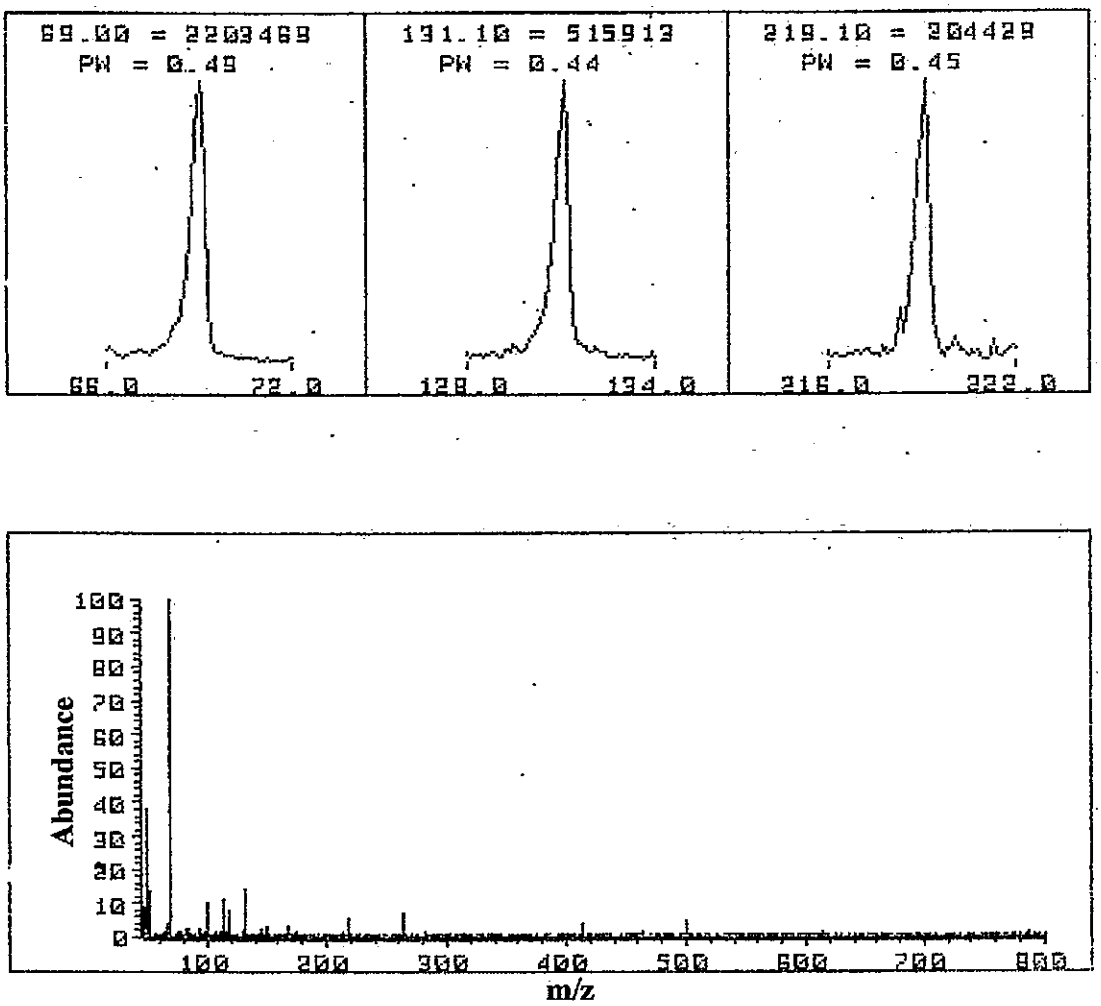

m/z	Fragment
69	$^{+}CF_3$
131	$^{+}CF_2CF_3$
219	$^{+}CF_2CF_2CF_2CF_3$
502	$^{+}CF_2$-N-$(CF_2CF_2CF_2CF_3)_2$

Figure 5.2: Mass spectrum of PFTBA.

The mass spectrum obtained is similar to that obtained by electron impact ionisation. The assignment of the four most abundant fragments is also given. It can be seen from the peak shape and width of less than 0.5 that good resolution and calibration was achieved. The abundance of the three fragments was similar to that obtained under previous operation of the instrument[202].

Figure 5.3 shows the effect of forward power on the signal intensity of the four most abundant fragments of PFTBA. The maximum signal for the three higher mass fragments (i.e. m/z 131, 219 and 502) occurred at a forward power of 6 W. Above this power their signals decrease suggesting fragmentation which would lead ultimately to the production of an atomic spectrum. The maximum signal for m/z 69 occurred at 8 W and above this power the decrease in signal was not as rapid as the decrease in the signals of m/z 219 and 502. It is likely that the fragmentation of the higher mass fragments leads initially to the formation of more m/z 69 before it is also fragmented giving rise only to atomic spectra. For the same reason the decrease in the signal for m/z 131 was also less rapid than for the signals for m/z 219 and 502. These findings are similar to those found previously[202]. Figure 5.4 shows the effect of the plasma gas flow rate on the signal intensities of the four most abundant fragments of PFTBA. It can be seen that increasing the plasma gas flow rate caused a rapid decrease in the analyte signal. At a flow rate of 6 ml min^{-1} He, the signal for each fragment was reduced to the background count rate. Hence, it is likely that at this flow rate only atomic information would be obtained from the instrument. Again this is consistent with previous findings[202]. The reason for this effect is that a chemical ionisation process dominates the LP helium plasma[202]. The rate of charge transfer is dependent on the partial pressure of the gas. Increasing the helium flow increases the partial pressure in the LP-ICP and hence the rate of charge transfer is increased. It is also likely that the presence of the RF magnetic field induces collisional energy exchange between the excited electrons and the analyte increasing the ionisation power of the plasma at higher gas flows. This leads

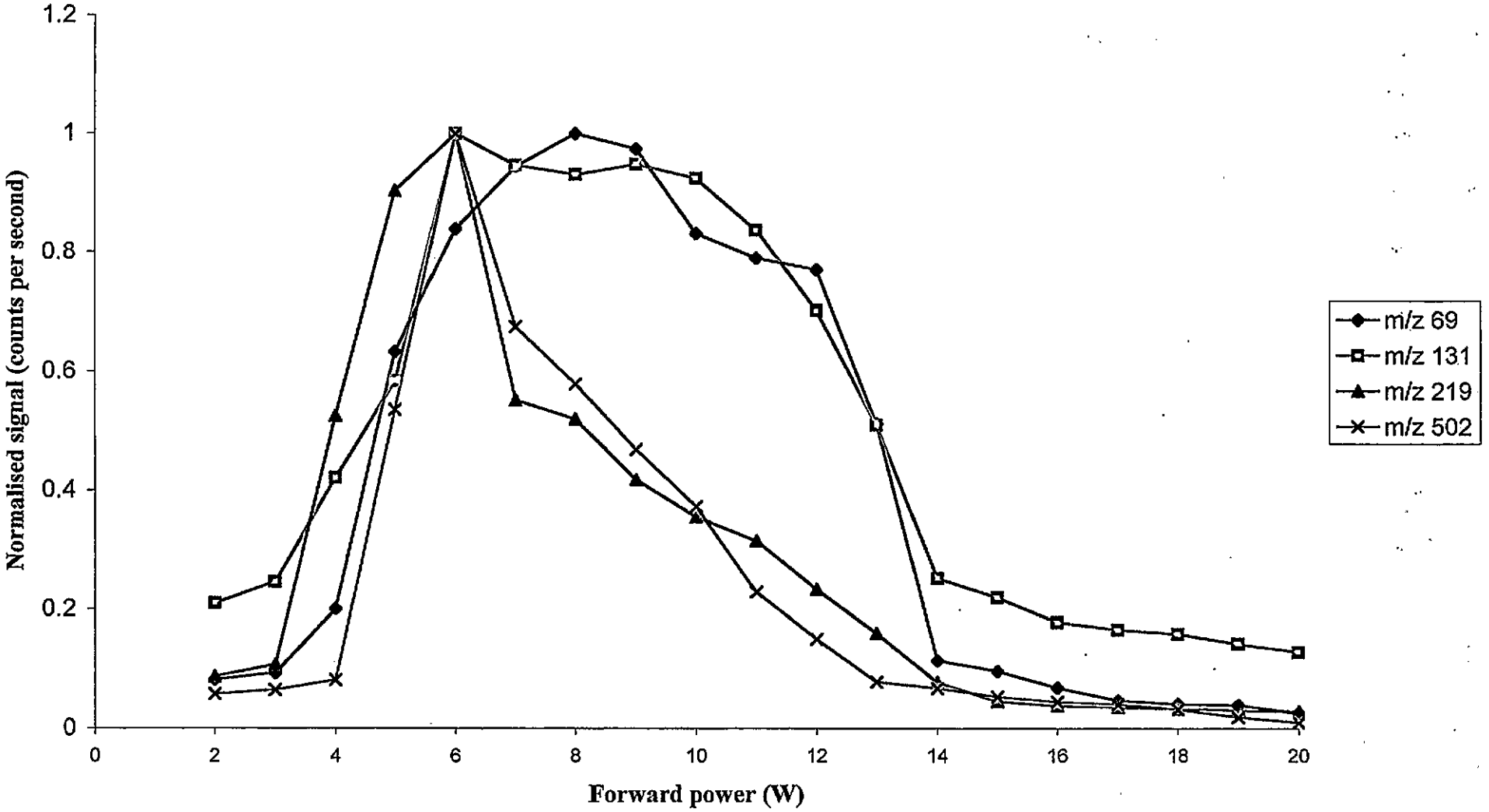

Figure 5.3: The effect of forward power on the signal intensities of the four most abundant fragments of PFTBA

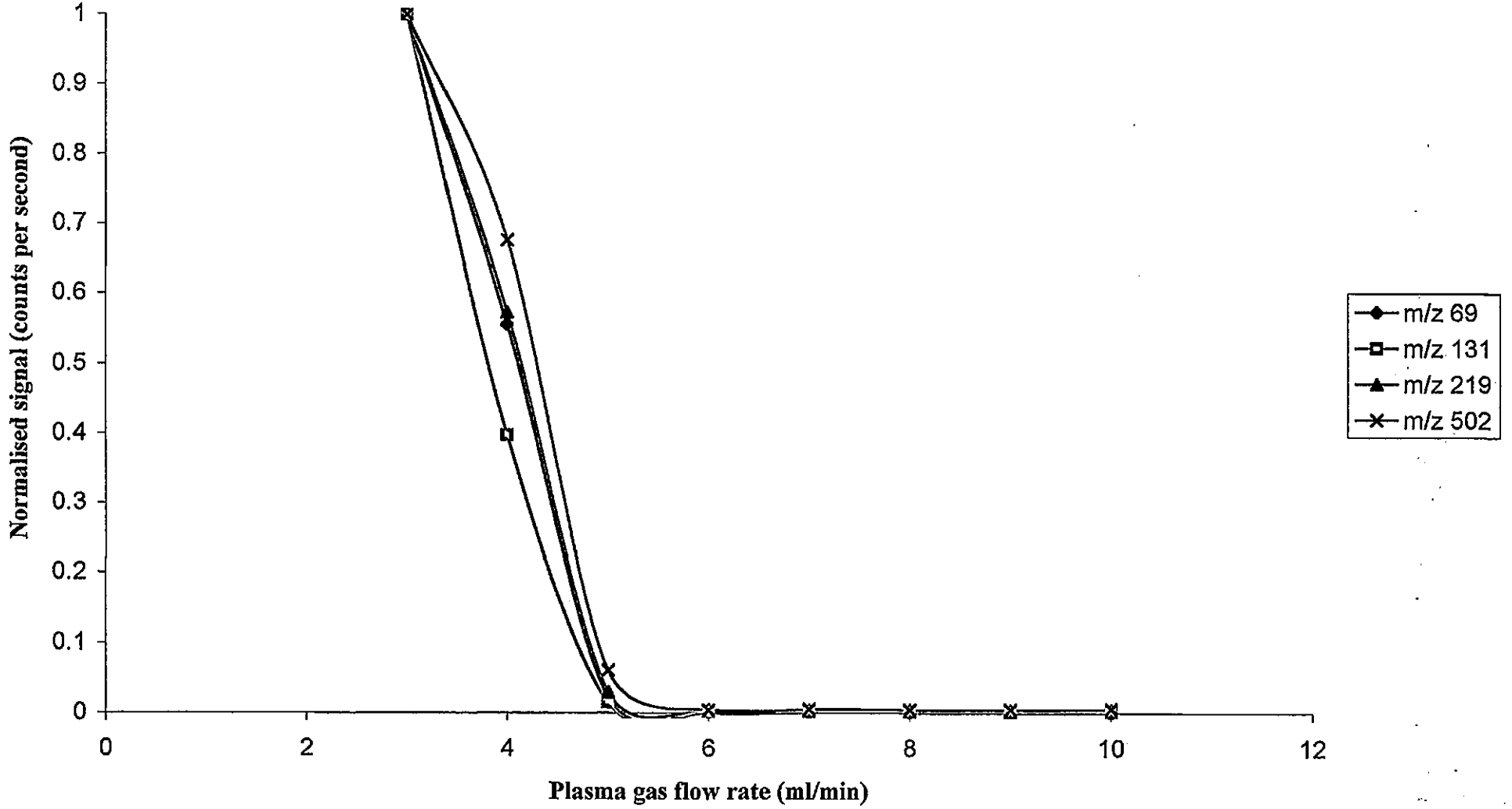

Figure 5.4: The effect of the plasma gas flow rate on the signal intensities of the four most abundant fragments of PFTBA

to greater fragmentation and eventually atomisation of the analyte molecule. The conclusion to these experiments is that the LP-ICP-MS system was working efficiently and the use of a forward power of 6 W with a plasma gas flow of 3 ml min^{-1} will lead to the production of molecular spectra provided adequate vaporisation of the sample is achieved.

5.3.2: Particle deposits in the particle beam interface

In order to asses particle loss in the PB interface, a 100 mg l^{-1} caffeine solution in methanol was allowed to flow continuously at 1 ml min^{-1} for 3 hours. The end of the transfer line was blocked off. After this time significant particle deposits were found around the orifice of skimmer 1 but the orifice was not blocked. No particle deposits were observed around the orifice of skimmer 2. A significant deposit of white powder was also found in the transfer line. This demonstrate that significant particle loss occurred in the first stage of the momentum separator between the nozzle and the first skimmer and that little particle loss occurred in between the first and second skimmer. The loss of particles in this region is consistent with the findings of other workers[210]. If the PB interface was not working efficiently it might be expected that the white powder of caffeine would be deposited around the two skimmers in a large annulus indicating deflection of the high mass, high momentum sample particles. This was not found. This experiment demonstrated that significant particle loss does occur in the PB interface but suggests that the PB interface was working efficiently since a significant build up of white powder was observed in the transfer line.

5.3.3: The first mass spectrum

The injection of increasing concentrations (1 % – 4 %) of the four compounds into the PB-LP-ICP-MS yielded no signal. Finally a 5 % solution of chlorobenzene yielded a molecular spectrum (Figure 5.5) with the following count rates:

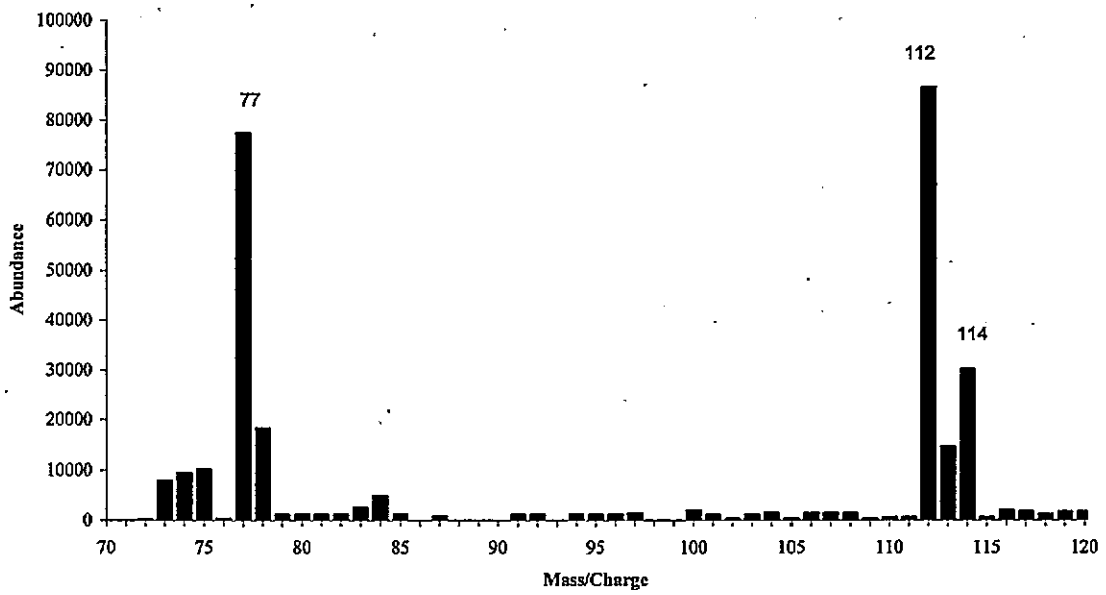

m/z	Fragment
77	$C_6H_5^+$
112	$C_6H_5{}^{35}Cl^+$
114	$C_6H_5{}^{37}Cl^+$

Figure 5.5: Mass spectrum of chlorobenzene (injection of 500 µl of 5 % sample solution)

m/z	Counts per second
77	5000
112	3500
114	4100

5.3.4: The effect of sample flow rate

Figure 5.6 shows the signal intensity at m/z 77 for chlorobenzene at different sample flow rates. It can be seen that initially the signal intensity increases as the sample flow rate increases due to more sample being delivered to the plasma and ultimately the mass spectrometer. A maximum signal was obtained at a flow rate of 0.5 ml min^{-1} and after this point there was a dramatic decrease in the signal intensity. At high flow rates the nebulisation process will be less efficient as the residence time of the solution in the capillary will be lower. A higher flow rate will also lead to a higher solvent load in the desolvation chamber which will mean less efficient desolvation of the sample. It is also possible that if there is less efficient desolvation more solvent vapour will pass into the plasma and cause quenching. The particle beam interface used in this study is optimised for a flow rate of 0.4 ml min^{-1} [209] and a sample flow rate of 0.5 ml min^{-1} was employed throughout this work.

5.3.5: The effect of the nebuliser pressure

The effect of changing the nebuliser pressure of the PB interface is shown in Figure 5.7. At low pressure the signal for m/z 77 was reduced due to the formation of large low velocity aerosol droplets that are difficult to vaporise in the desolvation chamber, and which will not be transmitted to and through the nozzle of the momentum separator. The signal increased to a maximum corresponding to a optimum nebuliser pressure of 40 psi. Further increasing the nebuliser pressure resulted in a drop in the

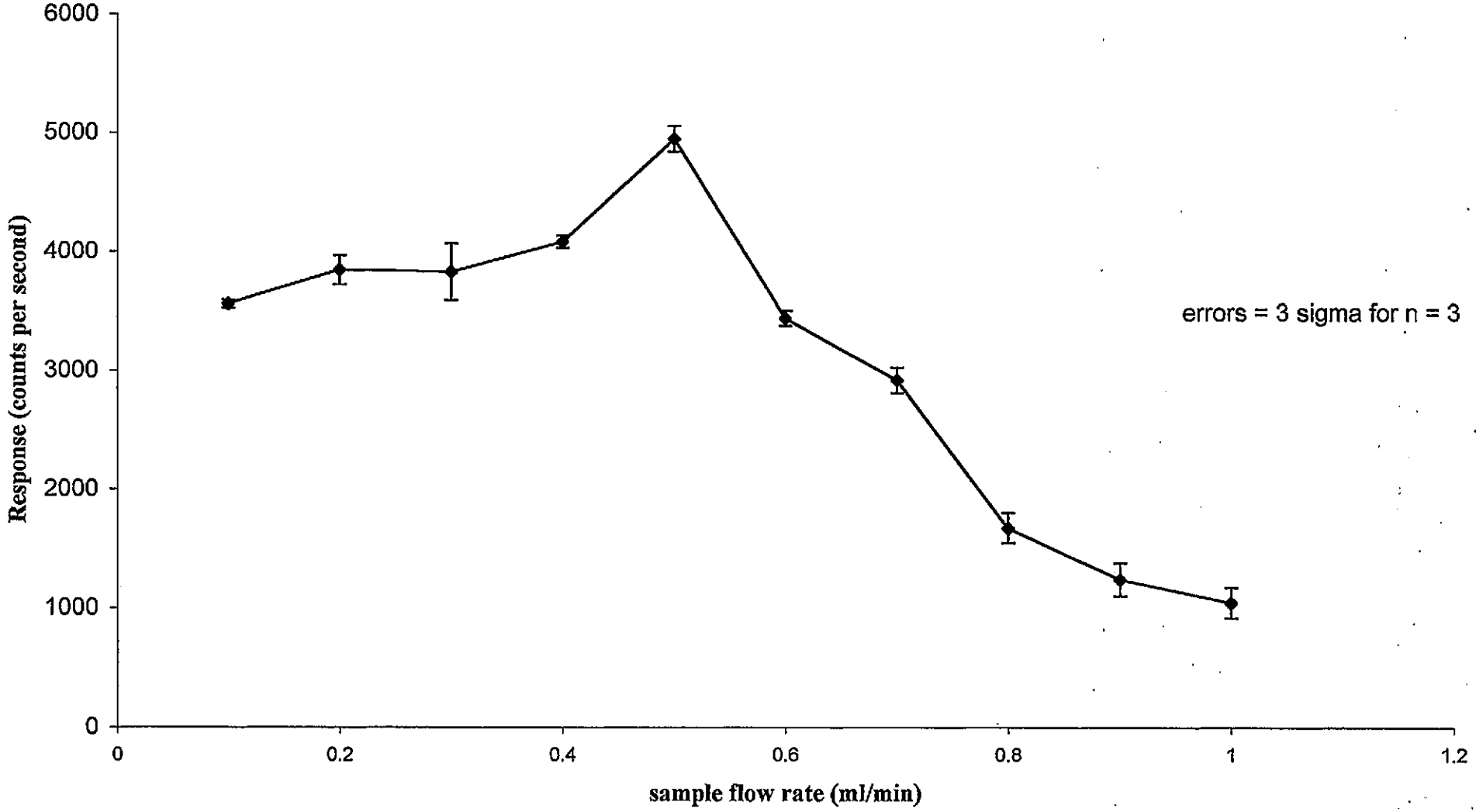

Figure 5.6: The effect of sample flow rate on the signal intensity for m/z 77 of chlorobenzene

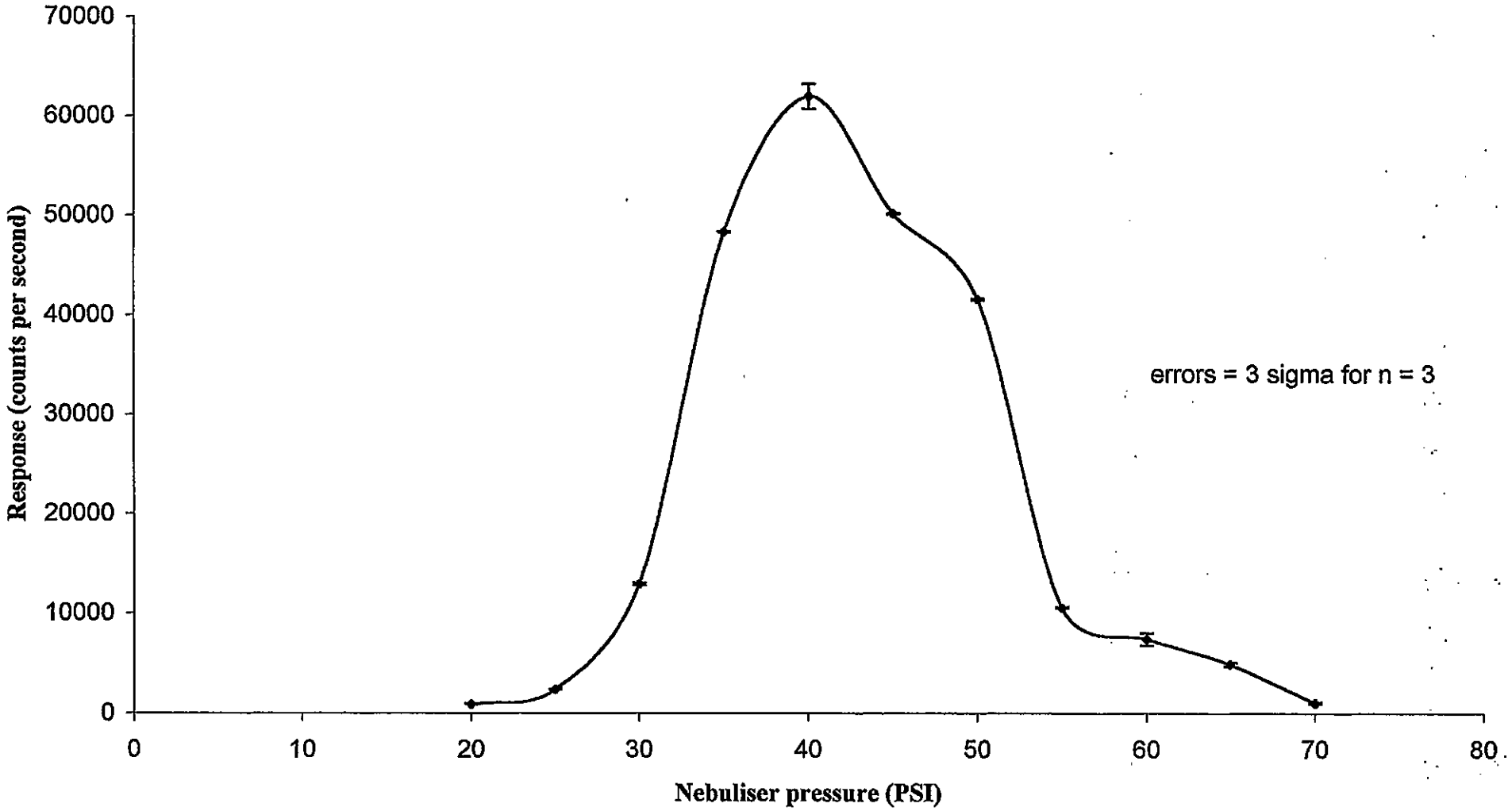

Figure 5.7: The effect of the nebuliser pressure on the signal intensity for m/z 77 of chlorobenzene

nebuliser efficiency and the signal for m/z 77 decreased. This drop at high nebuliser pressure is likely to be due to an increase in particle dispersion[211]. The desolvation chamber is equipped with a 1 inch viewing window that permits observation of the spray from the tip of the nebuliser. At high nebuliser pressures a more divergent aerosol was seen to exit the capillary.

5.3.6: The effect of the desolvation chamber temperature

Figure 5.8 shows the effect of the desolvation chamber temperature on the signal for m/z 77. Increasing the temperature resulted in an improvement in the signal with the maximum signal being obtained at a desolvation chamber temperature of 70 °C. This is the maximum desolvation temperature achievable. Figure 5.8 clearly shows that the signal did not reach a plateau indicating that the signal could be increased further if the desolvation chamber temperature could be increased further. However, at this stage it is important to efficiently separate solvent from solute without significant solute evaporation.

5.3.7: Vaporisation of the particles emerging from the particle beam interface

The low signals obtained for the fragments of chlorobenzene were attributed to the low thermal kinetic temperature of the LP-ICP which is less than 340 K[202]. This is insufficient to vaporise and dissociate the particles. In all particle beam interfaces there is some sort of heated target. Source vaporisation temperatures are often as high as 240 ^{0}C[212], 280 ^{0}C[208] and 340 ^{0}C[213]. In order to vaporise the particles a heating tape was wound around the transfer line so that the heated walls of the transfer line provided thermal energy for vaporisation of the clusters of molecules. A thermocouple was placed in between the transfer line and the heating tape. The O - rings in the ultra-torr fitting between the plasma torch and the transfer line are composed of a fluoro-elastomer that will degrade above 200 ^{0} C. Therefore in order to ensure a vacuum is

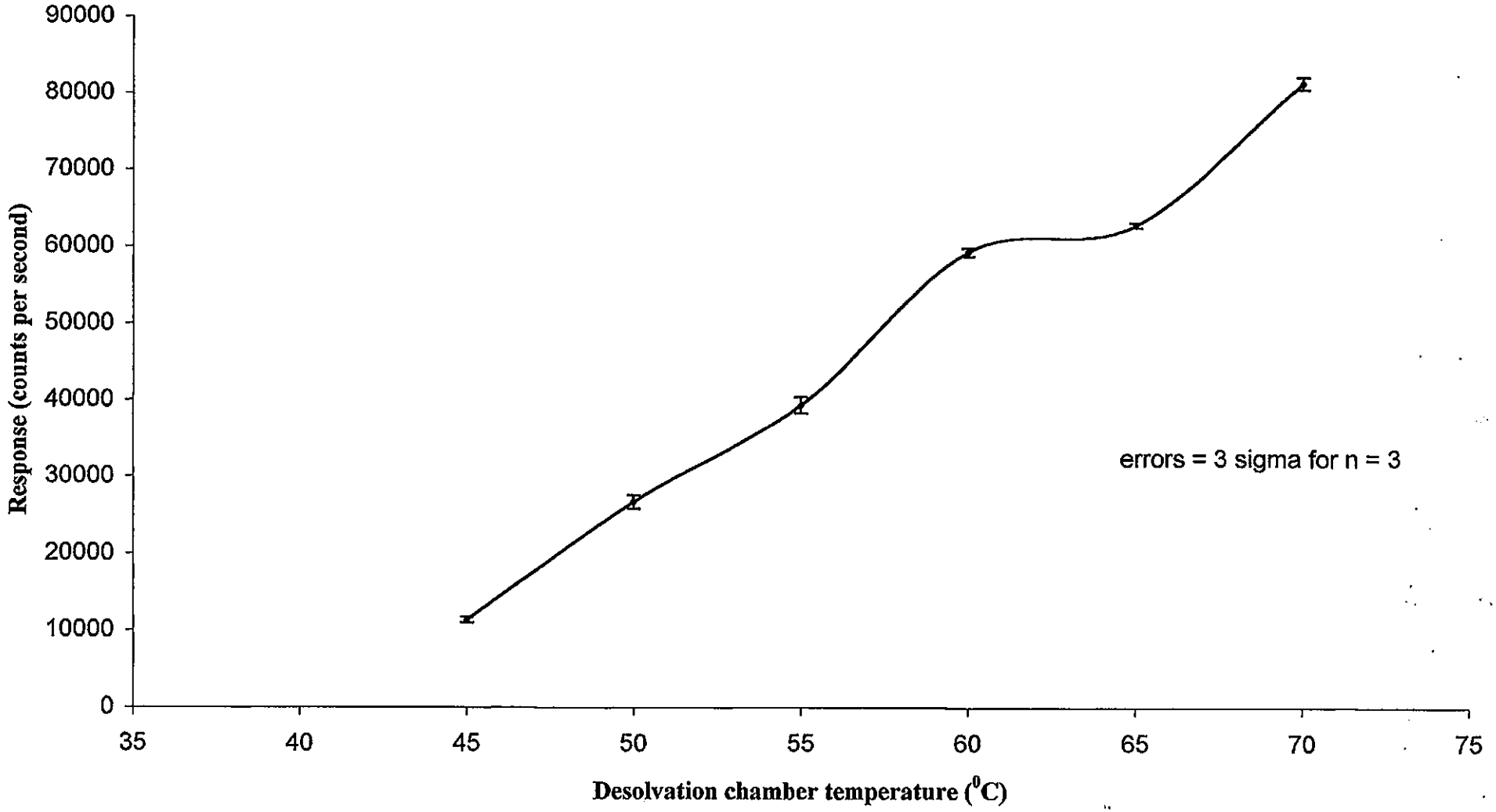

Figure 5.8: The effect of the desolvation chamber temperature on the signal intensity for m/z 77 of chlorobenzene

maintained the O-rings were replaced by graphite ferrules. The results are shown in Table 5.3.

It should be noted that the temperatures quoted in Table 5.3 are due to local hotspots on the outside surface of the transfer line and do not reflect the true temperature inside. It can be seen from Figure 5.9 that the count rate increased exponentially with temperature and that a plateaux was not reached, suggesting that improvement in the signal could still be gained by increasing the temperature further.

In order to help conduct heat into the transfer line a strip of wire was placed across the inside of the transfer line. At the highest voltage setting (corresponding to 420 ^{0}C in Table 5.3) the following counts were obtained:

m/z	**Counts per second**
77	175 811
112	156 115
114	101 470

This idea was taken further and a coil of copper wire was place inside the transfer line along its entire length and the following counts were obtained:

m/z	**Counts per second**
77	355 483
112	363 295
114	338 375

Figure 5.10 a and b show the mass spectra of chlorobenzene obtained for a 500 µl injection of 1 % sample solution when the temperature of the heating tape was 279 ^{0}C and 420 ^{0}C, respectively with the copper coil present in the transfer line. Figure 5.11 shows the mass spectrum of dibromobenzene recorded at 420 ^{0}C with the copper coil in the transfer line. The injection of caffeine and progesterone still yielded no spectra. It would be expected that the more volatile compounds would give a poorer response due to the transport efficiency through the PB interface being greatest for involatile solutes. However, since caffeine and progesterone are more thermally stable they will require higher temperatures for efficient vaporisation and dissociation. Hence the particles

Table 5.3: Counts per second obtained for a 1 % chlorobenzene solution at different temperatures

Temperature of heating tape ^{0}C	Counts at given m/z		
	77	**112**	**114**
50	2345	2134	2234
189	3256	3714	3101
207	7342	3726	3509
279	12867	6413	7609
405	48115	24718	56731
420	68392	65217	68918

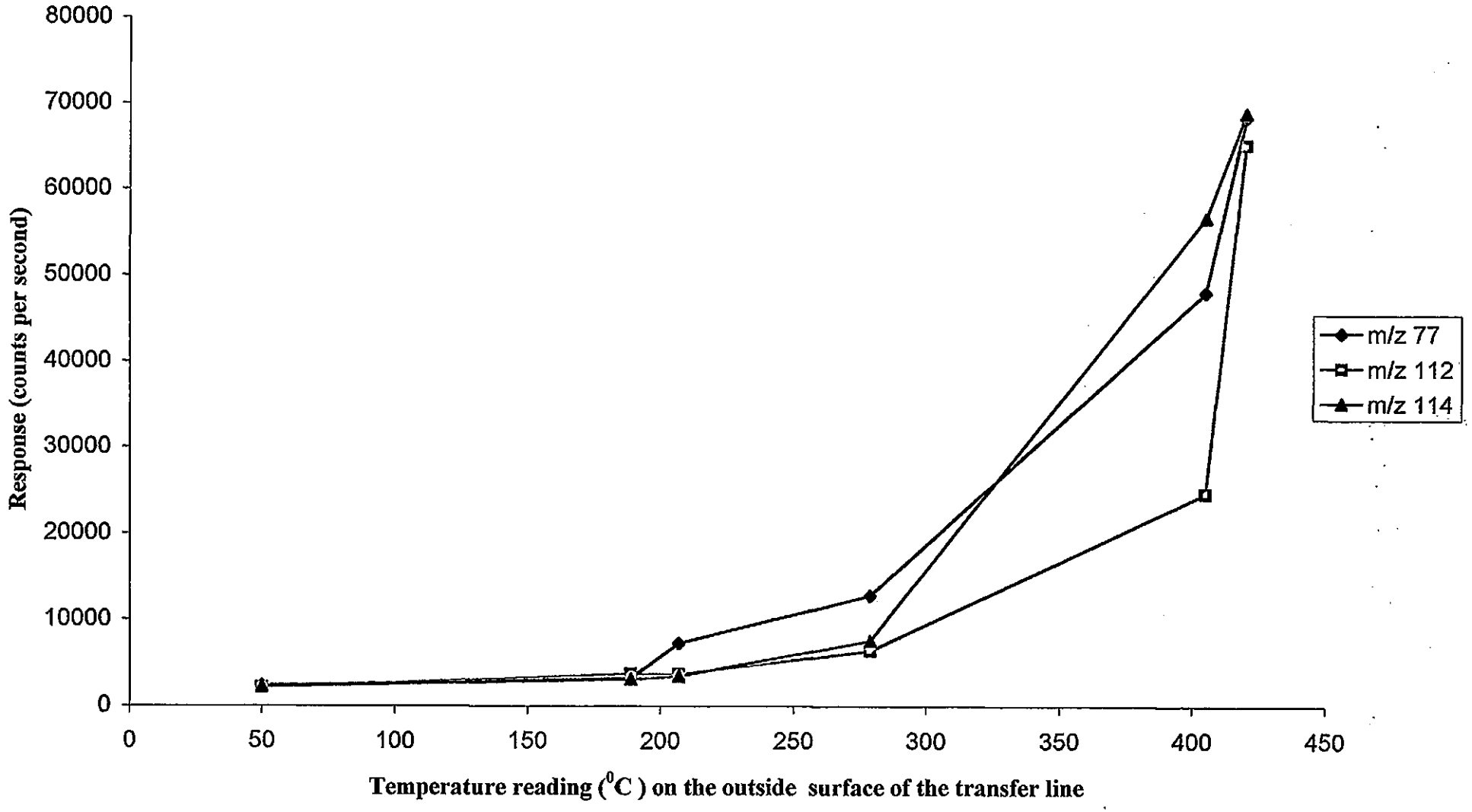

Figure 5.9: The effect of heating the transfer line on the signal intensity for m/z 77, 112 and 114 of chlorobenzene

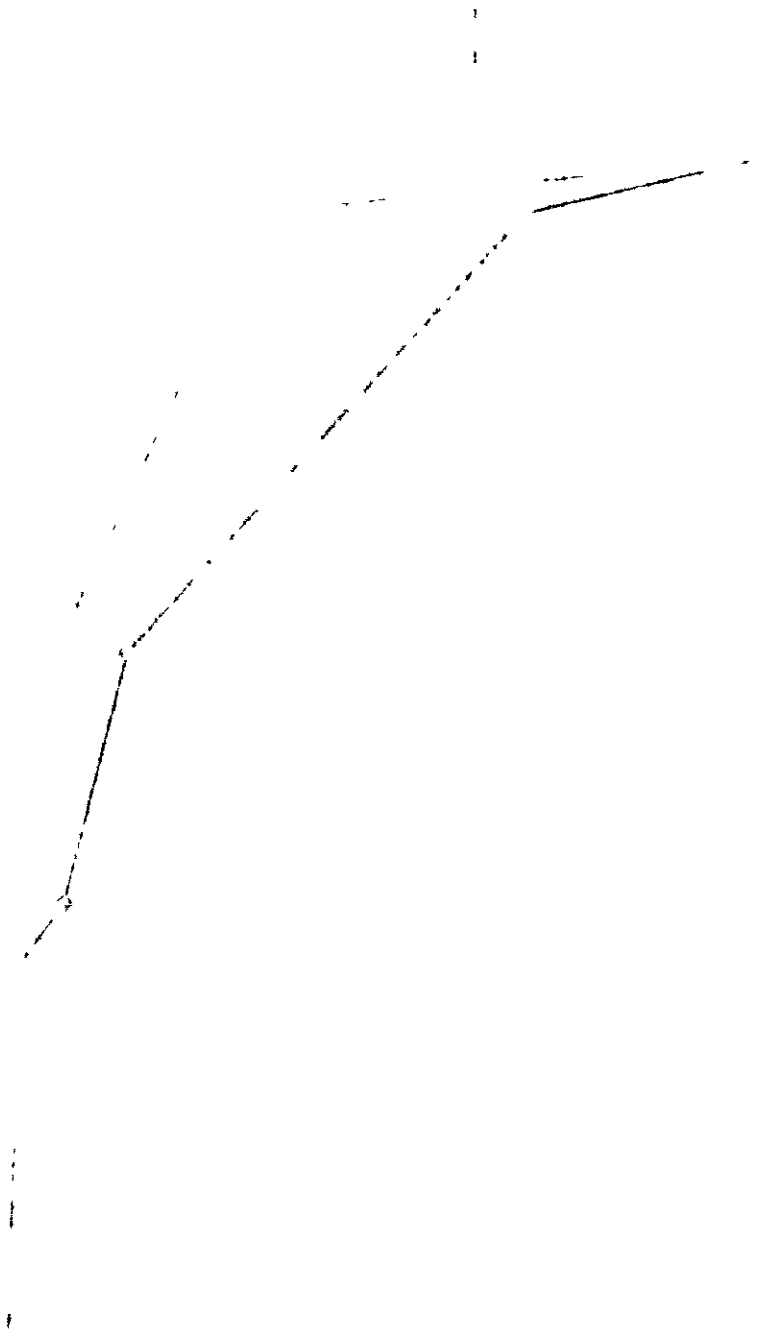

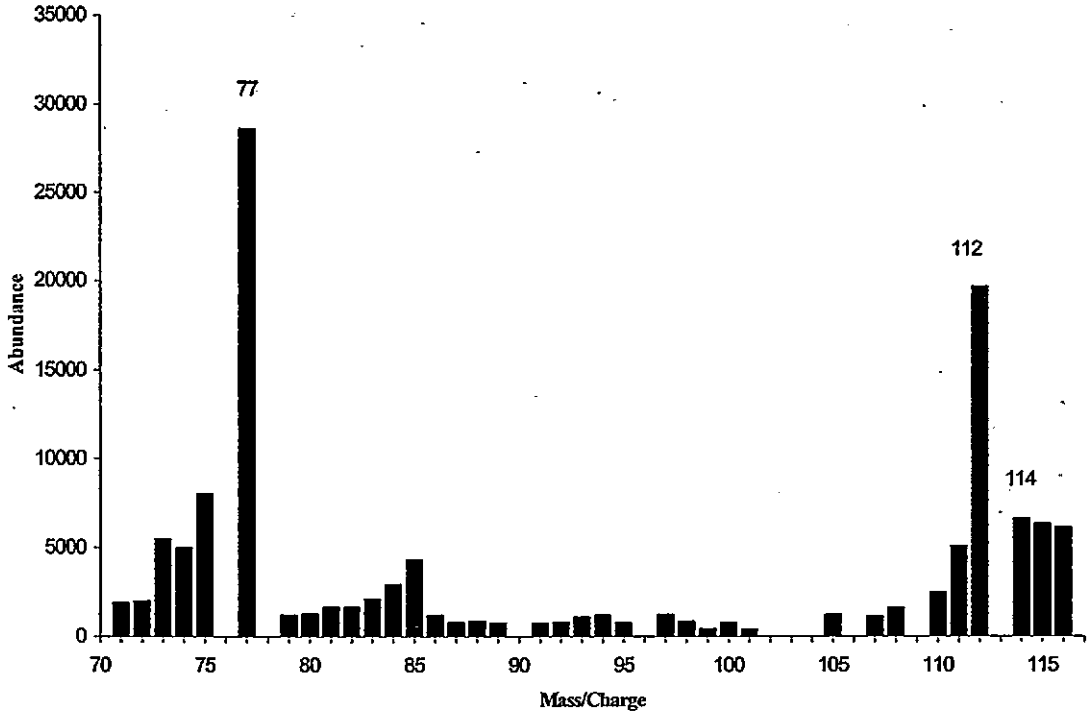

Figure 5.10 (a): Mass spectrum of chlorobenzene (sample solution 1 % and heating tape reading 279 ^{0}C)

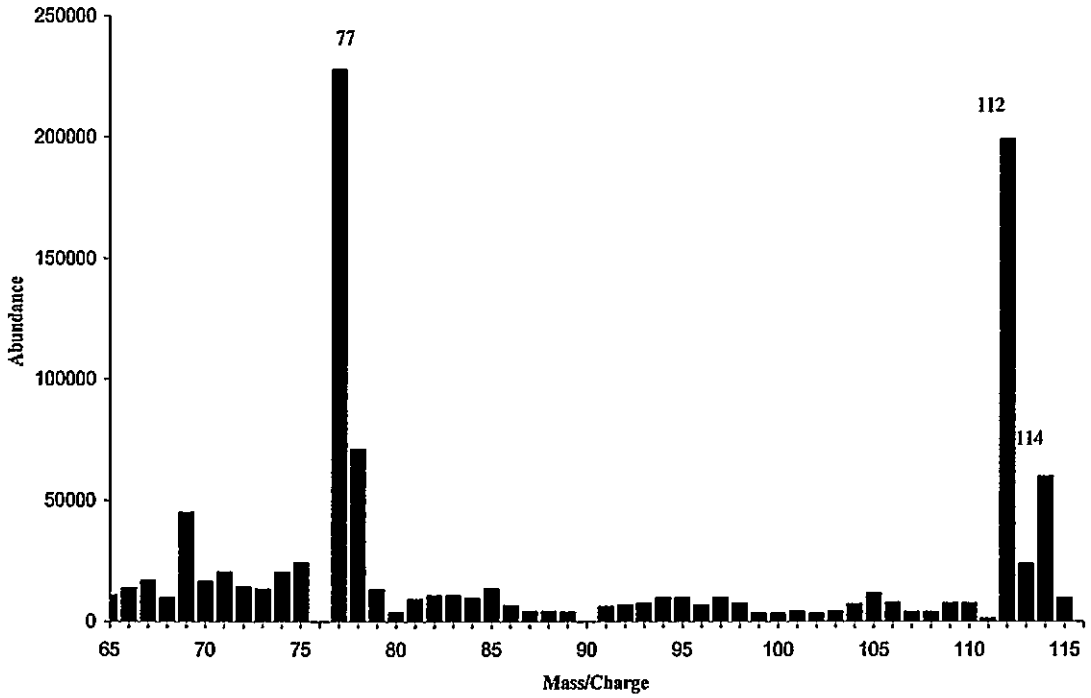

Figure 5.10 (b): Mass spectrum of chlorobenzene (sample solution 1 %, heating tape reading 420 ^{0}C and copper coil inside transfer line)

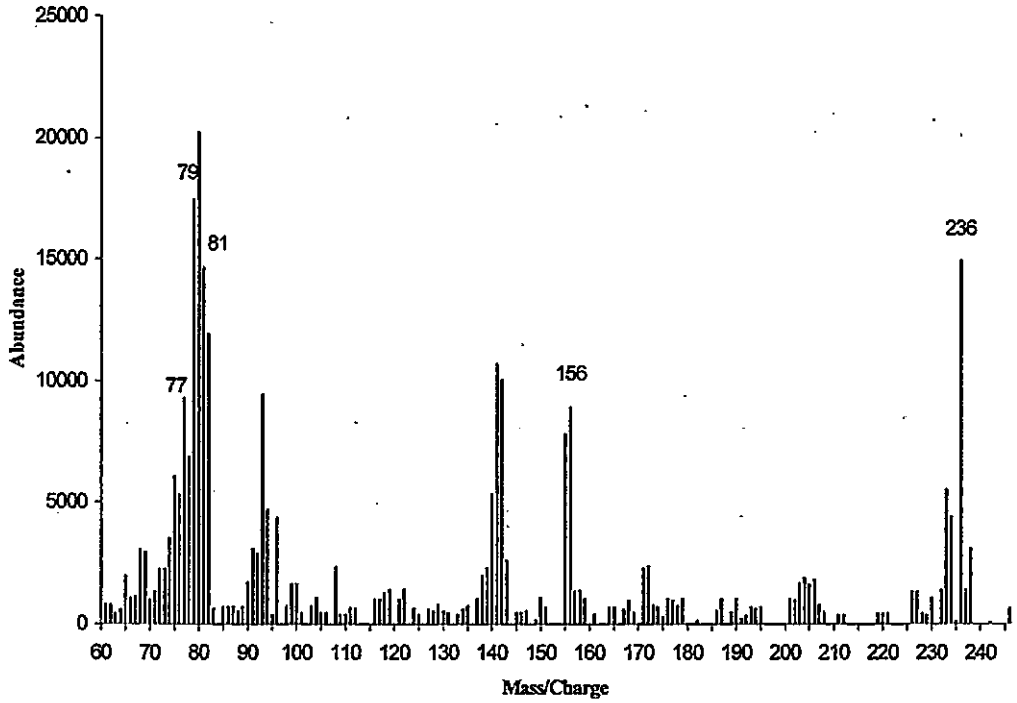

m/z	Fragment
77	$C_6H_5^+$
79	$^{79}Br^+$
81	$^{81}Br^+$
156	$C_6H_5\,^{79}Br^+$
236	$^{79}Br\,^{81}Br\,C_6H_4^+$

Figure 5.11: Mass spectrum of dibromobenzene (sample solution 1 %, heating tape reading 420 ^{0}C and copper coil in transfer line)

emerging from the particle beam are inadequately vaporised, resulting in lower signals for the less volatile compounds.

5.3.8: Chlorobenzene Calibration graph

A calibration graph was constructed for mass 77. A linear plot is shown in Figure 5.12. Nonlinearity is often observed for compounds that are analysed using a PB interface, although the reason for this is not understood[210]. However, in this case a linear response was observed for chlorobenzene with an R^2 value of 1 and a 3σ limit of detection of 30 mg l^{-1}.

5.3.9: Improving the uniformity of heating and thermal transfer

At this stage in the development of the PB-LP-ICP-MS attentions focused on modifying thermal transfer to the particles and improving the uniformity of heating. For this reason a cartridge heater (Length 3 inch, diameter 0.5 inch, Watlow, Linby, Nottingham, UK) containing a thermocouple at its tip was soldered into a T-piece as shown in Figure 5.13. The cartridge heater should provide a means of flash vaporisation of the particles as they emerge from the PB interface and an accurate measurement of the temperatures which the particles experience in the transfer line. Table 5.4 show the response obtained for the fragments of chlorobenzene with the cartridge heater set at different temperatures.

One interesting point to note is that the counts obtained at the highest temperature (i.e. 168 ^{0}C) were comparable to those obtained at the highest voltage setting when the heating tape was used and the copper strip was placed in the transfer line. This therefore seems a promising approach to solving the problem of thermal transfer to the particles once they have emerged from the particle beam interface. Unfortunately the cartridge heater could not be operated under these conditions and

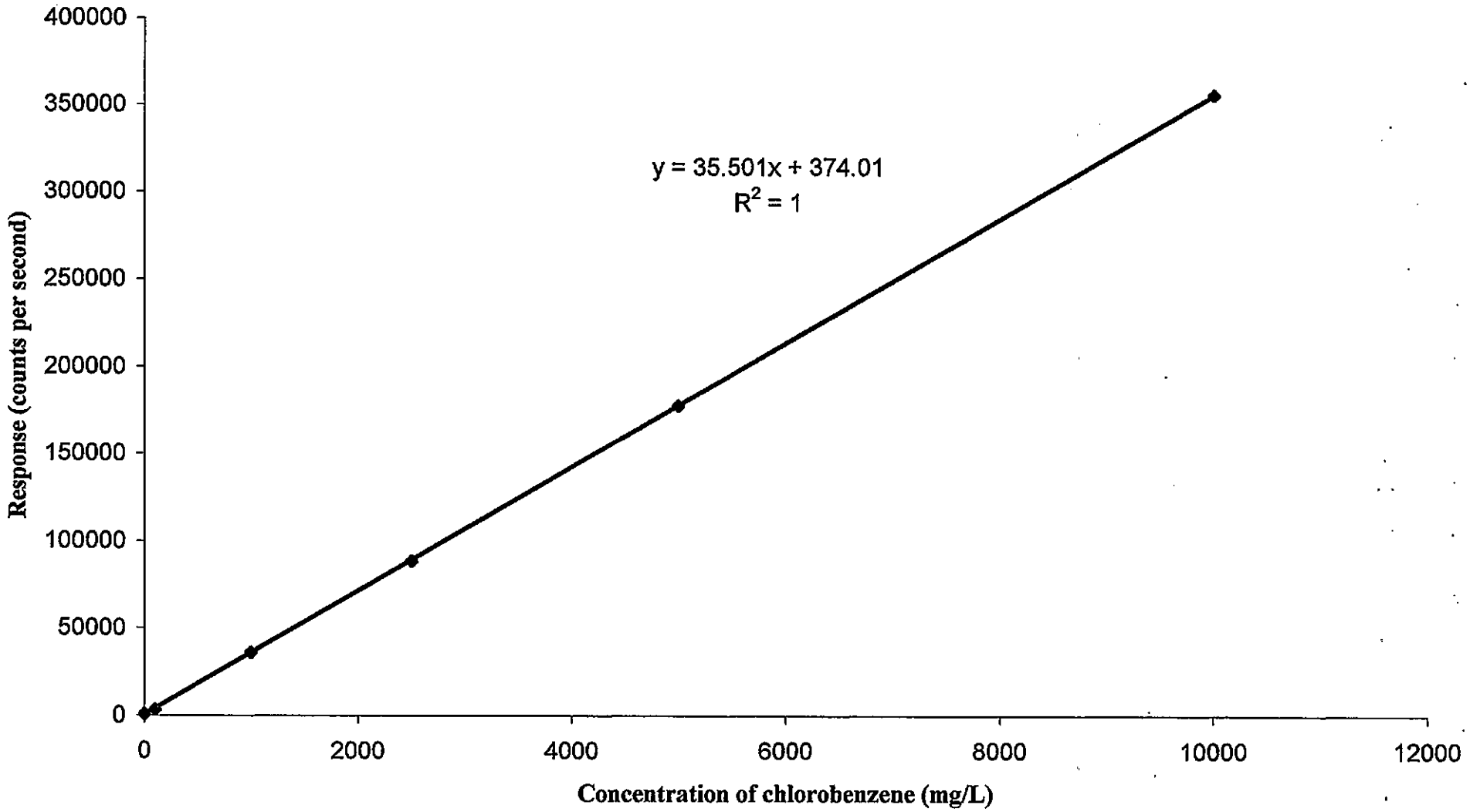

Figure 5.12 calibration graph for chlorobenzene (m/z 77)

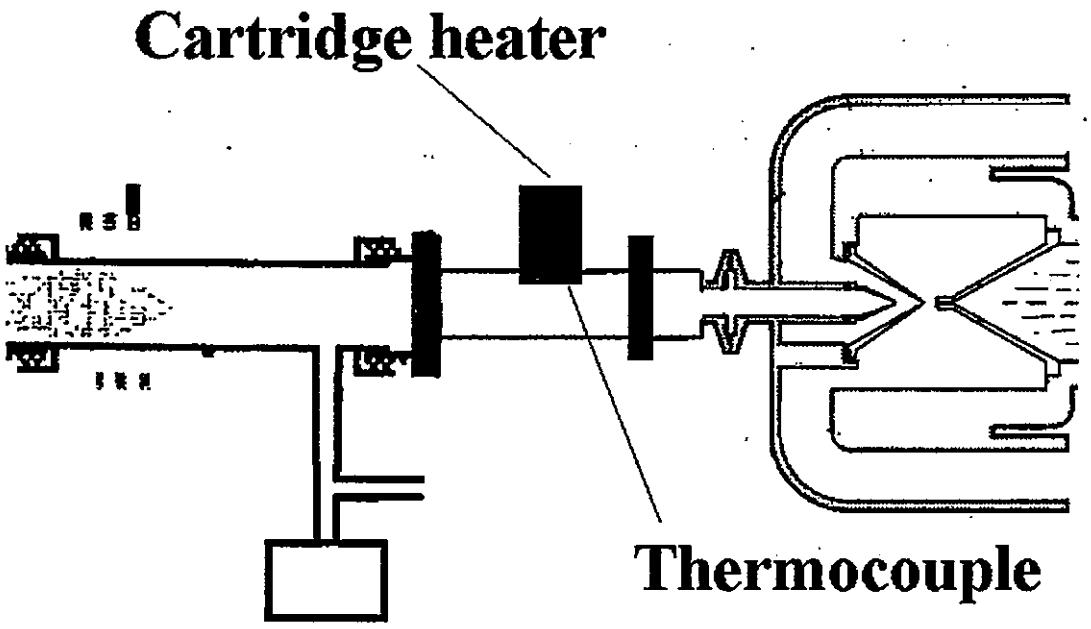

Figure 5.13: Schematic of PB-LP-ICP-MS interface for improving the uniformity of heating and thermal transfer

Table 5.4: Counts per second obtained for 1 % chlorobenzene solution at different temperatures using a cartridge heater

Temperature of cartridge heater ^{0}C	Counts at given m/z		
	77	112	114
97	2671	2895	2243
112	5963	6144	5726
121	67391	65218	60314
168	286002	241894	231218

after several hours of operation it burnt out. Hence the problem of efficient thermal transfer to the particles still exists.

5.4: Conclusions

The introduction of liquid samples into a LP-ICP-MS to allow its use as a liquid chromatography detector has so far met with limited success. The major challenge with the use of a particle beam interface seems to be providing an efficient source of thermal energy for vaporising the particles. The gas kinetic temperature of the LP-ICP is less than 340 K which means the LP-ICP is an inadequate excitation source to vaporise, dissociate and ionise the particles emerging from the particle beam interface. Providing thermal energy by heating the walls of the transfer line resulted in a dramatic increase in the analyte signal. An efficient means of vaporisation must be sought if the PB-LP-ICP-MS is to be analytically useful. So far more volatile compounds have given better signals than less volatile compounds indicating inefficient vaporisation rather than inefficient transport through the PB interface.

It was found that the sample flow rate, nebuliser pressure and desolvation chamber temperature were all critical parameters in the use of the particle beam interface. Furthermore, the greatest loss of particles occurs in the first stage of the momentum separator with little or no loss occurring in the second stage. Such loss will inevitably limit the use of a PB-LP-ICP-MS.

CHAPTER 6: SILICON SPECIATION

6.1: Introduction

Silicon is the second most abundant element on the earth's surface, after oxygen, and constitutes approximately 28 % by weight[214]. The most common form of silicon in nature is silica which is composed of silicon dioxide, SiO_2. Silica is an important commercial material, forming a substantial constituent of concrete, ceramics and other building materials[215]. Inhalation of dust from these sources can accumulate in lung tissue and in lymph nodes[214]. Silica also finds many applications as a drying agent in the form of silica gel as it readily absorbs moisture from the air. Other forms of silicon are the silicates, containing SiO_4 units. Natural silicates form the major component of most rocks and are used in analgesics and antacids being excreted in the urine within hours of exposure[216]. Silicon may also be encountered as silicones, polymeric compounds containing chains of silicon alternating with oxygen, with the silicon being linked to organic groups. In the body, silicon can occur as silica, found in hair, bones, epidermis and dental enamel[214].

Due to the great range of viscosity exhibited by silicones, and the elasticity of silicone rubbers, it has been possible to fabricate silicone-based materials that mimic body tissues as diverse as bone and mammary tissue[217, 218]. Polydimethylsiloxanes (PDMS), which have the general formula $(CH_3)_3Si\text{-}O\text{-}[Si(CH_3)_2\text{-}O]_n\text{-}Si(CH_3)_3$ (where n = 0 - > 10 000), are the most important class of silicones with 700, 000 tonnes produced in 1990[219]. PDMS fluids come in a range of viscosities from water-like liquids to non-pourable fluids and all of them are essentially water insoluble. They have a variety of uses such as lubricants, electrical insulators, anti-foaming agents in foodstuffs, texturisers in personal care products such as antiperspirants, colognes and hair sprays, and biomedical applications. Among the biomedical uses of PDMS are therapeutic agents, (e.g. in anti-flatulence tablets), drug delivery systems and adjunct devices such

as rubber tubing in catheters. The most common medical use of PDMS is in plastic and re-constructive surgery. Medical grade polymers are injected to restore facial contours in patients with facial disfigurements and they are constituents of replacement joints. In recent years PDMS have been widely used for cosmetic breast augmentation and reconstruction after mastectomy.

The silicone breast implant has been available since 1963. Polydimethylsiloxanes, which form the silicone gel of the implant, are manufactured from elemental silicon through a variety of chemical reactions to form polymers of varying length. The silicone rubber shell is composed of extensively crosslinked high-molecular weight components, together with 16.4-26.9 % amorphous fumed silica which is added as a strengthener. The composition of the gel has changed since 1963. In the modern implant, the gel contains 1-2 % of low molecular weight PDMS, which are usually cyclic and the other 98 % of the gel is composed of high molecular weight linear PDMS. To produce the desired viscosity the silicone gel is only partially cross-linked and much of the gel is composed of filler, long chain linear PDMS usually 1000 centistokes (cs)[217]. Solvent extraction of the shell and the gel has revealed 30 different types of linear and cyclic components[220].

Silicones are synthetic chemicals that do not occur naturally so the Si-O backbones in these long polymers should not be attacked by the enzymes of the body. Hence PDMS has been used in breast implants because it was considered to be non-biodegradable and chemically, immunologically and physiologically inert, and thus pose no harmful effects to humans. However, controversy has raged about immuonological responses to PDMS. Breast implants have been associated with connective tissue diseases or autoimmune diseases such as rheumatoid arthritis[221, 222]. Kossovsky *et al.* experimentally demonstrated that silicones evoke an immunologically-mediated inflammatory reaction in guinea pigs after they were injected with sterile medical grade silicone oil for 1 month[223]. A study conducted in Sweden involving 7442

women, with implants for cosmetic reasons or for reconstruction after breast cancer surgery, concluded there was no evidence of an association between breast implants and connective tissue disease[224]. Questions concerning an increased cancer risk to women with breast implants have also been raised, however, a detailed review of the literature by Edelman *et al.* showed there was no evidence to support this[225].

Nevertheless, it has been shown that the shell of the implant is not impermeable and that silicone can bleed from clinically intact implants and be detected visually in lymph nodes[226, 227]. Several studies have attempted to measure the rate of silicone bleed from clinically intact gel implants. Such studies usually involve the application of a 5 Kg weight to an implant and measuring the bleed rate into saline or simulated body fluids. Bleed rates of 100 mg and 200 mg per year have been reported for older implants[220]. Extrapolation of this data to the in *vivo* situation is difficult. The true bleed rate would be limited by the rate of diffusion through the shell of the implant and the rate of removal of the bleed fluid from the exterior surroundings of the implant. This is limited by silicone solubility and by the presence of capsular tissue, which provides an additional barrier to bleed[220]. It has been pointed out that over time, 10 years or more, the shell may erode and permit silicone gel to enter the surrounding fibrous tissue[228]. The implant may also deteriorate further due to the absorption of body fluids[229, 230].

Several studies have examined the possibility of migration of silicones from implants to local and distant sites throughout the body via the circulatory and lymphatic systems[231, 232, 233]. Kala *et al.*[231] examined the distribution of low molecular weight silicones in body organs by injecting mice with either breast implant distillate or silicone oil. After a single subcutaneous injection silicones were widely distributed throughout the body and persisted over an extended period. The silicone was found to accumulate in several organs of the mice including the liver, kidney, spleen, pancreas and ovary. Lukasiak *et al.*[233] fed rats with either PDMS fodder or a cyclic-PDMS (cPDMS) fodder. The accumulation and toxic effects of silicones were studied in the

blood, brain, kidneys, liver and spleen after 12 days. It was found that PDMS was preferentially absorbed by the brain and kidneys and cPDMS remained in the circulatory system and partly in the kidneys. The internal organs showed no pathological changes attributable to siloxanes. Pfleiderer and Garrido[232] used NMR to detect the migration and accumulation of silicones in the bodies of women with silicone gel-filled breast implants. These results clearly demonstrate that leaked silicone is not limited to the area surrounding the implant.

It is also known that PDMS is not chemically inert, but undergoes chemical degradation[234, 235, 236, 237] in *vivo* into products that appear in blood plasma. This degradation involves siloxane bond redistribution and hydrolysis, resulting in the formation of low molecular weight organosilicon compounds such as silanols, or volatile cyclic siloxanes. The biotransformation of injected siloxanes in the lymph nodes of rats has also been observed[238]. The authors report that all polymers (linear and cyclic) are biodegradable, but higher molecular weight polysiloxanes require longer to degrade[238]. Certain low molecular silicones, particularly the cyclic silicones may have potent biological activities that mimic estrogens[218, 239] or central nervous system-active drugs [218].

Estimates of the number of women with silicone breast implants vary from 815 000 to 2.2 million in the US and about 100 000 in the UK[240]. The literature suggests that the low molecular weight silicones, in particular the cyclic compounds are potentially toxic[218, 239], while the higher molecular weight compounds are relatively stable and inert in biological tissues[217, 218]. Nevertheless, the modern breast implant contains 98 % of the higher molecular weight silicones and PDMS has been shown to biodegrade over time[238] and therefore warrants the development of sensitive methodology for their determination in clinical samples.

Organosilicon compounds may be separated by a variety of techniques according to polarity, size and solubility of the analytes[241]. GC-MS[242, 243, 244, 231] and

GC-AED[242, 243] have been used to determine low molecular weight silicones in biological matrices. Octamethylcyclotetrasiloxane (D_4) and its metabolites have been extracted from plasma and blood of spiked samples of rats administered with radioactively labelled D_4 and separated by high performance liquid chromatography (HPLC) with radiometric detection[245].

It has been demonstrated that the combination of HPLC, for separation, and inductively coupled plasma atomic emission spectrometry (ICP-AES), for detection, is applicable to the determination of organosilicon compounds that may occur in environmental and industrial samples[241]. Size exclusion chromatography (SEC), also known as gel permeation chromatography (GPC), coupled to ICP-AES has been used to determine the environmental occurrence of PDMS[246] and its degradation in soil[247]. Tetrahydrofuran (THF)[246] and xylene[247] have been used as the mobile phase. In the latter work the silanols, the water soluble break down products of PDMS, were determined by reversed phase chromatography coupled to ICP-AES.

HPLC coupled to inductively coupled plasma mass spectrometry (ICP-MS) is a well established technique for trace element speciation studies, however, silicon suffers from severe interference from N_2^+ formed as a result of air entrainment into the plasma. This interference can be resolved using high resolution ICP-MS thereby allowing determination of silicon at m/z 28. A resolution of 958 is required to resolve N_2^+ from $^{28}Si^+$.

The introduction of organic solvents into ICP-MS is associated with a number of problems, including plasma stability and the deposition of carbon onto the torch and cones. In order to alleviate these problems cooled spray chambers, a reduction in sample uptake rate, increased forward power and desolvation devices have been employed. The major difficulty encountered in ICP-MS is that the interface is directly in contact with the plasma. In spite of the high temperatures associated with the ICP it does not fully combust the organic solvent and carbon atoms recombine to form graphite which

condenses on the relatively cool metal surface of the sampling cone. This problem is overcome by the introduction of oxygen into the nebuliser gas stream, which reacts with carbon atoms in the ICP to form CO, CO_2, CO_2^+ and CO^+, which is sampled from the plasma along with all other ions. This poses another potential problem in the analysis of $^{28}Si^+$, namely that $^{28}CO^+$ also becomes an interference at m/z 28 which must also be resolved. A resolution of 1557 is required to resolve $^{28}Si^+$ and $^{28}CO^+$. The mass spectrum around m/z 28 acquired at a resolution of 3000 is shown in Figure 6.1, indicating that $^{28}Si^+$ has been resolved from $^{28}CO^+$.

The impact of organosilicon compounds in the human body requires sensitive methodology to discriminate between the various forms of silicon which may be present in clinical samples[248]. The purpose of this work was to develop HPLC-ICP-MS methods for the determination of linear molecular weight PDMS including high molecular weight PDMS which cannot be determined by GC, and PDMS breakdown compounds which may be present in clinical samples. The use of SEC coupled to ICP-MS for the separation and determination of high molecular weight PDMS and the use of reversed phase chromatography coupled to ICP-MS for the separation and determination of silanols is presented.

6.2: Experimental

6.2.1: Determination of silicones

6.2.1.1: Instrumentation

The chromatography was performed using a Varian 9001 solvent delivery system, operated in isocratic mode, fitted with a Rheodyne 9010 injection valve with a 100 µl sample loop (Cotati, CA, USA). The separation of three polydimethylsiloxane polymers was performed at ambient temperature using a Phenogel 5 M3 size exclusion column 300 x 7.8 mm i.d. (5 µM) (Phenomenex, Macclesfield, Cheshire, UK), at a flow

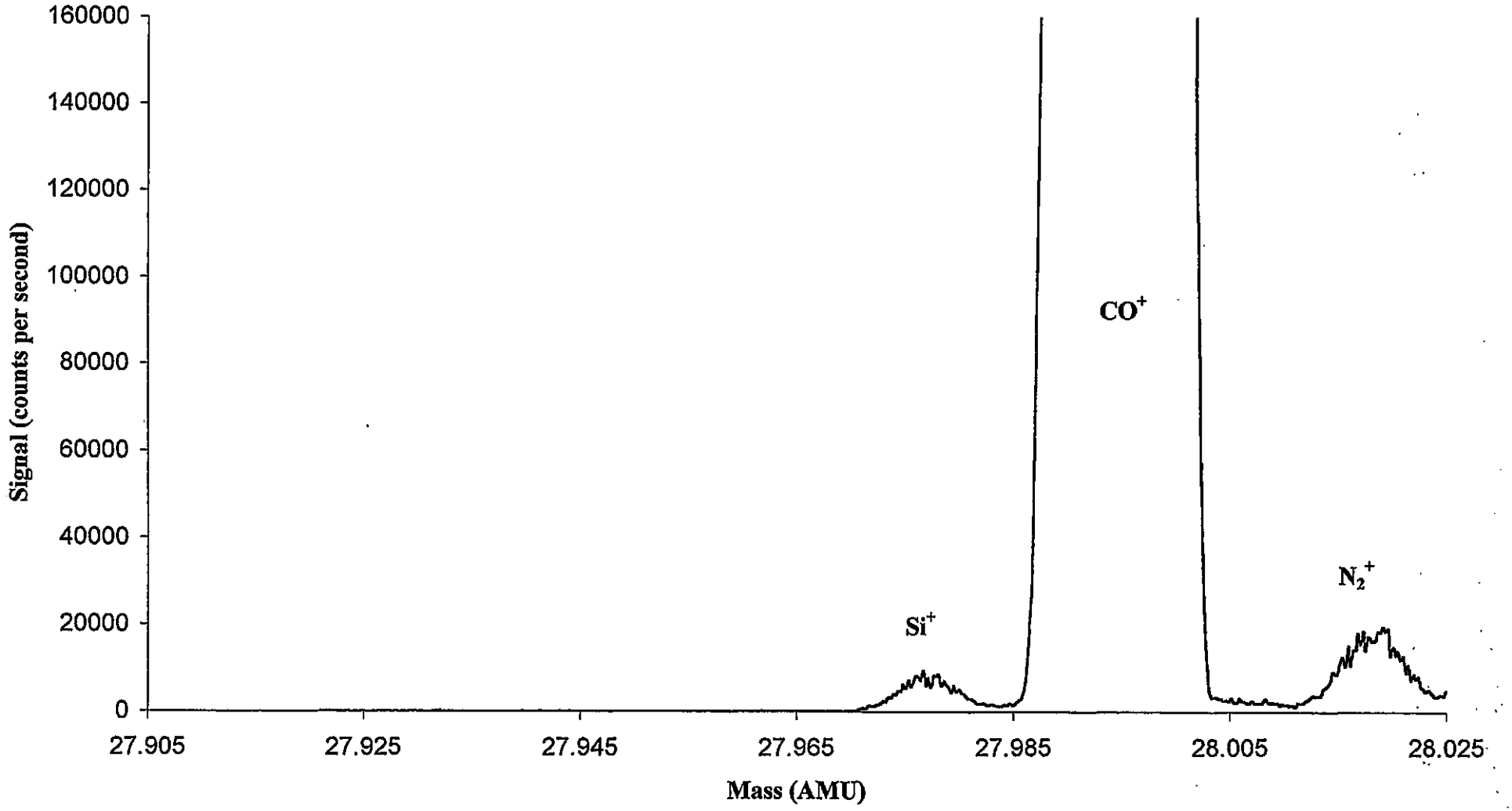

Figure 6.1: Mass spectrum around m/z 28

rate of 1 ml min^{-1} xylene (Anal R, BDH, Poole, Dorset, UK). A phenogel 5 guard column 50 x 7.8 mm i.d. was placed in front of the analytical column. Detection was performed using a sectorfield inductively coupled mass spectrometer (Axiom, Thermoelemental, Winsford, Cheshire, UK). The impact bead spray chamber was connected to the ICP torch via a T - piece with a gas inlet controlled by an external mass flow controller. Oxygen was added to the ICP, via this gas inlet, as a diluent gas from a 8: 92 % v/v oxygen/argon gas blender (Signal instruments, Camberley, Surrey, UK). The oxygen flow rate was optimised so that the green C_2 emission band did not impinge on the tip of the Pt cone. Operating conditions are shown in Table 6.1.

6.2.1.2: Data Acquisition

Data was acquired in single ion monitoring mode with a dwell time of 500 ms and saved as a CSV file. The peak area of the chromatograms was calculated using Un-Scan-It (Silk Scientific Corporation, Ormen, Utah, USA).

6.2.1.3: Reagents

Three PDMS fluids (BDH, Poole, Dorset, UK) of different viscosities, 0.65, 20 and 1000 centistokes were used. The average molecular weight attributed to these standards is shown in Table 6.2. Stock standard solutions were prepared, in xylene, from neat polymer standards and stored in amber coloured bottles due to the photo-sensitivity of the lowest molecular weight standard.

The mobile phase was degassed for 5 minutes with helium prior to use.

6.2.1.4: Spiking procedure

Blood was taken from one human male from the arm by venepuncture using a butterfly needle and 20 ml syringe, and dispensed into 10 ml glass tubes. Plasma was separated from blood by centrifugation at 2000 rpm and transferred to glass vials, using

Table 6.1: ICP-MS operating conditions for size exclusion separation of Silicones

Forward Power (W)	1280
Reflected power (W)	< 5
Coolant (l min^{-1})	14
Auxiliary (l min^{-1})	0.7
Nebuliser (l min^{-1})	0.35
O_2/Ar diluent gas (l min^{-1})	0.4 (32 ml min^{-1} O_2)
Spray Chamber	Jacketed Cyclone connected to impact bead
Spray chamber temperature (^{0}C)	5
Sampler	Pt
Skimmer	Ni
Ion mass (m/z)	$^{27.98}Si^+$
Resolution	3000
Dwell time (ms)	500

Table 6.2: The relationship between viscosity of the PDMS standards and the attributed molecular weight*

Viscosity of PDMS standard (centistokes, cs)	**Average molecular weight (g mol^{-1} *)**
0.65	162
20	1500
1000	16500

* Data supplied by BDH

glass pasteur pipettes, and stored in a freezer. Recovery studies of the three PDMS standards from plasma were made by spiking 995 µl of plasma, in 7 ml glass vials, with 5 µl of either a 200 µg ml^{-1} or 50 µg ml^{-1} PDMS standard made up in THF. The spiked samples were gently shaken and stored at 5^0C for 24 hours. The spiked plasma samples were extracted with 2 x 0.5 ml xylene, this involved the addition of 0.5 ml xylene vortex mixing (Hook and Turner Instruments Ltd) the solution for 5 minutes and the upper xylene layer being transferred to a 2 ml glass vial using glass pasteur pipette. All glass vials were surrounded in silver foil. Glass beads, 3 mm in diameter, were placed in the bottom of the 7 ml glass vials during the extraction step to improve solvent interaction with the blood plasma and greater agitation and thus aid extraction of the silicones. Each spiking experiment was repeated three times to estimate reproducibility. Three blanks were also extracted for silicones.

6.2.2: Determination of silanols

6.2.2.1: Instrumentation

The chromatography was performed using a Waters 600 mutisolvent delivery system, operated in isocratic mode, fitted with a Rheodyne 9010 injection valve with a 100 µl sample loop (Cotati, CA, USA). The separation of inorganic silicon and two silanols was performed at ambient temperature using a YMC - pack polymer C_{18} column 250 mm x 2.1 mm i.d. (6 µm) (Hichrom, Reading, Berkshire, UK) at a flow rate of 0.15 ml min^{-1} 80 % DDW:20 % Methanol (Hipersolv, BDH, Poole, Dorset, UK). An in line filter (Alltech, Carnforth, Lancashire, UK) was placed in front of the analytical column.

Detection was performed using a sectorfield ICP-MS instrument (Axiom, TJA Solutions Winsford, Cheshire, UK). ICP-MS operating conditions are shown in Table 6.3. Data was acquired in single ion monitoring mode as described in section 6.2.1.2.

Table 6.3: ICP-MS operating Parameters for Reversed Phase Separation of Silanols

Forward Power (W)	1280
Coolant (l min^{-1})	14
Auxiliary (l min^{-1})	0.7
Nebuliser (l min^{-1})	0.8
Spray Chamber	Jacketed Cyclone connected to impact bead
Spray chamber temperature (^{0}C)	5
Sampler	Ni
Skimmer	Ni
Ion mass (m/z)	$^{27.98}Si^+$
Resolution	3000
Dwell time (ms)	500

6.2.2.2: Reagents

The three silicon standards used in this work were i) inorganic silicon ($(NH_4)_2SiF_6$) (BDH, Poole, Dorset, UK) ii) dimethylsilanediol (monomer) (synthesised by Dr P. Sutton, DeMontfort University, Leicester, UK) and iii) tetramethyldisiloxane-1,3-diol(dimer) (synthesised by Mr A. Tonkin University of Plymouth, Plymouth, Devon, UK). Figure 6.2 shows the structure of the two silanols. Appendix 1 contains the NMR spectra and melting point data for the two silanols that were synthesised. Standards were made up in the mobile phase in plastic volumetric flasks and kept refrigerated prior to analysis due to the silanols adsorbing to glass surfaces and their ability to undergo polymerisation at room temperature.

All solutions were degassed for 5 minutes with helium prior to use.

6.3: Results and Discussion

6.3.1: Determination of silicones

6.3.1.1: Figures of merit

Size exclusion chromatographic separation with ICP-MS detection of three PDMS polymers using a mobile phase of xylene was successfully achieved. A typical chromatogram from the system is shown in Figure 6.3. Each of the three PDMS fluids was at a concentration of 1 $\mu g\ ml^{-1}$ PDMS or in terms of Si the 0.65 cs standard is at a concentration of 346 $ng\ ml^{-1}$ while the 20 cs and 1000 cs standards are both at a concentration of 375 $ng\ ml^{-1}$. The retention times of the three standards were 6.1, 8.6 and 11.4 minutes for the 1000 cs standard, 20 cs standard and 0.65 cs standard respectively.

Xylene was the solvent of choice as it readily dissolved the polymers of interest, which ranged from a molecular weight of 162 $g\ mol^{-1}$ to 16500 $g\ mol^{-1}$. The higher molecular weight PDMS are only soluble in a limited number of solvents including

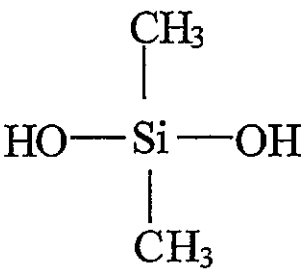

Dimethylsilandiol (Monomer)

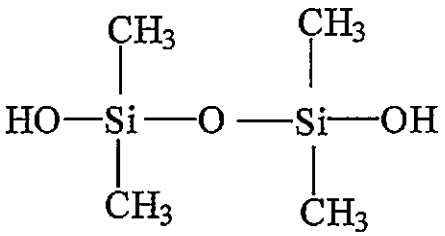

Tetramethyldisiloxane-1,3-diol (Dimer)

Figure 6.2: Structure of silanols used in reversed phase chromatography

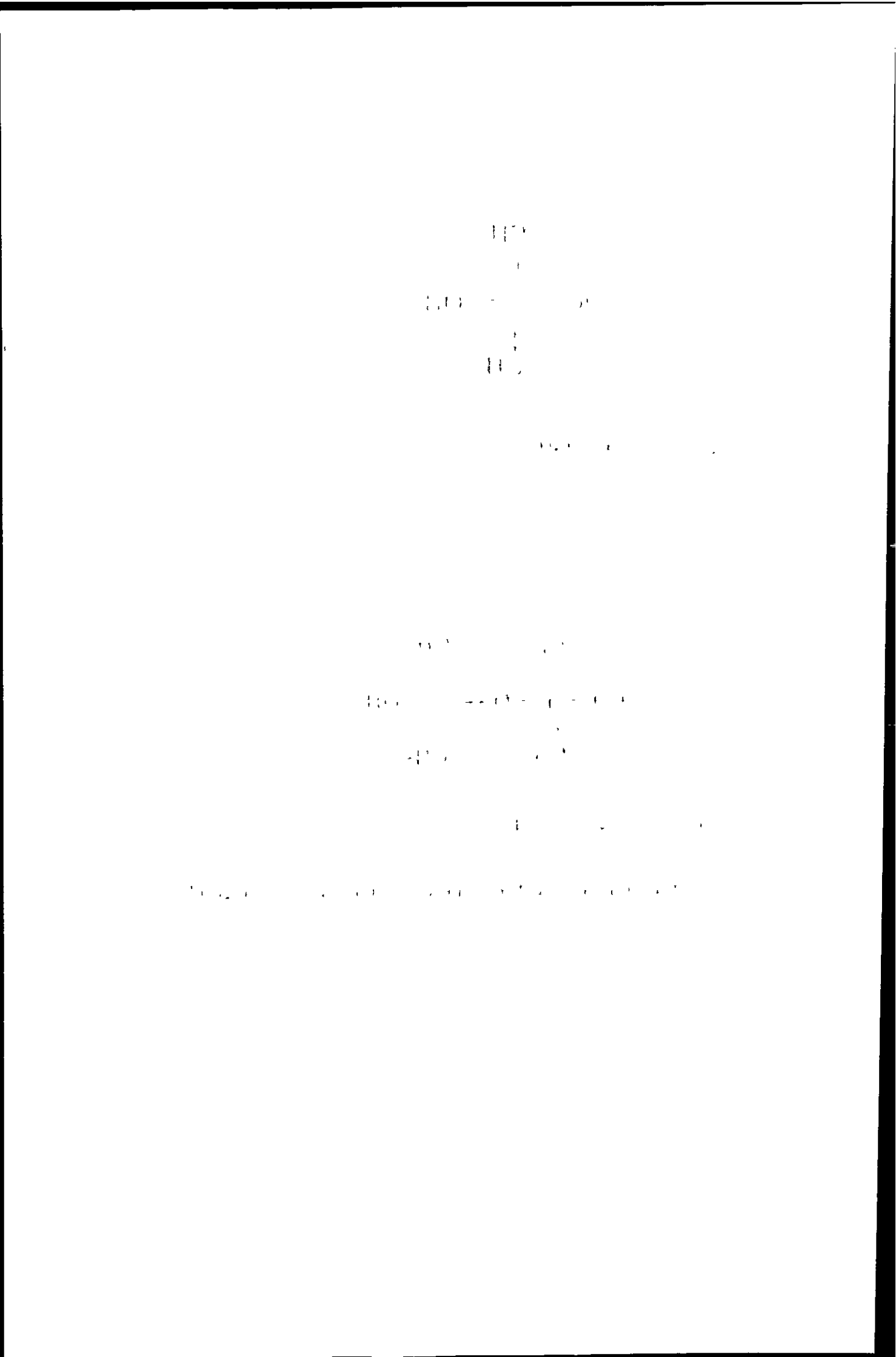

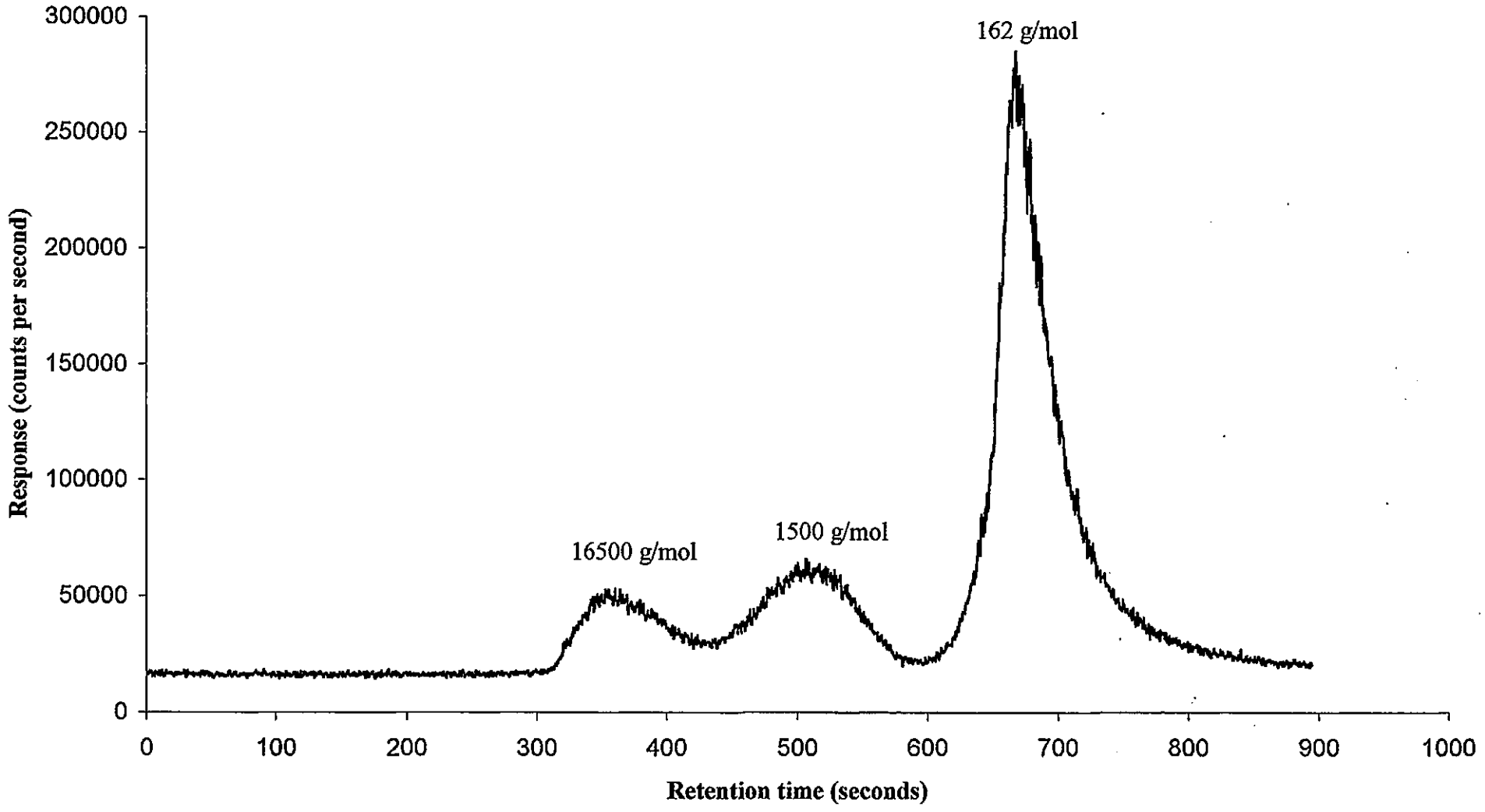

Figure 6.3: Size exclusion chromatographic separation of polydimethylsiloxanes

xylene and THF. Xylene was also a suitable solvent as it has a low vapour pressure. The three isomers of Xylene, ortho, meta and para, have vapour pressures of 0.88, 1.13 and 1.19 KPa at 25^0C respectively[31]. In comparison, THF has a vapour pressure, at 25^0C, of 21.6 KPa. Thus, it is easier to achieve a stable plasma at a higher flow rate of solvent with xylene than with THF.

Linearity was investigated using a stock standard solution of the three silicone polymers which was diluted serially. Calibration graphs are shown in Figure 6.4. Figure 6.4 shows that a linear response for the three standards was achieved. Other works have reported a non-linear response of PDMS using xylene as the mobile phase and ICP-AES detection[241], this was not found to be the case. However a linear response in xylene with ICP-AES detection has been reported elsewhere[249].

Figure 6.4 clearly shows that the response, Silicon concentration versus peak area, of the three standards is different. The 0.65 cs standard is a single monomer unit and therefore gives a sharp peak and not a 'hump' as it does not contain a distribution of molecular masses as do the other two standards and so its response is larger. The discrepancy between the 20 cs and 1000 cs standards in terms of response could be attributed to less efficient transport efficiency of the higher viscosity standard owing to its higher viscosity and incomplete decomposition in the plasma caused by its large molecular weight.

The 3 σ detection were 30 ng ml^{-1} Si for the 1000 cs standard, 26 ng ml^{-1} Si for the 20 cs standard and 12 ng ml^{-1} Si for the 0.65 cs standard.

The reproducibility of the system was investigated by making five replicate injections, the RSDs were 3.4 %, 3.4 % and 1.4 % for the 1000 cs, 20 cs and 0.65 cs standards respectively.

Silicon gel breast implants contain polydimethylsiloxanes ranging from low molecular weight to as high as 404, 000 g mol^{-1} [220]. Therefore there is a range of PDMS compounds that could potentially be detected in the blood of women who have such

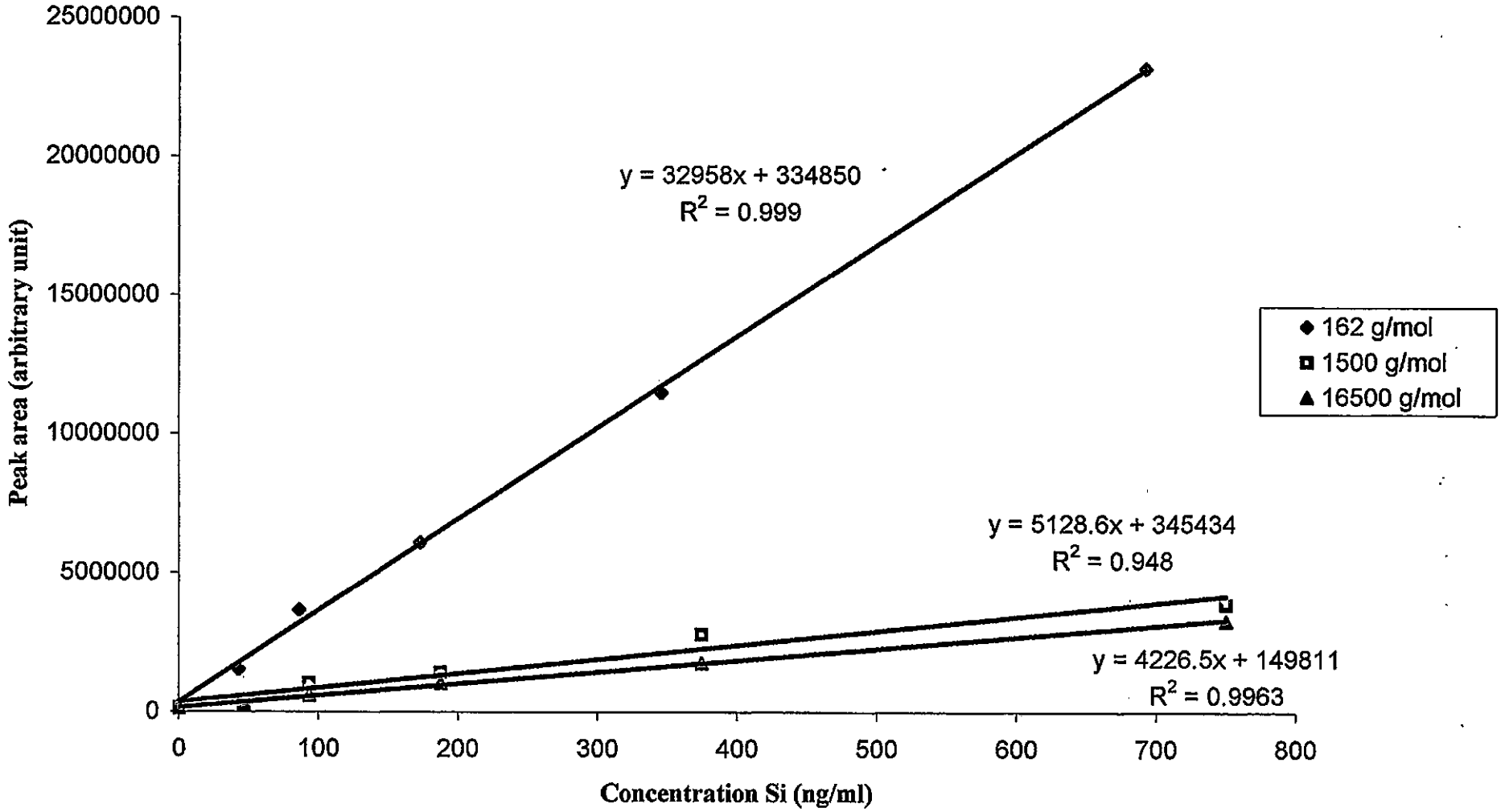

Figure 6.4: Calibration graph of Polydimethylsiloxanes

implants. It is necessary to calibrate the column in order to facilitate the identification of the molecular mass distribution of various molecular weight PDMS compounds in unknown samples. A plot of the log of the attributed molecular weight of the three silicone standards used versus their retention time is shown in Figure 6.5, a linear relationship was found.

6.3.1.2: Development of extraction method

In order to determine the silicones accurately in human plasma it was necessary to avoid contamination with PDMS or other silicones. Originally, blood was taken by venepuncture into vacutainers. It was found that the plasma became contaminated with silicone, which leached from the rubber seals of the vacutainers with an approximate molecular weight of 1500 g mol^{-1}. In addition, silicone contamination of the plasma occurred when using disposable plastic pasteur pipettes to transfer the plasma following centrifugation. The plastic pasteur pipettes contained a silicone lubricant with a molecular weight of approximately 16500 g mol^{-1}. These sources of contamination were differentiated from each other by passing a saline solution through the vacutainer and plastic pipette. These sources of contamination where of approximately the same molecular weight as two of the standards so had to be eliminated before analysis could proceed.

It was found that drawing a saline solution through a butterfly needle into a 20 ml syringe resulted in no detectable contamination of the solution with silicone. Hence, blood was taken using a butterfly needle and a 20 ml syringe and then dispensed into 10 ml glass vials for centrifugation. Following centrifugation, plasma was transferred to glass vials using disposable glass pipettes. All equipment was checked for traces of silicone. For example the glass vials used were shaken with xylene which was subsequently injected onto the column. Similarly xylene was taken up in the pipettes

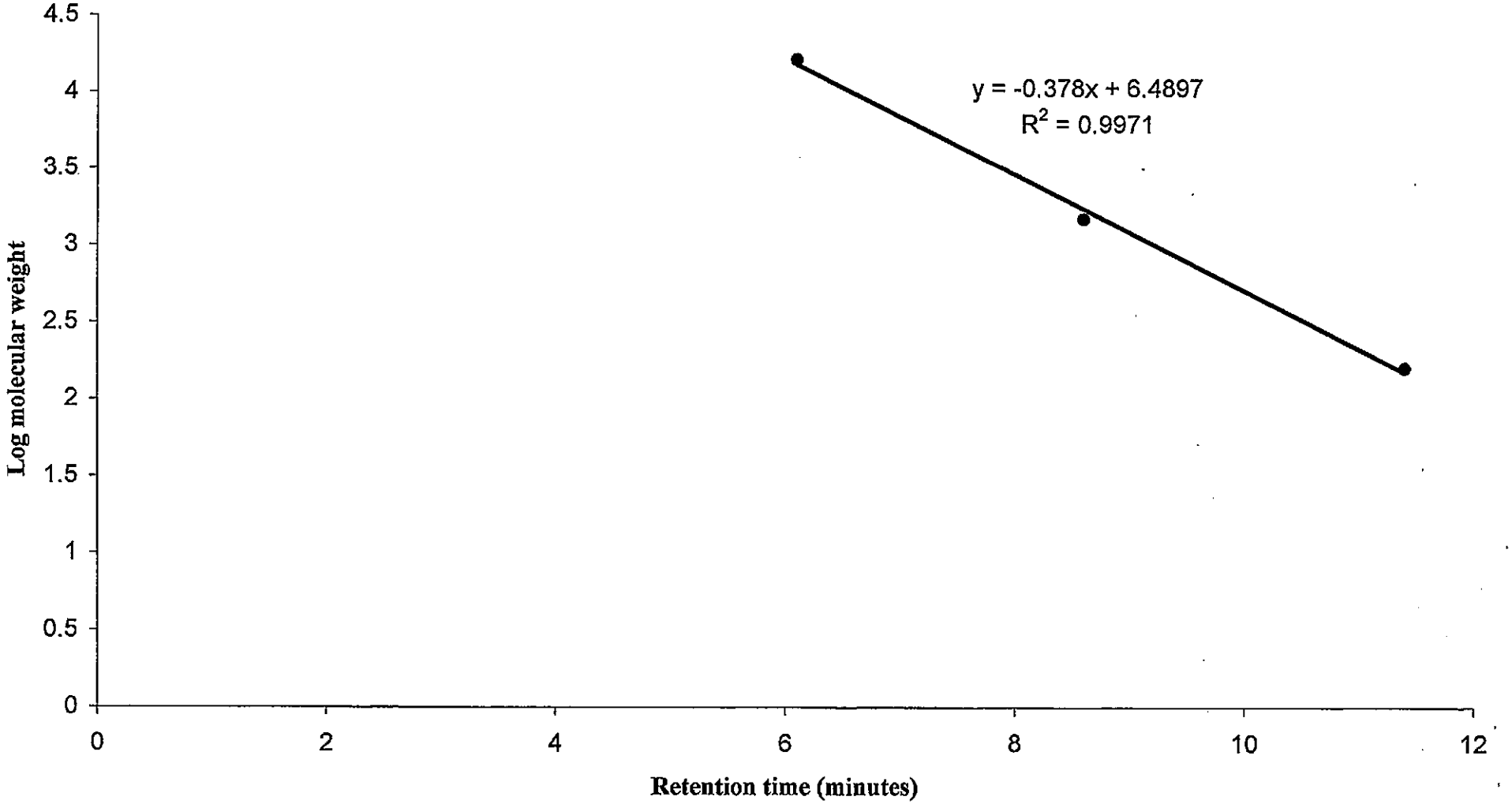

Figure 6.5: Calibration of size exclusion column

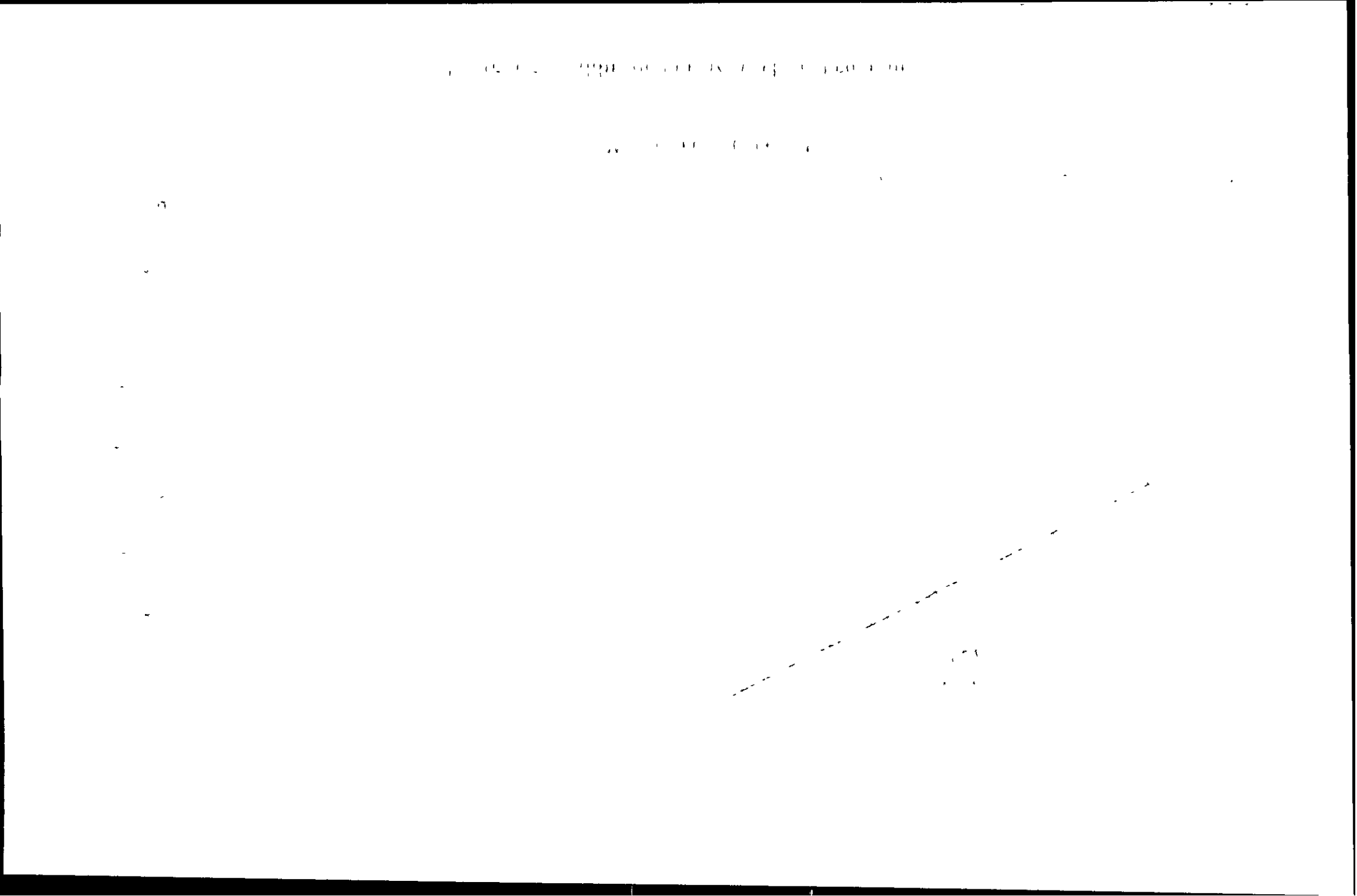

used and injected onto the column. No silicones were observed in three un-spiked plasma aliquots. Furthermore, blank xylene injections were made in between each standard and each plasma extraction. No carry over was observed.

Due to the low solubility of higher molecular weight silicones in aqueous media it proved difficult to spike human plasma samples. In contrast, spiking blood with low molecular weight silicones is easily achieved using methanolic spikes. Tetrahydrofuran is the preferred solvent with which to dissolve higher molecular weight PDMS compounds and has the added advantage that it is miscible with water and therefore plasma was spiked with standards made up in THF. Originally 900 μl aliquots of plasma were spiked with 100 μl of 10 μg ml^{-1} PDMS standards in THF. However, the volume of spike proved to be immiscible with the plasma. When 5 μl spikes were used a cloudy solution did not result. While spiking the plasma with a THF standard may not be ideal it was used as there was no alternative.

Extraction of PDMS from biological material has been undertaken successfully using ethyl acetate and THF, with extraction efficiencies of 80 % and 90% respectively[244, 245]. Similarly, hexane has also been used to extract low molecular weight silicones with over 90 % recoveries[242]. In this case, ethyl acetate and hexane could not be used because repeat injections of these solvents resulted in carbon build up on the cones. It is possible to evaporate the solvent and re-dissolve in xylene, however, this can lead to analyte losses, particularly when the sample size is small and the analyte concentration is low. It was considered inappropriate to use THF as the extraction solvent as this was used to prepare the spikes. Hence it was decided to use xylene as the extraction solvent, which had the advantage that it was also the mobile phase.

Originally PDMS was extracted from 1 ml spiked plasma samples using 1 ml xylene. This gave poor extraction efficiencies. In order to improve this extraction efficiency several approaches may be adopted. It is standard practice to repeat extractions three times with fresh solvent and combine individual extracts. This may

lead to large solvent volumes that will have to be concentrated for the determination of low analyte levels. This can lead to the loss of some of the more volatile extracted silicones. The lowest molecular weight standard used in this work, 162 g mol^{-1}, is more volatile than xylene and therefore the rotary evaporation of xylene from combined extracts would be unacceptable. This approach would work for the higher molecular weight standards which are not volatile. However, a similar approach was adopted which negated the need to reduce the volume of the extracting solvent, by dividing the 1 ml of xylene, used to extract the PDMS, into 2 lots of 0.5 ml. Varaprath *et al.*[245] found that performing the extraction of octamethyl-cyclotetrasiloxane in the presence of glass beads greatly improved the efficiency. This was attributed to providing a greater surface area for solvent interaction with the plasma and greater agitation of the solvent. This approach was also adopted.

6.3.1.3: Spiked recoveries

Extraction of the three silicone standards spiked into plasma aliquots was performed as described in section 6.2.1.4. No silicone was observed in three un-spiked plasma samples. Therefore any silicone contamination of the blood was below the limit of detection. Injection of 100 µl of xylene between the injections of samples revealed no carry over.

Table 6.4 shows the results of the extraction efficiency of the three PDMS compounds used in this work. The extraction efficiency of the lowest molecular weight silicone standard is over 70 % for the 1 µg ml^{-1} spike and over 65 % for the 0.25 µg ml^{-1} spike. The extraction efficiencies of the two higher molecular weight silicone standards was very poor.

The spiking and extraction procedure used was tested on water samples before using plasma. The extraction efficiencies for the three silicone standards for the 1 µg ml^{-1} spike were over 90 %. The 0.25 µg ml^{-1} spikes still showed poor extraction

Table 6.4: Extraction efficiencies of linear silicones from spiked Human plasma a) 0.25 μg ml^{-1} spike and b) 1 μg ml^{-1} spike.

a)

Molecular weight g mol^{-1}	**Extraction efficiency %**		
16500	46	0	26
1500	15	0	35
162	65	0	82

b)

Molecular weight g mol^{-1}	**Extraction efficiency %**		
16500	49	50	61
1500	41	53	22
162	73	82	107

efficiencies, although not to the same extent as the plasma samples.

High extraction efficiencies have been reported elsewhere for some low molecular weight silicones. In the work performed by Flassbeck *et al.*[242] they extended their research to cover whole blood. They found extraction efficiencies of approximately 80 % in comparison to 90 % for plasma. As pointed out by the authors this was unexpected as the composition of blood is much more complex than that of plasma, and siloxanes may be expected to adsorb onto the surface of various blood components. The fact the extraction efficiencies were still very high showed this not to be the case. However, higher molecular weight siloxanes may exhibit a greater tendency to adsorb on various blood components and although plasma is less complex than whole blood it nevertheless contains many components that the silicones may adsorb to such as glucose, urea, fats, amino acids, vitamins and various hormones.

6.3.2: Determination of silanols

Reversed phase chromatographic separation of inorganic silicon and two potential polar PDMS breakdown compounds with ICP-MS detection has been achieved.

A polymer (polymethacrylate) C_{18} column was used as silanols interact too strongly with silica-based packing material[241]. It was also found that the silicon background from a capped C_{18} (ODS) column was too high making these columns unsuitable for use. The background from such a column at m/z 28 was found to be 9.5 x 10^5 cps. A typical chromatogram is shown in Figure 6.6, inorganic silicon is present at a concentration of 200 ng ml^{-1} Si while the two silanols are present at a concentration of 2 μg ml^{-1} silanol. The retention times were 3.0 minutes, 4.7 minutes and 27 minutes for inorganic silicon, dimethysilanediol and tetramethyldisiloxane-1,3-diol respectively and the reproducibility of 5 replicate injections was 11 % for inorganic silicon, 4.0% for dimethysilanediol and 6.5 % for tetramethyldisiloxane-1,3-diol.

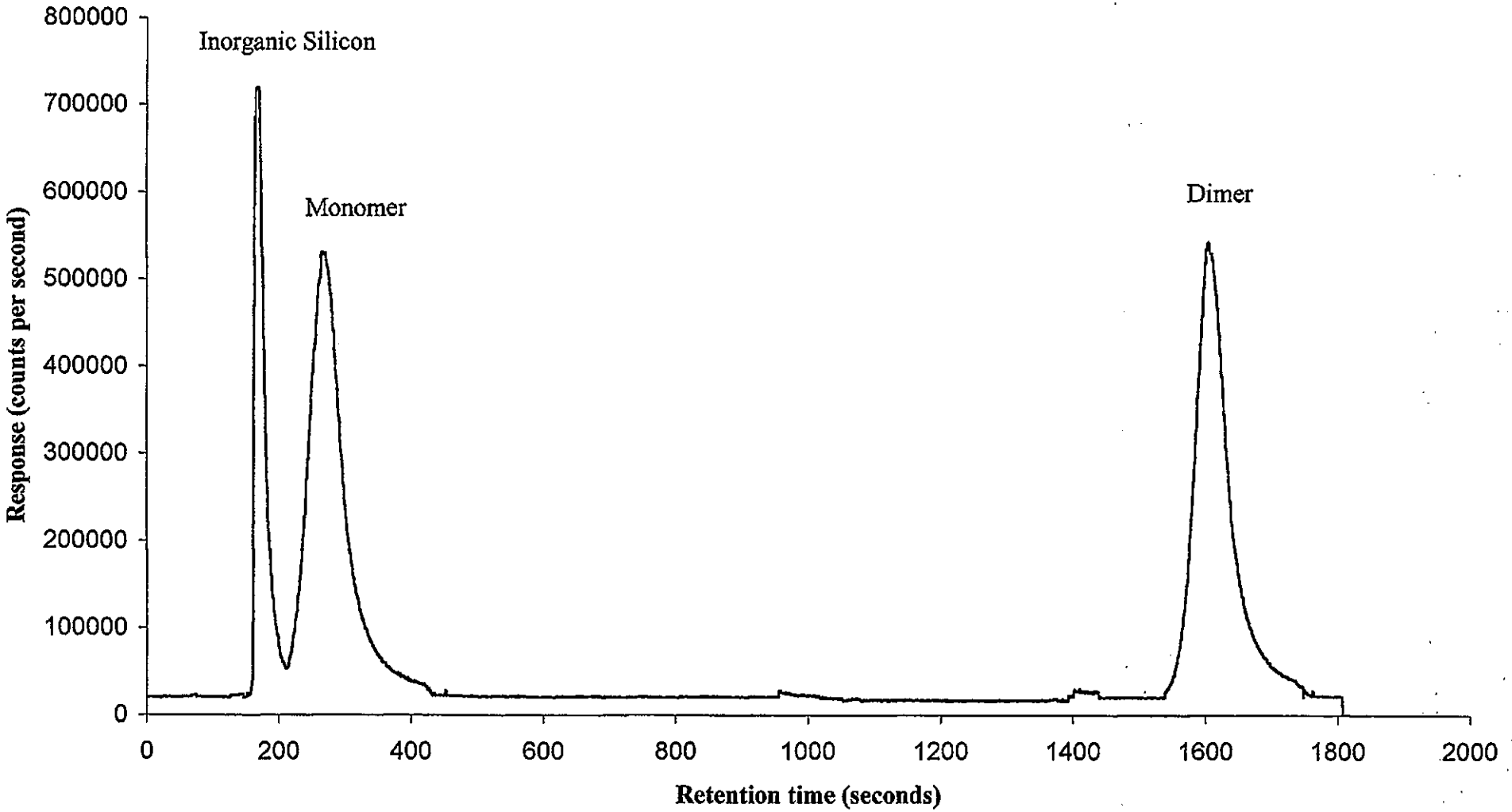

Figure 6.6: Reversed phase chromatographic separation of polar silicon compounds

Figure 6.6 shows that inorganic silicon comes of as a sharp peak and the response of the two silanols is not significantly different from each other.

Linearity was investigated using a stock solution of the three standards which was diluted serially. Figures 6.7 and 6.8 show that a linear response for silicate and the silanols was achieved.

The 3σ detection limits were 0.1 ng ml^{-1} Si, 4 ng ml^{-1} Si and 4 ng ml^{-1} Si for silicate, dimethylsilandiol and tetramethyldisiloxane-1,3-diol respectively.

Due to synthesis of the silanols, which are not available commercially, proving to be difficult this only represents a preliminary investigation into the separation and detection of the silanols. Insufficient sample was available to investigate the extraction of these compounds from plasma.

6.4: Conclusions

Conventional ICP-MS with a quadrupole mass analyser cannot be used for the determination of silicon as it suffers from interference by N_2^+, as a result of air entrainment into the plasma, and CO^+ formed when organic solvents are aspirated into the plasma. Using a sectorfield ICP-MS instrument N_2^+ and CO^+ can be resolved from $^{28}Si^+$ allowing its determination. This work has demonstrated the use of a sectorfield ICP-MS for the speciation of silicon.

Linear polydimethylsiloxanes ranging from 162 g mol^{-1} to 16500 g mol^{-1} which are found in the silicone gel of breast implants have been separated by size exclusion chromatography and detected by high resolution ICP-MS. PDMS Polymers can be determined and characterised by molecular mass using this system. It has been demonstrated that the response was sufficiently uniform, under the conditions described, to calibrate the system using any single PDMS polymer and hence for its determination in biological samples. The reproducibility of the system was very good.

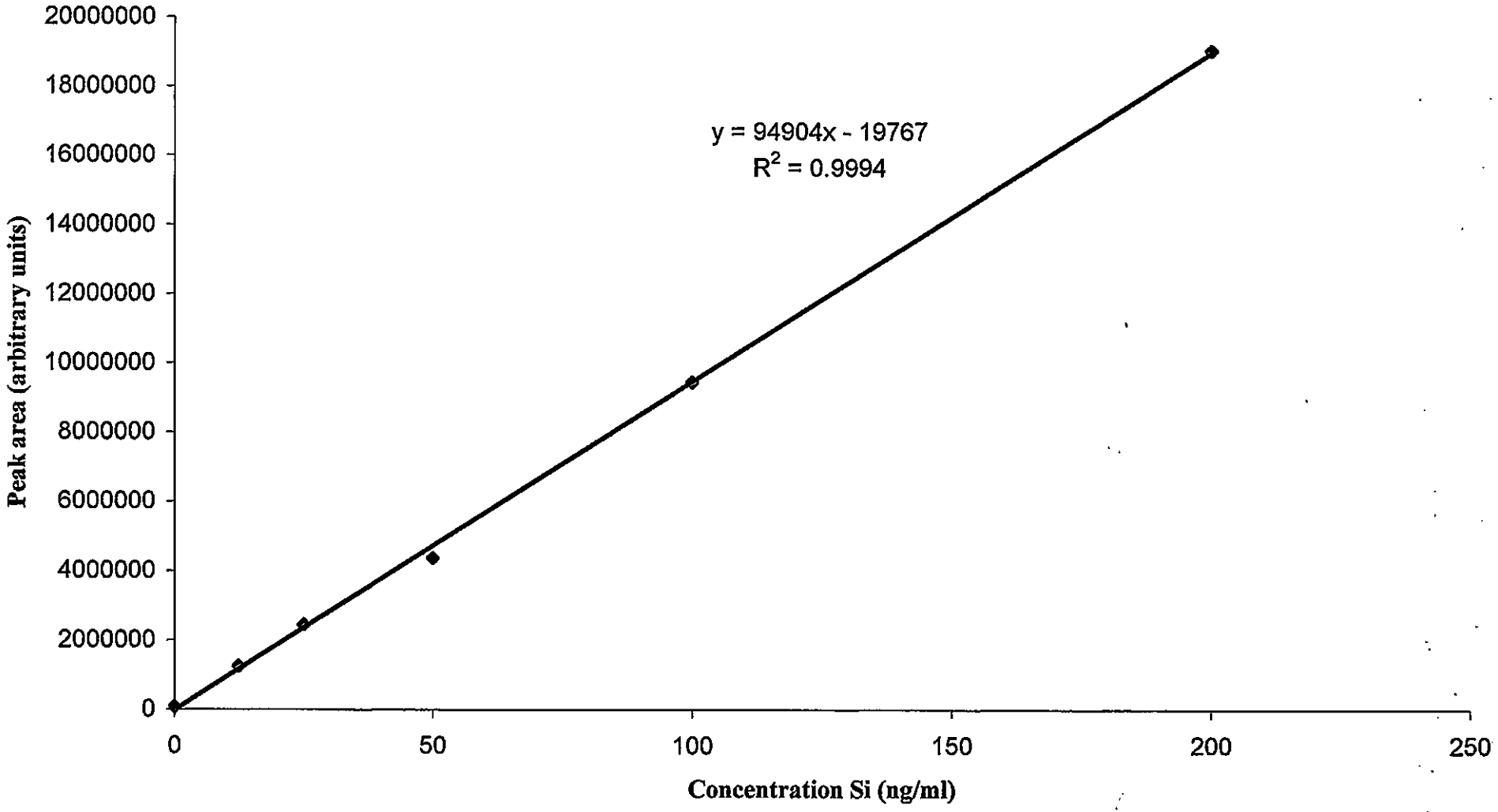

Figure 6.7: calibration graph of inorganic silicon

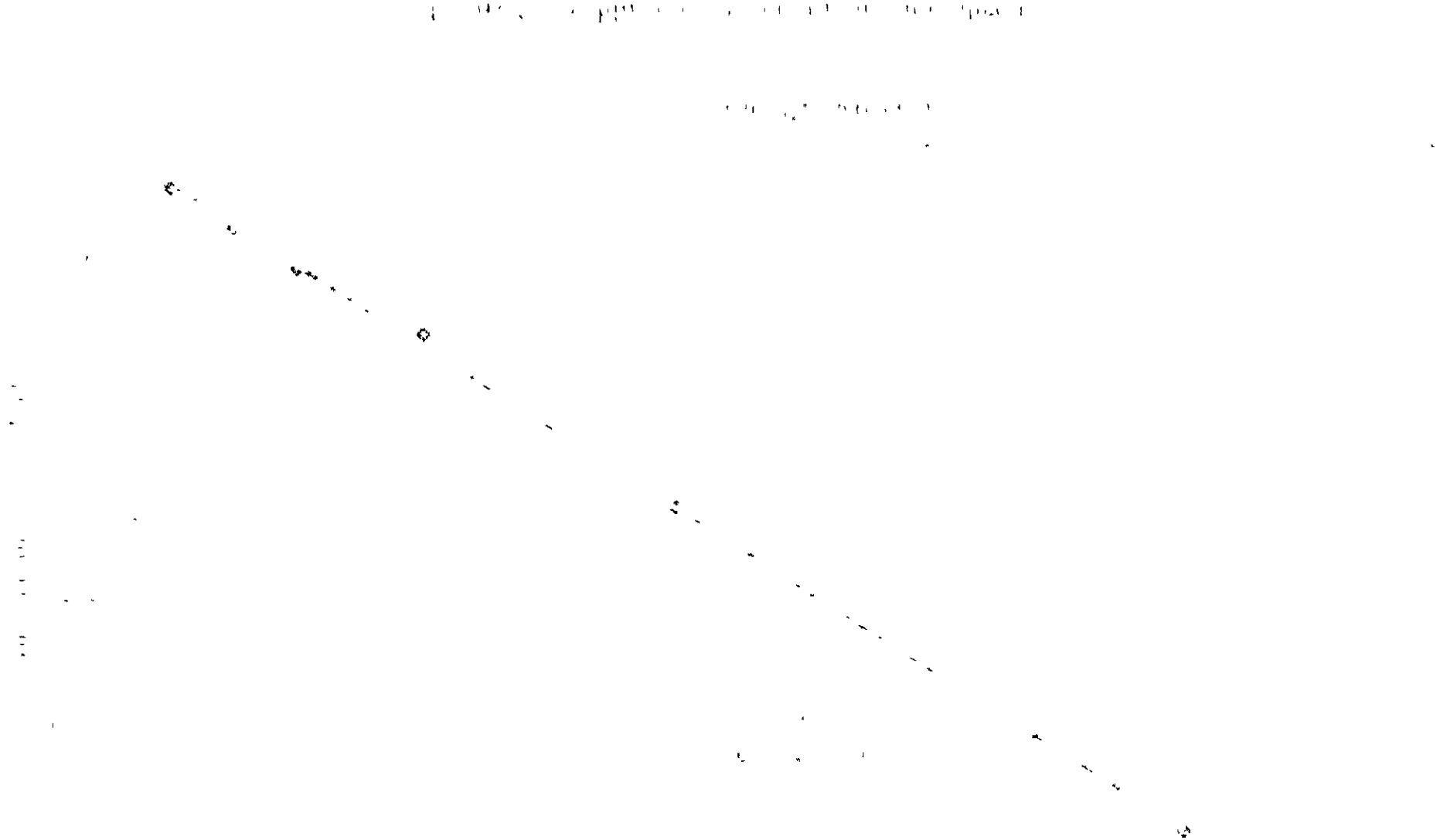

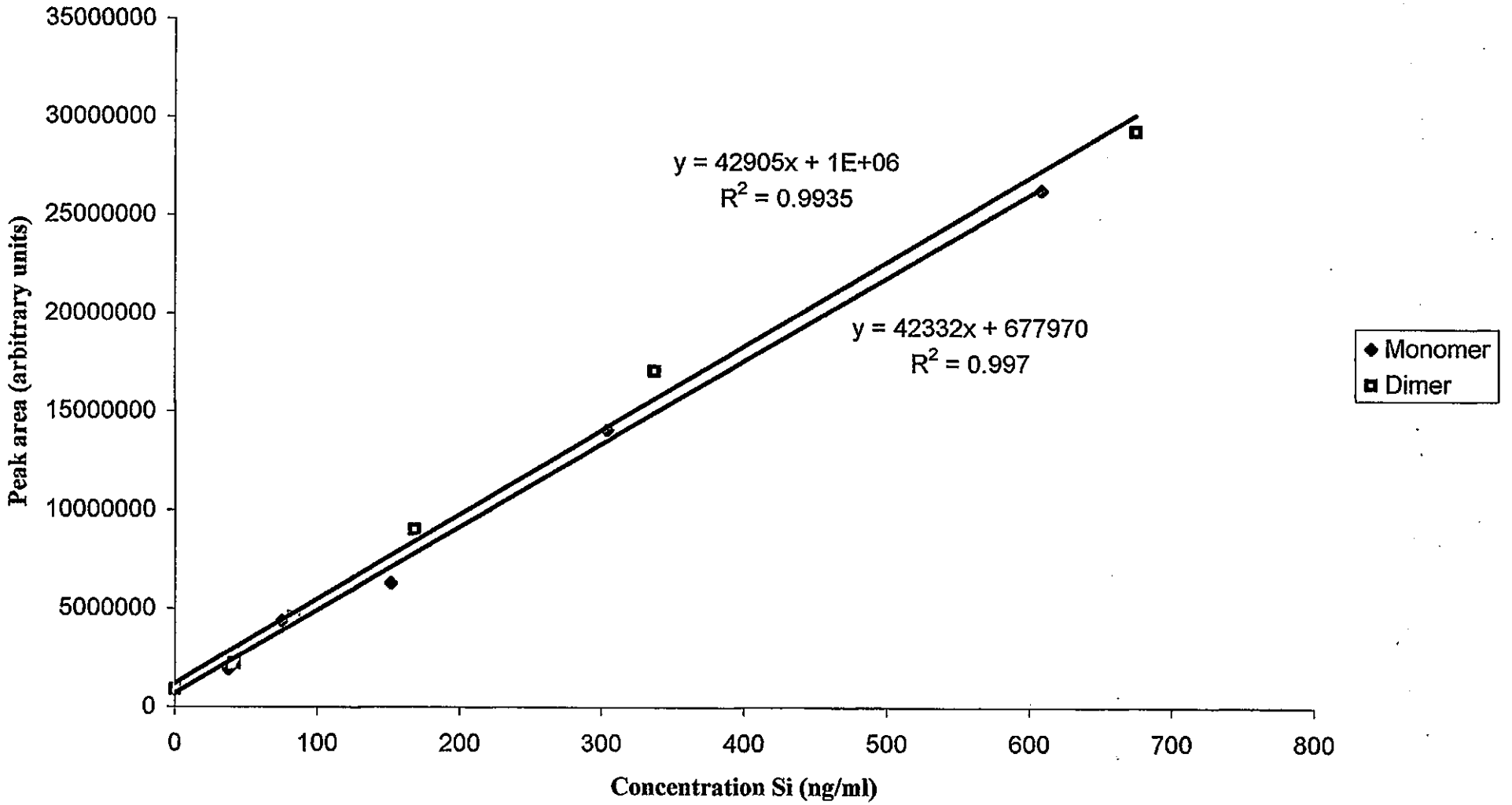

Figure 6.8: Calibration graph of Silanols

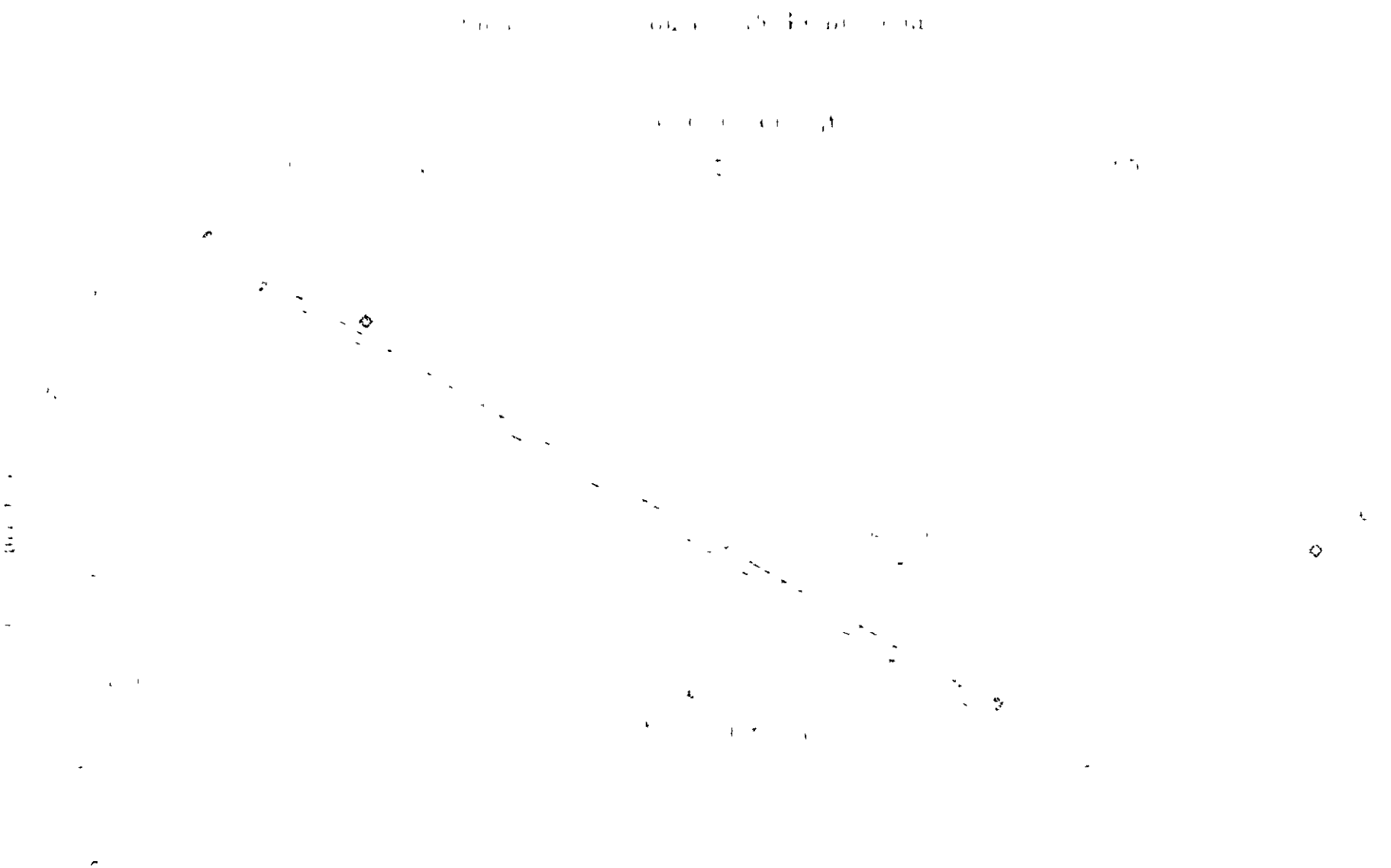

Normal serum silicon levels of 14 ± 1.0 ng ml^{-1} and 17 ± 10 ng ml^{-1} have been reported[250, 251].

The extraction efficiency was poor, and there is considerable room for improvement. These improvements must be made if real samples are to be determined. However, this work clearly demonstrates the feasibility of using SEC-ICP-MS to determine organosilicon polymers in biological samples.

Silicate and potential breakdown products of PDMS, the silanols, were successfully separated and detected using reversed-phase HPLC coupled to ICP-MS detection.

CHAPTER 7: PHOSPHORUS SPECIATION

7.1: Introduction

Phosphorous is a mono-isotopic, non-metallic element belonging to group V of the periodic table. It occurs in various phosphate rocks, from which it is extracted by heating with carbon and silicon (IV) oxide. Phosphorus is an essential element to all life, and it is almost without exception utilised as the phosphate anion. The ability of the phosphate anion to form polymers is vital to most life processes. The transfer of a phosphate unit from the tripolyphosphate portion of ATP (adenosine triphosphate) is the means of energy transfer in most biochemical reactions in living organisms.

However, phosphorus is an element that is difficult to determine accurately at very low levels by most analytical techniques, and ICP-MS is by no means an exception. Using a quadrupole ICP-MS instrument $^{31}P^+$ suffers from severe interference from NOH^+ and NO^+, however, using a sector-field instrument $^{31}P^+$ can be resolved from the polyatomic ions NOH^+ and NO^+ allowing the determination of $^{31}P^+$. The mass spectrum around m/z 31 acquired at a resolution of 3000 is shown in Figure 7.1, indicating $^{31}P^+$ has been resolved from NOH^+ and NO^+.

7.1.1: Organophosphates

Organophosphate pesticides (OPs) are esters of alcohols with phosphoric acids and are characterised by a central phosphorus atom and numerous side chains, Figure 7.2.

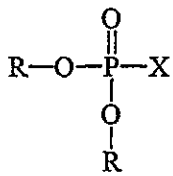

Figure7.2: The generic structure of organophosphate pesticides

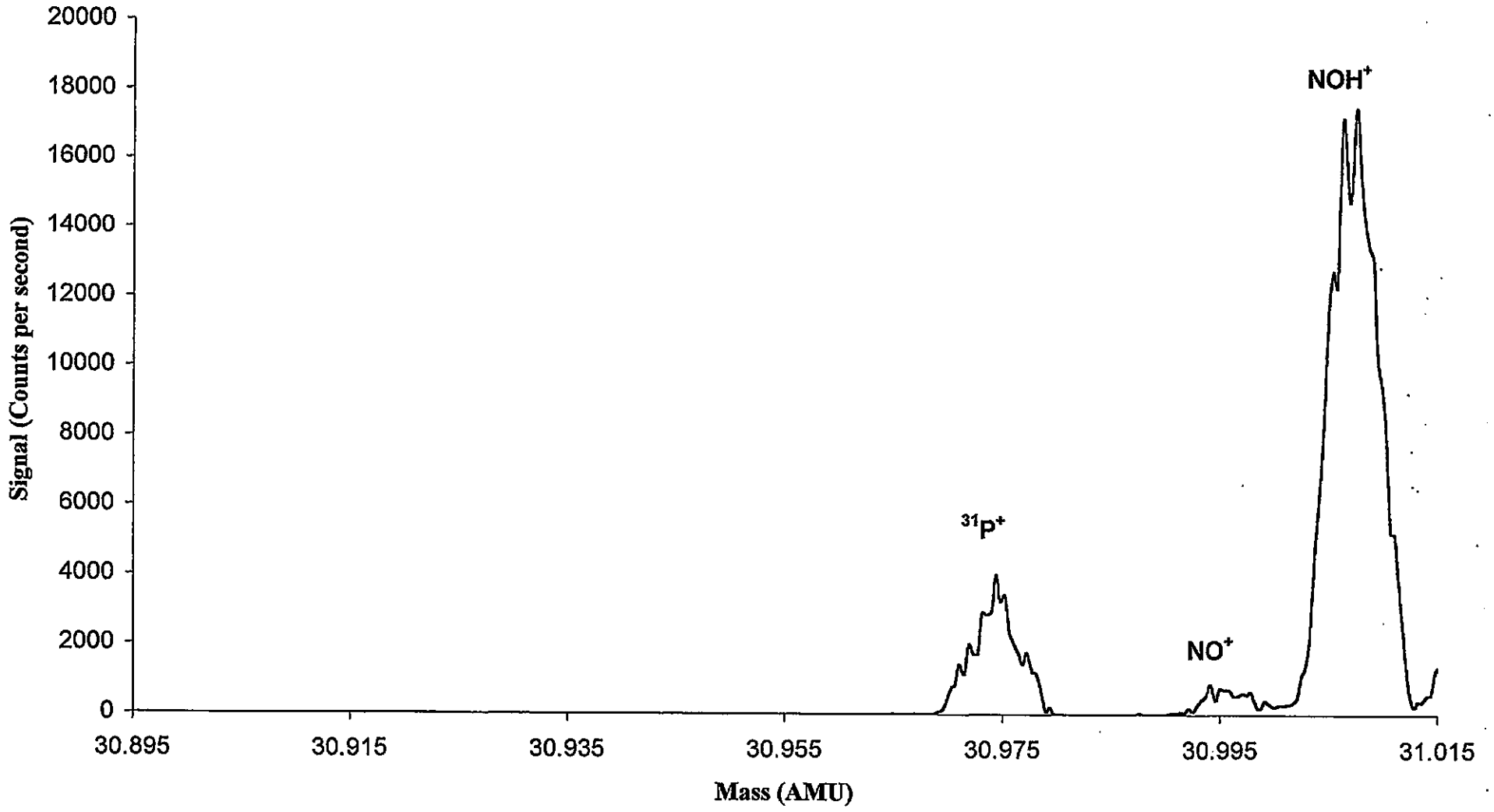

Figure 7.1: Mass spectrum around m/z 31

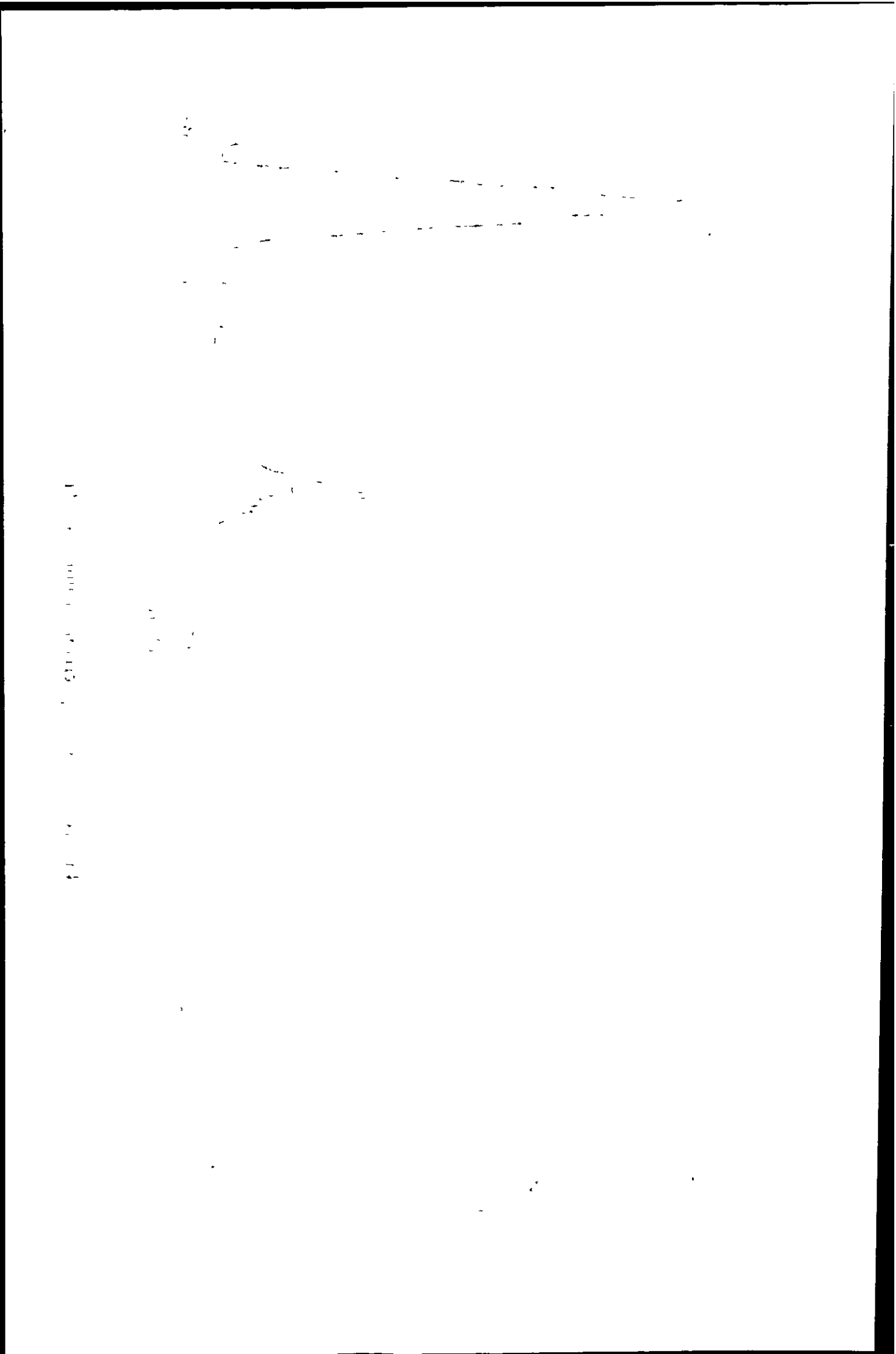

They are the most widely used insecticides and they are also used as herbicides and fungicides. Organophosphate pesticides were first developed in the early 19th century but their effect on insects was not discovered until 1932. Their wide use in agriculture and in the home in various formulations, is due mainly to their low persistence in the environment compared with the organochlorines.

Organophosphate insecticides are effective whether they are ingested or absorbed through the skin of the pest and are used against a variety of insects and mites. Organophosphates are used extensively on vegetables, fruits, rice and crops such as cotton, coffee, tea, wheat, corn, tobacco and spices. They are also used as veterinary medicines, for example, to protect farmed salmon against salmon lice and as aerosols against cat and dog fleas. They are also used in aerosol insecticides to control household and public health insect pests such as flies, mosquitoes, cockroaches and bedbugs. Some organophosphates, such as dichlorvos, are administered orally to livestock to control internal parasites or used externally, as in the case of sheep dipping, to control parasites on the animals' skins.

However, organophosphate pesticides have long been known for their potentially fatal effects on humans[252]. They have been linked to suicidal, intentional and accidental poisonings. Farmers and pesticide factory workers in developing countries have daily exposure to organophosphate pesticides at work[253] and long term occupational exposure can cause adverse health effects[254]. Furthermore, studies have demonstrated that home environments are commonly contaminated with pesticides including organophosphates[255, 256, 257, 258, 259]. Young children are particularly vulnerable to accidental poisoning due to their tendency to explore their environment[260]. For these reasons the determination of organophosphates in biological samples is important.

Organophosphate pesticides have been separated by HPLC following liquid-liquid extraction from water[261, 262] and food samples[263, 264]. Normal phase HPLC has

been used to separate organophosphate and carbamate pesticides from blood and tissue samples following pesticide poisoning[265].

7.1.2: Polyphosphates

Phosphorus, in the form of the polyphosphate anion, plays an important function in food processing. General functions of phosphates in food include: (1) inactivation of metal ions by complexation; (2) complexation of food constituents such as proteins; (3) direct chemical reaction with food constituents; (4) buffering or pH stabilisation; (5) dispersion of food constituents; (6) increasing hydration and water binding; (7) mineral supplementation; (8) acidification or lowering pH; (9) alkalisation or raising pH; and (10) food preservation. In beverages, phosphates are mainly used for acidification and complexing metal ions responsible for off flavours or loss of carbonation.

The production, processing and preservation of meat to maximise palatability has been of major concern in the technology of meat processing. The palatability of meat is judged largely by its colour in the raw and cooked states, its tenderness and flavour. Each of these characteristics is directly affected by chemical and physical factors that can be controlled to some extent, and phosphates play an important role in this control. Phosphate applications in meat include: (1) colour preservation; (2) increasing tenderness; (3) moisture retention; (4) improving flavour and (5) preventing off flavours and microbial spoilage.

An excess intake of phosphates, in common with all inorganic salts, may upset mineral balance in the body, adversely affect the osmotic pressure of body fluids, and prevent the absorption or utilisation of essential mineral nutrients[266]. An excess of phosphate may inhibit the absorption of calcium from the intestine, so the level of phosphates in foods must be controlled. Furthermore, the stability of phosphates in food is not fully understood, so the determination of the degree of polymerisation for phosphates in food is also important.

Numerous analytical methods have been employed for the determination of phosphates, including anion exchange HPLC with post column molybdate colourimetric detection[267, 268] or with indirect photometric detection[269]. Capillary electrophoresis has been employed to separate phosphates with indirect photometric detection[270]. ICP-AES[271] and ICP-MS[272] have been employed as a phosphorus specific detectors following separation by ion - exchange chromatography.

Hydroxide solutions are commonly employed as eluents in gradient ion chromatographic separation with suppressed conductivity detection[273, 274]. Naphthalene sulphonate derivatives such as NDS and NTS have been employed as pH-independent mobile phases for ion exchange chromatography for the separation of inorganic ions such as F^-, Cl^-, NO_2^-, Br^-, NO_3^-, SO_4^{2-}, I^-, and SCN^- [275] and polycarboxylates and polyphosphates[276]. Such mobile phases ensure reproducible elution and retention times without the need for precise control of the pH of the mobile phase.

Recently, ion chromatography with conductivity detection has been used to determine phosphates in food products[277, 278].

The aim of this work was to use high resolution ICP-MS for the speciation of phosphorus in food and clinical samples.

7.2: Experimental

7.2.1: Organophosphates

7.2.1.1: Instrumentation

The chromatography was performed using a Dionex GP40 gradient pump fitted with a Rheodyne 9010 injection valve with a 100 µl sample loop (Cotati, CA, USA). The separation of four organophosphate pesticides was performed at 40 ^{0}C using a Nova - Pak C_{18} column 3.9 mm i.d x 150 mm (Waters) at a flow rate of 1 ml min^{-1} 50:50 methanol (BDH, Poole, Dorset, UK): DDW(18 MΩ from a milli-Q analytical grade

water purification system, Millipore, Bedford, MA, USA). An inline filter (Alltech, Carnforth, Lancashire, UK) was placed prior to the analytical column.

Detection was performed using a sector-field inductively coupled plasma mass spectrometer (Axiom, TJA Solutions, Winsford, Cheshire, UK). Operating conditions are shown in Table 7.1. Data was acquired in single ion monitoring mode with a dwell time of 500 ms and saved as a CSV file as described in section 6.2.1.2.

7.2.1.2: Reagents

Four different organophosphate pesticide standards (Supleco, Poole, Dorset UK) (Figure 7.3) were used. Stock standard solutions were prepared in methanol and then stored in amber coloured bottles and kept in a refrigerator for further use.

7.2.1.3: Spiking procedure

Recovery studies of the four organophosphate pesticides from human plasma, taken as described in section 6.2.1.4, were made by spiking 990 µl of plasma with 10 µl of 200 µg ml^{-1} mixed methanolic standard of the pesticides. The sample was then left in a refrigerator for 24 hours. The pesticides were extracted from the plasma using 3 x 5 ml of petroleum ether (BDH, Poole Dorset, UK). The three organic fractions were combined and rotary evaporated to dryness at 40^0C and the residue was dissolved in 1 ml of methanol.

7.2.2: Inorganic phosphates

7.2.2.1: Instrumentation

The Chromatography was performed using a Dionex GP40 gradient pump fitted with a Rheodyne 9010 injection valve with a 100 µl sample loop (Cotati, CA, USA). The separation of three inorganic phosphate ions was performed at ambient temperature

Table 7.1: ICP-MS operating conditions for organophosphate separation

Forward Power (W)	1280
Coolant (l min^{-1})	14
Auxiliary (l min^{-1})	0.7
Nebuliser (l min^{-1})	0.7
Spray Chamber	Jacketed Cyclone connected to impact bead
Spray chamber temperature (^{0}C)	-5
Sampler	Ni
Skimmer	Ni
Ion mass (m/z)	$^{30.97}P^+$
Resolution	3000
Dwell time (ms)	500

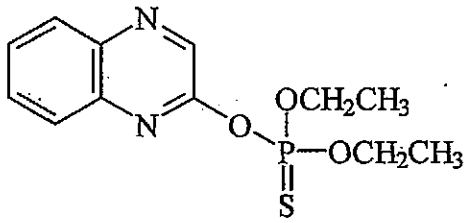

Quinolphos (O-O-diethyl-O-2-quinoxalinylphosphorothioate)

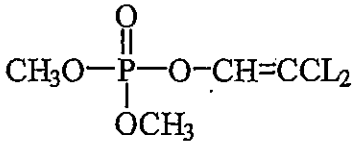

Dichlorvos (2,2-dichlorovinyl dimethyl phosphate)

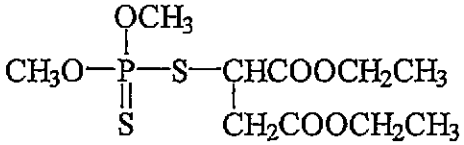

Malathion (S-1,2-bis(ethoxy-carbonyl)ethyl-O,O-dimethyl phosphorodithioate

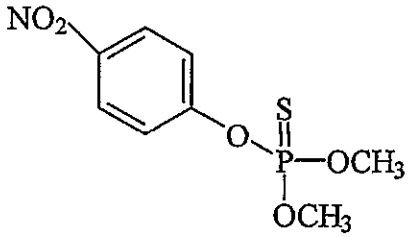

Methyl Parathion (O,O-dimethyl O-4-nitrophenylphosphorothioate

Figure 7.3: Organophosphate pesticides separated by reversed-phase chromatography

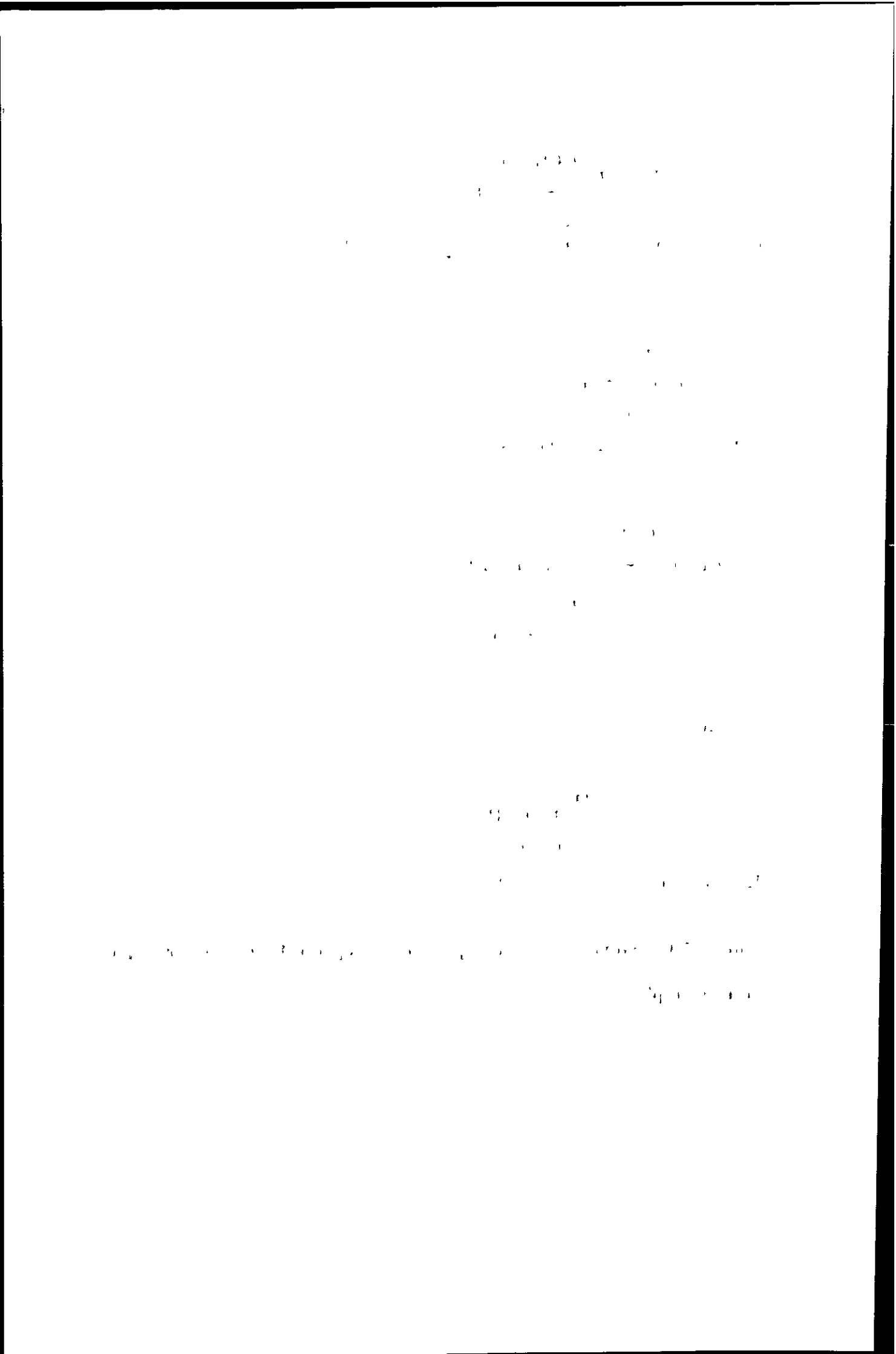

using a 4.6 mm i.d x 150 mm analytical PEEK column (Alltech, Carnforth, Lancashire, UK) packed with Hamilton PRP- X100, 10 μm, anion exchange resin (Phenomenex, Macclesfield, Cheshire, UK) at a flow rate of 1 ml min^{-1}. The mobile phase was 0.15 mM NTS (1, 3 -6-naphthalene sodium trisulphonate, Sigma - Aldrich, Poole Dorset, UK) made up in DDW (18 MΩ from a milli-Q analytical grade water purification system, Millipore, Bedford, MA, USA) with 5 % methanol added. An inline filter (Alltech, Carnforth, Lancashire, UK) was placed prior to the analytical column. The mobile phase was degassed for 5 minutes with helium prior to use.

Detection was performed using a sector-field inductively coupled plasma mass spectrometer (Axiom, TJA Solutions, Winsford, Cheshire, UK). Operating conditions are shown in Table 7.2. Data was acquired in single ion monitoring mode with a dwell time of 500 ms and saved as a CSV file as described in section 6.2.1.2.

7.2.2.2: Reagents

Three inorganic phosphate anion standards (Sigma-Aldrich, Poole, Dorset, UK), (Figure 7.4), were used. Stock standard solutions were prepared in DDW and then stored in a refrigerator.

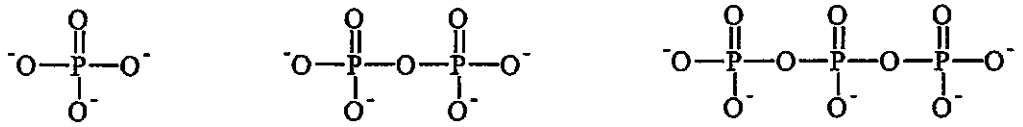

Orthophosphate Pyrophosphate Tripolyphosphate

Figure 7.4. Inorganic phosphate species separated by ion exchange chromatography

Table 7.2: ICP-MS operating conditions for inorganic phosphate separation

Forward Power (W)	1280
Coolant (l min^{-1})	14
Auxiliary (l min^{-1})	0.7
Nebuliser (l min^{-1})	0.8
Spray Chamber	Cyclone connected to impact bead
Spray Chamber Temperature (^{0}C)	5
Resolution	3000

A 2 M sodium hydroxide solution was prepared by dissolving 8 g of sodium hydroxide pellets (BDH, Poole, Dorset, UK) in 100 ml DDW.

A 20 % trichloroacetic acid solution was prepared by dissolving 20 g of trichloroacetic acid (BDH, Poole, Dorset, UK) in 100 ml of DDW.

7.2.2.3: Sample preparation

A previously reported sample treatment procedure was used[278]. Food samples (5 g solid or 5 ml liquid) were homogenised and 50 ml of DDW was added, the solution was then extracted ultrasonically for 15 minutes. The solid was removed by vacuum filtration, then 5 ml of 20 % trichloroacetic acid was added to the solution. The resulting precipitate was removed by vacuum filtration.

The pH of the solution was increased to a pH of 10 by the addition of 2 M sodium hydroxide and then the solution was made up to 100 ml with DDW. Further dilution of the sample solution was performed where necessary with DDW.

7.3: Results and discussion

7.3.1: Determination of organophosphates

A methanolic solution of all four pesticides was prepared and analysed at different flow rates, mobile phase compositions and column temperatures. The best separation was achieved at a column temperature of 40 ^{0}C, flow rate of 1 ml min^{-1} and mobile phase composition of 50 % methanol (Figure 7.5).

The elution pattern of the pesticides was in the order of: dichlorvos (184 seconds), methyl parathion (500 seconds), malathion (732 seconds) and quinolphos (1488 seconds). Calibration graphs for the four organophosphate pesticides are shown in Figure 7.6. The reproducibility of the system was investigated by testing five duplicates and the RSDs were 3.8 % for dichlorvos, 8.6 % for methyl parathion, 9.2 % for malathion and 8.4 % for quinolphos. The 3σ detection limits (in terms of P) were 0.9

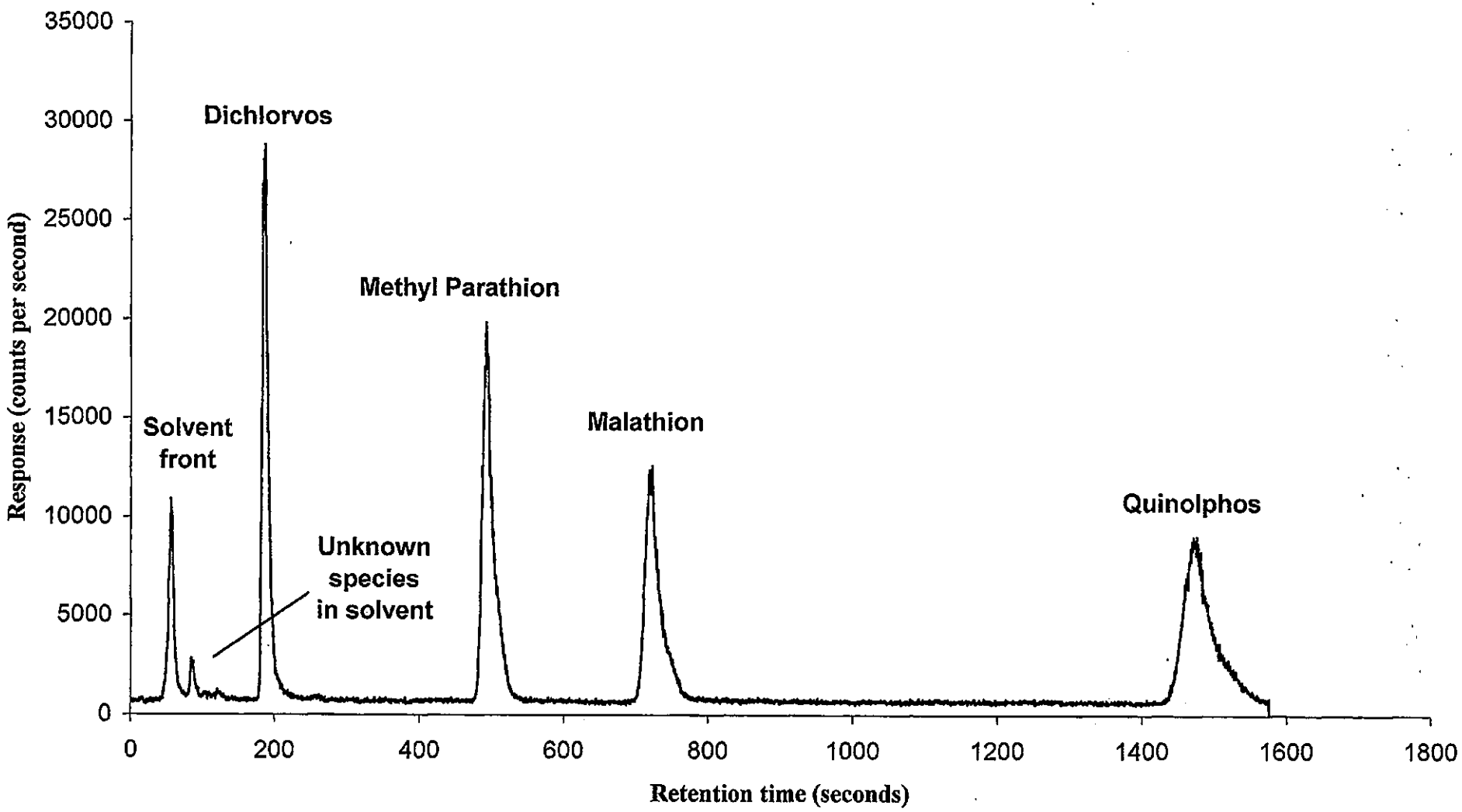

Figure 7.5: Reversed phase chromatographic separation of four organophosphate pesticides

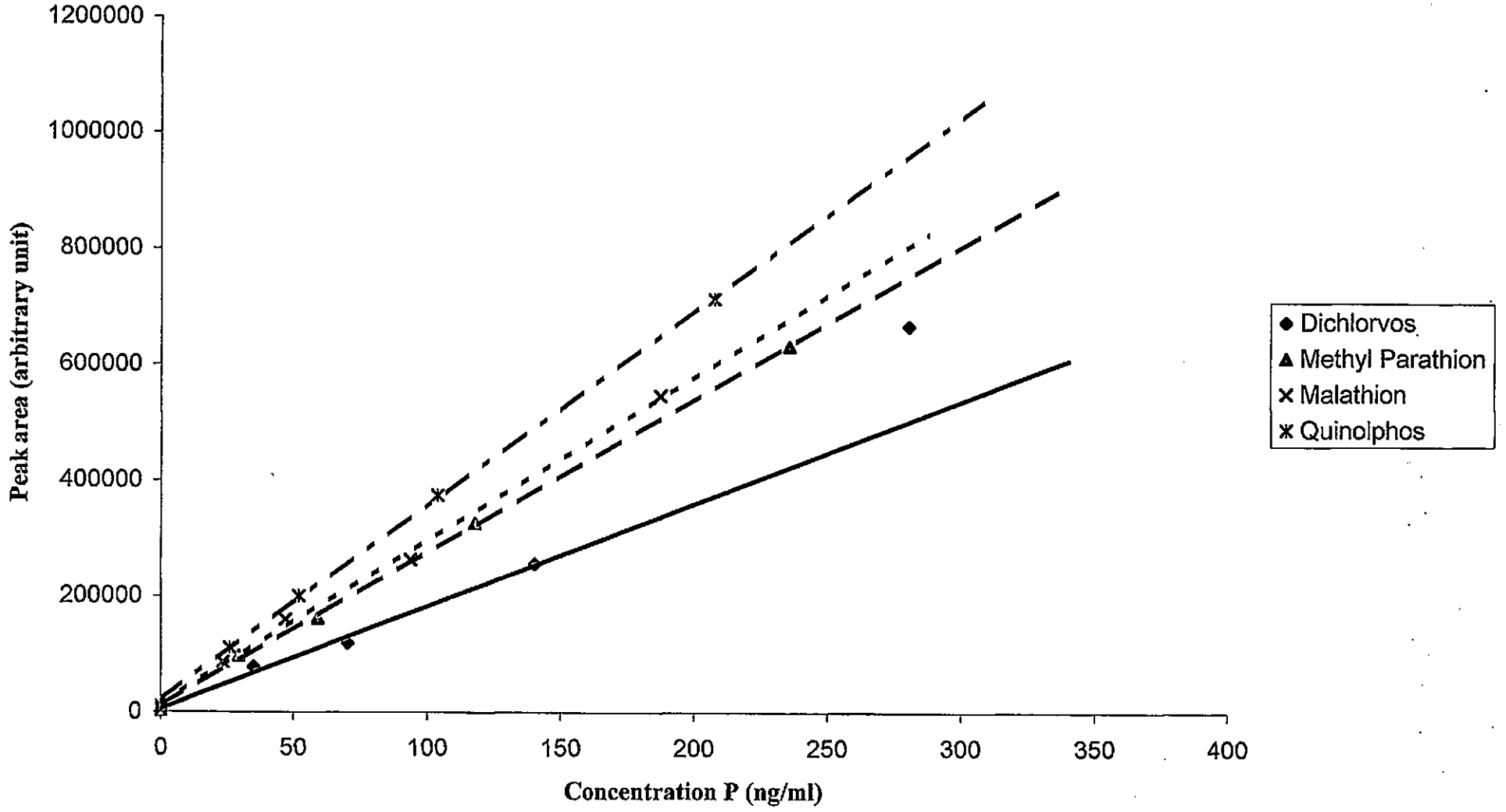

Figure 7.6: Calibration graph of organophosphate pesticides

ng ml^{-1}, 1.8 ng ml^{-1}, 1.6 ng ml^{-1} and 3.0 ng ml^{-1} for dichlorvos, methyl parathion malathion and quinolphos, respectively.

Table 7.3 shows the percentage recoveries of the four pesticides from spiked plasma samples. Recoveries were between 55 - 81 %.

7.3.2: Determination of inorganic phosphate anions

7.3.2.1: Figures of merit

Figure 7.7 shows a separation of three inorganic phosphate anions achieved using a mobile phase of 0.15 mM NTS. The retention times of the three inorganic phosphate anions were 133 seconds, 183 seconds and 562 seconds for PO_4^{3-}, $P_2O_7^{4-}$ and $P_3O_{10}^{5-}$, respectively. Lowering the concentration of NTS did not result in improved resolution of PO_4^{3-} and $P_2O_7^{4-}$. The retention times of the three phosphate anions were directly proportional to the effective charge, ionic radius and polarisability and inversely proportional to the hydration energy[279].

Calibration graphs are shown in Figure 7.8 for the three phosphate anions. The RSDs of five replicate injections were 2.5 % for PO_4^{3-}, 7.9 % for $P_2O_7^{4-}$ and 8.9 % for $P_3O_{10}^{5-}$. The 3σ detection limits (in terms of P) were 1.0 ng ml^{-1}, 2.3 ng ml^{-1} and 39 ng ml^{-1} for PO_4^{3-}, $P_2O_7^{4-}$ and $P_3O_{10}^{5-}$ respectively.

7.3.2.2: Application to food samples

Ion exchange chromatograms of the food extracts are shown in Figures 7.9 - 7.10. Figure 7.9 shows the presence of an unknown phosphate species at a retention time of 210 seconds eluted directly after $P_2O_7^{4-}$.

Polyphosphates are not stable in aqueous solution, and for this reason samples were analysed within two hours of extraction. Only ortho- and pyrophosphate were found in sausage meat and the ingredients label indicates the presence of these two

Table 7.3: Recoveries of Organophosphate pesticides from plasma

% Recovery				
Sample	**Dichlorvos**	**Methyl Parathion**	**Malathion**	**Quinolphos**
1	69.0	60.8	69.5	55.2
2	64.1	63.6	72.6	60.3
3	63.8	62.7	64.5	80.9

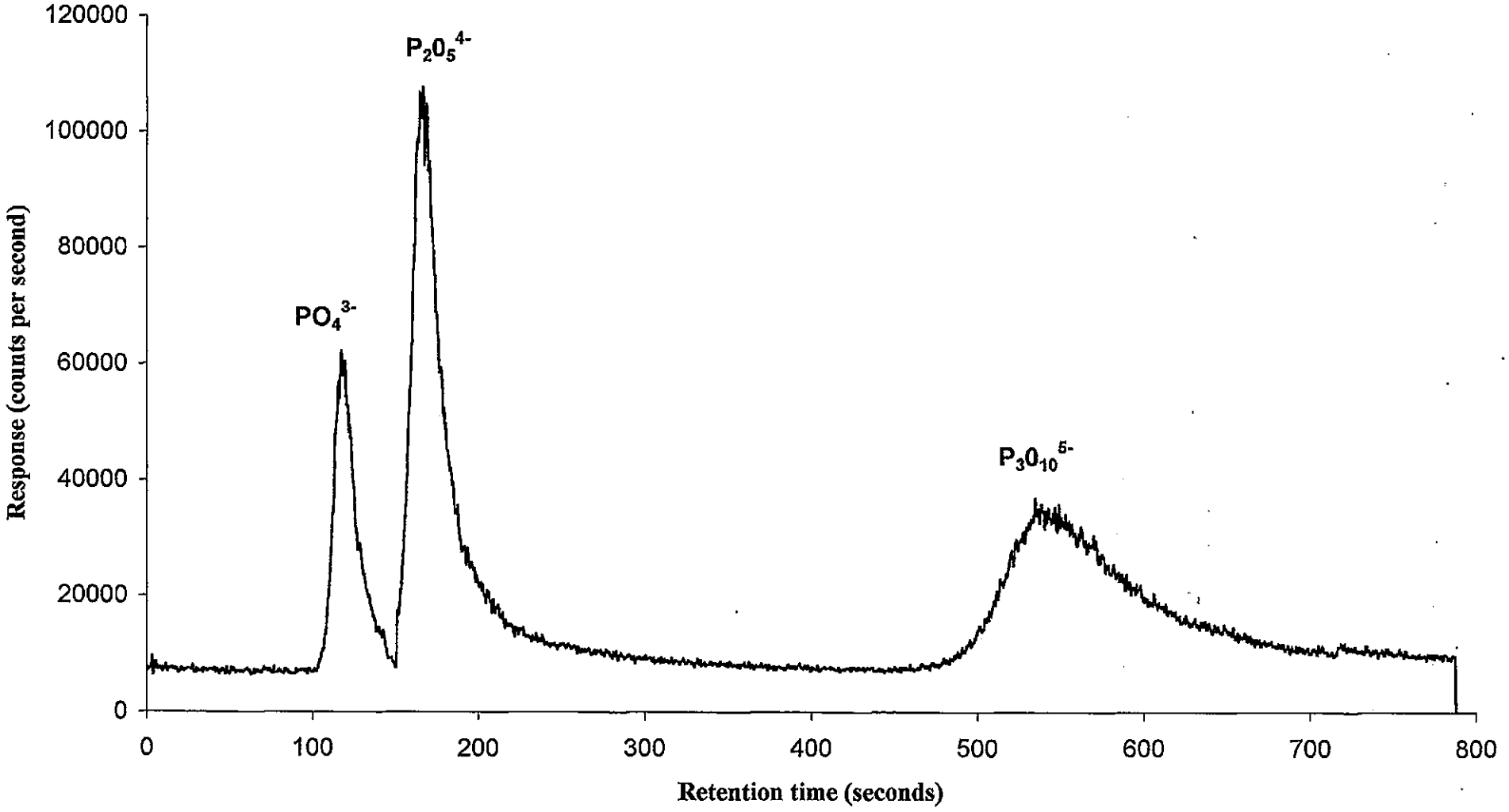

Figure 7.7: Ion exchange chromatograpahic separation of inorganic phosphates

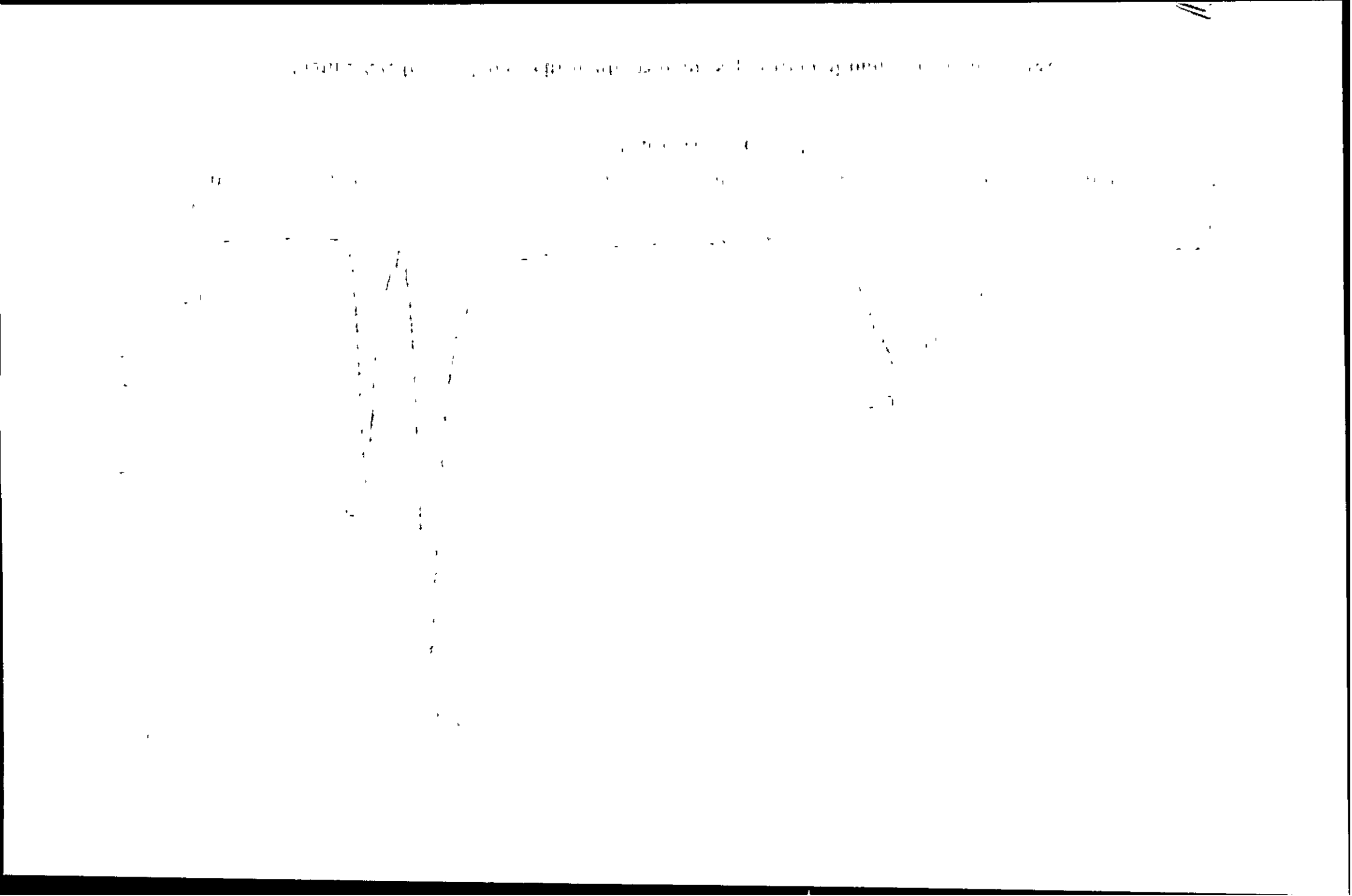

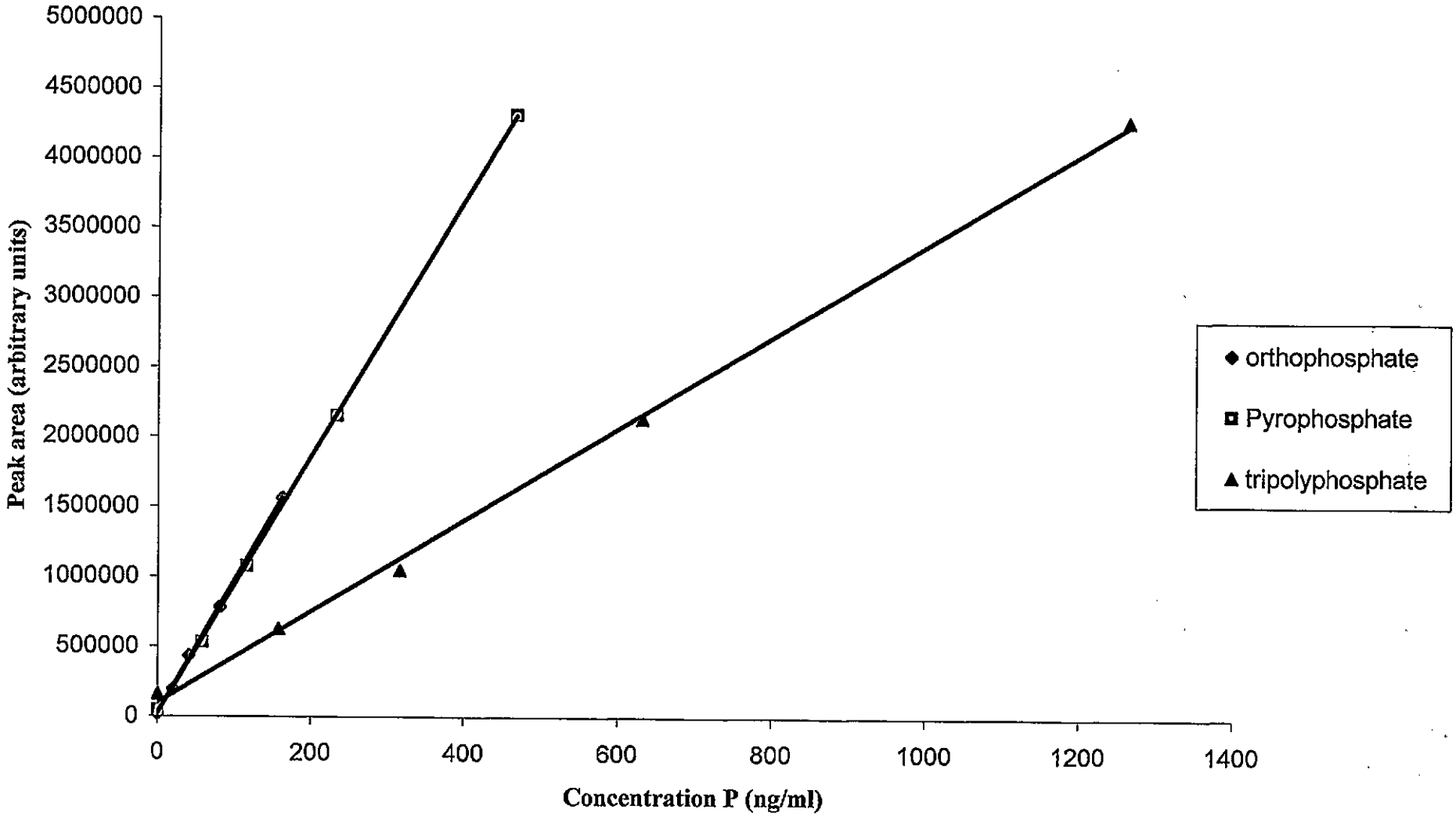

Figure 7.8: Calibration graph of inorganic phosphate species

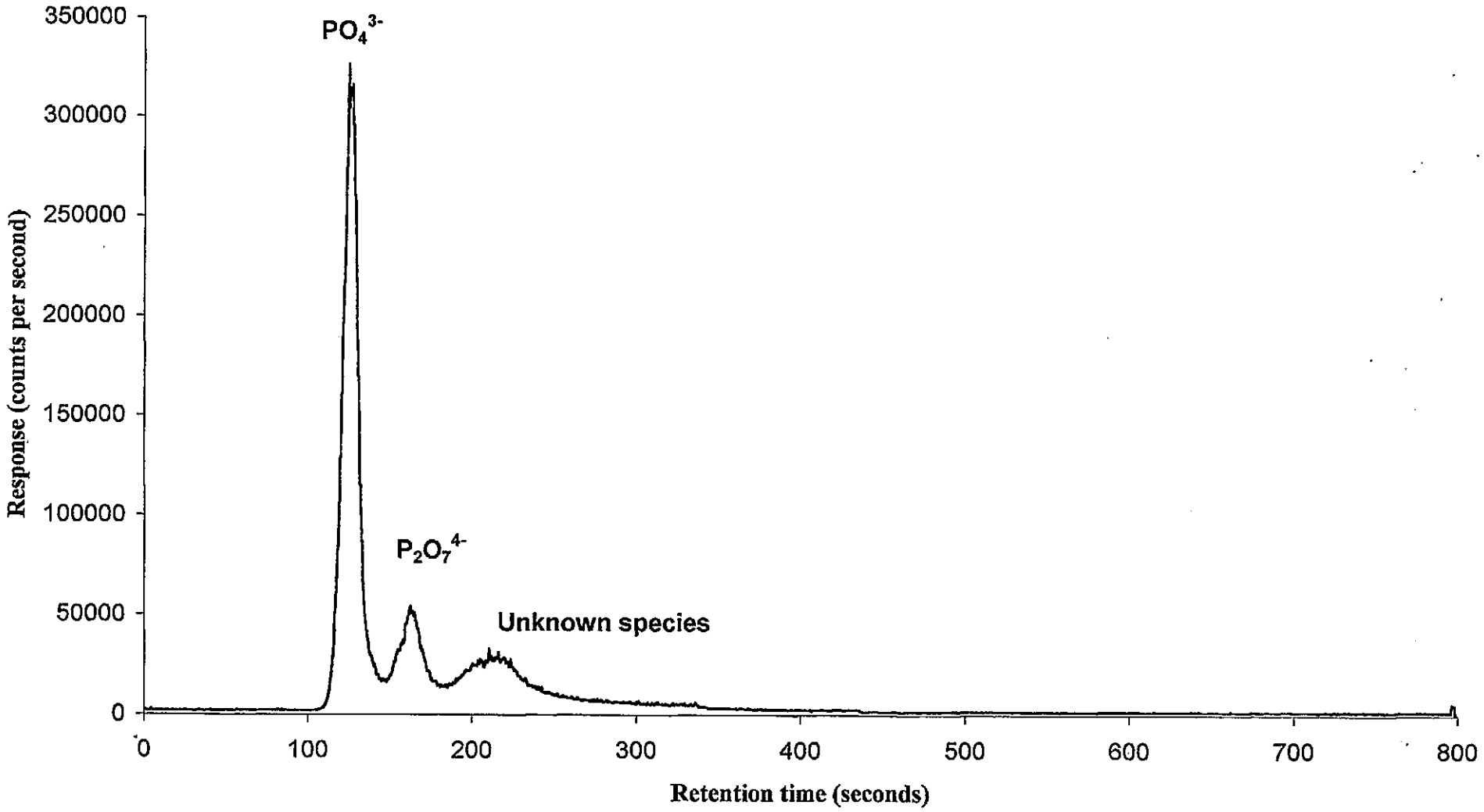

Figure 7.9: Chromatogram of phosphates extracted from pure orange juice
sample solution diluted tenfold

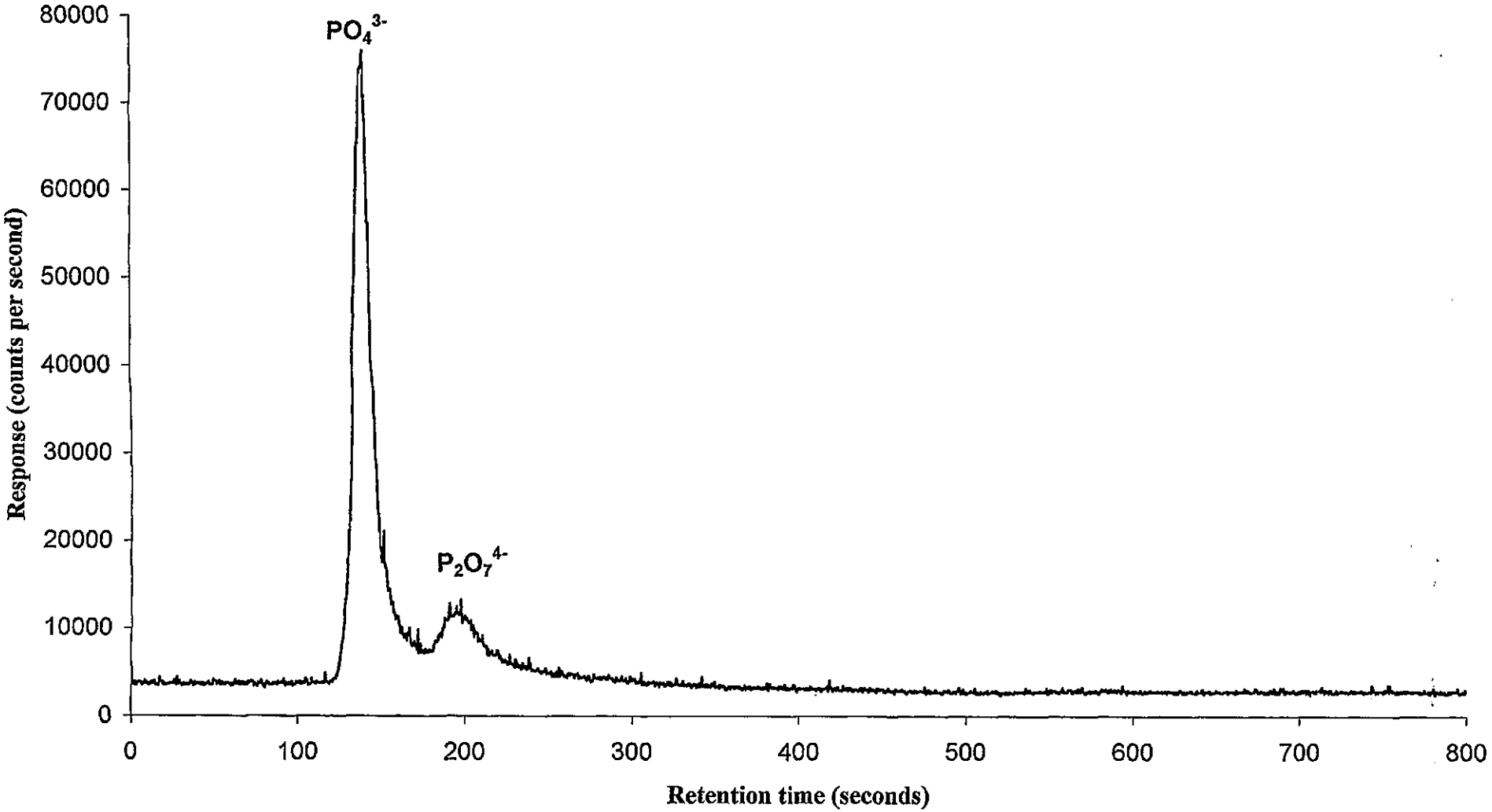

Figure 7.10: Chromatogram of phosphates extracted from sausage meat
sample solution diluted one hundredfold

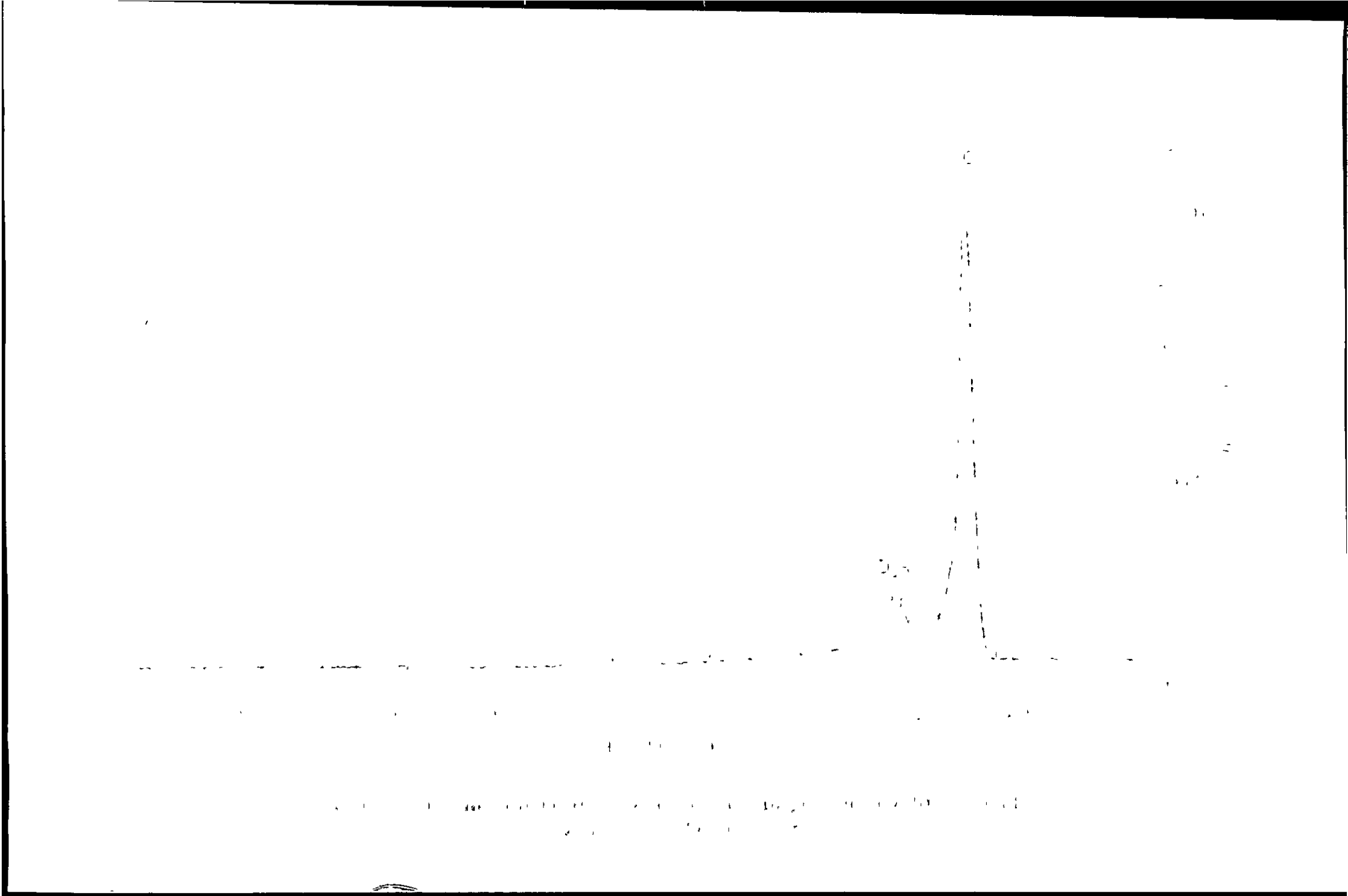

species. Polyphosphates were not found in the orange juice. Hydrolysis of phosphate is accelerated by low pH and thus any tripolyphosphate added may be hydrolysed over time to orthophosphate and pyrophosphate. However, the concentration of ortho- and pyrophosphate found in an orange flavoured drink showed no apparent change in concentration after 7 days. Furthermore, tripolyphosphate spiked into the orange drink also exhibited no change in concentration after this time.

The quantification of phosphates was achieved by the standard addition method. The concentrations of phosphates found are shown in Tables 7.4 and 7.5.

7.4: Conclusions

This work has demonstrated the use of ICP-MS as a phosphorus specific detector. Using a resolution setting of 3000 the spectral interference on $^{31}P^{+}$ from the NOH^{+} and NO^{+} polyatomic ions was eliminated. A quantitative and reproducible method was developed for the analysis of four common organophosphorous pesticides using ICP-MS detection which would be suitable for the analysis of biological samples where organophosphate pesticide poisoning is expected. This method would also be suitable for determination of organophosphorous pesticides in food products.

Inorganic phosphate anions were easily extracted, with high recoveries, into water from various food products, separated by ion exchange chromatography and detected using ICP-MS.

Table 7.4: Inorganic phosphate in pure orange juice

Phosphate Species	Content (µg/ml)	Phosphate added to sample (µg/ml)			Recovery (%)		
PO_4^{3-}	731	1000	1500	2000	79.7	83.8	83.9
$P_2O_7^{4-}$	48.1	60	80	100	83.7	85.9	88.5

Table 7.5: Inorganic phosphate in sausage meat

Phosphate species	Content (ng/g)
PO_4^{3-}	1900
$P_2O_7^{4-}$	12.9
$P_3O_{10}^{5-}$	ND*

* Not detected, the content is below the limit of detection

CHAPTER 8: CONCLUSIONS AND SUGGESTIONS FOR FUTURE WORK

8.1: Conclusions

The temperature of the plasma is an important parameter for its efficient use for analytical purposes. The measurement of the dissociation temperature of polyatomic ions is one method of determining the plasma temperature. Controlled vapour loading into the plasma was achieved using a Dreschel bottle. This allowed accurate determinations of the density of species in the plasma without the need to make any assumptions on the nebuliser efficiency.

The mass spectra obtained in this study highlight a fundamental problem with using mass spectral data for temperature determinations. Elements present in the ingredients added to the plasma cause isobaric overlap with the polyatomic ions whose signals are to be measured in order to calculate their dissociation temperatures. This leads to erroneous signal measurements and hence inaccurate dissociation temperatures being calculated. Using a sector-field mass spectrometer unambiguous identification and quantification of the polyatomic ion signals were made leading to the calculation of more reliable dissociation temperatures.

This work has demonstrated that the polyatomic ion chosen as the thermometric probe cannot be picked arbitrarily and only those ions that are strongly bound will truly reflect temperatures of the plasma.

The determination of the dissociation temperature is a useful and non-invasive technique for the determination of the site of formation of a polyatomic ion *i.e.* whether they are formed in the plasma or the interface region of the ICP-MS. The weakly bound ions ArO^+ and ArC^+ were found to form in the interface region due to gross deviation of the calculated temperature from those expected for a system in thermal equilibrium. The temperatures calculated using the strongly bound ions C_2^+ and CO^+ as the thermometric

probes were similar to those expected for the plasma indicating these ions are formed in the plasma.

The use of a hexapole collision cell pressurised with helium gas resulted in the attenuation of ArH^+ Ar^+, ArO^+, ArC^+, $ArCl^+$ and Ar_2^+. The most dramatic attenuation occurred for the Ar_2^+ signal, which was attenuated six orders of magnitude. The other polyatomic ions were attenuated between 2 - 4 orders of magnitude. The results demonstrated that different analytes may require different collision cell conditions for determination which severely limits the multi-element capabilities of ICP-MS when using a hexapole collision cell. Analyte ions not plagued by polyatomic ions were affected by the helium in the collision cell. Initially the ions were thermalised by the helium gas resulting in improved sensitivity while at higher helium gas flow rates the sensitivity was reduced as ions were lost by scattering. Improved limits of detection over standard operating conditions were attained for $^{39}K^+$, $^{40}Ca^+$, $^{56}Fe^+$, $^{52}Cr^+$, $^{75}As^+$ and $^{80}Se^+$ in standard solutions.

In order to improve limits of detection and accuracy any signal that does not arise solely from the sample being analysed must be removed or minimised. Following controlled contamination of the skimmer cone with various analytes only Be^+ gave a measurable signal. Since the kinetic energy of these ions sampled from the skimmer cone was found to be very low, then these ions under most operating parameters will make no significant contribution to the analytical signal.

Molecular spectra of chlorobenzene and 1,2-dibromobenzene were obtained using sample solution introduction into a LP-ICP via a particle beam separator, although at very high concentration. The low signal was due to the low kinetic temperature of the LP-ICP which is insufficient to vaporise, dissociate and ionise the particles. Increasing the thermal energy provided to the particles emerging from the particle beam separator resulted in significant increases in the signal. The desolvation chamber temperature, the

nebuliser pressure and sample flow rate were all found to be important parameters for efficient use of the particle beam separator.

The final part of this study demonstrated the feasibility of using HPLC coupled to sector-field ICP-MS for the speciation of silicon and phosphorous. The use of sector-field ICP-MS as a chromatographic detector for Si^+ and P^+ in speciation studies eliminated the interference problems encountered using conventional ICP-MS with a quadrupole mass analyser.

Size exclusion chromatography coupled to ICP-MS was used to separate and detect long chain, high molecular weight silicones that cannot be characterised by GC-MS. Reversed phase HPLC was used to separate low molecular weight polar silanols. The spiking of human plasma was not easily achieved, as there is a limited number of solvents which the silicones are soluble in that are also miscible with water. The extraction efficiency of the silicones from plasma was poor.

Four common organophosphorous pesticides were separated by reversed phase HPLC and inorganic phosphates were separated by ion exchange HPLC. Quantification was achieved using ICP-MS as a P^+ specific detector. The extraction efficiency of organophosphorous pesticides from plasma are generally high, making this method suitable for the analysis of biological samples where organophosphorous poisoning is expected. High recoveries were also obtained for inorganic phosphates from food products.

8.2: Suggestions for future work

The temperature prevailing in the interface cannot be determined from the dissociation temperatures of polyatomic ions. The use of a fibre optic to determine an optical temperature would provide a non-invasive technique for the determination of the temperature of the plasma and the interface allowing a direct comparison between the two to be made.

Preliminary studies involving the use of a hexapole collision cell resulted in lower limits of detection being attainable for several analytes in standard solutions. This work must be continued with real samples if the full capabilities and limitations of the hexapole collision cell are to be realised. In particular the application of the hexapole collision cell to the speciation of $^{75}As^{+}$, $^{80}Se^{+}$ and $^{56}Fe^{+}$ would be worthy of study. The use of other gases in the collision cell such as N_2, NH_3 and Xe should also be investigated.

In this study only a limited number of analytes were investigated for signals arising from material deposited on the skimmer cone. ICP-MS has multi-element capabilities and analytes across the periodic table are routinely analysed. Other analytes, in particular those with low ionisation potential such as Li^{+}, Cs^{+} and La^{+}, should be investigated to see if they are deposited on the skimmer cone in sufficient quantity to give a measurable signal. If they are then their kinetic energy should be determined. This will indicate if they will contribute significantly to the signal.

Solution sample introduction into a LP-ICP should be feasible with proper vaporisation of the particles emerging from the particle beam separator. Therefore attention must focus on providing an efficient means of heat to the transfer line. This could be achieved in several ways. A transfer line with several cartridge heaters or a heating coil hanging in free space inside the transfer line could both be used. Furthermore, the addition of other gases, such as H_2 or N_2, to the helium plasma may increase the gas kinetic temperature and aid vaporisation of the particles.

A study involving the speciation of silicon has been presented. While the separation and quantification of silicones using a mobile phase of 100 % xylene was successfully achieved the extraction recoveries from plasma was very poor. This must be improved if blood samples from patients with silicone implants are to be analysed. Xylene may not be the most suitable solvent for extraction and alternative solvents will have to be investigated. Only a preliminary study involving the separation of silanols

was presented, due to the difficulty in their synthesis. Improved separation of these compounds using acetonitrile and gradient elution must be investigated. In these circumstances a desolvation device of some kind will have to be employed. Furthermore, the extraction of the silanols from biological samples must be investigated. Moreover, the sequential extraction of silicones and silanols from biological samples should be investigated.

Once these issues have been addressed biological samples may be analysed to obtain information regarding the breakdown mechanisms of silicones in the human body. At present little is known about the degradation of silicones to the water soluble silanols in the human body.

The feasibility of the use of sector-field ICP-MS as a phosphorus specific detector has been demonstrated. The use of sector-field ICP-MS could be applied to the quantitative determination of DNA adducts using the signal of P^+ to determine modified DNA components as a result of carcinogenic compounds.

REFERENCES

1 Reed, T. B., J. Appl. Phys., 1961, **32**, 821.

2 Greenfield, S., Jones, I. L., and Berry, G. I., Analyst, 1964, **89**, 713.

3 Wendt, R. H., and Fassel, V. A., Anal. Chem, 1965, **37**, 920.

4 Gray, A. L., Proc. Soc. Anal. Chem., 1974, **11**, 182.

5 Houk, R. S., Fassel, V. A., Flesch, G. D., Svec, H. J., Gray, A. L., and Taylor, C. E., Anal. Chem., 1980, **52**, 2283.

6 Date, A. R., and Gray A. L., Analyst, 1981, **106**, 1255.

7 Evans, E. H., Giglio, J. J., Castillano, T. M., and Caruso, J. A., 'Inductively Coupled and Microwave Induced Plasma sources for Mass spectrometry., RSC, Cambridge, 1995.

8 Guo, X., and Lichte, F. E., Analyst, 1995, **120**, 2707.

9 Lichte, F. E., Anal. Chem., 1995, **67**, 2479.

10 Ebdon, L., Foulkes, M., and Sutton, K., J. Anal. At. Spectrom, 1997, **12**, 213.

11 Fonseca, R. W., and Miller-Ihli, N. J., Appl. Spectros., 1995, **49**, 1403.

12 Chapple, G., and Byrne, J. P., J. Anal. At. Spectrom., 1996, **11**, 549.

13 Naka, H., and Gregoire, D. C., J. Anal. At. Spectrom., 1996, **11**, 359.

14 Shibata, N., Fudagawa, N., and Kubota, M., Spectrochim. Acta, 1992, **47B**, 505.

15 Gregoire, D. C., and Sturgeon, R. E., Spectrochim. Acta, 1993, **48B**, 1347.

16 Huang, M. F., Jiang, S. J., and Hwang, C. J., J. Anal. At. Spectrom., 1995, **10**, 31

17 Thompson, J. J., and Houk, R. S., Anal. Chem., 1986, **58**, 2541.

18 Crews, H. M., Dean, J. R., Ebdon, L., and Massey, R. C., Analyst, 1989, **114**, 895.

19 Jarvis, K. E., J.Anal.At.Spectom., 1989, **4**, 563.

20 Vanhoe, H., Vandecasteele, C., Versieck, J., and Dams, R., Anal. Chem. Acta., 1991, **244**, 259.

21 Lyon, T. D. B., Fell, G. S., Hutton, R. C., and Eaton, A. N., J. Anal. At. Spectom., 1988, **3**, 265.

22 Vijayalakshmi, S., Krishna Prabhu, R., Mahalingam, T. R., and Matthews, C. K., At. Spectrom, 1992, **13**, 61.

23 Roig-Navarro, A. F., Martinez-Bravo, Y., Lopez, F. J., and Hernandez, F., J. Chromatogr. A., 2001, **912**, 319.

24 Rosland, E., and Lund, W., J. Anal. At. Spectrom., 1998, **13**, 1239.

25 Balarm, V., At. Spectrom., 1993, **14**, 174.

26 Paul, M., and Vollkopf, U., Fres. Z. Anal. Chem., 1989, **334**, 680.

27 Alswaidan, H. M., Sci. Total. Environ., 1994, **145**, 157.

28 Munro, S., Ebdon, L., and McWeeny, D. J. , J. Anal. At. Spectrom., 1986, **1**, 211.

29 Odegard, K. E., and Lund, W., J. Anal. At. Spectrom., 1997, **12**. 403.

30 Park, C. J., Cho, K. H., Suh, J. K., and Han, M. S., J. Anal. At. Spectrom, 2000, **15**, 567.

31 'CRC Handbook of Chemistry and Physics', 73rd edition, Lide, D. R. (ed), CRC publishing company, 1992.

32 Gray, A. L., and Williams, J. G., J. Anal. At. Spectrom., 1987, **2**, 81.

33 Tan, S. H., and Horlick, G., Appl. Spectros., 1986, **40,** 445.

34 Lajunen, L. H. J., Spectrochemical analysis by atomic absorption and emission, RSC, Cambridge, 1992.

35 Douglas, D. J., and Kerr, L., J. Anal. At. Spectrom., 1988, **3**, 749.

36 Tan, S. H., and Horlick, G. J., J. Anal. At. Spectrom., 1987, **2**, 745.

37 Beauchemin, D., McLaren, J. W., and Berman, S. S., Spectrochim. Acta, 1987, **42B**, 467.

38 Gregoire, D. C., Appl. Spectrosc., 1987, **41**, 897.

39 Gregoire, D. C., Spectrochim. Acta, 1987, **42B**, 895.

40 Gillson, G. R., Douglas, D. J., Fullford, J. E., Halligan, K. W., and Tanner, S. D., Anal. Chem., 1988, **60**, 1472.

41 Vaughan, M., Horlick, G., and Tan, S., J. Anal. At. Spectrom., 1987, **2**, 765.

42 Gray, A. L., and Williams, J. G., J. Anal. At. Spectrom., 1987, **2**, 599.

43 Gray, A. L., Spectrochim. Acta, 1986, **41**, 151.

44 Horlick, G. A., Tan, S. H., Vaughan, M. A., and Rose, C. A., Spectrochim. Acta., 1985, **40B**, 1555.

45 Longerich, H. P., Fryer, B. J., Strong, D. F., and Kantipuly, C. J., Spectrochim. Acta., 1987, **42B**, 75.

46 Jen-Jiang, S., Houk, R. S., Stevens, M. A., Anal. Chem., 1988, **60**, 1217.

47 Wang, J., Shen, W., Sheppard, B. S., Evans, E. H., and Caruso, J. A., J. Anal. At. Spectom., 1990, **5**, 445.

48 Vaughan, M. A., and Horlick, G., Spectrochim. Acta., 1990, **45B**, 1289.

49 McLaren, J. W., Beauchemin, D., and Berman, S. S., J. Anal. At. Spectom., 1987, **2**, 277.

50 Jarvis, K. E., Mason, P., Platzner, T., and Williams, J. G., J. Anal. At. Spectrom., 1998, **13**, 689.

51 Lam, J. W. H., and Horlick, G., Spectrochim. Acta, 1990, **45B**, 1327.

52 Vanhoe, H., Goossens, J., Moens, L., and Dams, R., J. Anal. At. Spectrom., 1994, **9**, 177.

53 Date, A. R., Cheung, Y. Y., and Stuart, M. E., Spectrochim. Acta, 1987, **42B**, 3.

54 Ketterer, M. E., Reschl, J. J., and Peters, M. J., Anal. Chem., 1989, **61**, 2031.

55 Zhu, W., Deleer, E. W. B., Kennedy, M., Kelderman, P., and Alaerts, G. J. F. R., J. Anal. At. Spectrom., 1997, **12**, 661.

56 Ebdon, L., Foulkes, M. E., Parry, H. G. M., and Tye, C. T., J. Anal. At. Spectrom., 1988, **3**, 753.

57 Mochizuki, T., Sakashita, A., Iwata, H., Ishibashi, Y., and Gunji, N., Anal. Sci., 1989, **5**, 311.

58 Jarvis, K. E., and Williams, J. G., Chem. Geol., 1989, **77**, 53.

59 Shabani, M. B., Akagi, T., Shimizu, H. and Masuda, A., Anal. Chem., 1990, **62**, 2709.

60 McLaren, J. W., Mykytiuk, A. P., Willie, S. N., and Berman, S. S., Anal. Chem., 1985, **57**, 2907.

61 Lyon, T. B. D., Fell, G. S., Hutton, R., and Eaton, A. N., J. Anal. At. Spectrom., 1988, **3**, 601.

62 Boomer, D. W., Powell, M. J., and Hipfner, J., Talanta, 1990, **37**, 127.

63 Gregoire, D. C., J. Anal. At. Spectrom., 1990, **5**, 623.

64 Hutton, R. C., and Eaton, A. N., J. Anal. At. Spectrom., 1987, **2**, 595.

65 Zhu, G., and Browner, R. F., J. Anal. At. Spectrom., 1988, **3**, 781.

66 Weir, D. G. J., and Blades, M. W., Spectrochim. Acta, 1990, **45B**, 615.

67 Gustavsson, A., and Hietala, P., Spectrochim. Acta, 1990, **45B**, 1103.

68 McLaren, J. W., Lam, J. W., and Gustavsson, A., Spectrochim. Acta, 1990, **45B**, 1091.

69 Tsukahara, R., and Kubota, M., Spectrochim. Acta, 1990, **45B**, 581.

70 Alves, L. C., and Daniel, D. R., and Houk, R. S., Anal. Chem., 1992, **64**, 1164.

71 Lam, J. W. H., and Horlick, G., Spectrochim. Acta., 1990, **45B**, 1313.

72 McLaren, J. W., Lam, J. W., and Gustavsson, A., Spectrochim. Acta., 1990, **45B**, 1091.

73 Lam, J. W., and McLaren, J. W., J. Anal. At. Spectrom., 1990, **5**, 419.

74 Branch, S., Ebdon, L., Ford, M., Foulkes, M., and O' Neill, P., J. Anal. At. Spectrom., 1991, **6**, 151.

75 Wang, J., Evans, E. H., and Caruso, J. A., J. Anal. At. Spectrom., 1992, 7, 929.

76 Houk, R. S., Montaser, A., and Fassel, V. A., Appl. Spectrosc., 1983, **5**, 425.

77 Evans, E. H., and Ebdon, L., J. Anal. At. Spectrom., 1989, **4**, 299.

78 Evans, E. H., and Ebdon, L., J. Anal. At. Spectrom., 1990, **5**, 425.

79 Lam, J. W. H., and Horlick, G., Spectrochim. Acta., 1990, **45B**, 1313.

80 Beauchemin, D., and Craig, J. M., Spectrochim. Acta., 1991, **46B**, 603.

81 Ford, M., Ebdon, L., and Hill, S. J., Anal. Proc., 1992, **29**, 104.

82 Sheppard, B. S., Shen, W., Davidson, T. M., and Caruso, J. A., J. Anal. At. Spectrom., 1990, **5**, 697.

83 Smith, F. G., Wiederin, D. R., and Houk, R. S., Anal. Chem., 1991, **63**, 1458.

84 Hutton, R. C., Bridenne, M., Coffre, E., Marot, Y., and Simondet, F., J. Anal. At. Spectrom, 1990, **5**, 463.

85 Hill, S. J., Ford, M. J., and Ebdon, L. , J. Anal. At. Spectrom., 1992, **7**, 1157.

86 Ebdon, L., Ford, M. J., Hutton, R. C., and Hill, S. J., Appl. Spectrosc., 1994, **48**, 507.

87 Montaser, A., Chan, S., and Koppenaal, D. W., Anal. Chem., 1987, **59**, 1240.

88 Koppenaal, D. W., and Quinton, L. F., J. Anal. At. Spectrom., 1988, **3**, 667.

89 Tanner, S. D., Paul, M., Beres, S. A., and Denoyer, E. R., At. Spectrosc., 1995, **16**, 16.

90 Tanner, S. D., J. Anal. At. Spectom., 1995, **10**, 905.

91 Koppenaal, D. W., Barinaga, C. J., and Smith, M. R., J. Anal. At. Spectrom., 1994, **9**, 1053.

92 Koppenaal, D. W., Barinaga, C. J., Rapid. Commun. Mass Spectrom., 1994, **8**, 71.

93 Koppenaal, D. W., Barinaga, C. J., and Eiden, G. C., J. Anal. At. Spectrom., 1996, **11**, 317.

94 Hieftje, J. Anal. At. Spectrom, 1996, **11**, 401.

95 Reed, N. M., Cairs, R. O., and Huton, R. C., J. Anal. At. Spectrom., 1994, **9**, 881.

96 Rodushkin, I., and Ruth, I., J. Anal. At. Spectrom., 1997, **12**, 1181.

97 Jakubowski, N., Moens, L., and Vanhaecke, F., Spectrochim. Acta, 1998,**53B**, 1739.

98 Becker, S. J., and Dietze, H. J., J. Anal. At. Spectrom., 1997, **12**, 881.

99 Douglas, D. J., and French, J. B., Anal. Chem., 1981, **53**, 37.

100 Douglas, D. J., Quan, E. S. K., and Smith, R. G., Spectrochim. Acta, , 1983, **38B**, 39.

101 Brown, P. G., Davidson, T. M., and Caruso, J. A., J. Anal. At. Spectrom., 1988, **3**, 763.

102 Creed, J. T., Mohamad, A. H., Davidson, T. M., Ataman, G., and Caruso, J. A., J. Anal. At. Spectrom., 1988, **3**, 923.

103 Suyani, H., Creed, J., Caruso, J., and Satzger, R. D., ., J. Anal. At. Spectrom., 1989, **4**, 777.

104 Mohamad, A. H., Creed, J. T., Davidson, T. M., and Caruso, J. A., Appl. Spectrosc., 1989, **43**, 1127.

105 Satzger, R. D., Fricke, F. L., Brown, P. G., and Caruso, J. A., Spectrochim. Acta, 1987, **42B**, 705.

106 Wilson, D. A., Vickers, G. H., and Hieftje, G. M., Anal. Chem., 1987, **59**, 1664.

107 Satzger, R. D., Fricke, F. L., and Caruso, J. A., ., J. Anal. At. Spectrom., 1988, **3**, 319.

108 Creed, J. T., Davidson, T. M., Shen, W., Brown, P. G., and Caruso, J. A., Spectrochim. Acta, 1989, **44B**, 909.

109 Shen, W., Davidson, T. M., Creed, J. T., and Caruso, J. A., Appl. Spectrosc., 1990, **44**, 1003.

110 Shen, W., Davidson, T. M., Creed, J. T., and Caruso, J. A., Appl. Spectrosc., 1990, **44**, 1011.

111 Evans, E. H., Caruso, J. A., and Satzger, R. D., Appl. Spectrosc., 1991, **45**, 1478.

112 Niu, H., and Houk, R. S., Spectrochim. Acta, 1996, **51B**, 799.

113 Olivares, J. A., and Houk, R. S., Anal. Chem., 1985, **57**, 2674.

114 Lichte, F. E., Meier, A. L., and Crock, J. G., Anal. Chem., 1987, **59**, 1150.

115 Boomer, D. W., and Powell, M. J., Anal. Chem., 1987, **59**, 2810.

116 Wilson, D. A., Vickers, G. H., and Hieftje, G. M., J. Anal. At. Spectrom., 1987, **2**, 365.

117 Nonose, N., Matsuda, N., Fudagawa, N., and Kubota, M., Spectrochim. Acta, 1994, **49B**, 955.

118 Shao, Y., and Horlick, G., Appl. Spectrosc., 1992, **45**, 143.

119 Sakata, K., and Kawabata, K., Spectrochim. Acta, 1994, **49B**, 1027.

120 Becker, J. S., Seifert, G., Saprykin, A. I., and Dietze, H., J. Anal. At. Spectrom., 1996, **11**, 643.

121 Douglas, D. J., and French, J. B., J. Anal. At. Spectrom., 1988, **3**, 743.

122 Togahi, H., Hashizume, A., and Niwa, Y., Spectrochim. Acta, 1992, **47B**, 561.

123 Van Heuzen, A. A., and Nibbering, N. M. M., Spectrochim. Acta, 1993, **48B**, 1013.

124 Mermet, J., Poussel, E., and Deruaz, D., J. Anal. At. Spectrom., 1994, **9**, 61.

125 Tanner, S. D., J. Anal. At. Spectrom., 1993, **8**, 891.

126 Shibata, N., Fudagawa, N., and Kubota., Spectrochim. Acta., 1993, **48B**, 1127.

127 Furuta, N., Spectrochim. Acta., 1985, **40B**, 1013.

128 Mermet, J. M., in 'Inductively coupled plasma spectrometry and its application', Hill, S. J., (ed), Sheffield Academic Press, Sheffield, 1999.

129 Hasegawa, T., Umemoto, M., Haraguchi, H., Hsiech, C., and Montaser, A., in 'Inductively coupled plasmas in analytical atomic spectrometry', 2nd edition., Montaser, A., and Golightly, D. W., (eds)., VCH, New York, 1992.

130 Ishii, I., and Montaser, A., Spectrochim. Acta., 1991, **46B**, 1197.

131 Kawaguchi, H., Ito, T., and Mizuike, A., Spectrochim. Acta., 1981, **36B**, 615.

132 Human, H. G. C., and Scott, R. H., Spectrochim. Acta., 1976, **31B**, 459.

133 Douglas, D. J., and French, J. B., Spectrochim. Acta., 1986, **41B**, 197.

134 Longerich, H. P., Fryer, B. J., Strong, D. F., and Kantipuly, C. J., Spectrochim. Acta, 1987, **42B**. 75.

135 Longerich, H. P., J. Anal. At. Spectrom., 1989, **4**, 491.

136 Kubota, M., Fudagawa, N., Kawase, A., Anal. Sci, 1989, **5**, 701.

137 Rowley, L K., Ph.D Thesis, University of Plymouth, 2001.

138 Houk, R. S., and Praphairaksit, N., Spectrochim. Acta., 2001, **56**, 1069.

139 Jarvis, K. E., Gray, A. L., and Houk, R. S., 'Handbook of Inductively Coupled Plasma Mass Spectrometry', Blackie, Glasgow, 1992.

140 Douglas, D. J., and Tanner, S. D., in 'Inductively Coupled Plasma Mass Spectrometry' Montaser, A. (ed), Wieley - VCH, New York, 1998.

141 Atkins, P.W., 'Physical Chemistry' Fifth edition, Oxford University Press, Oxfodrd, 1994.

142 De Galan, L., Smith, R., and Winefordner., Spectrochim. Acta., 1968, **23B**, 521.

143 Alberty, R. A., and Silbey, R. J., 'Physical Chemistry', Wiley and Sons, New York, 1997.

144 Huber, K. P., and Herzberg, G., 'Molecular spectra and Molecular structure, vol IV constants of diatomic molecules'. Van Nostrand, New York, 1979.

145 Radon, L., and Wong, M. W. J. Phys. Chem, 1989, **93**, 6303.

146 Frenking, G., Koch, W., Cremer, D., Gauss, J., and Liebman, J. F., J. Phys. Chem, 1989, **93**, 3410.

147 Evans, E.H., Rowley, L., and Ebdon, L., University of Plymouth unpublished results.

148 Olesik, J. W., Appl. Spectrosc, 1997, **51**, 158A.

149 Winge, R. K., Chen, X., and Houk, R. S., J. Anal. Atomic. Spectrom., 1997, **12**, 1139.

150 VG Elemental Plasmaquad 3 Operating Manual.

151 Zhu, G., and Browner, R. F., J. Anal. At. Spectrom., 1988, **3**, 781.

152 Murrillo, M., and Mermet, J. M., Spectrochim. Acta, 1989, **44B**, 359.

153 Boumans, P. W. and De Boer J. M., Spectrochim. Acta, 1976, **31B**, 355.

154 Boorn, A. W., and Browner, Anal. Chem., 1982, **54**, 1402.

155 Benli, H., Spectrochim. Acta, 1983, **38B**, 81.

156 Goldfarb, V. M., and Goldfarb, H. V., Spectrochim. Acta, 1985, **40B**, 177.

157 Blades, M. W., and Caughlin, B. L., Spectrochim. Acta., 1985, **40B**, 579.

158 Murrillo., M., and Mermet, J.M., Spectrochim. Acta, 1987, **42B**, 1151.

159 Tang, Y. Q., and Trassy, C., Spectrochim. Acta, 1986, **41B**, 143.

160 Alder, J. F., Bombelka, R. M., and Kirkbright, G. F., Spectrochim. Acta., 1980, **31B**, 163.

161 Hattendorf, B., and Gunther, D., Fres J. Anal. Chem., 2001, **370**, 483.

162 Douglas, D. J., and French, J. B., J. Am. Soc. Mass Spectrom., 1992, **3**, 398.

163 Douglas, D. J., Can. J. Spectrosc., 1989, **34**, 38.

164 Rowan, J. T., and Houk, R. S., Appl. Spectrosc., 1989, **43**, 976.

165 Eiden, G. C., Barrinaga, C. J., and Koppenaal, D. W., Rapid. Commun. Mass. Spectrom, 1997, **11**, 37.

166 Turner, P., Merren, T., Speakman, J., and Haines, C., in 'Plasma Source Mass Spectrometry' Holland, G (ed)., RSC, Cambridge, 1997.

167 Feldmann, I., Jakubowski, N., and Stuewer, Fresenius. J. Anal. Chem., 1999, **365**, 415.

168 Feldmann, I., Jakubowski, N., Thomas, C., and Stuewer, Fresenius. J. Anal. Chem., 1999, **365**, 422.

169 Dexter, M. A., Appelbald, P. K., Ingle, C. P., Batey, J. H., Reid, H. J., and Sharp, B. L., J. Anal. At. Spectrom., 2002, **17**, 183.

170 Turner, P. J., Mills, D. J., Schroder, E., Lapitajs, G., Jung, G., Iacone, L. A., Haydar, D. A., and Montaser, A., in 'Inductively Coupled Mass Spectrometry' Montaser, A. (ed). VCH, USA, 1988.

171 Bandura, D. R., and Tanner, S. D., At. Spectrosc., 1999, **20**, 69.

172 Baranov, V. I., and Tanner, S. D., J. Anal. At. Spectrom., 1999, **14**, 1133.

173 Tanner, S. D., and Baranov, V. I., J. Am. Soc. Mass Spectrom., 1999, **10**, 1083.

174 Tanner, S. D., Baranov, V. I., and Vollkopf, U., J. Anal. At. Spectrom., 2000, **15**, 1261.

175 Marchante-Gayon, J. M., Feldman, I., Thomas, C and Jakubowski, N., J. Anal. At. Spectrom., 2000, **15**, 1093.

176 Marchante-Gayon, J. M., Feldman, I., Thomas, C and Jakubowski, N., J. Anal. At. Spectrom., 2001, **16**, 457.

177 Chang, Y., and Jiang, S., J. Anal. At. Spectrom., 2001, **16**, 858.

178 Vollkopf, U., Klemm, K., and Pfluger, M., At. Spectrosc., 1999, **20**, 53.

179 Bollinger, D. S., and Schleisman, A., At. Spectrosc., 1999, **20**, 60.

180 Neubauer, K., and Vollkopf, U., At. Spectrosc., 1999, **20**, 64.

181 Hattendorf, B., and Gunther, D., J. Anal. At. Spectrom., 2000, **15**, 1125.

182 Bandura, D. R., Baranov, V. I., Tanner, S. D., J. Anal. At. Spectrom., 2000, **15**, 921.

183 Du, Z., and Houk., R. S., J. Anal. At. Spectrom., 2000, **15**, 383.

184 Moens, L. J. Vanhaecke, F. F., Bandura, D. R., Baranov, V. I., and Tanner, S. D., J. Anal. At. Spectrom., 2001, **16**, 991.

185 Vollkopf, U., Baranov, V., and Tanner, S., in 'Plasma Source Mass Spectrometry: Developments and applications., Holland, G., and Tanner, S.,(eds) RSC, Cambridge, 1999.

186 Date, A. R., and Gray, A. L.,(eds), 'ICP-MS ', Blackie, London, 1989.

187 PlasmaQuad system manual, (PQ2),VG Elemental.

188 Olivares, J. A., and Houk., R. S., Appl. Spectrosc., 1985., **39**, 1070.

189 Fulford, J. E., Douglas, D. J., Appl. Spectrosc., 1986, **40**, 971.

190 Jakubowski, N., Raeymaekers, B. J., Broekaert, J. A. C., and Stewer, D., Spectrochim. Acta., 1989, **44B**, 219.

191 Chambers, D. M., and Hieftje, G. M., Spectrochim. Acta, 1991, **46B**, 761.

192 Douglas, D. J., in ' Inductively Coupled Plasmas in Analytical Atomic Spectrometry, Second Edition, Montaser, A., and Golightly, D. W., (eds), VCH, New York, 1992.

193 Tanner, S. D., J. Anal. At. Spectrom., 1993, **8**, 891.

194 Evans, E. H., and Caruso, J. A., J. Anal. At. Spectrom., 1993, **8**, 427.

195 Castillano, T. M., Giglio, J.J., Evans, E. H., Caruso, J. A., J. Anal. At. Spectrom., 1994, **9**, 1335.

196 Evans, E. H., Pretorious, W., Ebdon, L., and Rowland, S., Anal. Chem., 1994, **66**, 3400.

197 O' Connor, G., Ebdon, L., Evans, E. H., Ding, H., Olson, L. K., and Caruso, J. A., J. Anal. At. Spectrom., 1996, **11**, 1151.

198 O' Connor, G., Ebdon, L., and Evans, E. H., J. Anal. At. Spectrom, 1997, **12**, 1263.

199 Rosenkranz, B., O'Connor, G., and Evans, E. H., J. Anal. At. Spectrom, 2000, **15**, 7.

200 Castillano, T. M., Giglio, J. J., Evans E. H., and Caruso, J. A., J. Anal. At. Spectrom., 1997, **12**, 383.

201 Sung, Y., and Lim, H. B., J. Anal. At. Spectrom., 2001, **16**, 767.

202 O' Connor, G. T., PhD Thesis, University of Plymouth, 1998.

203 You, J., Depalma, P. A., and Marcus, R. K., J. Anal. At. Spectrom., 1996, **11**, 483.

204 You, J., Fanning, J. C., and Marcus, R. K., Anal. Chem., 1994, **66**, 3916.

205 Dempster, M. A., Marcus, R. K., J. Anal. At. Spectrom., 2000, **15**, 43.

206 Marcus, R. K., Dempster, M. A., Gibeau, T. E., and Reynolds, E. M. Anal. Chem., 1999, **71**, 3061.

207 Strange, C. M., and Marcus, R. K.,Spectrochimica. Acta., 1991, **46B**, 517.

208 Gibeau, T. E., and Marcus, R. K., Anal. Chem., 2000, **72**, 3833.

209 HP 5989A Engine Hardware manual, Volume 2, Hewlett Packard.

210 Bier, M. E., Winkler, P.C., and Herron, J. R., J. Am. Soc. Mass. Spectrom., 1993, **4**, 38.

211 Israel, G. W., and Friedlander, S. K., J. Colloid. Interface. Sci., 1967, **24**, 330.

212 Winkler, P. C., Perkins, D. D., Williams, W. K., and Browner, R. F., Anal. Chem., 1988, **60**, 489.

213 Ligon, W. V., and Dorn, S. B., Anal. Chem., 1990, **62**, 2573.

214 Carlise, E. M. in ' Biochemistry of the essential ultratrace elements' Freiden, E. (ed), Plenum Press, New York, 1984.

215 LeVier, R. R., Harrison, M. C., Cook, R. R., and Lane, T. H., Plast. Reconstr. Surg., 1993, **92**, 163.

216 Dobbie, J. W., and Smith, M. J. B., in 'Silicon Biochemistry Ciba Foundation Symposium 121', Evered, D. (ed). J. Wiley, New York, 1986.

217 Potter, M., and Rose, N. R., (eds) 'Immunology of Silicones'. Springer-Verlag, Berlin, 1996.

218 LeVier, R. P., Chandler, M. L., and Wendel, S. R., in 'Biochemistry of Silicon and Related Problems'. Bendz, G., and Lindquist, I., (eds), Plenum, Press, New York, 1978.

219 Stroh, A., in 'Frontiers of Organosilicon Chemistry' Bassingdale, A. R. and Gasper, P. P., (eds), RSC, Cambridge, 1991.

220 Peters, W., Smith, D., and Lugowski, S., Ann. Plast. Surg, 1999, **43**, 324.

221 Kumagi, Y., Shiokawa, Y., Medsger, T. S., and Rodnan, G. P., Arthritis. Rheum., 1984, **27**, 1.

222 Sergott, T. J., Limoli, J. P., Baldwin, C. M., and Laub, D. R., Plast. Reconst. Surgy., 1986, **78**, 104.

223 Kossovsky, N., Heggers, J. P., and Robson, C., J. Biomed. Mater. Res., 1987, **21**, 1125.

224 Nyren, O., Yin, L., Josefsson, S., McLaughlin, J. K., Blot, W. J., Engqvist, M., Hakelius, L., Boice, J. D., and Adami, H., BMJ., 1998, **316**, 417.

225 Edelman, D. A., Grant, S., and Van Os, W., Int. J. Fertil, 1995, **40**, 274.

226 Barker, D. E., Retsky, M. I., and Schultz, S., Plast. Reconstr. Surg., 1978, **61**, 836.

227 Hausner, R. J., Schoen, F. J., and Pierson, K. K., Plast. Reconstr. Surg., 1978, **62**, 381.

228 Wolf, C. J., Brandon, H. J., Young, V. J., Jerina, K. L., and Srivastava, A. P., in 'Immunology of Silicones', Potter, M., and Rose, N. R., (eds) Springer-Verlag, Berlin, 1996.

229 Carmen, R., and Kahn, P., J. Biomed. Mater. Res., 1968, **2**, 457.

230 Allwork, S. P., and Norton, R., Thorax, 1976, **31**, 742.

231 Kala, S. V., Lykissa, E. D., Neely, M. W., and Libeberman, M. W., Am. J. Pathol., 1998, **152**, 645.

232 Pfleiderer, B., and Garrido, L., Magn. Reson. Med., 1995, **33**, 8.

233 Lukasiak, J., Jamrogiewicz, Z., Jachowska, D., Czarnowski, W., Hrabowska, M., Prokopowicz, M., and Falkiewicz, B., Polimery., 2001, **46**, 546.

234 Garrido, L., Pfleiderer,, B., Papisov, M., and Ackerman, J. L., Magn. Reson, Med., 1992, **29**, 839.

235 Pfleidener, B., Ackerman, J. L., and Garrido, L., Magn. Reson, Med., 1993, **30**, 534.

236 Garrido, L., Pfleiderer,, B., Jenkins, B. G., Hulkes, C. A., and Kopans, D. B., Reson, Med., 1994, **31**, 328.

237 Garrido, L., Bogdanova, A., Cheng, L., Pfleiderer,. B., Tokareva, E., Ackerman, J. L., and Brady, T. J., in 'Immunology of Silicones' Potter M., and Rose, N. R., (eds)., Springer-Verlag, Berlin, 1996.

238 Pfleiderer,, B., Moore, A., Tokareva, E., Ackerman, J. L., and Garrido, L., Biomaterials, 1999, **20**, 561.

239 Hayden, J. F., and Barlow, S. A., Toxicol. Appl. Pharmacol., 1972, **21**, 68.

240 Park, A. J., Black, R. J., Sarhadi, N. S., Chetty, U., and Watson, A. C. H., Plast. Reconstr. Surg., 1998, **101**, 261.

241 Dorn, S. B., and Skelly Frame, E. M., Analyst, 1994, **119**, 1687.

242 Flassbeck, D., Pleiderer, B., Grumping, R., and Hirner, A., Anal. Chem, 2001, **73**, 606.

243 Lykissa, E. D., Kala, S. V., Hurley, J. B., and Lebovitz, R. M., Anal. Chem, 1997, **69**, 4912.

244 Lykissa, E. D., Kala, S. V., and Lebovitz, R. M., Anal. Chem, 1997, **69**, 1267.

245 Varaprath, S., Salyers, K. L., Plotzke, K., and Nanavati, S., Anal. Biochem., 1998, **256**, 14.

246 Fendinger, N. J., McAvoy, D. C., Eckhoff, W.S., and Price, B. B., Environ. Sci. Technol., 1997, **31**, 1555.

247 Carpenter, J. C., Cella, J.A., and Dorn, S. B., Environ. Sci. Technol., 1995, **29**, 864.

248 Cavic-Vlasak, B. A., Thompson, M., and Smith, D. C., Analyst, 1996, **121**, 53R.

249 O' Hanlon, K. L., Ph. D Thesis, University of Plymouth., 1996.

250 Roberts, N.B., and Williams, D., Clin. Chem., 1990, **36**, 1460.

251 Gitelman, H. J., and Alderman, F. R., J. Anal. At. Spectrom., 1990, **5**, 687.

252 World Health Organisation. Public Health impact of pesticides used in agriculture. WHO, 1990.

253 Jeyaratnan, J., 'Acute Pesticide Poisoning and Developing Countries', Oxford University Press, Oxford, 1992.

254 Padungtod, C., Savitz, D. A., Overstreet, J. W., Christiani, D. C., Ryan, L. M., and Xu, X., J. Occup. Environ. Med., 2000, **42**, 982.

255 Colt, J.S., Zahm, S. H., Camann, D. E., and Hartge, P., Environ. Health Perspect., 1998, **106**, 721.

256 Bradman, M. A., Harnly, M. E., Draper, W., Seidel, S., Teran, S., Wakeham, D., and Neutra, R., J. Expo. Anal. Environ. Epidermiol, 1997, **7**, 217.

257 Whitmore, R. W., Immerman, F. W., Camann, D. E., Bond, A. E., Lewwis, R. G., and Schaum, J. L., Arch. Environ. Contam. Toxicol., 1994, **26**, 47.

258 Roinestad, K. S., Louis, J. B., and Rosen, J. D., J. AOAC International,1993, **76**, 1121.

259 Lewis, R. G., Fortmann, R. C., and Camann, D. E., Arch. Environ. Contam. Toxicol., 1994, **26**, 37.

260 Eskenazi, B., Bradman, A., and Castorina, R., Environ. Health. Perspect., 1999, **107**, Supplement 3, 409.

261 Hernandez, F., Beltran, J., and Sancho, J. V., Science. Total Environ., 1993, **132**, 297.

262 Bhushan, R., Thapar, S., and Mathur, R. P., Bio. Chromatogr., 1997, **11**, 143.

263 Ioerger, B. P., and Smith, J. S., J. Agric. Food Chem., 1993, **41**, 303.

264 Coulibaly, K., and Smith, J. S., J. Agric. Food Chem., 1994, **42**, 2035.

265 Sharma, V. K., Jadhav, R. K., Rao, G. J., Saraf, A. K., and Chandra, H., Forensic Science International., 1990, **48**, 21.

266 Ellinger, R. H., in ' Handbook of Food Additives' Furia, T. E. (ed), CRC press, Ohio, 1972.

267 Linares, P., Luque de Castro, M. D., and Valcarcel, M., J. Chromaatogr, 1991, **585**, 267.

268 Halliwell, D. J., Mckelvie, I. D., Hart, B. T., and Dunhill, R. H., Analyst. 1996, **121**, 1089.

269 Svoboda, L., and Schmidt., J. Chromatogr. A., 1997, **767**, 107.

270 Wang, T., Li, S. F. Y., J. Chromatogr. A., 1998, **802**, 159.

271 Urasa, I. T., Mavura, W. J., Lewis, V. D., and Nam, H. S., J. Chromatogr., 1991, **547**, 211.

272 Jiang, S. J., and Houk, R. S., Spectrochim Acta., 1988, **43B**, 405.

273 Shintani, H., and Dasgupta, P. K., Anal. Chem., 1987, **59**, 802.

274 Baluyot, E. S., and Hartford, C. G., J. Chromatogr. A., 1996, **739**, 217.

275 Maki, S. A., and Danielson, N. D., J. Chromatogr., 1991, **542**, 101.

276 Shamsi, S. A., and Danielson, N. D., J. Chromatogr A., 1993, **653**, 153.

277 Sekiguchi, Y., Matsunaga, A., Yamamoto, A., and Inoue, Y., J. Chromatogr. A., 2000, **881**, 639.

278 Cui, H., Cai, Fa., and Xu, Q., J. Chromatogr. A., 2000, **884**, 89.

279 Gjerde, D. T., and Fritz, J. S., 'Ion Chromatography', second edition, Huthig, Heidelberg, 1987.

280 Balaram, V., Current Science., 1995, **25**, 640.

281 Dean, J. R., 'Atomic Absorption and Plasma Spectroscopy', Wiley and Sons, Chichester, 1997.

APPENDIX 1: SILANOL DATA

The two silanols used in chapter six were synthesised according to the method developed by Cella and Carpenter[1].

Figure A1.1 shows the ^{1}H NMR spectrum of dimethylsilandiol, in DMSO, which was synthesised by Dr P. Sutton, DeMontfort University, Leicester, UK. Table A1.1 shows the assignment of the chemical shifts. The white plates gave a melting point of 98 - 102^0 C, literature melting point 98 - 100^0 C [1].

Table A1.1: Assignment of chemical shifts for dimethylsilandiol

Chemical shifts, δ	Group	Integration
-0.08	-C<u>H</u>$_3$	6
5.76	-O<u>H</u>	2
3.45	<u>H</u>$_2$O (from DMSO)	-

Figure A1.2 shows the ^{1}H NMR spectrum of tetramethyldisiloxane-1,3-diol, in DMSO, which was synthesised by Mr A. Tonkin, University of Plymouth, Plymouth, Devon, UK. Table A1.2 shows the assignment of the chemical shifts. The white needles gave a melting point of 61 - 64^0 C, literature melting point 63 - 64^0 C [1].

Table A1.2: Assignment of chemical shifts for tetramethyldisiloxane-1,3-diol

Chemical shifts, δ	Group	Integration
-0.02	-C<u>H</u>$_3$	12
6.06	-O<u>H</u>	2
3.39.	<u>H</u>$_2$O (from DMSO)	-

1 Cella, J. A., and Carpenter, J. C., J. Organomet. Chem, 1994, **480**, 23.

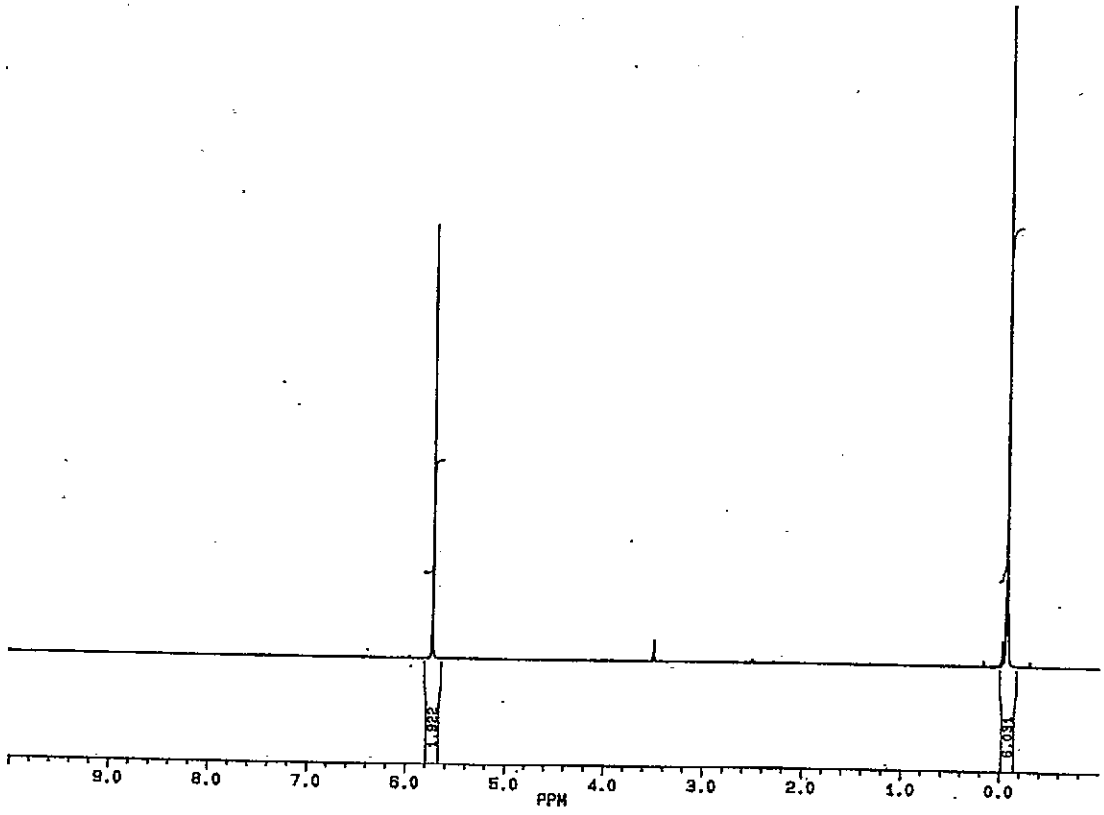

Figure A1.1: ^{1}H NMR spectrum of dimethylsilandiol

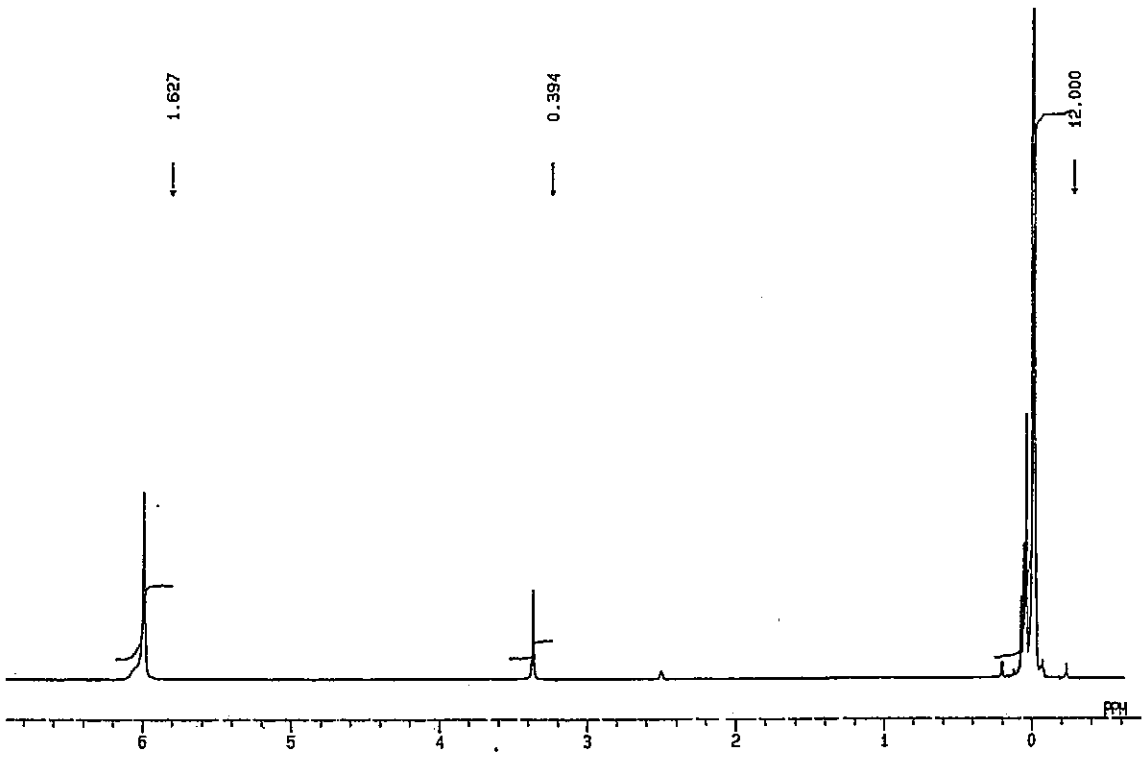

Figure A1.2: ^{1}H NMR spectrum of tetramethyldisiloxane-1,3-diol